DOCTOR OF PHILOSOPHY

Emerging anabolic drugs - investigation of the in vitro and in vivo metabolism of selective androgen receptor modulators

Holderbaum, Anna

Award date:
2020

Awarding institution:
Queen's University Belfast

Link to publication

Emerging Anabolic Drugs -
Investigation of the *in vitro* and *in vivo* Metabolism of
Selective Androgen Receptor Modulators

A thesis submitted for the degree of
Doctor of Philosophy

School of Biological Sciences
Queen's University Belfast

By

Anna Holderbaum, Mag.pharm.

April 2020

Declaration for Submission of Research Thesis

I declare that:

(i)   the thesis is not one for which a degree has been or will be conferred by any other university or institution;

(ii)   the thesis is not one for which a degree has already been conferred by this University;

(iii)   the work for the thesis is my own work and that, where materials are submitted by me for another degree or work undertaken by me as part of a research group has been incorporated into the thesis, the extent of the work thus incorporated has been clearly indicated;

(iv)   the composition of the thesis is my own work.
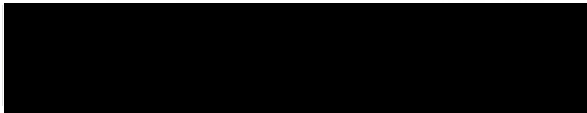
Signed: █████████████████   Date: 10th of April 2020

Dedicated with gratitude

to my parents.

Acknowledgements

Abstract

Selective androgen receptor modulators (SARMs) are a novel class of orally active, tissue-selective small molecule androgen receptor ligands with potential use for human therapeutic purposes. While SARMs show similar myoanabolic effects to anabolic androgenic steroids with reduced side effects, their exact underlying molecular mechanisms remain unclear. Their abuse has been reported in human and animal sports and further potential for abuse exists in livestock species. SARMs abuse therefore poses a threat to sports and food integrity as well as public health. To advance forensic testing of illicit use of SARM compounds in several relevant species and better understand their physiological impact, this thesis studies the *in vitro* and *in vivo* metabolism of key SARM compounds.

To evaluate the use of liver homogenates as an *in vitro* tool to rapidly produce SARM metabolites, cattle liver homogenates, S9 fractions, and microsomes were isolated, characterised (protein concentration, P450 and cytochrome b_5 content, enzymatic activity), and incubated with SARM compounds ostarine, andarine, or S-1 and respective cofactors to generate phase I and II metabolites followed by ultra-high performance liquid chromatography- quadrupole time of flight mass spectrometry (UHPLC-QTOF MS) analysis. All fractions produced metabolites that have previously been described as important target analytes of the investigated SARM compounds, demonstrating that the proposed simple and low-cost liver homogenate approach holds potential for use in the rapid development of metabolite-based screening methods.

Further, the *in vitro* metabolism of key SARM compounds across several relevant sports (horse), livestock (cattle, pig) and laboratory (rat) species, and the correlation of *in vitro* to *in vivo* generated metabolites was investigated. After isolation and characterisation of the liver fractions, microsomes alone or in combination with S9 fractions were incubated with SARM compounds ostarine, LGD-4033, or RAD140 to generate phase I and II metabolites respectively. To characterise *in vivo* generated metabolites, urine samples were collected after initial and repeated administration of ostarine, LGD-4033, or RAD140 to rats. Prepared *in vitro* and *in vivo* samples were analysed by UHPLC-ion mobility-QTOF MS. Interspecies differences within determined *in vitro* metabolite profiles were observed, highlighting the necessity of studying the metabolism of emerging anabolic agents such as SARMs on a by-species basis. The majority of detected urinary metabolites were also produced *in vitro*. While RAD140 was metabolically relatively stable, ostarine and LGD-4033 were extensively metabolised *in vitro* in all investigated species as well as *in vivo* - Subsequently,

cytochrome P450 (CYP) isoenzymes responsible for the formation of ostarine and LGD-4033 phase I metabolites using cattle, horse, pig, or rat liver microsomes were identified using a CYP-selective inhibitor reaction phenotyping approach followed by UHPLC-tandem mass spectrometry (UHPLC-MS/MS). Bovine, equine, murine, and porcine orthologues of human CYP2A6, CYP2B6, CYP2C8, CYP2C9 (only ostarine), and CYP3A4 were implicated in metabolism of ostarine and LGD-4033 across species.

To expand on the liver-based *in vitro* tools employed in this thesis, the metabolism of SARM compounds ostarine, LGD-4033, and RAD140 by multiple equine tissue microsomal and S9 fractions from liver, lung, kidney, and small intestines was investigated by UHPLC-QTOF analysis. Although it was shown that SARMs are not only metabolised by hepatic but also extrahepatic equine tissues, no additional metabolites were produced by extrahepatic tissue fractions.

Administration of SARM compounds ostarine or LGD-4033 to rats at sub-toxic levels for 17 days was shown (via two-dimensional difference gel electrophoresis (2-D DIGE) to identify differential protein levels with subsequent matrix-assisted laser desorption/ionization-time of flight mass spectrometry (MALDI-TOF MS) analysis to cause a response to the hepatic proteome. Subsequent differential centrifugation of livers into subcellular fractions (nuclei, mitochondria, cytosol, and microsomes) and 2-D DIGE analysis enabled detection of more subtle changes to the protein levels in response to SARM treatment. While all investigated SARM compounds triggered changes to 12 protein spots, each compound exhibited a unique response profile. Pathway enrichment analysis revealed that identified proteins were mainly involved in metabolic processes related to amino acid, carbohydrate and energy metabolism. Several proteins involved in protein processing within the endoplasmic reticulum had elevated differential abundances suggesting a potential cellular stress response following SARM treatment.

This thesis describes *in vitro* strategies and *in vitro*/*in vivo* metabolite profiles of key SARM compounds in sports, livestock and laboratory species and the *in vivo* effects of SARMs on hepatic protein levels. It is anticipated that the results will help to inform SARM metabolite-based screening approaches in veterinary species and provide a better understanding of SARMs effects on liver as a key metabolic tissue.

Table of Contents

Abbreviations

2-D	Two-dimensional
3-D	Three-dimensional
AAF	Adverse Analytical Finding
AAS	Anabolic androgenic steroids
ALT	Alanine aminotransaminase
ANOVA	Analysis of variance
APS	Ammonium persulfate
AR	Androgen receptor
AWERB	Animal Welfare and Ethical Review Body
BCA	Bicinchoninic acid
BCAA	Branched-chained amino acids
BEH	Ethylene bridged hybrid
cDNA	Complementary DNA
C. elegans	*Cunninghamella elegans*
CCS	Collision cross section
CE	Collision energy
CES	Carboxylesterase
CHAPS	3-[(3-Cholamidopropyl)dimethylammonio]-1-propanesulfonate
CHCA	α-Cyano-4-hydroxycinnamic acid
CO	Carbon monoxide
Cy	Cyanine
CYP	Cytochrome P450 isoform
Da	Dalton
DHT	Dihydrotestosterone
DIGE	Difference gel electrophoresis
DMA	Differential mobility analyzer
DME	Drug metabolising enzyme
DMSO	Dimethyl sulfoxide
DT	Dithionite
DTIMS	Drift tube ion mobility spectrometry
DTT	Dithiothreitol
EDTA	Ethylenediaminetetraacetic acid

EIC	Extracted ion chromatogram
ER	Endoplasmic reticulum
ERAD	ER-associated degradation
ESI	Electrospray ionisation
FAD	Flavin adenine dinucleotide
FDR	False discovery rate
FEI	Fédération Équestre Internationale
FI	Fragment ion
FMN	Flavin mononucleotide
FMO	Flavin-containing monooxygenase
GC	Gas chromatography
GE	Gel electrophoresis
GO	Gene Ontology
GRP	Glucose-regulated protein
HLB	Hydrophilic-lipophilic balance
HR	High resolution
IABRW	International Agreement on Breeding, Racing and Wagering
IEF	Isoelectric focusing
IFHA	International Federation of Horseracing Authorities
ILAC	International Laboratory Accreditation Cooperation
IM	Ion mobility
IMS	Ion mobility spectrometry
IPG	Immobilised pH gradient
iv.	Intravenous
KEGG	Kyoto Encyclopedia of Genes and Genomes
LC	Liquid chromatography
LLE	Liquid-liquid extraction
LM	Liver microsomes
LOD	Limit of detection
LS9	Liver S9 fractions
m/z	Mass-to-charge ratio
MALDI	Matrix-assisted laser desorption/ionisation
M_{mi}	Monoisotopic mass

M_r	Relative molecular mass
MRM	Multiple reaction monitoring
MS	Mass spectrometry
MS/MS	Tandem mass spectrometry
NAD^+	Nicotinamide adenine dinucleotide (oxidized form)
NADH	Nicotinamide adenine dinucleotide (reduced form)
NADPH	Nicotinamide adenine dinucleotide phosphate
NAT	*N*-Acetyltransferase
NHS	N-Hydroxysuccinimide ester
NL	Non-linear
NMR	Nuclear magnetic resonance
NSCLC	Non-small cell lung cancer
p.o.	Per os
P450	Cytochrome P450
PAPS	3'-Phospho-adenosyl-5'-phosphosulfate
PBS	Phosphate-buffered saline
PDI	Protein di-sulfide isomerase
PEG	Polyethylene glycol
PI	Precursor ion
pI	Isoelectric point
PMF	Peptide mass fingerprinting
POWER	Prevention and treatment of muscle wasting in patients with cancer
PPAR	Peroxisome proliferator-activated receptor
QTOF	Quadrupole time of flight
RT	Retention time
SARM	Selective androgen receptor modulator
SDS	Sodium dodecyl sulfate
SEM	Standard error of the mean
SFC	Supercritical fluid chromatography
SPE	Solid phase extraction
STRING	Search Tool for the Retrieval of Interacting Genes/Proteins
SULT	Sulfotransferase

$t_{1/2}$	Half-life
TCA	Trichloroacetic acid
TEMED	Tetramethylethylenediamine
TFA	Trifluoroacetic acid
TIC	Total ion chromatogram
TIMS	Trapped ion mobility spectrometry
TOF	Time of flight
TQ	Triple quadrupole
Tris	Tris(hydroxymethyl)aminomethane
TWIMS	Travelling wave ion mobility spectrometry
UDPGA	Uridine 5'-diphospho-glucuronic acid
UGT	Uridine 5'-diphospho-glucuronosyltransferase
UHPLC	Ultra-high performance liquid chromatography
UPLC	Ultra performance liquid chromatography
UPR	Unfolded protein response
v/v	Volume per volume
w/v	Weight per volume
WADA	World Anti-Doping Agency

Chapter 1: Introduction

1.1.   An emerging class of anabolic compounds: SARMs

Testosterone and anabolic androgenic steroids (AAS) have important anabolic effects, however, the lack of tissue specificity leads to several dose-dependent side effects, such as increased risk of prostate cancer in men and virilisation in women and children[1–3], often preventing their long-term clinical use. Selective androgen receptor modulators (SARMs), an emerging class of anabolic agents, have been widely studied as potential therapeutic drugs in humans because of their tissue-selective anabolic activities since their discovery in 1998 by Dalton et al.[4] They act as full androgen receptor (AR) agonists in anabolic organs (e.g. muscle and bone) via coactivator recruitment, but act as AR antagonists or weak AR agonists in androgenic tissues (e.g. prostate and seminal vesicles) via corepressor recruitment.[5,6] They are not substrates for 5α-reductases and aromatases in contrast to testosterone, which is converted by these enzymes leading to an undesirable metabolic amplification of androgenic or estrogenic functions in off-target tissues. Therefore, SARMs have similar anabolic effects to AAS, but with a reduced side effect profile.[6] The mechanistic basis for SARM tissue-selective action is not yet fully understood. Several mechanisms such as ligand-dependant conformational changes of the AR[7], the varied expression of coactivators and corepressors in different tissues[8,9], and distinct genomic and non-genomic signalling pathways[10] are likely to contribute to the tissue selectivity of SARMs.

Despite high specificity for the AR and tissue selectivity, an "ideal" SARM has high oral bioavailability and reasonably long half-life ($t_{1/2}$) that is consistent with daily dosing.[11] Advanced modifications to SARM chemical structures improved these properties to achieve an ideal pharmacokinetic profile. For example, the structural development of the first described non-steroidal aryl-propionamide-derived SARM compounds[4] was based on the AR antagonist bicalutamide (**Figure 1.1**). Notably the sulfone group was replaced by a thioether substituent in acetothiolutamide[12], an AR agonist *in vitro* exhibiting anabolic effects but unfavourable short half-lives due to oxidation of the thioether to sulfoxides and sulfones.[13] Through replacing the thioether by an ether resulting compounds acted as AR agonists in castrated male rats with unprecedented tissue-selective actions.[14] S-1 and andarine were identified as the first potent tissue-selective anabolic compounds[15], however, both the acetamido group in andarine and the nitro group in S-1 rendered them metabolically labile.[16,17] In ostarine the nitro group of S-1 was replaced with a cyano group resulting in a metabolically stable SARM compound.[18] To improve the pharmacokinetic and pharmacological profiles, SARMs have developed into an increasingly heterogeneous group

of compounds with regards to their chemical structure (**Figure 1.2**) and can be clearly categorized into steroidal and non-steroidal structures. The majority of reported SARM compounds have a non-steroidal core structure according to which they can in many cases be further classified (**Table 1.1**).

Bicalutamide
AR antagonist

Acetothiolutamide
AR agonist *in vitro*
$t_{1/2}$ 26 min (5 or 10 mg/kg iv.)[13]

Andarine
SARM
$t_{1/2}$ 2.88 hours (10 mg/kg p.o.)[17]

S-1
SARM
$t_{1/2}$ 4.72 hours (10 mg/kg p.o.)[16]

Ostarine
SARM
$t_{1/2}$ 14 ± 3.4 hours (10 mg/kg p.o.)[19]
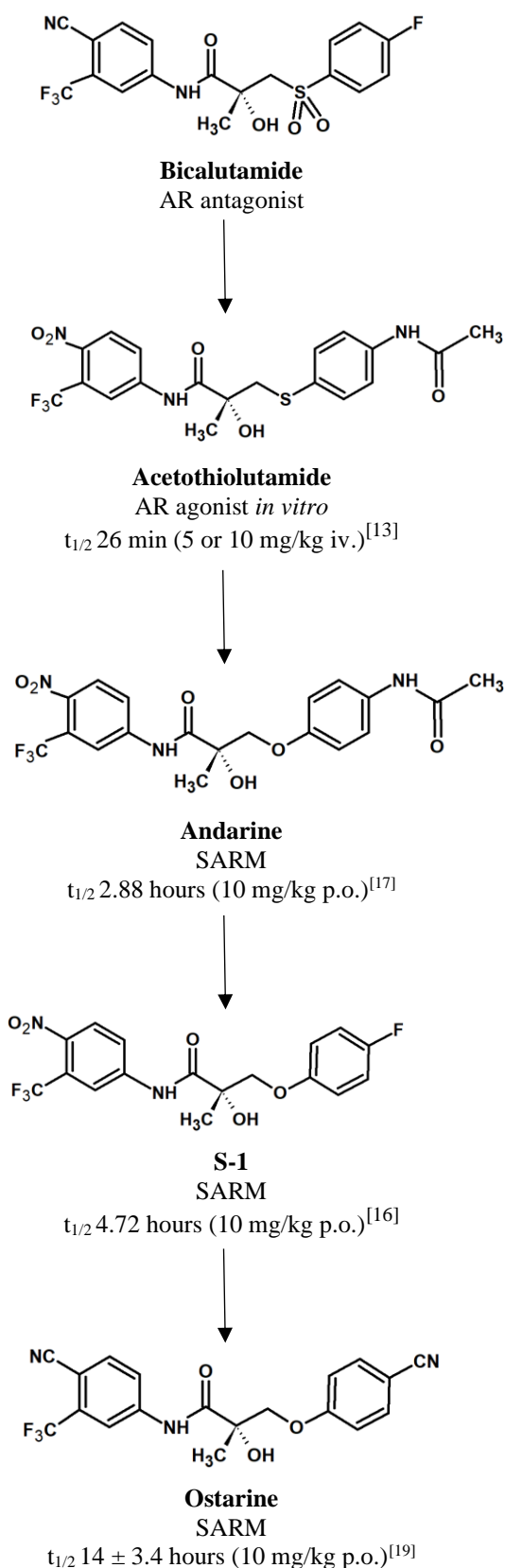
Figure 1.1 Development of aryl-propionamide-derived SARM compounds: From AR antagonists (bicalutamide) to agonists (acetothiolutamide) and metabolically labile (andarine, S-1) to stable (ostarine) SARM compounds.[16,17,19] (p.o. = per os; iv. = intravenous)
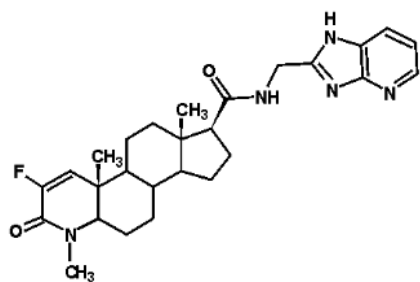
MK-0733
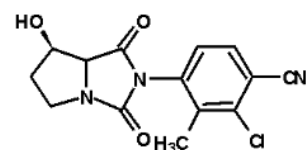
BMS 564929
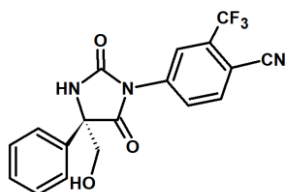
GLPG0492
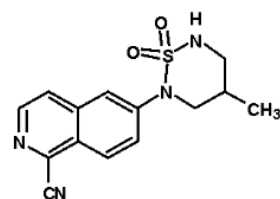
PF-06260414
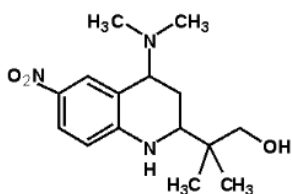
S-40503
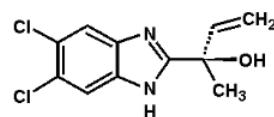
JNJ-37654032
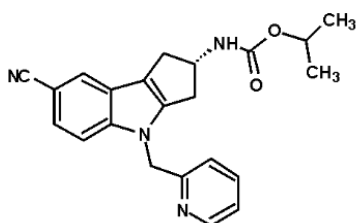
LY2452473
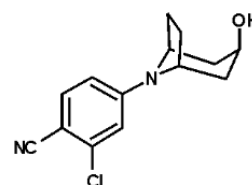
ACP-105
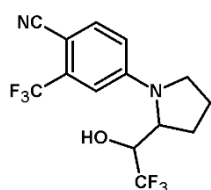
LGD-4033
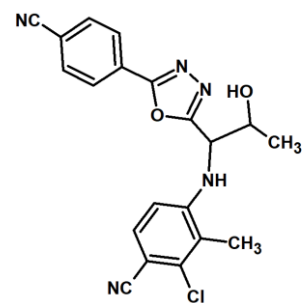
RAD140

Figure 1.2 Chemical structures of selected SARM compounds

Table 1.1 List of selected SARM compounds according to their chemical core structures. Compounds in bold have been studied in clinical trials and will be further discussed in **Section 1.1.1**.

Chemical core structure		Representative compounds	Ref.
Steroidal		MK-0733	[20]
		S42	[21]
		YK-11	[22,23]
		TFM-4AS-1	[24]
Non-steroidal	Aryl-propionamide	**Ostarine** (S-22, Enobosarm, GTx-024, MK-2866)	[18]
		Andarine (S-4, GTx-007)	[15]
		S-1	[15]
		S-9	[14]
		S-23	[25]
		S-24	[26]
		C-6	[27]
	Phenylmethanamide	MK-3984	[28]
	Hydantoin	BMS-564929	[29,30]
		GLPG0492 (DT-200)	[31]
	Quinoline	**PF-06260414**	[32]
	Quinolinone	LGD-2226	[33]
		LGD-2941	[34]
		LGD-3033	[35]
		LG121071	[36]
	Tetrahydroquinoline	S-40503	[37]
		S-101479	[38,39]
		S-49288	[39]
	Benzimidazole	JNJ-37654032	[40]
	Indole	**LY2452473** (TT701, OPK-88004)	[41]
		GSK2881078	[42]
		JNJ-26146900	[43,44]
	Tropanole	ACP-105	[45]
		AC-262536	[46]
	Imidazolopyrazole		[47,48]
	Pyrrolidinyl-benzonitrile	**LGD-4033** (Ligandrol, VK5211)	[49]
		SARM-2f	[32,50]
	Pyrazoline	JNJ-28330835	[51]
	Thiophene	NEP28	[52]
	Phenyloxadiazole	**RAD140**	[53]

1.1.1 SARM compounds in clinical development

SARMs are compounds that have emerged from human drug development for potential clinical applications. Promising SARM compounds from preclinical studies have advanced to testing in humans, and numerous clinical trials for SARMs have been completed (**Table 1.2**) to investigate their potential use for various conditions including muscle-wasting disorders, Duchenne muscular dystrophy, stress urinary incontinence, osteoporosis, and breast cancer.[54] Yet, to date no SARM compound has gained clinical approval.

An aryl-propionamide-derived SARM compound that holds great promise to gain approval is ostarine. A phase II clinical trial with 120 healthy elderly men and women evaluated four doses (0.1, 0.3, 1, or 3 mg daily) of ostarine for 86 days and showed a dose-dependent improvement of lean body mass, i.e. muscle, and physical function compared to the placebo.[55] While ostarine was generally well tolerated and no effects on hair growth nor sebum production in women were observed, alanine aminotransaminase (ALT) fluctuations to above the upper limit were observed in eight participants. One of them (3 mg regime) had to be discontinued due to the high level of ALT. However, an increase in ALT plasma levels may not be linked to drug toxicity but androgen action of the drug in non-hepatic tissue.[56] 12 weeks of treatment with ostarine (3 mg) or the phenylmethanamide-derived SARM compound MK-3984 (50 mg or 125 mg) in postmenopausal women were shown to increase lean body mass, however, seven women in the MK-3984 groups discontinued the trial due to elevations in liver enzymes.[57] SARM compounds are promising drugs in the treatment of breast cancer that express the AR.[58] AR-positive tumours are associated with improved overall and disease-free survival rates compared to AR-negative tumours[59] likely due to modulating ER signaling and hence supressing metastasis[60]. In postmenopausal women with estrogen receptor positive metastatic breast cancer administration of 9 mg ostarine daily was well tolerated and showed no drug-related serious adverse effects.[61,62] Upon administration of ostarine (1 mg or 3 mg) for 16 weeks, not only lean body mass but also stair climb performance and quality of life in patients with cancer cachexia were improved.[63] Another study in cancer patients showed that treatment with a daily dose of 1 mg or 3 mg of ostarine increased body mass with no observed change in prostate specific antigen concentration when compared to the placebo group.[64,65] Growth and functions of the prostate depend on DHT and its interaction with the AR[66] and higher levels of serum free testosterone were linked to an increased risk of aggressive prostate cancer[67]. Therefore, prostate specific antigen concentration was measured as specific prostate marker with

increased levels associated with prostate cancer.[68] It has been suggested that SARMs form a complex of coactivators and -repressors at a cellular level in the prostate that will prevent maximal activation of the AR in this androgenic tissue while coactivators facilitate maximal activation of the AR in anabolic tissues.[54] In addition, ostarine was administered as daily dose of 1 mg or 3 mg to patients with non-small cell lung cancer (NSCLC), colorectal cancer, non-Hodgkin's lymphoma, chronic lymphocytic leukemia or breast cancer.[69] It was well tolerated and improved physical function in NSCLC patients. Two phase III studies on the effect of ostarine on the prevention and treatment of muscle wasting in patients with cancer (POWER) were subsequently initiated. Based upon the first-line chemotherapy, patients with stage IV and III NSCLC were either enrolled in POWER 1 (platinum+taxane, $n = 321$)[70] or in POWER 2 (platinum+non taxane, $n = 320$)[71]. At the time of initiation of the chemotherapy, patients received 3 mg ostarine once daily for 84 days. Primary endpoints were lean body mass and physical function after 84 days. Secondary endpoints looked at the overall survival, durability of benefits and quality of life. Overall, whilst ostarine was well tolerated, mixed results were obtained for the primary endpoints. Both trials reported an increase in lean body mass, however, significant improvement of physical performance was only observed in POWER 1.[28,72–74] Two phase II clinical trials investigating ostarine for stress urinary incontinence have been completed[75,76] while two other registered phase II trials to assess the long-term safety and response were terminated due to a lack of efficacy.[77,78] GTx is still evaluating ostarine for treatment of estrogen and androgen receptor positive breast cancer[79] and in combination with the monoclonal antibody pembrolizumab for use in patients with androgen receptor positive triple negative breast cancer.[80]

The pyrrolidinyl-benzonitrile-derived SARM compound LGD-4033 has been developed by Ligand Pharmaceuticals and is under investigation as VK5211 with Viking Therapeutics. When the drug was administered orally (0.1, 0.3, or 1 mg) to healthy young men between 21 and 50 years for 21 days, it was well tolerated at all doses, showed favourable pharmacokinetics and a dose-dependent increase in lean body mass even in this short period although muscle performance and physical function were not significantly different from the placebo group.[81] A phase II study evaluated the safety, tolerability and efficiency of LGD-4033 after 12 weeks of treatment in ≥ 65 year-old patients with acute hip fracture with results not yet published.[82]

Administration of 50 mg MK-7033, a steroidal SARM compound, orally twice daily for six months resulted in increased lean body mass in women with sarcopenia. Most of the increase occurred within the first three months. However, this did not lead to improved

strength or physical function when compared to the placebo group. Liver transaminase and haematocrit were elevated, which likely suspended further development of MK-7033.[83,84]

The first-in-human study with the quinoline-type SARM compound PF-06260414 in healthy subjects found that it was generally well tolerated.[32] A phase I clinical trial to investigate the bioavailability of PF-06260414 upon oral administration in a solid dose formulation compared to a nanosuspension was terminated before enrolling subjects.[85]

The safety, tolerability and pharmacokinetics of the hydantoin-type SARM compound GLPG0492 in healthy subjects was investigated in phase I trials with a single ascending oral dose[86] of the hydantoin-type SARM and subsequently multiple ascending doses[87] In addition, the pharmacodynamics and metabolism of GLPG0492 in healthy male volunteers were studied.[88] Results of these studies have not been openly published yet. GLPG0492 is still in development for potential treatment of Duchenne muscular dystrophy or other neuromuscular disorders.[89]

GlaxoSmithKline assessed the safety, tolerability, pharmacokinetics and -dynamics of GSK2881078[42,90–92], GSK2849466 (structure undisclosed)[93], and GSK971086 (structure and study results undisclosed)[94]. The indole-derived SARM compound GSK2881078 was well tolerated and had good pharmacokinetic characteristics, which supports further clinical development and another phase II trial in patients with chronic obstructive pulmonary disease that suffer from muscle weakness has been initiated.[95] GSK2849466 was well tolerated as single dose, however, the study was terminated before advancing to repeat dosing due to cardiac necrosis in a pre-clinical 13-week rat study.[96]

Disposition of another indole-derived SARM compound LY2452473 was studied in humans by administering a ^{14}C labelled analogue of the drug.[41,97] A phase I trial studied the bioavailability of LY2452473 taken orally as 5 mg capsule and 5 mg tadalafil tablet compared to three combination tablets with small, intermediate and large particle sizes.[98] In a phase II trial the efficacy of LY2452473 with tadalafil to tadalafil alone in volunteers with erectile dysfunction was evaluated.[99,100] The idea was to achieve synergistic effects when combining an androgen agonist with a phosphodiesterase type 5 inhibitor.[41,101] However, the studies showed a lack of efficacy of LY2452473 with tadalafil in erectile dysfunction non/partial responders.[101] Transition therapeutics has acquired the rights for LY2452473 from Eli Lilly & Company and has renamed the compound to TT701. In 2016, the company announced that they will evaluate in a phase II study how save and efficient the drug is in improving the life quality of men with prostate cancer after radical prostatectomy surgery.[99,102] Transition therapeutics was acquired by OPKO health that kept

LY2452473 in its pipeline as OPK-88004 and enrolled patients with benign prostatic hyperplasia in a phase II trial, which has been terminated due to variability in the employed method for endpoint measurement of prostate volume and increased liver enzymes at higher doses (15 mg and 25 mg) in several patients.[103]

In 2017 a phase I trial for treatment of hormone positive breast cancer with the phenyloxadiazole-derived SARM compound RAD140 has been registered with the aim to evaluate the drug's safety, tolerability and pharmacokinetics with results not yet available.[104]

Overall, the results from clinical studies indicate a superior safety profile of SARMs over AAS.[6] Generally, they were well tolerated and led to an increase in lean body mass. While ostarine is the most advanced SARM clinically with two phase III trials completed, the findings from these were insufficient for a new drug application as definite demonstration that the increase in lean body mass is associated with an improvement in physical function was not achieved.[105] Lessons learned from these trials (e.g. choice of primary endpoints, dosage, methodology) are valuable and will help to shape future trials in the field, where guidance on regulatory aspects and study design is highly relevant.[106,107] In addition, improved understanding of the targeted mechanisms in specific tissues may also help the development of SARMs.

SARM compounds in clinical trials phase of commercial development are routinely abused in sports (**Section 1.1.2**). The information published from clinical trials investigating SARM compounds has been used by various Internet outlets to promote SARM compounds as safe alternatives to AAS for muscle mass gain to prospective customers potentially fuelling their abuse. Therefore, it is imperative for forensic testing laboratories to remain informed on the most recent drug and clinical trial research which will enable them to anticipate and detect the abuse of emerging substances. Such information was used to inform selection of the specific compounds studied in this project (i.e. ostarine, LGD-4033, and RAD140 for **Chapter 3-7**) and the sub-toxic dosage of SARM compounds for administration in the *in vivo* study (**Section 3.2.2** and **6.2.2**).

Table 1.2 Completed clinical trials with SARM compounds

Clinical trial phase	SARM compound	Sponsor	ClinicalTrials.gov identifier	Condition of subjects	Findings
Phase I	GSK971086	GlaxoSmithKline	NCT00540553[94]	Healthy	No results posted
	GSK2881078	GlaxoSmithKline	NCT02045940[90]	Healthy	No results posted
			NCT02567773[42,91,92]		Pharmacodynamic effects with acceptable tolerability.
	GSK2849466	GlaxoSmithKline	NCT01696604[93]	Healthy	Terminated due to cardiac necrosis in rat toxicology study
	PF-06260414	Pfizer	NCT02070939[32]	Healthy	Well tolerated with no serious adverse events
	GLPG0492	Galapagos NV	NCT01130818[86] NCT01397370[87] NCT01538420[88]	Healthy	No results posted.
	Ostarine + anastrozole	Havah Therapeutics Pty Ltd	NCT03264651[108]	Pre-menopausal women with high mammographic breast density	No results posted
	LY2452473	Eli Lilly & Company	NCT01275157[41,97]	Healthy	Extensive metabolism through multiple pathways.
	LY2452473 + tadalafil	Eli Lilly & Company	NCT01401543[98]	Healthy	Pharmacokinetics (maximum plasma concentration c_{max})
Phase II	Ostarine	GTx	NCT00467844[64,65]	Cachexia	Increase in total lean body mass. No drug related serious adverse events
			NCT01616758[61,62]	Metastatic breast cancer	Well tolerated with no serious adverse events
			NCT02658448[76]	Stress urinary incontinence	No results posted
			NCT03241342[75]		Did not meet primary endpoint (change in stress incontinence episodes)
	MK-0733	Merck Sharp & Dohme Corp.	NCT00529659[83,84]	Sarcopenia	Increase in lean body mass, no improvement in strength or function
	LGD-4033	Viking Therapeutics	NCT02578095[82]	Hip Fractures	No results posted
	LY2452473 +tadalafil	Eli Lilly & Company	NCT01160289[100,101]	Erectile dysfunction	Lack of efficacy
	LY2452473	Dana-Faber Cancer Institute	NCT02499497[99,102]	Prostate cancer	No results posted
	LY2452473	Transition Therapeutics	NCT03297398[103]	Benign prostatic hyperplasia	Terminated (method of endpoint measurement)
Phase III	Ostarine	GTx	NCT01355484[70,72,73] NCT01355497[71–73]	Muscle wasting, NSCLC	Did not meet primary endpoints (physical function and lean body mass)

1.1.2 Abuse of SARM compounds as doping agents and strategies for their detection in control analysis

Whether it is in human sports, animal racing or the agricultural industry – where there is an incentive to cheat, fraudsters try to circumvent current legislation and monitoring schemes to maximize their profits. Besides their clinical potential (**Section 1.1.1**) SARMs may be used by athletes or in the animal sports and livestock industry due to their myoanabolic affects. Some athletes may try to gain an advantage by consuming anabolic substances such as SARMs to increase muscle mass and hence enhance performance. For the same reason these drugs might be administered to sports animals such as horses or greyhounds, whilst in food producing animals, anabolic agents improve muscle mass and therefore meat production. However, such practices are illegal and combating the misuse of anabolic agents poses a major challenge in animal husbandry and sports.

The prohibited list published and updated annually by the World Anti-Doping Agency (WADA) states that anabolic agents including SARMs are prohibited at any time in- and out-competition.[109] The WADA also sets international standards for the testing of samples and laboratory accreditation.[110,111] In horse racing the International Agreement on Breeding, Racing and Wagering (IABRW) published by the International Federation of Horse Racing Authorities (IFHA) states that anabolic agents including SARMs are not to be administered to racehorses at any time and it specifies requirements for testing laboratories.[112] However, the adoption of this guideline depends on the individual racing authorities, e.g. Horse Sport Ireland and the British Horse Racing Authority.[113,114] The Fédération Équestre Internationale (FEI) is the international governing body for equestrian sports and sole controlling authority for all international events enforcing the Equine Prohibited Substance List that includes controlled medication and banned substances such as several SARM compounds.[115] Accredited horseracing laboratories must adhere to the requirements and criteria outlined in the International Laboratory Accreditation Cooperation (ILAC)-G7 guidelines to test for prohibited substances.[116] In livestock, council directive 96/22/EC[117] prohibits the use of all substances that have hormonal (such as SARMs) or thyrostatic action and β-agonists for growth promotion. Council directive 96/23/EC[118] requires that each member state implements a national residue control plan to monitor specified prohibited substances that has to be submitted to the European Commission for annual approval. Levels and frequencies of sampling are outlined in Commission Decision 97/747/EC[119] and analyses of samples can only be conducted by officially approved

accredited laboratories using validated analytical methods as outlined in Commission Decision 2002/657/EC.[120] Furthermore, European Union reference laboratories function as competent authorities to provide analytical support for national reference laboratories and provide the Commission with scientific expertise (Regulation (EC) No. 882/2004).[121] Together, these documents are part of the current legal framework for controlling the misuse of anabolic substances in human sports, horse racing, and food producing animals.

A new and ever-expanding range of SARMs deriving from drug discovery and development processes with potential for abuse emerges on the black market.[122–124] Although safety criteria for the approval of new drugs increase and SARMs still lack approval for therapeutic purposes, they are readily available on the Internet with the SARM compounds andarine, ostarine, and LGD-4033 previously identified in confiscated black market products[122–124] and in test purchases from online vendors.[49,125–129] As discussed earlier the use of SARMs by athletes or administration to sports and livestock animals is prohibited due to their anabolic properties, but cases of abuse of SARMs in athletes and horses have been widely reported.[130–133] WADA testing figures reports from 2012-2018 show a steep rise in Adverse Analytical Findings (AAFs) of SARMs based on analysis of urine and blood samples (**Figure 1.3**).[134–140] In 2012, five samples tested positive for SARMs, whereas, in 2013, this figure rose to 13. From 2014 to 2015, the number more than doubled again from 15 to 32 - of these, 28 tested positive for ostarine, with two each returning positive for LGD-4033 and andarine respectively. The number of samples that tested positive for SARMs increased again in 2016 to 39, including 30 samples that tested positive for ostarine, six for LGD-4033, two for RAD140, and one positive sample for andarine. Another rise was observed in 2017 when 65 samples were tested positive for SARMs including 47 samples positive for ostarine, nine for LGD-4033, six for RAD140, and three for andarine. In 2018, the number of AAFs of SARMs reached another high with 77 samples testing positive. Thereof 45 were attributed to ostarine misuse, 26 to LGD-4033, five to RAD140, and one to andarine. This observed rise could be due to improvement of detection methods and/or an actual increase of athletes taking SARMs. To provide further context, the reports show that the overall number of analysed samples from Olympic and non-Olympic athletes has steadily risen from 267,645 in 2012 to 344,177 in 2018 while the percentage of overall AAFs relating to the overall number of samples fluctuated: 1.19 % (2012), 1.31 % (2013), 1.11 % (2014), 1.26 % (2015), 1.60 % (2016), 1.43 % (2017), and 1.42 % (2018).
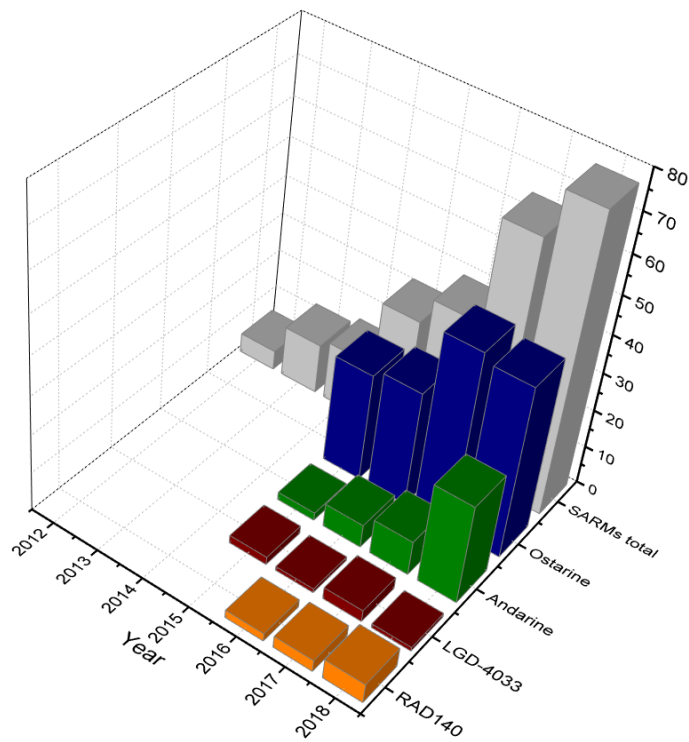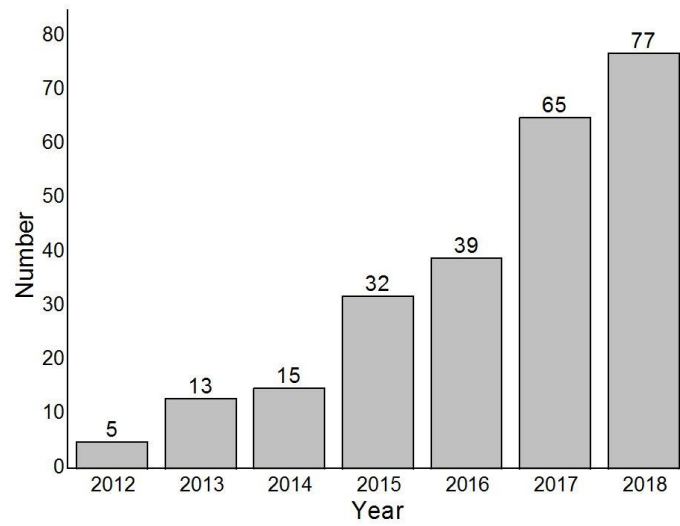
Figure 1.3 Number of athletes' samples tested positive for SARMs by the WADA (2012-2018) [134–140]

Moreover, the potential use of SARMs in food producing animals, including cattle, for increasing muscle growth and decreasing fat mass has been described in several patents, e.g. WO2011119544 A1 and WO2014087298 A1 and in a number of scientific publications.[141–143] Consequently, the free availability of SARMs and the increasing instances of their abuse and misuse emphasise the need to study the *in vitro* and *in vivo* metabolism of this class of emerging anabolic compounds.

The chemical diversity and ever-expanding range of SARMs poses an analytical challenge for control laboratories. Various methods based on hyphenated mass spectrometry techniques have been established to monitor either the intact SARM compound(s) or also their metabolites as determined from *in vivo* and/or *in vivo* drug metabolism studies (**Table 1.3**). Hyphenated mass spectrometry instruments such as ultra-high performance liquid chromatography-tandem mass spectrometry (UHPLC-MS/MS) or gas chromatography-mass spectrometry (GC-MS) are especially useful and advantageous tools for monitoring illicit drugs because multiple analytes can be detected from complex sample matrices with one sample injection. Routine analyses for SARMs are often performed with UHPLC-MS/MS due to their high sensitivity, selectivity, and specificity. For doping control in athletes, dedicated liquid chromatography (LC)-MS/MS methods have been developed for aryl-propionamide-[144], 2-quinolinone-[145], tricyclic tetrahydroquinolinone-[146], benzimidazole- and bicyclic hydantoin-derived[147] SARMs. Aryl-propionamides were analysed by solid phase extraction (SPE) of human urine followed by LC-MS in negative electrospray ionization (ESI) mode with simultaneous multiple reaction monitoring (MRM) and precursor ion scanning.[144] When human urine samples were analysed after intake of andarine, LC-MS was found to give more comprehensive information than GC-MS and is therefore the preferred detection method for aryl-propionamides.[148] Benzimidazole- and bicyclic hydantoins were analysed with the same strategy as aryl-propionamides in positive mode.[147] For detection of 2-quinolinones and tricyclic tetrahydroquinolinones, human urine samples were enzymatically hydrolysed followed by liquid-liquid extractions (LLE) and analysed by LC-MS/MS in positive ESI in MRM and precursor ion mode.[145,146] Generally, MRM mode allowed for lower limit of detections (LODs) of 1-10 ng/mL, whereas, precursor ion scans needed 20-50 ng/mL of the compound in urine to produce distinct signals.[149] However, precursor ion experiments scan for core ions as part of the drug and therefore, additionally allow for the detection of metabolites with the intact product ion and structurally similar or modified drugs. In addition, GC-MS methods were established for 2-quinolinones and bicyclic hydantoin-derived SARMs.[150,151] Bicyclic hydantoins showed low ionisation

with ESI and therefore, GC-MS is preferred over LC-MS.[150] For example, the LOD of BMS-564929 with LC-MS was 20 ng/mL, whereas, GC-MS leads to an improved LOD of 10 ng/mL.[147,150]

Besides dedicated methods, SARM compounds have also been implemented in multi-analyte methods. For example, Musenga et al. developed a high-throughput screening method for a wide range of prohibited substances, including andarine and ostarine, in human urine by LC-high resolution (HR)-MS.[152] Guddat et al. included andarine and one of its main metabolites formed by *O*-dephenylation in a multi-target approach by direct injection of human urine samples onto LC-MS/MS.[153] Further, a method for detection of 12 prohibited substances, including YK-11, in exhaled human breath has been established.[154]

In general, SARMs are not only at risk of abuse in human sports, but also in equine sports and livestock farming due to their anabolic properties. For equine doping control, e.g. a method for detecting 100 drugs, including the SARM compounds andarine and ostarine, in horse urine was developed using automated on-line SPE coupled to LC-HR-MS.[155] Multi-target screening methods covering a broad range of prohibited substances including andarine and ostarine in equine hair have been established in order to extend detection windows.[156,157] Recognizing the need for veterinary control of SARMs in cattle, a major food-producing animal, methods for detecting ostarine and andarine by LC-MS/MS in bovine urine[141,158,159] and faeces[159] were validated. Another study applied supercritical fluid chromatography (SFC)-ion mobility (IM)-MS to validate a method to detect andarine and ostarine in bovine urine.[143] Recently, targeted screening methods dedicated to the detection of fourteen SARM compounds that is applicable to the analysis of urine samples from several species (bovine, equine, canine, murine, human)[160] and bovine muscle[161] have been validated.

By using *in vivo* and/or *in vitro* studies, or authentic samples when available (see **Section 1.3**), not only the intact drug but also phase I (PHI) and phase (PHII) metabolites (see **Section 1.2**) have been implemented in control strategies (**Table 1.3**). In order to identify previously unknown metabolites LC-HR-MS is a popular technique to measure the mass-to-charge ratio (*m/z*) of analyte precursor and product ions with high accuracy.[162,163] *In vivo* drug administration studies serve the purpose to provide authentic specimens such as urine and plasma. After a single administration of the drug, samples are collected over an extended period of time to help establish an excretion profile of the drug and associated metabolites. This helps to demonstrate the applicability of the procedure to the analysis of authentic samples obtained after drug administration, provide detection time windows, and appropriate

long-term target analytes. For example, in equine urine SARMs S-1, ostarine, and andarine were quickly eliminated after three hours and a metabolite that could be detected up to 96 hours (S-1) and 48 hours (ostarine and andarine) was proposed as target analyte.[164] While metabolite monitoring prolonged the detection time for andarine (18 hours compared to 12 hours) in equine plasma, the main metabolites of ostarine and S-1 had the same detection time as the unchanged SARM compounds (96 hours for S-1 and 18 hours for ostarine).[165] Moreover, an excretion study of ostarine in bovine showed that faeces had a 500 times higher concentration of ostarine than urine and detection of ostarine beyond 21 days after a single high oral dose (200 mg/animal) in faeces was possible. Although *in vivo* samples are the gold standard in drug metabolism studies, authentic samples are limited and drug administration studies take a lot of time and resources. Alternatively, *in vitro* metabolism experiments of SARMs (**Table 1.3**) using human, bovine or equine liver microsomes (LM) and/or liver S9 fractions (LS9) have been used to generate metabolites (see **Section 1.3.2.4** for microsomes and S9 fractions) that were subsequently implemented into existing control procedures, and hence provide potential target analytes for efficient control analyses.

Altogether, the ease of availability and use, advantageous effects and short detection window[164] of SARMs increases their potential for abuse and demonstrate the need for in *vitro* and *in vivo* SARM metabolism studies to provide appropriate target analytes enabling monitoring laboratories to sensitively test for emerging SARM compounds, especially in sports and food producing animals. Relating to this context the following sections will discuss general aspects of drug metabolism (**Section 1.2**) and methods for studying drug metabolism (**Section 1.3**)

Table 1.3 Strategies for the detection of SARM compounds and associated metabolites in humans, sport and food producing animals based on analysis using hyphenated mass spectrometry techniques.

Core structure	SARM compounds	Species	Matrix	Metabolites	Analysis	Ref.
Method development and validation						
Aryl-propionamide	S-1, andarine, S-9, S-24	Human	Urine		HPLC-MS/MS	[144]
	Andarine	Human	Urine		UHPLC-MS/MS	[166]
	Andarine, ostarine	Human	Urine		UHPLC-HR-MS	[152]
					UHPLC-MS/MS	[167]
	Andarine	Human	Urine	O-Dephenyl-andarine	HPLC-MS/MS	[153]
	Andarine, ostarine, S-23, S-24	Human	Urine	Ostarine glucuronide	HPLC-HR-MS	[168]
	S-1, andarine, S-9, S-24	Human	Plasma		UHPLC-HR-MS	[169]
	Andarine, S-1	Human	Blood		UHPLC-HR-MS	[170]
	Andarine, ostarine	Equine	Urine		UHPLC-HR-MS	[155]
	Andarine, ostarine	Equine	Hair		UHPLC-MS/MS	[157]
	Andarine, ostarine	Equine	Hair		UHPLC-MS/MS	[156]
	Andarine, ostarine	Bovine	Urine		UHPLC-MS/MS	[141]
	Andarine, ostarine	Bovine	Urine		HPLC-MS/MS	[158]
	Andarine, ostarine	Bovine	Urine Faeces		UHPLC-MS/MS	[159]
Quinolinone	LGD-2226, 3 quinolinone-derived SARMs	Human	Urine		HPLC-MS/MS	[145]
	US 6,462,038 LG121071	Human	Urine		GC-MS	[151]
	LGD-2226, 2 quinolinone-derived SARMs	Human	Urine		GC-μAPPI-MS	[171]
	LG121071	Human	Urine		HPLC-HR-MS/MS	[172]
Tetrahydroquinoline	S-40503	Human	Plasma		HPLC-MS/MS	[173]
	Tricyclic tetrahydroquinolinone-derived SARMs	Human	Urine		HPLC-MS/MS	[146]
Steroidal	YK-11	Human	Exhaled breath		UHPLC-MS/MS	[154]
Aryl-propionamide, pyrrolidinyl-benzonitrile	Andarine, ostarine, LGD-4033	Human	Urine	O-Dephenyl-andarine, O-Dephenyl-ostarine	GC-HR-MS	[174]
Bicyclic hydantoin, quinolinone	BMS-564929, LGD-2226	Human	Urine		GC-MS/MS GC-MS	[150]
Benzimidazole, bicyclic hydantoin	BMS-564929, JNJ-37654032, 3 benzimidazole-derived SARMs	Human	Urine		HPLC-MS/MS	[147]
Aryl-propionamide, pyrrolidinyl-benzonitrile, quinolinone, quinoline, hydantoin, tropanole, indole	S-1, andarine, ostarine, S-6, S-9, S-23, LGD-4033, LGD-2226, PF-06260414, GLPG0492, BMS-564929, AC-262536, RAD140, LY3452473	Bovine Equine Canine Human Murine	Urine		UHPLC-MS/MS	[160]
		Bovine	Muscle		UHPLC-MS/MS	[161]
***In vivo* drug administration studies (* in combination with method development and validation)**						
Aryl-propionamide	Ostarine	Human	Urine	PHI, PHII	UHPLC-HR-MS(/MS)	[175]
	Andarine	Human	Urine	PHI, PHII	HPLC-MS(/MS) HPLC-MS^n GC-MS(/MS)	[148]

Table 1.3 *continued*

Core structure	SARM compounds	Species	Matrix	Metabolites	Detection strategy	Ref.
	Andarine, ostarine	Human	Urine	PHI, PHII	UHPLC-MS/MS GC-MS	[176]
	Ostarine, S-23	Canine	Urine	PHI, PHII	HPLC-MS/MS	[177]
	S-1, andarine, ostarine	Equine	Urine	PHI, PHII	UHPLC-HR-MS(/MS)	[164]
	S-1, andarine, ostarine	Equine	Plasma	PHI, PHII	UHPLC-HR-MS(/MS)	[165] *
	Ostarine	Bovine	Urine Faeces	PHI, PHII	UHPLC-MS/MS	[142] *
	Ostarine	Bovine	Urine	PHI (ostarine)	UHPLC-MS/MS	[141]
	Andarine, ostarine	Bovine	Urine	Excretion profile ostarine	UHPLC-MS/MS SFC-IM-HR-MS	[143] *
Pyrrolidinyl-benzonitrile	LGD-4033	Human	Urine	PHI, PHII	UHPLC-MS/MS UHPLC-HR-MS GC-MS	[178]
	LGD-4033	Human	Urine		UHPLC-HR-MS(/MS) GC-MS	[179]
	LGD-4033	Equine	Urine Plasma	PHI, PHII	UHPLC-HR-MS	[180] *
Phenyloxadiozole	RAD140	Human	Urine	PHI, PHII	UHPLC-MS/MS	[181]
Tropanole	ACP-105	Rat	Urine	PHI	UHPLC-HR-MS(/MS)	[182]
Case studies						
Aryl-propionamide	Andarine	Human	Urine		HPLC-MS/MS	[130]
	Andarine	Human	Urine	Andarine-M (*O*-dephenyl) Andarine glucuronide	LC-MS/MS UHPLC-HR-MS(/MS)	[133]
	Ostarine	Human	Hair		HPLC-MS/MS	[183]
	Andarine	Equine	Plasma		HPLC-HR-MS	[131]
Pyrrolidine	LGD-4033	Human	Urine	PHI	UHPLC-MS/MS UHPLC-HR-MS	[132]
***In vitro* studies**						
Aryl-propionamide	S-1, andarine, S-9, 1 aryl-propionamide-derived SARM	Human	LM LS9	PHI, PHII	HPLC-MS(/MS) HPLC-HR-MS	[184]
	Ostarine, S-23	Human	LM	PHI, PHII	HPLC-HR-MS(/MS)	[177]
	Andarine, S-24	Equine	LM + LS9	PHI, GLUC	HPLC-MS/MS HPLC-HR-MS	[185]
Pyrrolidine	LGD-4033	Human	LM	PHI	UHPLC-MS/MS UHPLC-HR-MS GC-MS	[178]
	LGD-4033	Human	LM	PHI	UHPLC-HR-MS(/MS)	[49]
	LGD-4033	Human	LM LS9	PHI, GLUC	GC-MS(/MS) UHPLC-HR-MS	[127]
Quinolinone	LG121071	Human	LM	PHI, PHII	HPLC-HR-MS/MS	[172]
Steroidal	MK-0773	Human	LM	PHI	HPLC-HR-MS(/MS) HPLC-MS/MS	[186]
Phenyloxadiozole	RAD140	Human	LM	PHI	UHPLC-MS/MS	[181]
Aryl-proprionamide, Quinolinone	Andarine, ostarine, S-9, S-24, bicalutamide, 2 quinolinone-derived SARMs	Bovine	LS9	PHI	UHPLC-MS/MS UHPLC-HR-MS	[141]

1.2.   Drug metabolism

In principle, biotransformation processes help to eliminate drugs from the body by metabolising lipophilic substrates to more hydrophilic products. Generally, metabolic reactions can be classified as phase I and phase II reactions. Phase I reactions are also referred to as functionalization reactions, introducing or exposing functional groups on the chemical structure of the compound on which further phase II reactions can occur. Phase II or conjugative reactions modify the compound by attaching groups such as sulfo and/or glucuronosyl groups. A thorough understanding of drug metabolism is important to determine the pharmacological activity, pharmacokinetics and/or toxicity of the drug and its metabolites.

Phase I reactions typically involve oxidation, reduction and hydrolysis reactions catalysed by flavin-containing monooxygenase (FMO), dehydrogenase, esterase, epoxide hydrolase, amidase, and most importantly cytochrome P450 (P450) enzymes. Phase II reactions include glucuronidation by uridine 5'-diphospho-glucuronosyltransferases (UGTs), sulfation by sulfotransferases (SULTs), acetylation by *N*-acetyltransferases (NATs), and methylation by methyltransferases. Except for methylation and acetylation, these reactions result in increased water solubility of the metabolites, and besides elimination and/or inactivation of a drug, biotransformation can result in activation or toxification.[187,188]

Most drugs undergo metabolism by several and/or combined pathways at different sites of the molecule. Identification of produced metabolites provides crucial information to analytical tests for monitoring drugs. Knowledge of drug metabolism, particularly if urine is the test matrix, is a crucial prerequisite in order to implement and detect drugs by analytical screening methods as the parent compound may not be present or detectable, and its associated metabolites have to be monitored instead. This subchapter gives a brief overview of common biotransformation reactions of drugs and xenobiotics in mammals and the enzymes involved. Several textbooks delve into the topic of drug metabolism to provide a more comprehensive overview.[189–191]

1.2.1.   Phase I metabolism

1.2.1.1   Oxidations catalysed by cytochrome P450

Cytochrome P450 (P450) is a superfamily of enzymes containing a haeme prosthetic group that catalyse a range of phase I metabolic reactions via oxidation, reviewed by Guengerich et al.[192] Besides a hydrocarbon substrate (RH), all these reactions require the presence of molecular oxygen (O_2), nicotinamide adenine dinucleotide phosphate (NADPH) as cofactor, and the mixed-function oxidase system consisting of P450 and NADPH-cytochrome P450 reductase.[190,193,194] The substrate binds to the P450 haeme in its ferric iron Fe^{3+} state, which causes a substrate-dependent lowering of the redox potential by approximately 100 mV[195], e.g. in microsomal systems the redox potential of P450 is lowered from -300 to -225 mV upon binding of the substrate benzphetamine[196]. The transfer of an electron from NADPH reduces Fe^{3+} to the ferrous state Fe^{2+}. O_2 binds to the Fe^{2+} forming a complex. A second electron from either NADPH-cytochrome P450 reductase or cytochrome b_5 is transferred to the complex reducing the $Fe-O_2$ adduct to a superoxo state. This is the rate-limiting step of the catalysis.[195] Two protons from the surrounding solvent break the O-O bond, forming water, and a hydroxylated form of the substrate while the enzyme returns to its initial Fe^{3+} state.

NADPH-cytochrome P450 reductase is a flavoprotein containing flavin adenine dinucleotide (FAD) and flavin mononucleotide (FMN) bound to the cytoplasmic membrane of the endoplasmic reticulum and transfers electrons from NADPH to P450.[197] The endoplasmic reticulum is a membrane tubular network that crosses the cytoplasm from the nucleus membrane to the plasma membrane. FAD is the electron acceptor from NADPH and FMN donates electrons to P450.[198,199] Therefore, NADPH-cytochrome P450 reductase is essential for the reduction of the P450 haemeprotein, which subsequently binds molecular oxygen and oxidises the substrate.

NADPH-cytochrome P450 reductase not only transfers its electrons to P450 but also to the haemoprotein cytochrome b_5. Besides NADPH-cytochrome P450 reductase, cytochrome b_5 and its electron donor cytochrome b_5 reductase play an important role in the electron transfer to P450[200,201] and it has been shown that the deletion of cytochrome b_5 in mice significantly affected hepatic and extrahepatic drug metabolism and P450 expression.[202] Cytochrome b_5 reductase is a flavoprotein containing FAD that can bind and oxidize nicotinamide adenine dinucleotide (NADH) to NAD^+. The reduced enzyme transfers its

electrons to cytochrome b_5, which serves as an electron donor for P450 and various desaturases that synthesize unsaturated fatty acids.

P450, NADPH-cytochrome P450 reductase, cytochrome b_5 reductase, and cytochrome b_5, are integral membrane proteins primarily anchored to the cytoplasmic surface of the endoplasmic reticulum of eukaryotic cells.[197,203–205] They are widely expressed proteins, present in all tissues, most notably in the liver, but also in kidney, lung, and intestines.[206] Measurements of NADPH-cytochrome P450 reductase activity, cytochrome b_5 content, and total P450 content can be used as markers for the integrity of a biological system.[207] Using cytochrome c as a surrogate electron acceptor, NADPH-cytochrome P450 reductase activity in biological samples can be measured with a spectrophotometer by reducing cytochrome c in the presence of NADPH. In this assay, NADPH-cytochrome P450 reductase accepts electrons from NADPH, which are passed on to cytochrome c. The reduction of cytochrome c results in the formation of distinct bands in the absorption spectrum and increase in absorbance at 550 nm over time.[207] The assay is an indirect measure of the NADPH-cytochrome P450 reductase activity towards P450 as the reduction rate of cytochrome c and not P450 is measured. Measurement of the actual NADPH-cytochrome P450 reductase reduction rate of P450 requires anaerobic conditions and rapid reaction techniques.[208] NADPH-cytochrome P450 reductase may be cleaved by proteolysis and still reduce cytochrome c, but not P450, however, proteolytic cleavage may not be significant and the cytochrome c reduction rate is a generally accepted surrogate substrate for NADPH-cytochrome P450 reductase activity measurements.[209] The amount of cytochrome b_5 can also be determined spectrophotometrically through the absorbance difference of the oxidized cytochrome b_5 at 410 nm and the NADH-reduced cytochrome b_5 by cytochrome b_5 reductase at 425 nm using a molar extinction coefficient of 185 mM^{-1} cm^{-1}.[203]

In 1958, the presence of a carbon monoxide (CO) binding pigment was reported in rat liver microsomes, which has a distinctive absorbance maximum at 450 nm.[210,211] Therefore, in "P450", the "P" stands for pigment and "450" refers to the absorbance of the distinctive carbon monoxide-bound state of reduced P450. The principle of this characteristic P450 spectral assay is that when the P450 haemeprotein is reduced to the ferrous form Fe^{2+} it can react with CO to form a stable complex that shows a maximum absorbance at 450 nm. In the CO-difference method, both the sample and reference cuvette are reduced with sodium dithionite, a baseline is recorded with the reference cuvette, and then the sample cuvette is bubbled with CO and a difference spectrum is recorded. The content of total P450 can be calculated by the difference between the isobestic absorbance at 490 nm and the Soret peak

at 450 nm divided by the molar extinction coefficient of 91 mM^{-1} cm^{-1}.[203] This method may not be suitable for preparations from non-perfused samples or in liver homogenates due to the presence and interference of haemoglobin, and therefore the dithionite (DT)-difference method was established whereby both the sample and reference cuvette are bubbled with CO.[212–215] As haemoglobin is mostly in its ferrous state to bind oxygen, both the haemoglobin in the sample and reference cuvette bind CO and the absorbance of this CO-haemoglobin complex is compensated for in the difference spectra. A molecular extinction coefficient of 104 mM^{-1} cm^{-1} is used with the DT-difference method.[214] Although the molar extinction coefficients were determined using rat liver preparations, these are generally valid for most P450s.[207]

On the basis of protein sequences, similarities and phylogeny, a common nomenclature for P450 genes across all organisms has been established.[216] Each P450 gene is rooted as CYP followed by a number associated with the gene family (> 40 % homology), a letter linked to the subfamily (> 59 % homology), and a further number designating the isoform. The Cytochrome P450 Homepage gives an overview of P450 sequences and nomenclature in various organisms.[217] In mammals, CYP1, CYP2, and CYP3 gene families are responsible for most drug metabolism[218–221], whereas others are involved in biosynthetic pathways (e.g. steroidogenesis and cholesterol biosynthesis). A characteristic of CYP isoforms is that they can be induced or inhibited, which plays a major role in the development of new chemical entities as it may lead to drug-drug interactions and subsequent failure of therapeutics or toxicity.[222] Inhibitors and inducers of human CYPs were reviewed by Pelkonen et al.[223] With regards to potential pitfalls in the drug approval process, the expression, regulation, and interaction of CYPs has been intensively studied in humans and laboratory species, however, drug metabolising enzyme (DME) expression profiling in veterinary species is still in its early stages.[224]

1.2.1.2 Oxidations not catalysed by cytochrome P450

Like P450, flavin monooxygenases (FMOs) are a family that require oxygen and NADPH to catalyse oxidations. FMO is a non-haeme microsomal enzyme localised in the endoplasmic reticulum with a FAD prosthetic group that catalyses the oxidation of nucleophilic nitrogen- and sulfur-containing xenobiotics. These reactions are not only catalysed by FMO, but also P450. In order to distinguish between FMO and P450 catalysed reactions and/or assess their relative contribution, CYP activity can be abolished under the

addition of 1 % *v/v* Triton X-100 or over 80 % of FMO activity can be diminished by heating microsomes for 1-2 min at 50 °C.[225,226] Mammalian FMOs can be grouped into five families (FMO1, FMO2, FMO3, FMO4, FMO5) based upon their amino acid sequence.[227,228] Based on FMO mRNA levels, human FMO1 is highly expressed in the kidneys, whereas FMO3 and FMO5 are primarily expressed in the liver and FMO2 in the lungs. FMO4 was mainly detected in liver and kidney. Additionally, small amounts of FMO1-5 were present in the small intestine.[229] Although not readily inducible or inhibitable in contrast to CYPs, there is also a degree of underlying genetic variability in FMOs.[230]

Other oxidative enzymes include dehydrogenases, such as aldehyde dehydrogenases as well as alcohol dehydrogenases, and aldehyde oxidases. Aldehyde dehydrogenases are a group of enzymes that catalyse the oxidation of aldehydes to carboxylic acids. Alcohol dehydrogenases are a group of enzymes that catalyse the oxidation of alcohols to the corresponding aldehyde. Both enzymes use NAD^+ as cofactor and are localised in the cytosol[231], whereas no cofactor is required for oxidations catalysed by aldehyde oxidases.

1.2.1.3 Reductions

Although most P450-catalysed reactions are oxidations, reductive reactions such as reductions of nitro and azo compounds leading to amino derivatives can also be catalysed by P450. They are primarily observed under anaerobic conditions unlike the P450-catlaysed oxidations. These reactions can also be catalysed by NADPH-cytochrome P450 reductase. For example, a nitro reduction metabolite was formed from the nonsteroidal antiandrogen flutamide in liver microsomal incubations by NADPH-cytochrome P450 reductase under aerobic, and to a greater level under anaerobic conditions.[232]

1.2.1.4 Hydrolysis

Various esterases can hydrolyse substrates such as esters, amides, and thioesters.[233] Esters may be hydrolysed by plasma esterases (non-specific acetylcholinesterases, pseudocholinesterases, and other esterases) or liver esterases (specific esterases). The hydrolysis of amides may be slowly catalysed by esterases in the plasma, however, they are mainly hydrolysed by amidases in the liver.[234] A notable representative of esterases are carboxylesterases (CES), which are located both in the endoplasmic reticulum (ER) and cytosol of various tissues including the liver, small intestine, lungs, and kidneys.

Carboxylesterases are a mammalian multigene family that based on homology of amino acid sequences can be classified into four families: CES1, CES2, CES3, and CES4.[235]

Epoxides may be hydrated by epoxide hydrolase, which converts the epoxide to two hydroxyl group under addition of water. This hydration reaction is a special form of the hydrolysis, where water is added without cleaving the compound.[234]

1.2.2. Phase II metabolism

1.2.2.1 Glucuronidation

The uridine 5'-diphospho-glucuronosyltransferase (UGT) superfamily catalyses the conjugation of glucuronic acid to a nucleophilic substrate and are involved in the glucuronidation of bilirubin, steroids, and xenobiotics. The mammalian UGT gene superfamily can be divided into four families, namely UGT1, UGT2, UGT3, and UGT8.[236] The tissue distribution of UGTs is similar to CYPs as they are predominantly expressed in the liver with some isoforms also present at high levels in the kidneys and intestines contributing to significant extrahepatic glucuronidation.[237] They are anchored in the membrane of the ER with the active site of the enzyme being localised lumenally.[238] Therefore, latency of activity occurs in preparations of the ER (i.e. microsomes), where the closed microsomal membranes pose a barrier for diffusion of substrates, cofactors, and products to the active side of UGTs.[239] *In vitro* UGT is activatable, for example by the antimicrobial peptide alamethicin isolated from the fungus *Trichoderma viride*. It inserts into the membranes forming pores[240] that remove the latency[241] and allow free diffusion of substrate, cofactor, and products without affecting intrinsic membrane structures. Endogenous β-glucuronidases are located inside the ER lumen and their presence can lead to underestimation of glucuronide formation.[242] *In vivo* glucuronides are eliminated by the kidneys into urine and bile into the small intestine, where they can be excreted by faeces or undergo enterohepatic recirculation by β-glucuronidase-catalysed hydrolysis and subsequently deconjugated substrates can be reabsorbed in the intestine.[243] The intestinal β-glucuronidase was shown to be produced by bacteria rather than native epithelial cells.[244] Firstly described in 1952, saccharolactone is frequently used as a β-glucuronidase inhibitor within *in vitro* assays.[242,245] However, it has been shown that saccharolactone may not or not significantly alter the rate of glucuronidation and even moderately inhibit it at a concentration of 20 mM.[244]

1.2.2.2   Sulfation

Sulfotransferases (SULTs) are cytosolic enzymes that catalyse the transfer of a sulfo group from 3'-phospho-adenosyl-5'-phosphosulfate (PAPS) to substrates that contain hydroxy or amine groups subsequently forming sulfate or sulfamate conjugates. They are expressed in human liver, intestines, lungs, and kidneys[246] and further studies in mice showed their expression in other tissues such as the brain, placenta, and gonads.[247] At least 47 mammalian SULT isoforms have been identified and classified into six families – SULT1, SULT2, SULT3, SULT4, SULT5, and SULT6 - based on their amino acid sequence similarities.[248] SULT1 and SULT2 are primarily involved in xenobiotic metabolism.[249] Generally, sulfations tend be high affinity and low capacity reactions due to the limited availability of PAPS[250], whereas UGTs are low affinity and high capacity enzymes. For example, in humans paracetamol sulfate reached a plateau after administration of 20 mM paracetamol. This saturation was compensated by an increased excretion of paracetamol glucuronide in patients administered up to 66 mM of paracetamol.[251] Moreover, SULTs can exhibit partial or complete substrate inhibition at high substrate concentrations.[252] Both sulfation and glucuronidation form more hydrophilic conjugates of the parent drug and/or metabolites, which facilitates their elimination by the kidneys into urine and by bile into the gastrointestinal tract, where sulfate conjugates can be excreted into faeces or undergo enterohepatic recirculation via hydrolysis by sulfatase present in the gut microflora.[253]

1.2.2.3   Methylation

During methylation, methyltransferases catalyse the transfer of a methyl group from the cofactor *S*-adenosylmethionine to substrates with *O*-, *N*-, or *S*-heteroatoms. Methylations mainly occur in endogenous metabolism and it is a common but minor biotransformation pathway for drugs. Most methyltransferase catalyse specific endogenous substrate groups. For example, catechol *O*-methyltransferases methylate catechols and *S*-methyltransferases methylate thiols. Drugs can be methylated by non-specific methyltransferases found only in the lung.[234]

1.2.2.4   Acetylation

N-Acetyltransferases (NATs) catalyse the transfer of acetyl groups from the cofactor acetyl coenzyme A to aryl amines and are localised in the cytosol of liver, spleen, lung, kidney, and intestinal cells.[254,255] In 1995 a consensus nomenclature was established, which

has been kept updated since.[256–259] Two NAT enzymes have been documented for humans and rabbits, NAT1 and NAT2, while only NAT2 was reported in monkeys. Hamsters express two enzymes as well, designated as Nat1 and Nat2, whereas mice express three enzymes (Nat1, Nat2, and Nat3). Rats were shown to express Nat2 and Nat3.[259] In humans, rabbits, mice, rats, and hamsters genes for *N*-acetylation have been described as polymorphic resulting in different levels of expression amongst individuals.[260]

1.2.3.   Factors affecting drug metabolism

A huge number of variables are known to influence drug metabolism and enzyme activities. Internal factors such as species, genetic polymorphisms, strain, sex, age, hormonal status, and physio-pathological conditions (e.g. pregnancy, diseases) and external factors such as diet, drug administration, and the environment may affect drug metabolism.[261] For example, age dependent differences between the cattle breeds Charolaise, Piedmontese, and Blonde d'Aquitaine in females and males have been described showing that breed, age, and gender can affect expression of DMEs.[262,263] P450, UGT, and carboxylesterase activities showed an age-dependent increase in female horses, whereas glutathione *S*-transferase activity declined with age.[264]

Several species are relevant in veterinary research (**Table 1.4**).[265] Therefore, species-specific differences in the expression of DMEs and metabolism of drugs are of particular interest. Differences in pharmacodynamics and -kinetics between species are numerous, and this can be due to species defects in certain metabolic reactions (e.g. glucuronidation in cats[266], *N*-acetylation in dogs and guinea pigs[267]) and/or species differences to the relative extent of various reactions.[265,268] Even among phylogenetic subfamilies, small differences in the gene sequence can alter catalytic specificities and activities.[269] By using substrates that are specific for one human isoenzyme, species-differences in catalytic activities were reported.[270–272] While investigating different species with this substrate approach, it has to be considered that the substrate might be catalysed by a different isoenzyme (change in selectivity) or by several (loss of selectivity).[273] Species differences are so profound that prediction of results is not possible[272] and drug metabolism should be studied in the species of interest. However, a number of factors as mentioned above, such as genetic polymorphisms, sex, diet, age and pathophysiological conditions (e.g. pregnancy, diseases), may alter the regulation of DMEs within a species and contribute to interspecies differences. Also, results from comparison of species will be limited to the strains studied.[274]

Table 1.4 Taxonomic classification of some mammalian species of interest in veterinary research

Cohort	Order	Family	Representative species
Glires	Rodentia	Muridae	Rats
			Mice
	Lagomorpha	Leporidae	Rabbits
Ferungulata	Carnivora	Canidae	Dogs
		Felidae	Cats
	Artiodactyla	Bovidae	Cattle
			Goat
			Sheep
		Suidae	Pig
	Perissodactyla	Equidiae	Horse
			Donkey

1.3. Methods for studying drug metabolism

Drug metabolism studies play a pivotal role in drug discovery[275,276], are a prerequisite for developing clinical and forensic screening procedures[277–279] and surveillance schemes in sports and food producing animals[279–282]. Different methods are available to study the metabolic fate of a drug and the choice of system depends on the research question which a study aims to answer and investigate. In addition, ethical and financial factors as well as availability of subjects and tissues play a decisive role in the choice of method, with each system possessing strengths and limitations, which ultimately govern their applicability. This subchapter describes the most commonly employed methods used in drug metabolism studies that precede drug surveillance outlining their relative advantages and disadvantages and their potential applications.

1.3.1 *In vivo* metabolism

In vivo studies are the gold standard to elucidate the metabolism of a drug and post drug administration to the species under investigation, authentic biological samples such as urine, blood, faeces, and/or hair may be collected and analysed. Depending on the study design, drugs can be administered per os, intravenous, intraarterial, intraperitoneal, intramuscular, or via subcutaneous injection, inhalation, topical or ocular as single or multiple doses in toxicological relevant concentrations.[283] Administration of radiolabelled drug analogues with ^{14}C or ^{3}H in a single dose are common practice in pharmaceutical industry studies. Subsequent quantitative whole body autoradiography and ADME/mass balance studies provide a comprehensive picture of covalent binding of the drug to macromolecules, distribution, rates and routes of excretion.[284] However, radiolabelled materials are often not commercially available and preparation thereof is technically difficult, time-consuming, and expensive.[285] Moreover, due to the radioactivity these studies are accompanied with regulatory issues and ethical concerns and additional precautions have to be taken when handling acquired samples.

Blood and urine are the typical biological matrices samples and analysed during drug surveillance procedures. Drugs can be detected in blood just after intake prior to metabolism and filtration and it is the sample of choice for quantification purposes. However, urine is often the preferred sample of choice for screening as drugs are detectable longer than in blood and urine contains more metabolites, which provide further evidence of drug use. Hair samples can provide information on presence of drugs over an even longer period of time

compared to urine and long-term detection of testosterone in horse hair samples highlight the use of hair as complimentary matrix to urine and blood.[286] Interestingly, higher concentrations of β-agonists have been observed in black than in white hair of heifers.[287,288]

Before GC-MS analysis, enzymatic or acid hydrolysis of urine samples is necessary prior to extraction to hydrolyse phase II metabolites.[289] Different deconjugation protocols exist and have been extensively studied especially for steroids.[290] For enzymatic hydrolysis, urine samples are incubated with β-glucuronidase from *Escherichia coli* or *Helix pomatia*, or β-glucuronidase/arylsulfatase from *Helix pomatia*. Enzymatic hydrolysis with arylsulfatase may not sufficiently cleave sulfate conjugates as in the case of 19-nortestosterone-17β-sulfate, which requires further cleavage by chemical hydrolysis using sulfuric acid in ethyl acetate and methanol.[291] Enzymatic hydrolysis is a gentle but time-consuming method and preferred in metabolism studies, whereas acid hydrolysis is more rapid and preferred for systematic toxicological analysis.[289] The possibility of artefact formation with both methods has to be considered to avoid misleading results.[292,293] Deconjugated phase II as well as phase I metabolites are derivatised to improve their gas chromatographic characteristics.[289] The hydrolysis leads to deconjugation of sulfate and glucuronide moiety resulting in a loss of information on phase II metabolites. Phase II metabolites are directly detectable with LC-MS for which urine samples are prepared without hydrolysis.[277] Hydrolysis of samples is also employed prior to LC-MS analysis where the method of choice is based on the detection of the deconjugated drug and/or metabolites.[294,295]

Metabolites, which are detectable for a longer duration, make more effective targets for drug testing. Excretion studies can help to establish such long-term metabolites and expand detection windows. For example, long-term metabolites for the AAS metandienone, namely 18-nor-17β-hydroxymethyl-17α-methylandrost-1,4,13-triene-3-one[296], methyltestosterone, namely 17β-methyl-5α-androstan-3α,17α-diol 3α-sulfate[297], methasterone, namely 18-nor-17β-hydroxymethyl-2α, 17α-dimethyl-androst-13-en-3α-ol-ξ-O-glucuronide[298], and oxandrolone, namely 17β-hydroxymethyl-17α-methyl-18-nor-2-oxa-5α-androsta-13-en-3-one and 17α-hydroxymethyl-17β-methyl-18-nor-2-oxa-5α-androsta-13-en-3-one, were identified by analysing post-administration human urine samples. Sulfate and glucuronide long-term metabolites show the importance of studying phase II metabolism and including them as targets in screening approaches.

Due to ethical reasons, laboratory animals commonly serve as replacement *in vivo* models for human metabolism studies. However, findings from such studies may not always

correlate to actual drug metabolism in humans due to species-related differences. Humanized mice are a promising *in vivo* model to overcome such issues whereby transgenic mice with overexpressed homozygous urokinase-type plasminogen activator (uPA$^{+/+}$) and severe combined immune deficiency (SID) are bred. The induced conditions of severe chronic liver disease by overexpression of uPA and immunodeficiency allow the transfer of human hepatocytes without rejection to this model.[299] In doping control research, metabolism of steroids in human liver uPA$^{+/+}$-SID mouse chimeras showed close resemblance to human *in vivo* or *in vitro* metabolism and detection methods for AAS were established based upon results.[300–305]

In the UK any research involving animals must comply with the Animals (Scientific Procedures) Act 1986.[306] Besides an establishment and personal licence, the work has to be approved by a project licence before experiments commence. However, *in vivo* studies can be hard to justify for emerging drugs of abuse when there is limited available information on the drugs' safety profile. Furthermore, for animal studies appropriate approved facilities as well as experienced personnel are needed. In addition, relatively large amounts of the drug may be needed, especially when studies are carried out in larger animals such as cattle or horses. This makes *in vivo* studies a time-consuming and expensive approach. Furthermore, *in vivo* studies cannot differentiate between hepatic, renal, pulmonary or intestinal biotransformation. In an effort to reduce, refine, and replace animal experiments, regulatory agencies such as the U.S. Food and Drug Administration encourage the investigation of drug metabolism and potential drug-drug interactions using *in vitro* approaches.[307]

1.3.2   *In vitro* methods for assessment of drug metabolism

In vitro strategies represent a rapid and cost-effective method to draw initial conclusions about the metabolic fate of a drug and potential target analytes in drug surveillance, particularly when *in vivo* studies are ethically and financially hard to justify for emerging drugs. These strategies can be used to help elucidate metabolite structures as well as identify targets for control using hyphenated mass spectrometry techniques. Furthermore, determination of drug metabolites' chromatographic retention times and mass spectrometric behaviour facilitates further method development. Although *in vitro* studies cannot fully replace *in vivo* studies, they can help to reduce and refine *in vivo* experiments. Additionally, the use of *in vitro* strategies can provide mechanistic insights into metabolic pathways, e.g. specify the enzyme(s) and/or tissue(s) involved in the reaction – this information cannot be gained by analysing typical samples such as urine and blood obtained from *in vivo* studies.[308]

Drug metabolism and toxicity are closely linked to the liver, hence, *in vitro* models are typically liver-based and *in vitro* experiments to characterise the metabolic fate of a drug are primarily performed using cellular systems, tissue fractions or recombinant isoenzymes. As a rule of thumb, the more complex *in vitro* systems have a lower throughput and higher cost.

1.3.2.1   Isolated perfused organs

The preservation of the full organ structure in isolated perfused organs makes it the most complete *in vitro* system. Isolation and perfusion techniques for organs and their applications have been described.[309] In experiments with isolated perfused liver, the perfusate, bile and liver tissue can be analysed.[309,310] Bile canaliculi are functional, which therefore makes it a good model for bile collection and analysis.[310,311] As it is a very costly, time-consuming low-throughput technique, it is not a viable option in control analysis considering the substantial number of emerging drugs of abuse, limited availability of organs, and extensive size of such organs in larger animals.

1.3.2.2   Organ slices

Precision-cut organ slices represent a multicellular three-dimensional (3-D) *in vitro* model that closely mimics the *in vivo* biomicroarchitecture of the tissue with all cells preserved in their natural arrangement. Following preparation of cores from tissues using a coring tool, precision slices are cut with a tissue slicer, e.g. Krumdieck, and cultured.[312,313]

Preparation and incubation procedures have been described for tissues from rats and humans.[314] Cell viability and corresponding enzyme activities decrease over time and when incubated intestinal and liver slices showed to be viable for 24 and 96 hours, respectively.[313] Due to the limited cell viability, the use of organ slices is restricted as they rapidly deteriorate upon culturing. It has been shown that only slices from livers classified as high quality can be cold- or cryopreserved[315], however, with an optimised cryopreservation procedure, cryopreserved and subsequently cultured slices retained 60 to 90 % biotransformation capacity of fresh livers.[316] Some issues of viability, e.g. cell degradation and accumulation of waste products, have been addressed with the incorporation of organ slices in microfluidic devices to continuously deliver nutrients and oxygen, and remove waste products.[317]

Organ slices have been used for various purposes in drug metabolism research. For example, liver slices in combination with intestinal slices adequately predicted the *in vivo* drug metabolism of three drugs in development.[318] Intestinal slices were shown to be a useful tool to asses drug metabolite formation by intestinal DME.[319,320] Moreover, rat organ slices were capable of predicting *in vivo* metabolic clearance of model substrates.[321] Cattle liver slices were used to assess the biotransformation and additionally, transcriptomic effects of testosterone[322] and/or dehydroepiandrosterone[322,323] using a yeast androgen screen, an assay where the human AR is recombinantly expressed in yeast to investigate AR ligands. A microfluidic approach using liver and intestinal slices was suggested to assess interorgan interactions in drug metabolism.[324]

1.3.2.3   Isolated primary cells

Hepatocytes account for over 60 % of all liver cells and 80 % of the liver volume[325] and are recognised as the cells within the liver where metabolism primarily occurs. Procedures for the isolation of primary hepatocytes from human[326], horse[327,328], cattle[329–331], goat[330], rat[332,333], and pig[334] liver tissue have been described inter alia. In general, hepatocytes can be isolated from fresh intact liver tissue by perfusion with a calcium-free buffer followed by a buffer containing collagenase. Following collagenase digestion the remaining suspension of single cells can be used fresh or cryopreserved followed by direct use in suspension[335], or plating in monolayer or sandwich culture[336]. After hepatocytes have been isolated, their viability is limited, and dedifferentiation accompanied by loss of functionality occur over time. Cryopreservation may be accompanied by a loss of cell viability, and in suspension cells are only viable for a very limited time (hours), whilst they can be used for a longer

period (days) when cultured.[337] For short-term studies, monolayer cultures are sufficient but to study various aspects of drug metabolism over a prolonged period, the use of the sandwich culture is the most convenient model.[338] Different culture techniques, such as coincubation of collagen with heparin[339], micropatterned coculture with fibroblasts[340], coculture with liver sinusoidal endothelial cells[341], and use of microfluidic devices[342], maintain cell functions for prolonged periods. Furthermore, various more sophisticated 3-D cell culture approaches, such as 3-D membrane reactors[338], spheroids consisting of hepatocytes, non-parenchymal cells, and extracellular matrix[343,344], and 3-D hepatic microtissues[345] have shown promising results. Human cell lines are more stable and their use overcomes the issue of limited lifetime associated with primary human hepatocytes, however, they express DMEs at very low levels or not at all.[346,347]

Freshly isolated hepatocytes closely mimic *in vivo* metabolism processes as they possess a complete set of DMEs and cofactors at physiological concentrations. Furthermore, the influence of membrane transport proteins such as the apical/canicular transporters P-glycoprotein and multidrug resistance-associated protein 2 (MRP2) as well as basolateral/sinusoidal transporters (MRP3 and MRP4) can be studied.[348] Therefore, they represent a valuable *in vitro* system to derive the clearance[349] and metabolic profiles, quantitatively[350] and qualitatively[318,351], that can closely reflect actual *in vivo* metabolism. For example, with primary hepatocytes as *in vitro* model the metabolism of AAS in cattle[352,353] and humans[354,355] was predicted. In addition, cattle primary hepatocytes were used in an multiparametric approach to not only determine the metabolism of AAS, but also to investigate their effect on DME expression and regulation as well as cytotoxicity.[356]

To conclude, cellular systems are inherently dynamic models in a constant state of change retaining liver and/or cell structures only for a limited time. Samples are generally taken from one individual and batches can highly vary due to the interindividual variability among the donors. Furthermore, variability can also derive from how tissues are processed and maintained. Therefore, morphological, biochemical and functional parameters have to be extensively characterised.

1.3.2.4 Tissue fractions

Although perfused livers, liver slices, and isolated primary hepatocytes are the closest *in vitro* models to actual *in vivo* metabolism and describe a very comprehensive picture, their preparation and use is difficult as the viability of these models is only given for a limited period. Consequently, only a small number of experiments can be performed with one animal liver sample in a short time. Similar to intact hepatocytes, tissue fractions contain a wide spectrum of metabolic phase I enzymes such as P450s and/or phase II enzymes including UGTs and SULTs (**Table 1.5**), but no longer within living cells. For this reason, cofactors must be added to the respective incubation mixtures to initiate required reactions and the donor substrates for conjugation reactions are UDPGA for glucuronidation, PAPS for sulfation and acetyl CoA for acetylation, and NADPH and magnesium chloride for NADPH-dependent metabolism. The two coenzymes NADPH-cytochrome P450 reductase and cytochrome b_5 as described in **Section 1.2.1.1** are present at physiological levels.

Tissue fractions can be isolated through homogenization of tissue to break-up cells followed by differential centrifugation. This centrifugation approach is based on size (µm) and density of the particles in the homogenate (g/mL), where larger and denser particles pellet at lower centrifugal forces than smaller and less dense particles. For example, nuclei have a size of 16-144 µm and a density of > 1.30 g/mL in a sucrose gradient. They sediment at low centrifugal forces between 500 and $1000 \times g_{max}$, while mitochondria have a size of 0.16-6.3 µm, a density of 1.17-1.21 g/mL in a sucrose gradient and typically sediment at higher centrifugal forces between 3000 and $15\,000 \times g_{max}$.[357] For *in vitro* drug metabolism studies, subfractionation procedures are normally based on the presence of different DMEs (**Table 1.5**).

Homogenization leads to the disruption of the cell surface membrane and release of cytosol and internal organelles, including nuclei, mitochondria, lysosomes, and peroxisomes in an intact form, while the sheets and tubules of the ER (both rough and smooth) are disrupted by homogenization and fragment into small closed vesicles called microsomes.[358] **Figure 1.4** shows the vesiculation of sheets and tubules from the ER to microsomes when tissue is homogenized.[359] Microsomal vesicles can vary in size, density and surface charge[360] and despite such heterogeneity can be recovered in a relatively pure and high yield.[357] The outside of the microsomal membrane corresponds to the cytoplasmic surface of the ER.[360]

Table 1.5 Selection of metabolic enzymes in liver subcellular fractions

Metabolic Enzymes	Microsomes	S9 fractions	Cytosol
Aldehyde oxidase		x	x
CES	x	x	x
CYP	x	x	
FMO	x	x	
Epoxide hydrolase	x (microsomal-bound)	x	x (soluble)
NAT		x	x
Methyltransferase	x	x	x
SULT		x	x
UGT	x	x	
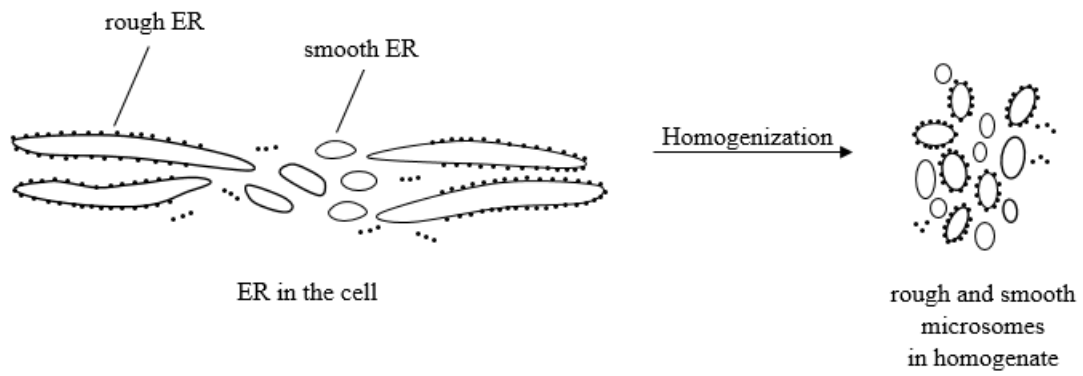
Figure 1.4 Fragmentation of the ER during homogenization

The supernatant that is obtained after homogenization and a single medium-speed centrifugation at $\geq 9000 \times$ g is denoted as the S9 fraction. 9000 x g is the centrifugal speed originally used for its preparation, however, a higher centrifugal speed can be employed in in an effort to obtain cleaner preparations (usually 12 000 to 15 000 $\times$ g). After centrifugation, the floating-lipid layer is removed with the remaining supernatant consisting of microsomal and cytosolic enzymes, whilst the pellet consisting of cells, mitochondria, and nuclei is discarded. The S9 fraction contains a complete set of both phase I enzymes, such as P450 and FMO, and phase II enzymes, such as SULTs and UGTs. These characteristics make it a good *in vitro* system to investigate phase I as well as phase II metabolic profiles. More types of enzymes are present in S9 fractions compared to microsomes and the cytosol, however, metabolites might be produced at lower concentrations with S9 fractions than with microsomes or cytosol due to a lower content of specific enzymes, e.g. microsomes typically have a higher P450 content and cytosol a higher SULT content than S9 fractions.

Microsomes can subsequently be attained as sediment after a second centrifugal step at $\geq 100\ 000 \times$ g. Microsomal preparations are a mixture of membranous elements and ribosomes or polysomes present either as separated entities or complexes derived from the ER[361] and contain P450s, FMOs, and UGTs (**Table 1.5**). These enzymes are enriched in microsomes and certain metabolites may therefore be generated at higher concentrations with microsomes compared to S9 fractions.

The supernatant of the 100 000 $\times$ g centrifugation step represents the cytosol containing soluble metabolic phase II enzymes at higher concentrations than in the S9 fraction, but they do not contain UGTs. Whilst *in vitro* studies do not commonly employ incubations with the cytosol, it can however be a useful tool when studying pathways that involve *N*-acetylation and/or sulfation.

Normally, tissue fractions are pooled from several donors to avoid interindividual variability and obtain a representative sample of a population. By selecting the pool of tissues, preparations can be tailored to study specific metabolic differences, for example, relating to gender (male compared to female pool), age (e.g. young versus middle-aged versus elderly pool) or species. Typically, characterisation of tissue fractions includes quantification of total P450 and cytochrome b_5 content, determination of NADPH-cytochrome P450 reductase activity, and quantitation of metabolic activities with specific probe substrates. Relative levels of CYP isoenzymes can be quantified by western blot analysis.[362] Several experimental variables including organic solvent[363], buffer type, pH,

ionic strength, cofactors and supplements, substrate concentration, protein concentration[364], incubation time[365], and sample preparation affect outcomes (personal observations) and are chosen depending on the research question.

For equine doping control applications, *in vitro* incubations can be used instead of *in vivo* post-administration samples due to a revision of the ILAC-G7 guidelines in 2009.[116] Scarth et al. compared the *in vitro* phase I metabolites generated by horse liver microsomes or S9 fractions of eight banned substances (acepromazine, azaperone, celecoxib, fentanyl, fluphenazine, tripelennamine, mepivacaine, and methylphenidate) to deconjugated post-administration samples from previous *in vivo* studies (acepromazine, azaperone, celecoxib, fentanyl, and fluphenazine), previous case reports (tripelennamine and mepivacaine), and the available literature (methylphenidate). The study concluded that at least two major *in vivo* metabolites were found to be generated *in vitro* and recommended the use of *in vitro* technologies in equine drug surveillance.[366] Furthermore, the *in vitro* phase I metabolism of stanozolol was studied using horse liver microsomes as well as liver and lung S9 fractions.[294] In addition, eight designer steroids were incubated with liver microsomes or S9 fractions from the horse. Following LC-HR-MS, LC-MS/MS, and GC-MS analysis, phase I metabolites were found to be formed in both fractions in similar abundances, however, a number of metabolites could only be detected in samples derived from S9 incubations and not from microsomal ones. Therefore, the use of both microsomal and S9 liver fractions was recommended.[295] Equine liver S9 fractions have also been described as a useful tool in producing phase II metabolites of drugs and facilitating the development of LC-MS assays based on intact metabolites omitting the hydrolysis step in sample preparation.[367] More recently, homogenized horse liver has been successfully employed as an alternative to microsomes and S9 fractions to study the *in vitro* phase I metabolism of five anabolic agents by GC-MS, the phase II metabolism of 17β-estradiol, morphine, and boldenone undecylenate as well as the phase I metabolism of tamoxifen and toremifene by LC-HR-MS.[368–370]

Tissue fractions have also been used in investigating the metabolism of steroids and steroids in cattle. Using cattle liver S9 the *in vitro* formation of prednisolone from endogenous levels of cortisol was demonstrated and based on the mean of prednisolone in 100 bovine urine samples a threshold level of 5 µg/L was recommended.[371] Cattle liver S9 were also used to bioactivate dehydroepiandrosterone with subsequent use of an androgen-activity yeast bioassay to screen for hormonal activity in resulting extracts.[372] Moreover, putative urinary markers for 17β-boldenone and boldione treatment were proposed based on

the results of *in vitro* incubations of compounds with bovine liver and kidney homogenate, S9 fractions, and microsomes.[373]

As described in **Section 1.1.2**, liver microsomes and S9 fractions are routinely used in human doping control for *in vitro* experiments to study metabolism and establish detection methodologies by determining retention times and studying mass spectrometric fragmentation patterns.

For reaction phenotyping, chemicals that selectively inhibit CYP isoenzymes can be added to the incubation mixture to identify the enzymes that are mainly responsible for metabolising the drug by comparing to incubations without the inhibitor added. A reduced production of metabolite following incubation with a particular inhibitor suggests that the inhibited isoform is involved in the metabolism. Various inhibitors that selectively inhibit specific human, rat, monkey, and dog CYP isoenzymes have been described.[374] A lot is known about the specificity of chemical inhibitors toward a range of different human P450s[223] and first steps have been taken to identify similar enzymes in other species using this chemical inhibitor approach as tested for stanozolol in equine. This study showed that ketoconazole, primarily a CYP3A4 inhibitor, and quercetin, primarily a CYP2C8 inhibitor, inhibited the metabolism of the major metabolites 16α- and 16β-hydroxy-stanozolol.[294] However, this does not mean that a homologous isoenzyme exists and/or is involved nor that an analogous isoenzyme does not exist and/or is involved in the horse. Also, at this point it is not possible to assess the selectivity and sensitivity of inhibitors towards certain isoforms in these species.

Tissue fractions are easy to prepare from fresh or frozen tissues and straightforward to use providing a level of convenience for systems intended for routine use. They can be conveniently stored at - 80 °C for years, freeze/thaw cycles do not significantly lead to a loss in enzyme activities[375], and they are cheaper to use compared to other *in vitro* models. However, tissue fractions are not a complete system and are therefore not fully representative of the *in vivo* situation. Whilst the absence of proteins and/or cofactors means certain metabolic reactions may/or may not be observed and their use in the extrapolation of quantitative measurements to replicate *in vivo* biotransformation may be limited, tissue fractions are a suitable *in vitro* model to rapidly predict phase I and II metabolism of emerging anabolic drugs in sports and food producing animals.

1.3.2.5   Heterologously expressed drug metabolizing enzymes

In addition to the chemical inhibitor approach, the use of recombinant metabolic enzymes provides an excellent way to identify the isoenzymes (CYPs, UGTs) involved in metabolic reactions (reaction phenotyping) and to study the kinetic profiles of the metabolites formed by specific isoenzymes in isolation. As only a single isoenzyme is represented, the metabolic contribution of other enzymes is not shown, and therefore, this *in vitro* system is often used in addition to others after the apparent metabolic pathway has been determined. Heterologously expressed drug metabolizing enzymes can be produced from complementary DNA (cDNA) cloning using a number of approaches. Commonly used expression systems include bacterial (*Escherichia coli*), fungal (*Saccharomyces cerevisiae*), insect cell expression (baculovirus-driven) and mammalian expression (e.g. V79 cells)[376] and Yun et al. has reviewed each system's advantages and disadvantages[377]: The use of bacterial expression is a cheap, easy and fast approach but cannot replicate the same post-translational modifications, which can affect protein folding and functioning. Yeast offers similar advantages but with a closer resemblance to mammalian cells. In baculovirus expression, a polyhedrin promoter drives expression to high yields and it is easy to scale up. However, it is time and labour intensive. Mammalian expression offers the best representation of wild-type protein, however, it is an expensive approach. NADPH-cytochrome P450 reductase and cytochrome b_5 are present at endogenous levels in mammalian and yeast host cells, whereas, they are not present in bacteria and baculovirus. They can be coexpressed with the CYP enzyme. The isoenzymes are not expressed to the same level as in normal cells and as a result have to be normalised. In general, all systems require substantial technical expertise and time to develop and use.

Despite advances in molecular biology and genome sequencing, the myriad of equine[378–382], bovine[383], and pig[384] isoenzymes is only partly characterised yet and isoenzymes are not commercially available. Establishing which isoenzymes are responsible and/or dominant for metabolite formation is therefore difficult. As described in the previous subchapter, using chemical enzyme inhibitors that are known to be selective for particular isoforms in other species within tissue fraction incubations represents an alternative approach.

1.3.3 Alternative approaches in drug metabolism studies

Typically, reference material of metabolites of emerging anabolic drugs are not commercially available. For this reason, electrochemistry has been used for simulation of drug metabolism and synthesis of metabolites in doping research.[385,386] As most biotransformations are redox reactions, they can be mimicked using electrochemistry, most commonly coupled to ESI-MS or LC-ESI-MS, to detect and identify produced metabolites.[387] Moreover, electrochemistry can be used to synthesise metabolites at a preparative scale that is sufficient for subsequent nuclear magnetic resonance (NMR) analysis and further use.[388]

Microorganisms can be used as microbial models of mammalian biotransformation.[389] For example, the fungus *Cunninghamella elegans* (*C. elegans*) has a broad spectrum of DMEs[390] and therefore serves as a tool to produce metabolites similar to those observed in mammals.[391] *C. elegans* has been used to produce relevant human[392,393] as well as equine[392,394,395] phase I and II drug metabolites for doping research purposes with yields of metabolites high enough for NMR analysis and subsequent use as reference material.[396,397]

Various computational models that can predict potential metabolites are available in the form of web services, free, or commercial softwares, which have been comprehensively described by Kirchmair et al.[398] For example, METEOR is a commercially available software that predicts phase I and II metabolites of xenobiotics based on knowledge and rules. However, it tends to produce false-positives by over predicting metabolites in comparison with *in vivo* observed metabolites.[399,400] Previous studies have observed that results can vary significantly across computational models.[400] For example, predictions from MetaSite, which is another commercial software that predicts the probability of metabolic sites to undergo metabolic phase I modifications, were found to be more precise albeit less sensitive when compared to results with METEOR.

1.4.   Objectives

Forensic testing of illicit drug use in sports and food producing animals is facing an increasing challenge to screen for novel anabolic drugs emerging from human drug development. One class of anabolic agents are SARMs that have received growing attention relating to their use for potential therapeutic applications. Compared to current therapies with testosterone or synthetic AAS, SARM compounds exhibit a favourable pharmacological profile demonstrating full anabolic activities in target tissues such as muscle and bone but reduced androgenic activities in other tissues such as prostate, heart, and liver with the underlying molecular mechanisms for dissociation of the anabolic and androgenic activities remaining unknown. Although several SARM compounds have been the subject of various human clinical trials, they still lack pharmaceutical approval. Daily oral delivery makes administration of SARMs easy whilst extensive metabolism and/or quick excretion from the body make their detection challenging. Such ease of use and availability over the Internet, advantageous effects, and short detection windows increase their potential for abuse and demonstrate the need to develop more advanced control screening methods for monitoring of emerging SARM compound use. Knowledge of SARM metabolism, particularly where urine is the test sample matrix, is a crucial prerequisite in order to establish appropriate target analytes as the parent compound might not be present or detectable, and compound metabolites have to be monitored instead. Using compound metabolites as additional target analytes besides the intact parent compound in screening methods may be beneficial for several additional reasons. Detection of a metabolite can corroborate a positive finding confirming SARM exposure and exclude potential contamination of a sample. Furthermore, metabolites have been shown to have extended detection windows (**Sections 1.1.2** and **1.3.1**) making it possible to detect drugs for a longer time after initial administration. Therefore, the overall aim of the thesis was to investigate the *in vitro* and *in vivo* metabolism of key SARM compounds to advance forensic testing based on drug metabolite profiling and to provide a better understanding of their physiological effects. *In vivo* drug administration studies can help to elucidate metabolic pathways, establish excretion time profiles of SARM compounds, and investigate the drug response, whereas *in vitro* tools can be used as alternative approach to produce SARM metabolites supporting efforts to reduce, replace, and refine animal experimentation.

Given the large number of SARM compounds emerging from drug development and the need to establish analytical targets, monitoring laboratories require a workflow for

metabolite generation and identification in relevant species (e.g. sports and food producing animals) that is suitable for even higher throughput than is presently available. Whilst, on the one hand larger scale *in vivo* studies are too time- and resource-consuming, on the other hand *in vitro* systems for metabolite generation such as liver microsomes and S9 fractions are not commonly commercially available for sports and food producing animals and the production thereof is tedious. To address this issue, work in **Chapter 2** aimed to assess the potential use of liver homogenates as an alternative *in vitro* approach to rapidly produce metabolites in place of S9 fractions and microsomes which can be adopted by testing laboratories to enable quicker incorporation of drug metabolites as target analytes into existing screening methods. For this purpose, several fractions including crude homogenates, homogenates, S9 fractions, and microsomes isolated from livers of cattle (which was chosen as representative and relevant species) were incubated with aryl-propionamide SARMs (S-1, andarine, and ostarine) and analysed by UHPLC-quadrupole time of flight (QTOF) MS to compare the formation of phase I and II metabolites by differently prepared fractions.

Generated drug metabolite profiles are often distinct to individual species (**Section 1.2.3**), adding to the complexity of detecting SARM abuse in various relevant species such as sports animals (i.e. horses) and food producing animals (i.e. cattle, pigs). Consequently, the objective of **Chapter 3** of this thesis was therefore to compare and identify the *in vitro* generated metabolites of SARM compounds ostarine, LGD-4033, and RAD140 in a variety of relevant species (horse, cattle, pig, and rat) in order to provide insights into shared and species-specific mammalian metabolism pathways. For this purpose, species-specific liver microsomes (alone or in combination with S9 fractions) were used for the generation of phase I and II metabolites of SARM compounds respectively, and metabolite analysis performed using UHPLC-ion mobility (IM)-QTOF MS. Moreover, generated metabolites from incubations with rat liver fractions were compared to rat urinary metabolites following *in vivo* administration in an attempt to characterise the direct relationship between findings from *in vitro* and *in vivo* drug metabolism experiments. This work aimed to provide a panel of SARM metabolites that can be subsequently included by laboratories for species-specific screening improving upon existing methods. To advance this initial investigation on interspecies differences in SARM compound metabolism further, **Chapter 4** aimed to identify the CYP isoenzyme(s) responsible for catalysing the formation of ostarine and LGD-4033 phase I metabolites in each species. This was achieved by using a reaction phenotyping approach based on addition of selective CYP inhibitors to incubations of the

SARM compounds with species-specific liver microsomes and necessitated the establishment of a MRM method for UHPLC-MS/MS analysis of ostarine and LGD-4033 phase I metabolites. These findings seek to examine whether there is potential for drug-drug interactions to occur, i.e. when SARM compounds are taken together with other drugs that may alter the metabolite profiles and mask SARM administration.

Conventional *in vitro* drug metabolism studies primarily focus on the use of liver-based strategies, and **Chapter 5** sought to expand on this approach by additionally examining equine lung, kidney, and small intestinal fractions besides liver to investigate if and to what extent metabolites of ostarine, LGD-4033, and RAD140 can be formed by other tissues. Microsomes, alone and in combination with S9 fractions, were used to generate phase I and II metabolites of SARM compounds, with resulting incubational samples from various equine tissues including liver, lung, kidney and small intestine analysed by UHPLC-HR-MS. The findings from these investigations provide a clearer understanding of involved tissues in SARM compound metabolite formation aiming to closer mimic actual *in vivo* metabolism and inform the monitoring of SARMs in specific tissues from horses.

Illicit administration of SARM compounds is not only considered a threat to the integrity of sports and animal products, but also poses a potential health risk as their mechanisms of actions have not been fully elucidated yet and unlicensed drugs are not monitored for drug safety concerns (pharmacovigilance). As SARMs are typically taken orally, an assessment of their effects on the liver as a key metabolic tissue is needed, and **Chapter 6** investigated the hepatic response at the functional protein level following oral administration of the SARM compounds ostarine, LGD-4033, and RAD140 in an *in vivo* rat model. Additionally, a subcellular proteomics approach (**Chapter 7**) was applied to enrich proteins and gain further insights into liver-specific proteomic signatures in response to SARM compound administration. These analyses were based on comparative proteomics using two-dimensional difference gel electrophoresis (2-D DIGE) for differential protein spot detection and subsequent matrix-assisted laser desorption/ionization-time of flight (MALDI-TOF) analysis for protein identification. This work sought to provide an improved understanding of the biological and molecular effects following SARM compound administrations.

The principle aims of this thesis can be summarised as follows:

- To investigate the use of bovine liver homogenates as compared to microsomes and S9 fractions for the rapid generation of metabolites of emerging aryl-propionamide SARM compounds (i.e. S-1, andarine, and ostarine) for subsequent LC-MS characterisation (**Chapter 2**)

- To establish species-specific *in vitro* metabolite profiles of SARM compounds (ostarine, LGD-4033, and RAD140) by using bovine, equine, porcine, and murine liver microsomal and S9 fractions, and to characterise the correlation between *in vitro* and *in vivo* generated metabolites by analysis through UHPLC-IM-QTOF MS (**Chapter 3**)

- To develop a targeted MRM UHPLC-MS/MS method for phase I metabolites of SARM compounds ostarine and LGD-4033, and subsequently characterise the CYP isoenzymes responsible for the formation of these phase I metabolites in cattle, horse, pig, and rat (**Chapter 4**)

- To compare *in vitro* generated metabolites of SARM compounds (ostarine, LGD-4033, and RAD140) by microsomal and S9 fractions from various equine tissues based on UHPLC-HR-QTOF MS analysis (**Chapter 5**)

- To profile the differential liver protein responses following SARM compound (ostarine, LGD-4033, and RAD140) administration using a proteomics approach (**Chapter 6**)

- To investigate the hepatic responses after SARM compound (ostarine, LGD-4033, and RAD140) administration using subcellular proteomic profiling (**Chapter 7**)

Chapter 2: Rapid *in vitro* Metabolite Generation of Emerging Anabolic Drugs for LC-MS Characterisation

2.1 Introduction

In recent years it has become evident that drugs from the pharmaceutical industry developed towards treatment of diseases or conditions have potential for abuse in animal husbandry and sports. Emerging drugs prone to abuse due to performance-enhancing effects include peroxisome proliferator-activated receptor (PPAR) δ agonists such as GW501516[401,402], calstabin-ryanodine receptor complex stabilizers such as S-107 and JTV-519[403], and selective androgen receptor modulators (SARMs)[54]. SARMs are particularly attractive alternatives to conventional anabolic androgenic steroids due to their anabolic effects, reduced androgenic properties, and favourable pharmacokinetics.[11] Whilst a range of issues are associated with the use of these emerging anabolic drugs and as such regulatory approval for use has not yet being gained, they are freely marketed and readily available for purchase, e.g. over the Internet.[126] Moreover, instances of SARM abuse for muscle gain and performance enhancement have been reported in both human athletes as well as sport animals[130–133], whilst such compounds may potentially also be illegally administered for economic gain to cattle to promote muscle growth posing a threat to animal welfare and consumers of food products.

Agents and methods of doping are constantly evolving and expanding, and therefore target analytes of interest and associated analytical methodologies are regularly updated to ensure ongoing effective detection.[404,405] In the period since introduction, liquid chromatography-mass spectrometry (LC-MS)-based approaches have largely replaced traditional gas chromatography-mass spectrometry (GC-MS) as the primary technique for monitoring a wide array of substances.[406] While targeted methods using multiple reaction monitoring (MRM) capabilities result in high sensitivity, they can only cover a limited range of compounds.[153,407] Furthermore, designer drugs whilst still bearing a close structural homology to known compounds can be devised to evade detection by such techniques. Therefore, MRM is commonly combined with less sensitive precursor ion scanning utilising diagnostic product ions to detect related unknown compounds.[144–146] On the other hand, non-targeted approaches such as LC-high resolution (HR)-MS provide for adequate sensitivity and enable retrospective data mining[152], but several factors still complicate endeavours to detect emerging drugs of abuse by existing methods. For novel compounds the structures are sometimes not fully disclosed and analytical reference standards may not be available. If blood or hair is used for testing, monitoring the unchanged compound may be sufficient to detect abuse, but if excreted matrices such as urine are used for analysis

additional knowledge on drug metabolism is necessary to establish the appropriate target analytes. This can be accomplished through *in vivo* drug metabolism studies that involve administration of drugs to experimental laboratory animals or to the particular species of interest. For investigational drugs that often lack toxicological profile data, *in vivo* studies may be ethically hard to justify. Furthermore, *in vivo* studies are time-consuming, laborious, expensive, and require extensive resources including animal facilities and qualified personnel. Alternatively, *in vitro* approaches can serve the purpose of initially producing candidate drug metabolites which can subsequently be identified as target analytes and incorporated into existing methods.[408] Simple, rapid, and cost-effective *in vitro* strategies that can promptly respond to analytical challenges presented by emerging illegal drugs of abuse are therefore required to ensure effective control and monitoring of use.

S9 fractions and microsomes are established *in vitro* tools used to produce and subsequently identify drug metabolites in drug discovery and doping control.[184,362,366] The preparation of liver homogenates by homogenisation of liver in suspension buffer with a Potter-Elvehjem tissue grinder was first described in 1936[409], with later studies employing ultracentrifugation of homogenates produced using this technique to facilitate the study of microsomes and S9 fractions.[410] S9 fractions are the post-mitochondrial supernatant obtained from homogenised tissue post centrifugation ($\geq$ 9000 x g) containing phase I (i.e. CYPs and FMOs) and phase II (i.e. UGTs and SULTs) enzymes. Through subsequent centrifugation of the S9 fraction at high-speed, microsomes as the fragmented membranous artefacts of the endoplasmic reticulum containing phase I and UGT enzymes can be sedimented. SULTs remain in the subsequent supernatant (cytosol) and sulfations cannot be observed using microsomes. Therefore, sulfations and glucuronidations may only be simultaneously observed using S9 fractions or homogenates. Such liver tissue preparations and fractions are commonly available for laboratory species and humans because of their high demand for research and development purposes, however, for sports animals and livestock species these materials are not always readily available and only expensive customised productions may be offered limiting their use in routine control labs. Whilst several drug metabolism studies using liver homogenates have been reported over the years[373,411–413], homogenates as an *in vitro* system are not widely used and have not been truly established besides/over microsomes and S9 fractions. More recently, homogenised livers have been used to identify phase I and II metabolites for drugs of abuse in place of liver microsomes in equine sports testing.[368–370]

The field of drug monitoring and control is an arms race, which demands a versatile approach to rapidly identify metabolites and target analytes for previously uncharacterised and constantly emerging anabolic compounds in sports and food producing animals. While conventional *in vitro* methods such as liver S9 fractions and microsomes have been proven effective and are available for humans and laboratory species, they are not readily available for sports or food producing animals. The production thereof is tedious, time-consuming and specialized equipment is needed, thus preventing many laboratories from establishing appropriate target analytes for metabolite-based screening by LC-MS. The aim of the present work was therefore to assess the potential for use of bovine liver homogenates as an alternative simple, rapid, and cost-effective *in vitro* approach to rapidly produce metabolites in place of S9 fractions and microsomes. Disadvantages of liver homogenates are the disruption of the cellular integrity in contrast to isolated primary cells and potential lower enzymatic activities in comparison to microsomes and S9 fractions due to the lack of (crude homogenates) or minimal (homogenates) enrichment. Cattle were chosen as a representative and relevant group of major food-producing animals commonly exposed to anabolic drugs and requiring residue control monitoring. The use of liver homogenates could in future be used to rapidly generate metabolites for optimisation of screening methods. Furthermore, these generated metabolites could be used as potential acceptable reference material enforcing National Residue Control Programmes. A variety of bovine liver fractions (liver crude homogenates, homogenates obtained from low-speed centrifugation, S9 fractions from mid-speed centrifugation, and microsomes isolated via high-speed centrifugation) were produced as outlined in **Figure 2.1**, and characterised and compared in terms of their protein/P450/cytochrome b_5 content and NADPH-cytochrome P450 reductase/ 7-ethoxycumerin *O*-deethylation activity. Prepared fractions were then used to produce phase I (microsomes, S9 fractions, crude homogenates, homogenates) and II (S9 fractions, crude homogenates, homogenates) metabolites of the SARM compounds ostarine, andarine and S-1 that were selected as model compounds and samples were analysed by UHPLC-QTOF MS. The aryl-propionamide SARMs ostarine, andarine, and S-1 were chosen for this study based upon their availability as analytical standards and reported abuse in human and animal sports. The formation of metabolites was compared between the fractions by looking at qualitative and quantitative differences and similarities to establish if liver homogenates can be used in place of S9 fractions and microsomes. This would enable quicker implementation of *in vitro* generated metabolites derived from emerging anabolic drugs as potential target analytes into existing methods whilst saving resources due to short, convenient, and simple

preparation and ensuring animal welfare and food integrity by effective detection of banned substances.

2.2 Experimental

2.2.1 Materials and reagents

Tris(hydroxymethyl)aminomethane (Tris), ethylenediaminetetraacetic acid (EDTA) and the Pierce bicinchoninic acid (BCA) Protein Assay Kit were from Thermo Fisher Scientific (Hemel Hempstead, UK). Nicotinamide adenine dinucleotide phosphate (NADPH) was purchased from Roche Diagnostics (Mannheim, Germany). 3′-Phosphoadenosine-5′-phosphosulfate (PAPS) was purchased from Merck (Darmstadt, Germany). Uridine 5′-diphospho-glucuronic acid (UDPGA) trisodium salt, alamethicin from *Trichoderma viride*, cytochrome c from bovine heart, nicotinamide adenine dinucleotide reduced disodium salt hydrate (NADH), potassium cyanide, sodium cholate hydrate, Triton N-101, glycerol, potassium phosphate monobasic and dibasic, magnesium chloride ($MgCl_2$) hexahydrate, potassium chloride (KCl), umbelliferone (7-hydroxycoumarin), 7-ethoxyoumarin, and chloroform HPLC Plus grade were bought from Sigma-Aldrich (Gillingham, UK). Carbon monoxide (CO) compressed in a gas cylinder was from BOC (Guildford, UK). Oasis hydrophilic-lipophilic balance (HLB) solid phase extraction (SPE) cartridges (1 cc, 30 mg, 30 μm) were obtained from Waters (Milford, MA, USA). Methanol and acetonitrile Chromasolv for LC-MS was from Honeywell Riedel-de Haën (Seelze, Germany). Ethyl acetate Chromasolv for HPLC and acetic acid eluent additive for LC-MS were from Sigma-Aldrich (Gillingham, UK). Ultrapure water was prepared by a Milli-Q water purification system from Merck (Darmstadt, Germany). Analytical standards of ostarine, andarine, and S-1 were purchased from Sigma-Aldrich (Gillingham, UK). S-1-d4 was obtained from Toronto Research Chemicals (Toronto, Canada).

2.2.2 Preparation of bovine liver fractions

Bovine liver samples were collected from six animals at a commercial beef-processing abattoir facility, including one Limousin heifer, one Limousin crossbreed heifer, one Limousin steer and three Limousin crossbreed steers as shown in **Table 2.1**, and stored on ice.

Table 2. 1 Information on cattle, which livers were included in the study, including gender, breed, and age at the time of slaughter

No.	Gender	Type	Breed	Age
1	Female	Heifer	Limousin	29 months 23 days
2	Female	Heifer	Limousin cross	30 months 3 days
3	Male	Steer	Limousin	30 months 3 days
4	Male	Steer	Limousin cross	26 months 9 days
5	Male	Steer	Limousin cross	29 months 25 days
6	Male	Steer	Limousin cross	32 months 8 days

Upon arrival in the laboratory, liver samples were washed and perfused using a plastic syringe stuck into visible blood vessels with ice-cold phosphate-buffered saline (PBS) and finely minced. The procedure for isolation of S9 fractions and microsomes was adapted from Pearce et al.[375] and is illustrated in **Figure 2.1**. Briefly, after pooling the liver pieces to obtain a representative sample, 3 volumes of ice-cold homogenization buffer (50 mM Tris, 150 mM KCl, and 2 mM EDTA pH 7.4 at 4 °C) were added and the mixture was homogenized at 4 °C in five x 45 second intervals at 2000 rpm with a Silverson L5M homogenizer with a vertical slotted head. Approximately a third of this crude homogenate was stored at -80 °C. The remaining crude homogenate was split in two. The first portion was centrifuged at low-speed (1000 × g for 5 min at 4 °C) and the subsequent supernatant (homogenate) was stored at -80 °C. The second portion was centrifuged at medium-speed (10 400 × g_{max} for 20 min at 4 °C). An aliquot of the resulting supernatant (S9 fractions) was frozen at -80 °C. The rest of the supernatant was centrifuged again at high-speed (105 000 × g_{max} for 60 min at 4 °C). The subsequently obtained microsomal pellet was washed by resuspension in 10 mL ice-cold resuspension buffer (150 mM KCl, 2 mM EDTA) and pelleted again by centrifugation at 105 000 × g_{max} for 60 min at 4 °C. The pellet was resuspended in 3 mL ice-cold storage buffer (250 mM sucrose) and stored at -80 °C. To summarise, the following fractions were prepared from bovine livers: crude homogenates, homogenates, S9 fractions, and microsomes.
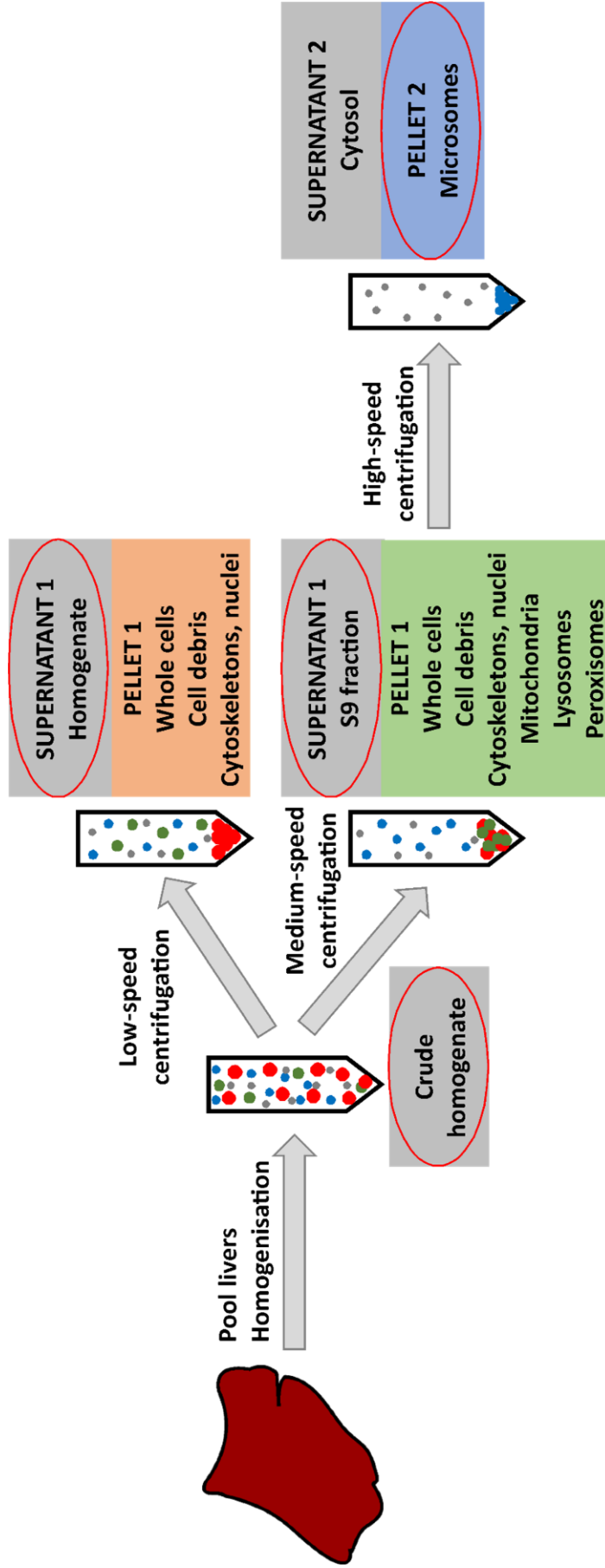
Figure 2.1 Overview of workflow utilised for the isolation of bovine liver fractions (crude homogenate, homogenate, S9 fraction, and microsomes) for *in vitro* metabolism studies

2.2.3 Characterisation of bovine liver fractions

2.2.3.1. Protein concentration determination

The protein content of all isolated fractions was determined with the colorimetric Pierce BCA assay to calculate the amount of protein to be added to subsequent incubation mixtures. The BCA kit was used according to instructions provided by the manufacturer using bovine serum albumin (0-1500 µg/mL) as calibration standard with samples prepared in triplicates and measured at 562 nm using a Tecan safire^2 plate reader (Tecan, Männedorf, Switzerland).

2.2.3.2. Cytochrome P450 content determination

Liver fractions were normalised to a final protein concentration of 2 mg/mL in a potassium phosphate buffer pH 7.4 containing 1 mM EDTA, 20 % glycerol (*v/v*), 0.5 % sodium cholate (*v/v*), and 0.4 % Triton N-101 (*w/v*).[207] P450 contents of the liver fractions were subsequently determined by using two methods; the CO-difference method and the DT-difference method (further detail in **Chapter 1 Section 1.2.1.1**). CO gas (10 bar) was transferred to a 45 mL parr reactor with a needle valve. For the CO-difference method as outlined by Omura and Sato[203], liver fractions (2 ml) were divided into two cuvettes, namely the sample and reference cuvette. Following the addition of approximately 5 mg of sodium dithionite to both cuvettes, only the sample cuvette was bubbled (at a rate of approximately 1 bubble/second by adjusting the valve opening of the reactor to control CO flow) with CO for one minute, and absorbance recorded between 400 and 500 nm with a Hitachi UV U-1900 spectrophotometer (Hitachi, Tokyo, Japan). At times the presence of contaminating haemoglobin can interfere with absorbance spectra. In anticipation of this, the DT-difference method was also used for crude homogenates, homogenates, and S9 fractions.[213–215,414] Here, CO was first bubbled through the sample and reference cuvette, then sodium dithionite was added to the sample cuvette only. The concentration of total P450 was calculated by the difference between the isosbestic absorbance at 490 nm and the Soret peak at 450 nm divided by the molar extinction coefficient of 94 mM^{-1} cm^{-1} for the CO-difference method[203] and 104 mM^{-1} cm^{-1} for the DT-difference method[214]. All samples were prepared in triplicates for measurements.

2.2.3.3. Cytochrome b$_5$ content determination

Cytochrome b$_5$ contents of tissue fractions were determined according to Omura and Sato.[203] 25 µL of the fractions were mixed with 970 µL of 100 mM potassium phosphate buffer at pH 7.4. After a baseline between 400 and 500 nm was recorded with a Cary WinUV spectrophotometer (Agilent Technologies, Santa Clara, CA, USA), 5 µL of 20 mM NADH at a final concentration of 0.1 mM was added to the sample cuvette and the spectrum difference recorded. Cytochrome b$_5$ contents were subsequently calculated by the difference between 424 and 409 nm divided by a molar extinction coefficient of 185 mM^{-1} cm^{-1}. All samples were prepared for measurements in triplicate.

2.2.3.4. NADPH-cytochrome P450 reductase activity measurements

NADPH-cytochrome P450 reductase activity was determined using a modified protocol as described by Lake et al.[415] and performed in 96-well microplates. The assay is based on using cytochrome c as a surrogate electron acceptor as it does not reoxidise with air.[207] Tissue fractions were diluted with 300 mM potassium phosphate buffer containing 5 mM MgCl$_2$ at pH 7.7 (assay buffer) to 0.4 mg/mL of protein. To 12.5 µL of the diluted fractions, 97.5 µL of assay buffer and 20 µL of an aqueous solution of 15 mM potassium cyanide (final concentration of 1.2 mM) were added to inhibit the oxidation of cytochrome c by mitochondrial cytochrome c oxidase. Then, 80 µL of 0.125 mM cytochrome c in 10 mM potassium phosphate buffer at pH 7.7 in a final concentration of 0.05 mM were added to samples and preincubated for five minutes at 37 °C and 400 rpm on a micro-plate shaker (VWR International, Dublin, Ireland). To initiate the reaction 20 µL of 5 mM NADPH dissolved in assay buffer were added to give a final concentration of 0.4 mM NADPH and a total assay volume of 250 µL. This resulted in a final protein concentration of 0.02 mg/mL that was found suitable providing a linear increase in absorbance over a period of up to three minutes. The increase in absorbance with time was measured at 550 nm for four minutes using a Tecan safire^2 plate reader ($n = 8$). The molar extinction coefficient of reduced cytochrome c at 550 nm has been determined previously to be 21 mM^{-1} cm^{-1}.[416] The NADPH-cytochrome P450 reductase activity was calculated based on the difference in absorbance in the first minute divided by the molar extinction coefficient and corrected for the sample dilution factor. Instead of the standard cuvettes with a path length of 1 cm as described by Lake et al. the assay was performed in a 96 well microplate. Therefore, based upon Lambert Beer's Law the absorbance was corrected for path length. From absorption

readings of the mixture at 975 and 900 nm as reference wavelengths in a 96-well microplate and a 1 cm standard cuvette respectively the path length of a well was deduced to be 0.714 cm.[417]

2.2.3.5. 7-Ethoxycoumarin *O*-deethylation activity measurements

7-Ethoxycoumarin is deethylated to 7-hydroxycoumarin by several CYP enzymes in the presence of NADPH, and therefore this reaction was utilised as a marker of general phase I drug metabolising activity (**Figure 2.2**). The rate of 7-hydroxycoumarine *O*-deethylation was measured using a modified procedure from Waxman and Chang.[418] 50 mM stock solutions of the standards 7-ethoxy- and 7-hydroxycoumarin were dissolved in methanol and further diluted with assay buffer (50 mM potassium phosphate buffer with 5 mM $MgCl_2$ at pH 7.4). Briefly, 4 µL of 10 mM 7-ethoxycoumarin (final concentration 200 µM) were added to 156 µL of assay buffer. Subsequently, 20 µL of liver fraction diluted with assay buffer to a protein concentration of 10 mg/mL (final concentration 1 mg/mL) were added and preincubated at 37 °C for 10 min in a shaking (300 rpm) incubator (Eppendorf Thermomixer comfort, Hamburg, Germany). The reaction was initiated by adding 20 µL of 10 mM NADPH. All samples were incubated at 37 °C for 30 min in a shaking incubator (300 rpm). For the calibration curve, liver fractions were firstly inactivated by incubation at 45 °C for 30 min. Then, 4 µL of 7-hydroxycoumarin at concentrations of 1 mM, 750 µM, 500 µM, 250 µM, 100 µM, or 25 µM (final concentrations 20, 15, 10, 5, 2, or 0.5 µM) were added to 156 µL of assay buffer. For the blank measurement, 160 µL of assay buffer was used. After addition of 20 µL of inactivated liver fractions diluted to 10 mg/mL, the samples were also preincubated, 20 µL of 10 mM NADPH were added and incubated at 37 °C for 30 min in a shaking incubator (300 rpm). All samples and calibrants were prepared in triplicates. The reaction was stopped by adding 25 µL of ice-cold 2 M HCl and placing the tubes on ice. 450 µL of chloroform was added to each sample and vortexed at 2500 rpm for 5 min in a DVX-2500 multi-vortexer (VWR International, Dublin, Ireland). Subsequently, samples were centrifuged at 3000 × g for 5 min, and 300 µL of the bottom organic layer transferred to a clean test tube and back-extracted with 1 mL of 30 mM sodium borate pH 9.2. Samples were again multi-vortexed at 2500 rpm for 5 min and centrifuged at 3000 × g for 5 min. 250 µL of the top aqueous layer was transferred into a black 96-well microplate and the fluorescence of 7-hydroxycoumarin at an excitation wavelength of 370 nm and an emission wavelength of 450 nm measured. The 7-ethoxycoumarin *O*-deethylation activity expressed as nmol 7-

hydroxycoumarin/min*mg protein was subsequently calculated. The chosen conditions for protein concentration (final concentration 1 mg/mL) and incubation time (30 min) showed linear metabolite formation.
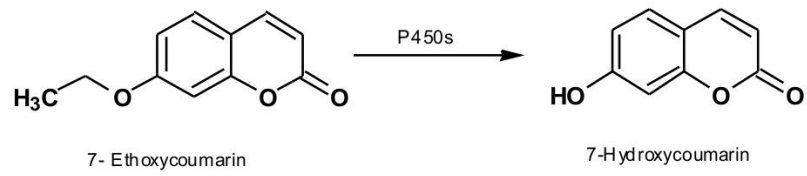
Figure 2.2 7-Ethoxycoumarin *O*-deethylation

2.2.4　*In vitro* generation of phase I and II SARM metabolites utilising liver fractions

Stock solutions of ostarine, andarine, and S-1 were prepared in acetonitrile at a concentration of 10 mM. The stock solutions were diluted in 50 mM potassium phosphate and 5 mM $MgCl_2$ at pH 7.4 to a concentration of 250 µM. Similarly, the liver fractions were diluted in the same buffer to 5 mg/mL. For the generation of phase I metabolites, 10 µL of 250 µM ostarine, andarine or S-1 (final concentration 50 µM) were added to 10 µL of 5 mg/mL liver microsomes, S9 fractions, homogenates, or crude homogenates (final concentration 1 mg/mL) and 20 µL of 50 mM potassium phosphate and 5 mM $MgCl_2$ at pH 7.4. After pre-incubation for 5 min at 37 °C, phase I reactions were initiated upon addition of 10 µL of 50 mM NADPH (final concentration 10 mM) as cofactor resulting in a total volume of 50 µL. Control samples in the absence of cofactor, test compound or tissue fraction were included as blanks to reveal non-cofactor dependent enzymatic degradation, distinguish any interfering components originating from the matrix, or compensate for chemical instability of the drug. All samples were incubated for two hours at 37 °C in a shaking (300 rpm) incubator (Eppendorf Thermomixer comfort) and reactions were stopped upon addition of three volumes (150 µL) of ice-cold acetonitrile spiked with S-1-d4 at a final concentration of 0.25 ng/mL.

To generate phase II metabolites, it was first necessary to produce phase I metabolites. Therefore, the phase I assay was carried out as described previously, and following the two hour incubation stage, 10 µL of 250 µg/mL alamethicin (final concentration 25 µg/mL) together with 10 µL of 5 mg/mL liver S9 fractions, homogenates, or crude homogenates (final concentration 0.5 mg/mL) in incubation buffer were added. Alamethicin and liver fractions were pre-incubated on ice for 10 min prior to use in the assay. Additionally, 10 µL of 250 µM PAPS (final concentration 25 µM), 10 µL of 50 mM UDPGA (final concentration 5 mM) were added as cofactors to initiate production of sulfated and glucuronidated phase II metabolites. Finally, 10 µL of 250 µM SARM compound were added resulting in a total volume of 100 µL. Samples were further incubated for another two hours at 37 °C 300 rpm and reactions were stopped by addition of 100 µL of ice-cold acetonitrile spiked with S-1-d4 at a final concentration of 2.5 µg/mL.

After reactions were stopped, samples were held on ice for 15 min and centrifuged at 12 000 × g (10 °C) for 15 min. 150 µL of the supernatant were transferred to 1.5 mL tubes and dried in a miVac Quatro vacuum-integrated centrifugal concentrator system (Fisher

Scientific; Loughborough, UK) at room temperature overnight. The samples were reconstituted in 500 µL of ultrapure water and vortexed at 2500 rpm for 3 min in a multi-vortexer. For liquid-liquid extraction, 500 µL of ethyl acetate were added to the aqueous samples and vortexed again (2500 rpm, 3min). The upper organic layer was transferred to a fresh tube. The extraction was repeated once more by adding 500 µL of ethyl acetate to the aqueous phase and vortexing (2500 rpm, 3min). The upper organic layer was removed; organic layers were combined and dried down in the miVac Quatro vacuum-integrated centrifugal concentrator system. The resulting residue was reconstituted in 75 µL of methanol:water (1:1, *v/v*). The aqueous lower layer was retained for solid phase extraction (SPE) of phase II conjugated metabolites. Oasis HLB SPE extraction cartridges were conditioned with 1 mL of methanol followed by 1 mL of water. Aqueous layers were loaded, washed with 1 mL of 5 % methanol, and eluted with 1 mL of methanol. Eluates were dried down at 40 °C under a stream of nitrogen and reconstituted in 75 µL of methanol:water (1:1, *v/v*). Samples were stored at -80 °C prior to LC-MS analysis.

2.2.5   UHPLC-HR-QTOF MS identification of *in vitro* generated phase I and II metabolites of SARM compounds

To identify generated phase I and II metabolites, 5 µL of the samples (**Section 2.2.4**) were injected onto an Agilent 1290 Infinity UHPLC system coupled to a 6560 drift tube ion mobility quadrupole time of flight (QTOF) mass spectrometer equipped with a dual Agilent jet stream electrospray ionisation source from Agilent Technologies (Santa Clara, CA, USA). The column oven was maintained at 45 °C and a reversed-phase Acquity UPLC ethylene bridged hybrid (BEH) C18 column (dimensions 2.1 x 100 mm, particle size 1.7 µm) from Waters (Milford, MA, USA) for chromatographic separation was used. Gradient elution with ultrapure water containing 0.1 % acetic acid (*v/v*) as mobile phase A and methanol containing 0.1 % acetic acid (*v/v*) as mobile phase B were used. The gradient and flow rate were programmed as follows: 0-0.5 min at 97 % A, 0.5-7.0 min 97 % A to 1 % A, 7-10 min hold 1 % A, and 10-12 min hold 97 % A, constantly at 0.4 mL/min. The autosampler temperature was maintained at 10 °C. The ESI source was operated with a nitrogen sheath gas temperature at 400 °C and nitrogen drying gas temperature at 150 °C both at a flow rate of 12 L/min. The capillary voltage was set at 4500 V and the nozzle voltage at 1600 V. The QTOF mass spectrometer was mass calibrated prior to analyses using an Agilent ESI-L low concentration tuning mix (P/N G1969-85000) and operated in negative

ESI, mass range *m/z* 100-1000 at a scan range of 5 spectra/sec in QTOF only mode with two scan segments at 0 V and 20 V collision energy. Prior to measurements a reference mix was prepared from ammonium trifluoroacetate, purine, and hexakis(1H, 1H, 3H-tetrafluoropropoxy)phosphazine (HP-0921) using the Reference Mass Solution Kit (P/N G1969-85001) according to the manufacturer's instructions (Agilent Technologies, Santa Clara, CA, USA). The calibrant delivery system introduced the reference mix (bottle A) to a reference sprayer for automatic recalibration during measurements. Reference mass correction was enabled using reference ions *m/z* 68.9958 (ammonium trifluoroacetate fragment CF_3), *m/z* 119.0363 (purine) and *m/z* 980.0164 (acetate ion HP-0921) in negative mode with the following parameters: average scans 1, detection window 50 ppm, and minimum height of 500 counts. A mixture of the SARM standards in acetonitrile (500 ng/mL) was injected before and after the samples (**Section 2.2.4**) to ensure mass accuracy and consistent retention times. Agilent MassHunter Workstation version B07.00 was used for data acquisition and analysis. Extracted ion chromatograms (EICs) were generated using exact masses of known and expected metabolites ± 10 ppm. The EICs of the proposed metabolites in the samples were compared to those of the controls. The identification of metabolites was based on accurate masses and fragmentation.

2.2.6   Statistical analysis

Descriptive statistics, including the mean ± standard error of the mean (SEM), for measurements of P450, cytochrome b_5, NADPH-cytochrome P450 reductase, and 7-ethoxycoumarin *O*-deethylation (**Section 2.2.3**) were calculated using IBM SPSS statistics version 22 software package. The stratification was crude homogenate, homogenate, S9 fractions and microsomes. Data were tested for normality and homogeneity of variance. Statistical tests utilised included one-way analysis of variance (ANOVA), and a two-tailed p-value of < 0.05 was considered statistically significant.

2.3   Results and discussion

2.3.1   Preparation and characterisation of bovine liver fractions

Four fractions, namely crude homogenate, homogenate, S9 fractions, and microsomes were successfully prepared from pooled bovine livers. Crude homogenate was prepared through homogenising minced pooled livers followed by centrifugation ($1000 \times g_{max}$, 5 min) with the resulting supernatant (homogenate) retained free of sedimented nuclei, cell debris, and erythrocytes. Subsequent centrifuging of crude homogenate ($10\,400 \times g_{max}$, 20 min) removed mitochondrial contents yielding the S9 fractions, with further centrifugation at $105\,000 \times g_{max}$ for one hour resulting in pelleted microsomes. Prepared crude homogenate, homogenate, and S9 fractions all contain a set of phase I and II enzymes allowing for the study of CYP-, FMO-, UGT-, and SULT-mediated biotransformation of a drug by addition of respective cofactors, such as NADPH, UDPGA, and PAPS. In contrast microsomes contain endoplasmic reticulum membrane bound enzymes such as CYP, FMO and UGT but lack cytosolic enzymes such as SULT. All fractions were characterised by measurements of their total protein content, cytochrome b_5 content, P450 content, NADPH-cytochrome P450 reductase activity and dealkylation activity towards 7-ethoxycoumarin as marker substrate (**Table 2.2**). Total protein content was used to normalise the volume of samples to result in a final assay concentration of 1 mg/mL. Most oxidations are catalysed by P450, therefore P450 and its accessory proteins cytochrome b_5 and NADPH-cytochrome P450 reductase were quantified in the liver fractions.[419] The rate of 7-ethoxycoumarin *O*-dealkylation by CYPs was quantified in all preparations as a measure of CYP-mediated rate of drug metabolism.

All measured contents and activities of prepared extracts were found to be significantly higher in microsomes (**Table 2.2**). Cytochrome b_5 content was lowest in S9 fractions and crude homogenates, whilst 7-ethoxycoumarin *O*-dealkylation activity was lowest in S9 fractions. The cytochrome b_5 content and 7-ethoxycoumarin *O*-dealkylation activity in homogenates were slightly higher than in S9 fractions. This is potentially due to the removal of mitochondria that contain cytochrome b_5 and P450.[206,420] Homogenates had slightly higher values than crude homogenates probably because of removal of cell debris and nuclei. The determined NADPH-cytochrome P450 reductase activity was increased only to a small degree in S9 fractions as compared to crude homogenates and homogenates, whilst P450 content was six times higher in microsomes than in crude homogenates, homogenates, and

S9 fractions. No significant variation in P450 contents of crude homogenates, homogenates, and S9 fractions was observed.

Two different methods (CO- or DT-difference method as described in **Section 2.2.3.2**) were used to determine the P450 contents (**Figure 2.3**). The ferrous (reduced) form of P450 can bind CO resulting in a distinctive wavelength maximum of this complex at 450 nm. The CO-difference method measures the difference between the CO complex of reduced P450 and reduced P450, whereas, the DT-difference method measures the difference between the CO complex of reduced P450 and oxidised P450.[203,214] **Figure 2.3 (A)** illustrates the absorbance spectrum of liver microsomes using the CO-difference method. No spectral change due to the formation of carboxyhaemoglobin (a complex formed from haemoglobin with CO) at 419 nm was observed.[421] Therefore, the CO-difference method was a suitable approach to determine the total P450 content. However, due to the presence of large amounts of contaminating haemoglobin in crude homogenates, homogenates and S9 preparations, the P450 content could only be determined with the DT-difference method. **Figure 2.3 (B)** shows the absorbance spectrum of a homogenate sample using the CO-difference method. Carboxyhaemoglobin results in an intense Soret band with a maximum wavelength at 419 nm. By saturating the reference and sample cuvette first with CO and then only adding DT to the sample cuvette as described for the DT-difference method, the effects of carboxyhaemoglobin can be precluded as shown in the absorbance spectrum of a homogenate sample in **Figure 2.3 (C)**. The Soret peak at 423 nm in **Figure 2.3 (C)** results from a reduction of cytochrome b_5 with DT.[422,423]

For measurements involving spectroscopy, homogenates were more suitable than crude homogenates. Centrifuging crude homogenates at a low-speed to produce homogenates removed tissue and cell debris which has the potential to interfere with spectral assays. While crude homogenates were observed to commonly clog up pipette tips, the low-speed centrifugations resulted in clear supernatants which ensures pipetting at accurate volumes.

Table 2.2 Characterisation of prepared bovine liver crude homogenates, homogenates, S9 fractions, and microsomes. Data are expressed as mean ± standard error of the mean ($n = 3\text{-}8$). Rows with different superscripts are statistically significant different ($p < 0.05$).

Liver fraction	Protein concentration (mg/mL) $n = 3$	Cytochrome b_5 content (pmol/mg protein) $n = 3$	P450 content (pmol/mg protein) $n = 3$	NADPH-cytochrome P450 reductase activity (nmol/mg protein/min) $n = 8$	7-Ethoxycoumarin O-deethylation activity (nmol/mg protein/min) $n = 3$
Crude homogenate	29.80 ± 0.46	99.61 ± 10.57[a]	163.14 ± 6.83[a]	28.46 ± 0.59[a]	92.44 ± 2.18[b]
Homogenate	21.42 ± 0.11	157.30 ± 1.63[b]	169.33 ± 5.04[a]	28.13 ± 0.96[a]	108.72 ± 2.26[c]
S9 fraction	18.76 ± 0.19	92.43 ± 2.30[a]	159.50 ± 4.33[a]	33.54 ± 1.39[b]	65.19 ± 1.71[a]
Microsomes	19.02 ± 0.08	786.28 ± 37.99[c]	988.33 ± 26.48[b]	100.52 ± 0.96[c]	545.96 ± 9.97[d]
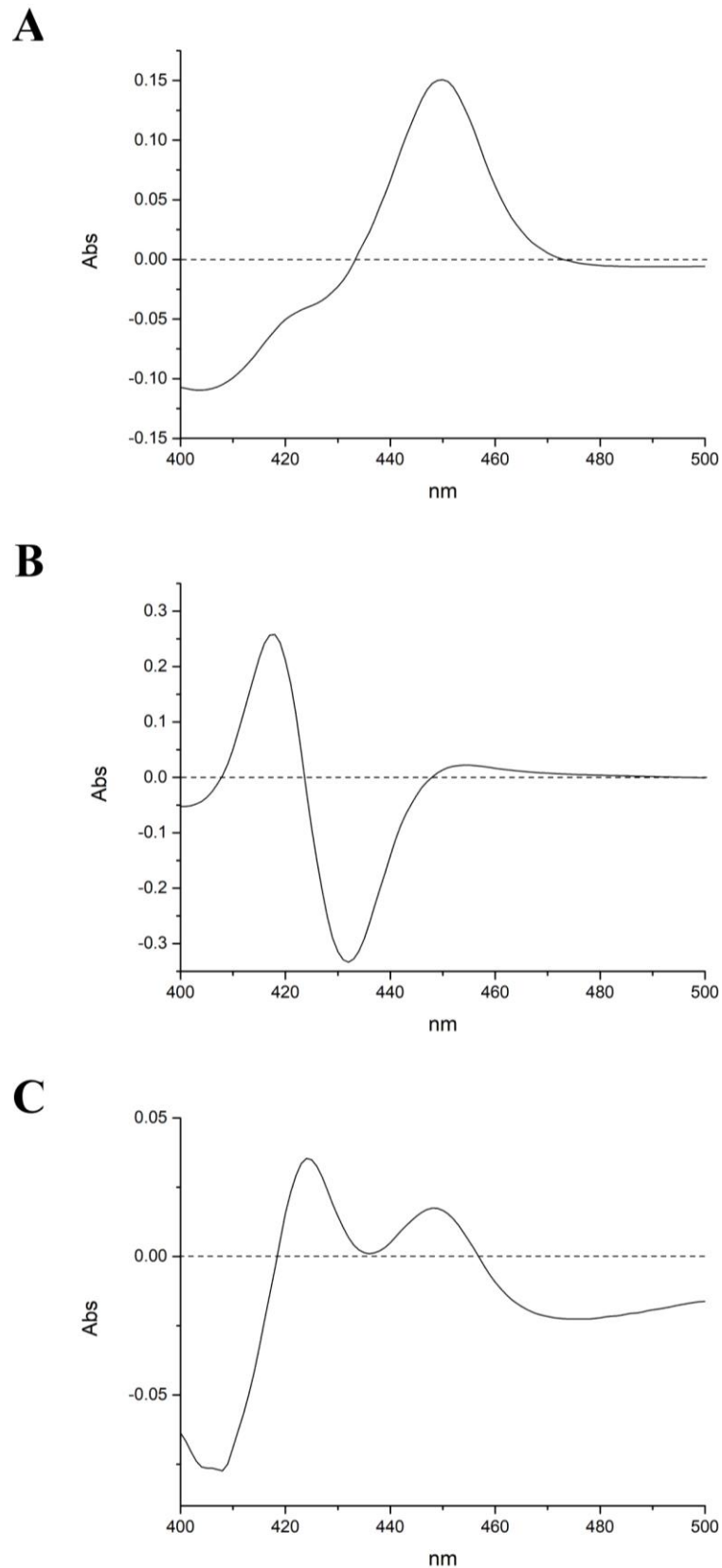
Figure 2.3 Absorbance spectra of P450 measurements with bovine liver **(A)** microsomes using the CO-difference method, **(B)** homogenate using the CO-difference method, and **(C)** homogenate using the DT-difference method. Soret peak of P450 evident at 450 nm.

2.3.2   *In vitro* generation of SARM metabolites by liver fraction preparations

Biotransformations of aryl-propionamide-derived SARMs ostarine, andarine, and S-1 were studied using bovine liver crude homogenates, homogenates, S9 fractions, or microsomes. Microsomes were used for the phase I metabolite assay only under addition of NADPH as cofactor, whereas the other fractions were also used for the phase I and subsequent phase II assay under addition of UDPGA and PAPS for UGT- and SULT-mediated reactions respectively. A final SARM substrate concentration of 50 µM was used in phase I and II metabolite generating incubations as preliminary experiments (data not presented) showed that lower concentrations (2 µM, 10 µM, or 25 µM) led to detection of less metabolites. Similarly, various incubation times were initially tested (30 min, 60 min, 90 min, 120 min, 150 min, 180 min, and 240 min) and an incubation time of two hours was chosen to be optimal for the formation of metabolites. Longer incubation times did not result in increased metabolite formation.

To identify the metabolites formed from incubations with different liver fractions, samples were injected onto the UHPLC-QTOF MS system. MS analysis was performed at altering low (0 V) and high (20 V) collision energies resulting in collation of two data sets; one scan segment for each collision energy. Data acquired at low collision energy displays mainly the molecular ions, whereas collision induced dissociation at the higher 20 V collision energy shows the fragment ions. This resulting "pseudo MS/MS" data can reveal fragment ions that not only derive from the molecular ion of interest but also from co-eluting components as all ions without previous precursor ion selection will be fragmented.[162] Using the deprotonated accurate masses of SARM metabolites from the available literature[16,19,130,133,141,142,148,164,165,177,184,185] and likely metabolic pathways, extracted ion chromatograms for both collision energy scan segments were displayed for samples and compared to respective controls (incubations without cofactors, substrate, or liver fractions). The measured accurate mass with a mass error $\pm < 10$ ppm from the calculated mass of the precursor and product ions characteristic for dissociation routes enabled the deduction of the metabolites generated and tentative elucidation of their chemical structures. Mass errors (ppm) were calculated by subtracting the theoretical mass (calculated as the monoisotopic mass) from the observed mass, divided by the theoretical mass, and multiplied by a 10^6 factor. The observed metabolites were typically non-polar and were found in the organic rather than the aqueous phase.

2.3.2.1.   Generated ostarine phase I and II metabolites

After incubating liver fractions with ostarine, the unmodified substrate ostarine was the most abundant analyte observed using UHPLC-QTOF MS analysis. Generated ostarine phase I and phase II metabolites with their observed precursor and fragment ions are listed in **Table 2.3** in ascending order by their retention times. Monohydroxylation (M1a and M1b) and *O*-dephenylation (M3) were the primary phase I metabolic pathways observed. Monohydroxylations of the cyanophenol moiety with fragment ions at *m/z* 134 (+16 Da from *m/z* 118) resulted in two positional isomers M1a and M1b. Two monohydroxylations of ostarine were previously observed in bovine urine samples following oral administration of ostarine[141,142] and also generated by bovine liver S9 fractions[141]. Bishydroxylations of the cyanophenol moiety identified by the fragment ion at *m/z* 150 resulted in two minor metabolites M2a and M2b. In previous studies, bishydroxylated metabolites were not found in post-administration bovine urine samples[141,142] and after bovine liver S9 incubations[141], but were generated by human liver S9 fractions and one bishydroxylated metabolite was found in post-administration canine urine[177]. *O*-Dephenylation cleaved the benzonitrile ring and yielded ostarine metabolite M3. Its formation was also observed to a minor degree in controls in the absence of NADPH indicating that it can also be formed NADPH-independently in the presence of enzymes. Thevis et al. described the *O*-dephenylated ostarine metabolite as a target analyte for doping control purposes.[177] The carboxyl analogue of M3 at *m/z* 301 as previously described in canine[177], bovine[141,142], and human urine[175] and metabolites deriving from amide hydrolysis at *m/z* 220[19,142] and amide hydrolysis plus hydroxylation at *m/z* 201[19,141,142] could not be detected in the current study. Main phase II metabolic pathways included glucuronidation of ostarine (M4) and glucuronidation of hydroxy-ostarine (M6). Moreover, the glucuronic acid conjugate of bishydroxy-ostarine (M7) and sulfated hydroxy-ostarine (M5) were detected.

Ostarine phase I metabolites were detected in crude homogenates, homogenates, S9 fractions, or microsomes as shown by the overlaid extracted ion chromatograms in **Figure 2.4**. The relative abundances of metabolites were highest in microsomes, followed by S9 fractions. Metabolites generated by crude homogenates and homogenates showed slightly lower relative abundances than by S9 fractions. A similar trend was observed for phase II metabolites generated by crude homogenates, homogenates and S9 fractions as illustrated by their overlaid extracted ion chromatograms in **Figure 2.5**.

Table 2.3 Ostarine and its phase I followed by phase II metabolites, in ascending order of retention time (RT), with their elemental compositions, observed masses in negative mode, and chemical structures with ESI fragmentation patterns found after incubation with crude homogenates (cH), homogenates (H), S9 fractions (S9), or microsomes (M). Collision energies at 20 V for fragment ions (FI), 0 V for precursor ions (PI).

Compound/ Metabolite	Elemental composition [M-H]⁻	Observed PI/FI ions [M-H]⁻ m/z	Error ppm	RT min	cH	H	S9	M	Chemical structure with proposed ESI fragmentation patterns
Ostarine	$C_{19}H_{13}F_3N_3O_3$	388.0892	-5.7	6.03	✓	✓	✓	✓	
	$C_{12}H_8F_3N_2O_2$	269.0560	6.3						
	$C_{11}H_8F_3N_2O$	241.0607	5.4						
	$C_8H_4F_3N_2$	185.0346	7.6						
	C_7H_4NO	118.0305	6.8						
Phase I					cH	H	S9	M	
Ostarine-M1a (Hydroxy-)	$C_{19}H_{13}F_3N_3O_4$	404.0882	4.5	5.95	✓	✓	✓	✓	
	$C_{12}H_8F_3N_2O_2$	269.0550	2.6						
	$C_8H_4F_3N_2$	185.0339	3.8						
	$C_7H_4NO_2$	134.0261	9.7						
Ostarine-M1b (Hydroxy-)	$C_{19}H_{13}F_3N_3O_4$	404.0875	2.7	5.79	✓	✓	✓	✓	
	$C_{12}H_8F_3N_2O_2$	269.0551	3.0						
	$C_8H_4F_3N_2$	185.0339	3.8						
	C_7H_4NO	134.0254	4.5						
Ostarine-M2a (Bishydroxy-)	$C_{19}H_{13}F_3N_3O_5$	420.0815	0.5	5.75	✓	✓	✓	✓	
	$C_7H_4NO_3$	150.0202	3.5						
Ostarine-M2b (Bishydroxy-)	$C_{19}H_{13}F_3N_3O_5$	420.0820	1.7	5.50	✓	✓	✓	✓	
	$C_{12}H_8F_3N_2O_2$	269.0552	3.3						
	$C_7H_4NO_3$	150.0206	6.2						
Ostarine-M3 (O-Dephenyl-)ᵃ	$C_{12}H_{10}F_3N_2O_3$	287.0659	3.5	5.04	✓	✓	✓	✓	
	$C_8H_4F_3N_2$	185.0342	5.4						
Phase II					cH	H	S9		
Ostarine-M4 (Glucuronide-)	$C_{25}H_{21}F_3NO_9$	564.1243	1.4	5.79	✓	✓	✓		
	$C_{18}H_{16}F_3N_2O_8$	445.0867	0.7						
	$C_{19}H_{13}F_3N_3O_3$	388.0915	0.3						
	$C_{12}H_{10}F_3N_2O_3$	287.0655	2.1						
	$C_{12}H_8F_3N_2O_2$	269.0550	3.0						
	C_7H_4NO	118.0304	5.1						

Table 2.3 *continued*

Compound/ Metabolite	Elemental composition [M-H]⁻	Observed PI/FI ions [M-H]⁻ *m/z*	Error ppm	RT min	cH	H	S9	Chemical structure with proposed ESI fragmentation patterns
Ostarine-M5 (Hydroxy-sulfate)	$C_{19}H_{13}F_3N_3O_7S$	484.0437	1.0	5.58	✓	✓	✓	
	$C_{19}H_{13}F_3N_3O_4$	404.0867	1.0					
	$C_8H_4F_3N_2$	134.0243	-3.7					
Ostarine-M6 (Hydroxy-glucuronide)	$C_{25}H_{21}F_3N_3O_{10}$	580.1192	1.2	5.44	✓	✓	✓	
	$C_{19}H_{13}F_3N_3O_4$	404.0866	0.7					
	$C_{12}H_8F_3N_2O_2$	269.0553	3.7					
	$C_7H_4O_2N$	134.0249	0.7					
Ostarine-M7 (Bishydroxy-glucuronide)	$C_{25}H_{21}F_3N_3O_{11}$	596.1132	-0.3	5.00	✓	✓	✓	
	$C_{12}H_{10}F_3N_2O_3$	287.0662	4.5					
	$C_8H_4F_3N_2$	185.0343	5.9					

[α] Also detected in lower intensity in absence of cofactor NADPH

GlcA … Glucuronic acid
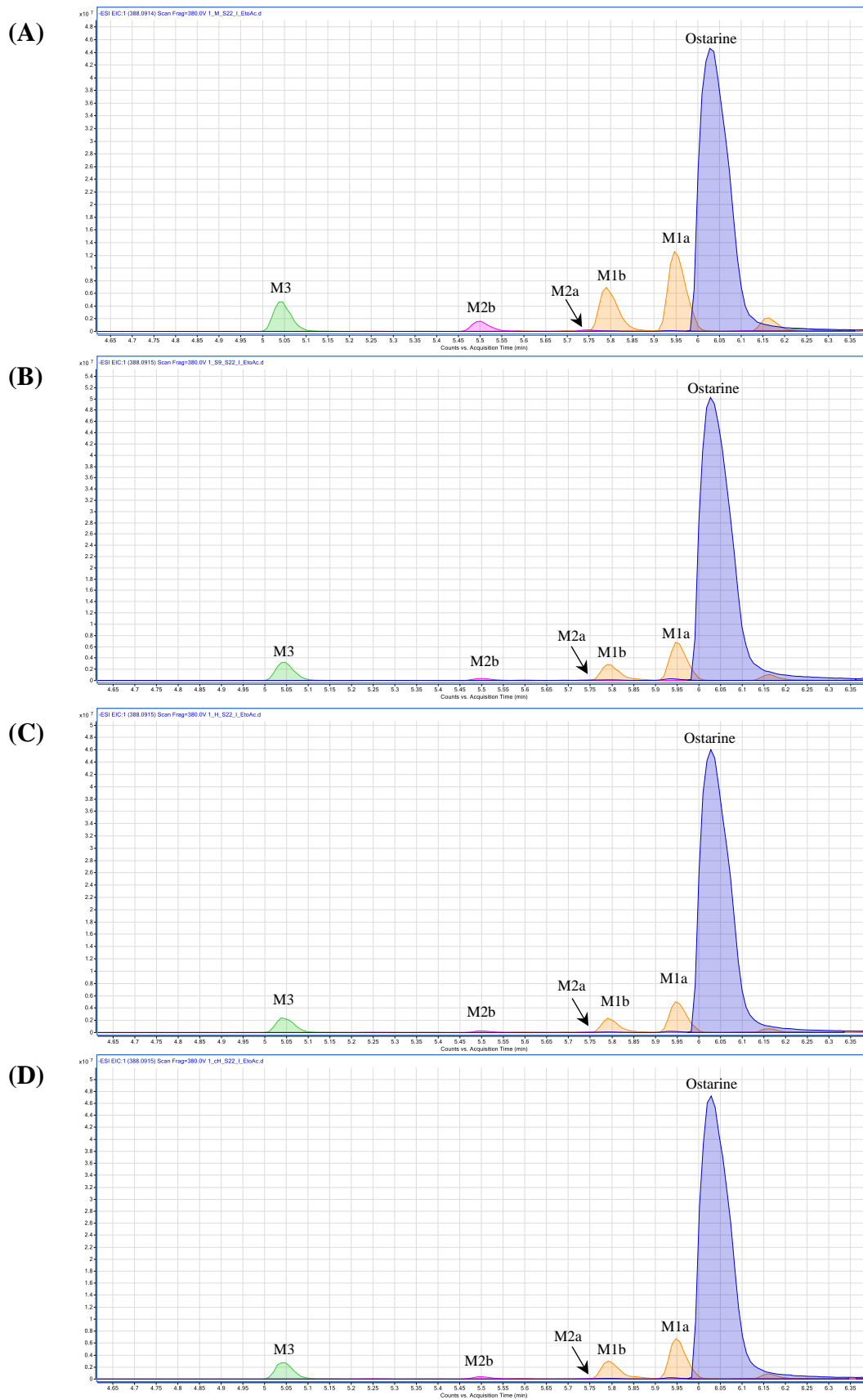
Figure 2.4 Overlaid extracted ion chromatograms in segment 1 (0 V) of ostarine and associated phase I metabolites generated by **(A)** microsomes, **(B)** S9 fractions, **(C)** homogenates, or **(D)** crude homogenates
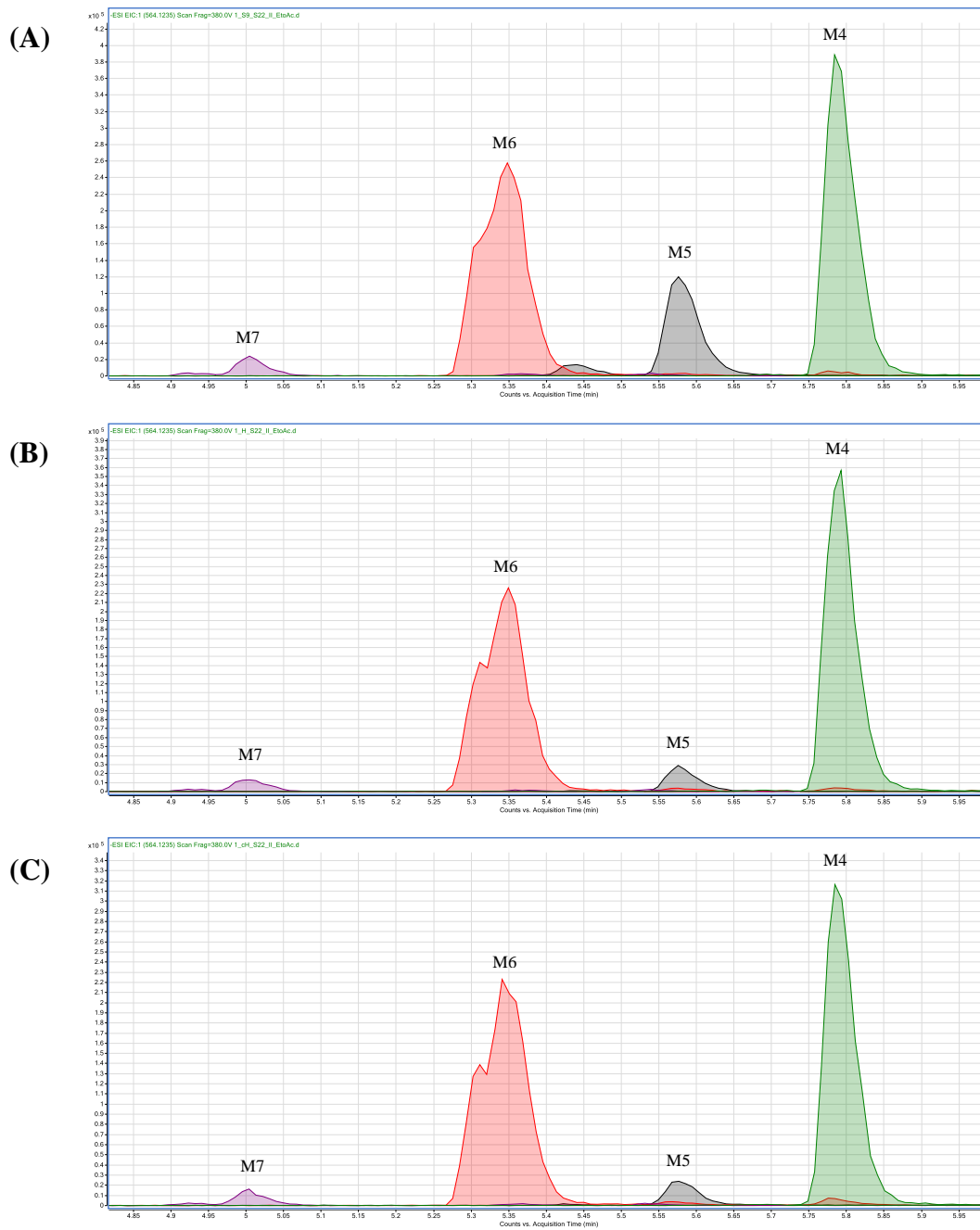
Figure 2.5 Overlaid extracted ion chromatograms in segment 1 (0 V) of ostarine phase II metabolites generated by **(A)** S9 fractions, **(B)** homogenates, or **(C)** crude homogenates.

2.3.2.2. Generated andarine phase I and II metabolites

For andarine, five phase I metabolites were generated by crude homogenates, homogenates, S9 fractions or microsomes (**Table 2.4**). Total ion chromatograms of phase I incubation samples are shown in **Figure 2.6**. The major metabolite was *O*-dephenyl-andarine (M4), which previously has also been described as a main metabolite in bovine liver S9 fractions[141], equine liver microsomes/S9 fractions[185], human[148] and equine[164] urine samples. Its formation was also observed to a minor degree in controls in the absence of NADPH or tissue fractions indicating that it can also be formed NADPH-independently in the presence of enzymes and due to chemical instability. Notably, M4 can be converted back to andarine by cytosolic *N*-acetyltransferases, however, *in vitro* this reaction would require the addition of cofactor acetyl-CoA and this reaction was not studied herein.[424] *O*-Dephenyl-andarine has the same chemical structure/formula as the dihydroxylated metabolite of the anti-prostate cancer drug flutamide.[425] Therefore, other relevant urinary metabolites should be monitored to discriminate andarine and flutamide intake. M1 corresponds to the demethylated andarine metabolite and its generation has previously been reported by bovine liver S9[141] and equine liver microsomal/S9 fractions[185], however, the presence of M1 in *in vivo* samples has not yet been confirmed. Furthermore, monohydroxylation annotated to the *N*-phenylacetamide ring (M2) with fragment ions at *m/z* 166 (deprotonated *N*-(4-hydroxyphenyl)acetamide) and *m/z* 205 (deprotonated 4-nitro-3-trifluoromethylaniline) was observed. M2 formation has been reported in studies with equine liver microsomes[185], human[184] and rat[426] liver microsomes/S9 fractions and its presence in human urine[176] has been confirmed. Additionally, in the present study demethylation plus hydroxylation (M3) with a molecular ion at *m/z* 442 and a distinctive fragment ion at *m/z* 152 (deprotonated *N*-(4-dihydroxyphenyl)formamide) was observed. A commonly described andarine metabolite formed by deacetylation[141,165,184,185,424,426] was also detected (M5) in this study. Nitro reduction has been described in previous studies[164,165,184,185], but a corresponding metabolite could not be detected in this study.

Using bovine liver crude homogenates, homogenates, or S9 fractions, three phase II metabolites of andarine were detected, mainly the glucuronic acid conjugate of andarine (M6), but also the glucuronic acid conjugate of hydroxy-andarine (M7), and *O*-dephenyl-andarine (M8). However, the site of glucuronidation could not be deduced from the fragment ions. In the present study sulfated conjugates were not generated for andarine or associated metabolites using bovine liver fractions. Previous studies described the formation of M6

using human[184] or equine[185] liver microsomes/S9 fractions and its presence in human urine samples[130,133,148,176] has been confirmed. Similarly, formation of M7 was previously reported by human[184] or equine[185] liver microsomes/S9 fractions and it was found in human urine. Thevis et al. reported two hydroxy-andarine glucuronides with different glucuronidation sites; by deducing chemical structures from the fragment ions of collision induced dissociation experiments, one site was attributed to C-14 and the other to the hydroxyl-group that was introduced on the *N*-phenylacetamide ring.[148] Two hydroxy-andarine glucuronides were also found in human urine samples by Grata et al.[133] M8 has not previously been described to be formed by *in vitro* incubations, however, it was detected in human urine samples[130,133,148].

Table 2.4 Andarine and associated phase I followed by phase II metabolites, in ascending order of retention time (RT), with their elemental compositions, observed masses in negative mode, and chemical structures with ESI fragmentation patterns found after incubations with crude homogenates (cH), homogenates (H), S9 fractions (S9), or microsomes (M). Collision energies at 20 V for fragment ions (FI), 0 V for precursor ions (PI).

Compound/ Metabolite	Elemental composition [M-H]⁻	Observed PI/FI ions [M-H]⁻ m/z	Error ppm	RT min	cH	H	S9	M	Chemical structure with proposed ESI fragmentation patterns
Andarine	$C_{19}H_{17}F_3N_3O_6$	440.1090	3.4	5.85	✓	✓	✓	✓	
	$C_{11}H_8F_3N_2O_4$	289.0453	3.8						
	$C_{10}H_8F_3N_2O_3$	261.0508	5.7						
	$C_7H_4F_3N_2O_2$	205.0243	6.3						
	$C_8H_8NO_2$	150.0570	6.0						
Phase I					cH	H	S9	M	
Andarine-M1 (Demethyl-)	$C_{18}H_{15}F_3N_3O_6$	426.0932	3.3	5.80	✓	✓	✓	✓	
	$C_{11}H_8F_3N_2O_4$	289.0454	4.2						
	$C_{10}H_8F_3N_2O_3$	261.0510	6.5						
	$C_7H_4F_3N_2O_2$	205.0243	6.3						
	$C_7H_6NO_2$	136.0415	8.1						
Andarine-M2 (Hydroxy-)	$C_{19}H_{17}F_3N_3O_7$	456.1031	1.5	5.72	✓	✓	✓	✓	
	$C_{11}H_8F_3N_2O_4$	289.0452	3.5						
	$C_{10}H_8F_3N_2O_3$	261.0503	3.8						
	$C_7H_4F_3N_2O_2$	205.0240	4.9						
	$C_8H_8NO_3$	166.0518	4.8						
Andarine-M3 (Demethyl-hydroxy-)	$C_{18}H_{15}F_3N_3O_7$	442.0877	2.0	5.68	✓	✓	✓	✓	
	$C_{11}H_8F_3N_2O_4$	289.0453	3.8						
	$C_{10}H_8F_3N_2O_3$	261.0503	3.8						
	$C_7H_4F_3N_2O_2$	205.0241	5.4						
	$C_7H_6NO_3$	152.0363	6.6						
Andarine-M4 (Dephenyl-)ᵃ	$C_{18}H_{15}F_3N_3O_7$	307.0560	4.2	5.37	✓	✓	✓	✓	
	$C_7H_4F_3N_2O_2$	205.0241	5.4						
Andarine-M5 (Deacetyl-)	$C_{17}H_{15}F_3N_3O_5$	398.0982	3.3	5.15	✓	✓	✓	✓	
	$C_{11}H_8F_3N_2O_4$	289.0450	2.8						
	$C_{10}H_8F_3N_2O_3$	261.0505	4.6						
	$C_7H_4F_3N_2O_2$	205.0243	6.3						

Table 2.4 *continued*

Compound/ Metabolite	Elemental composition [M-H]⁻	Observed PI/FI ions [M-H]⁻ *m/z*	Error ppm	RT min	cH	H	S9	Chemical structure with proposed ESI fragmentation patterns
Phase II					cH	H	S9	
Andarine-M6 (Glucuronide)	$C_{25}H_{25}F_3N_3O_{12}$	616.1396	0.0	5.56	✓	✓	✓	
	$C_{11}H_8F_3N_2O_4$	289.0449	2.4					
	$C_{10}H_8F_3N_2O_3$	261.0502	3.4					
	$C_7H_4F_3N_2O_2$	205.0240	4.9					
Andarine-M7 (Hydroxy-glucuronide)	$C_{25}H_{25}F_3N_3O_{13}$	632.1340	-0.8	5.44	✓	✓	✓	
	$C_{10}H_8F_3N_2O_3$	261.0504	4.2					
	$C_7H_4F_3N_2O_2$	205.0250	9.8					
Andarine-M8 (Dephenyl-glucuronide)	$C_{17}H_{18}F_3N_2O_{11}$	483.0868	0.0	4.96	✓	✓	✓	
	$C_{11}H_8F_3N_2O_4$	289.0448	2.1					
	$C_{10}H_8F_3N_2O_3$	261.0502	3.4					

α Also detected in lower intensity in absence of cofactor NADPH and in absence of tissue fractions

GlcA … Glucuronic acid

Figure 2.6 Total ion chromatograms of incubation samples with andarine and NADPH using **(A)** microsomes, **(B)** S9 fractions, **(C)** homogenates, or **(D)** crude homogenates as enzyme source for generation of phase I metabolites after liquid-liquid extraction (organic phase).

2.3.2.3. Generated S-1 phase I and II metabolites

S-1 is structurally very similar to andarine except that the *N*-acetyl group has been replaced by a fluoro group. Therefore, in this case deacetylation and demethylation reactions as previously described for andarine were not observed. This is the first study to look at the *in vitro* metabolism of S-1 in bovine. Tentative metabolites for S-1 are listed in **Table 2.5**.

Observed phase I reactions included monohydroxylations (M1a, M1b, M1c), bishydroxylations (M2a, M2b) and *O*-dephenylation (M3). M1a, M1b, and M3 were the major observed phase I metabolites *in vitro*. Kuuranne et al. reported the generation of three monohydroxylated metabolites by human liver microsomes/S9 fractions[184]. Bishydroxylated metabolites were not observed in any previous studies, however, they were only produced to a minor degree in the present study. An overlaid extracted ion chromatogram of *m/z* 417.0715 for the hydroxylated andarine metabolites M1a, M1b, and M1c from incubations with bovine liver microsomes, S9 fractions, homogenates and crude homogenates is presented as an example in **Figure 2.7**. Mass spectra from the two chromatographic traces were extracted for M1a from incubations with liver homogenates. Andarine-M4 is the same metabolite that has been formed by *O*-dephenylation of S-1 (M3). In previous studies M3 has been observed by incubations with human liver microsomes/S9 fractions[184] and in equine plasma[165] and urine[164] samples. Similarly to andarine, nitro reduction was not observed.

Six phase II metabolites were observed after incubations of S-1 with crude homogenates, homogenates, or S9 fractions. Observed metabolic reactions were glucuronidation of S-1 (M4), sulfation (M5a, M5b), and glucuronidation of hydroxylated S-1 (M6a, M6b, M6c). Kuuranne et al. have previously described the formation of glucuronic acid conjugate of S-1, sulfation of hydroxylated S-1, and three glucuronic acid conjugates of hydroxylated S-1 by human liver microsomes/S9 fractions[184]. Furthermore, sulfation of hydroxylated S-1was reported previously in a preclinical S-1 metabolism study in rat urine.[16] **Figure 2.8** shows a representative overlaid extracted ion chromatogram of *m/z* 593.1036 for the glucuronidated hydroxy-andarine metabolites M6a, M6b, and M6c generated from incubations with bovine liver S9 fractions, homogenates, or crude homogenates. Mass spectra were extracted for M6c from incubations with liver homogenates.

Table 2.5 S-1 and associated phase I followed by phase II metabolites, in ascending order of retention time(RT), with their elemental compositions, observed masses in negative mode, and chemical structures with ESI fragmentation patterns found after incubations with crude homogenates (cH), homogenates (H), S9 fractions (S9), or microsomes (M). Collision energies at 20 V for fragment ions (FI), 0 V for precursor ions (PI).

Compound/ Metabolite	Elemental composition [M-H]$^-$	Observed PI/FI ions [M-H]$^-$ m/z	Error ppm	RT min	cH	H	S9	M	Chemical structure with proposed ESI fragmentation patterns
S-1	$C_{17}H_{13}F_4N_2O_5$	401.0733	-8.2	6.59	✓	✓	✓	✓	
	$C_{11}H_8F_3N_2O_4$	289.0455	4.5						
	$C_{10}H_8F_3N_2O_3$	261.0507	5.4						
	$C_7H_4F_3N_2O_2$	205.0240	4.9						
	C_6H_4FO	111.0255	2.7						
Phase I					cH	H	S9	M	
S-1-M1a (Hydroxy-)	$C_{17}H_{13}F_4N_2O_6$	417.0743	6.7	6.47	✓	✓	✓	✓	
	$C_{11}H_8F_3N_2O_4$	289.0451	3.1						
	$C_{10}H_8F_3N_2O_3$	261.0502	3.4						
	$C_7H_4F_3N_2O_2$	205.0242	5.9						
	$C_6H_4FO_2$	127.0212	9.4						
S-1-M1b (Hydroxy-)	$C_{17}H_{13}F_4N_2O_6$	417.0724	2.2	6.08	✓	✓	✓	✓	
	$C_{11}H_8F_3N_2O_4$	289.0448	2.1						
	$C_{10}H_8F_3N_2O_3$	261.0501	3.1						
	$C_7H_4F_3N_2O_2$	205.0239	4.4						
	$C_6H_4FO_2$	127.0212	9.4						
S-1-M2a (Bishydroxy-)	$C_{17}H_{13}F_4N_2O_7$	433.0665	0.2	6.06	✓	✓	✓	✓	
	$C_{11}H_8F_3N_2O_4$	289.0449	2.4						
	$C_{10}H_8F_3N_2O_3$	261.0502	3.4						
	$C_7H_4F_3N_2O_2$	205.0239	4.4						
	$C_6H_4FO_3$	143.0156	4.2						
S-1-M1c (Hydroxy-)	$C_{17}H_{13}F_4N_2O_6$	417.0738	5.5	5.96	✓	✓	✓	✓	
	$C_{11}H_8F_3N_2O_4$	289.0451	3.1						
	$C_{10}H_8F_3N_2O_3$	261.0505	4.6						
	$C_7H_4F_3N_2O_2$	205.0240	4.9						
	$C_6H_4FO_2$	127.0208	6.3						

Table 2.5 *continued*

Compound/ Metabolite	Elemental composition [M-H]⁻	Observed PI/FI ions [M-H]⁻ m/z	Error ppm	RT min	cH	H	S9	M	Chemical structure with proposed ESI fragmentation patterns
S-1-M2b (Bishydroxy-)	$C_{17}H_{13}F_4N_2O_7$	433.0663	-0.2	5.76	✓	✓	✓	✓	
	$C_{11}H_8F_3N_2O_4$	289.0445	1.0						
	$C_{10}H_8F_3N_2O_3$	261.0503	3.8						
	$C_7H_4F_3N_2O_2$	205.0237	3.4						
	$C_6H_4FO_3$	143.0156	4.2						
S-1-M3 (*O*-Dephenyl-)[α]	$C_{18}H_{15}F_3N_3O_7$	307.0565	5.9	5.37	✓	✓	✓	✓	
	$C_7H_4F_3N_2O_2$	205.0246	7.8						
Phase II					**cH**	**H**	**S9**		
S-1-M4 (Glucuronide-)	$C_{23}H_{21}F_4N_2O_{11}$	577.1085	-0.3	6.33	✓	✓	✓		
	$C_{17}H_{13}F_4N_2O_5$	401.0769	0.7						
S-1-M5a (Hydroxy-sulfate)	$C_{17}H_{13}F_4N_2O_9S$	497.0289	1.2	6.02	✓	✓	✓		
	$C_{17}H_{13}F_4N_2O_6$	417.0722	1.7						
	$C_{11}H_8F_3N_2O_4$	289.0447	1.7						
	$C_{10}H_8F_3N_2O_3$	261.0500	2.7						
	$C_7H_4F_3N_2O_2$	205.0236	2.9						
	$C_6H_4FO_2$	127.0207	5.5						
S-1-M6a (Hydroxy-glucuronide)	$C_{23}H_{21}F_4N_2O_{12}$	593.1040	0.7	5.83	✓	✓	✓		
	$C_{17}H_{13}F_4N_2O_6$	417.0719	1.0						
	$C_{11}H_8F_3N_2O_4$	289.0449	2.4						
	$C_{10}H_8F_3N_2O_3$	261.0498	1.9						
	$C_7H_4F_3N_2O_2$	205.0237	3.4						
S-1-M6b (Hydroxy-glucuronide)	$C_{23}H_{21}F_4N_2O_{12}$	593.1038	0.3	5.64	✓	✓	✓		
	$C_{17}H_{13}F_4N_2O_6$	417.0715	0.0						
	$C_7H_4F_3N_2O_2$	205.0237	3.4						
S-1-M5b (Hydroxy-sulfate)	$C_{17}H_{13}F_4N_2O_9S$	497.0281	-0.4	5.59	✓	✓	✓		
	$C_{17}H_{13}F_4N_2O_6$	417.0717	0.5						
	$C_7H_4F_3N_2O_2$	205.0236	2.9						
S-1-M6c (Hydroxy-glucuronide)	$C_{23}H_{21}F_4N_2O_{12}$	593.1048	2.0	5.47	✓	✓	✓		
	$C_{17}H_{13}F_4N_2O_6$	417.0721	1.4						
	$C_{12}H_{12}F_4O_8$	303.0531	3.0						
	$C_{11}H_8F_3N_2O_4$	289.0448	2.1						
	$C_{10}H_8F_3N_2O_3$	261.0502	3.4						
	$C_7H_4F_3N_2O_2$	205.0237	3.4						

[α] Also detected in lower intensity in absence of cofactor NADPH and in absence of tissue fractions; GlcA … Glucuronic acid

Figure 2.7 Representative chromatograms and mass spectra: Extracted ion chromatograms of *m/z* 417.0715 (M1a-c) from incubations of S-1 with microsomes (red trace), S9 fractions, (black trace), homogenates (green trace), or crude homogenates (blue trace). Mass spectra were extracted from the green trace of M1a. **(A)** Segment 1 with 0 V and **(B)** Segment 2 with 20 V collision energy.
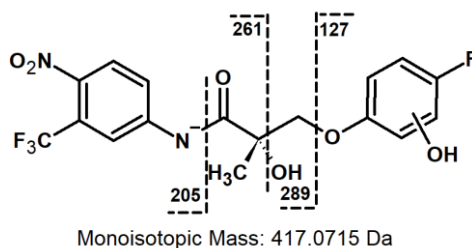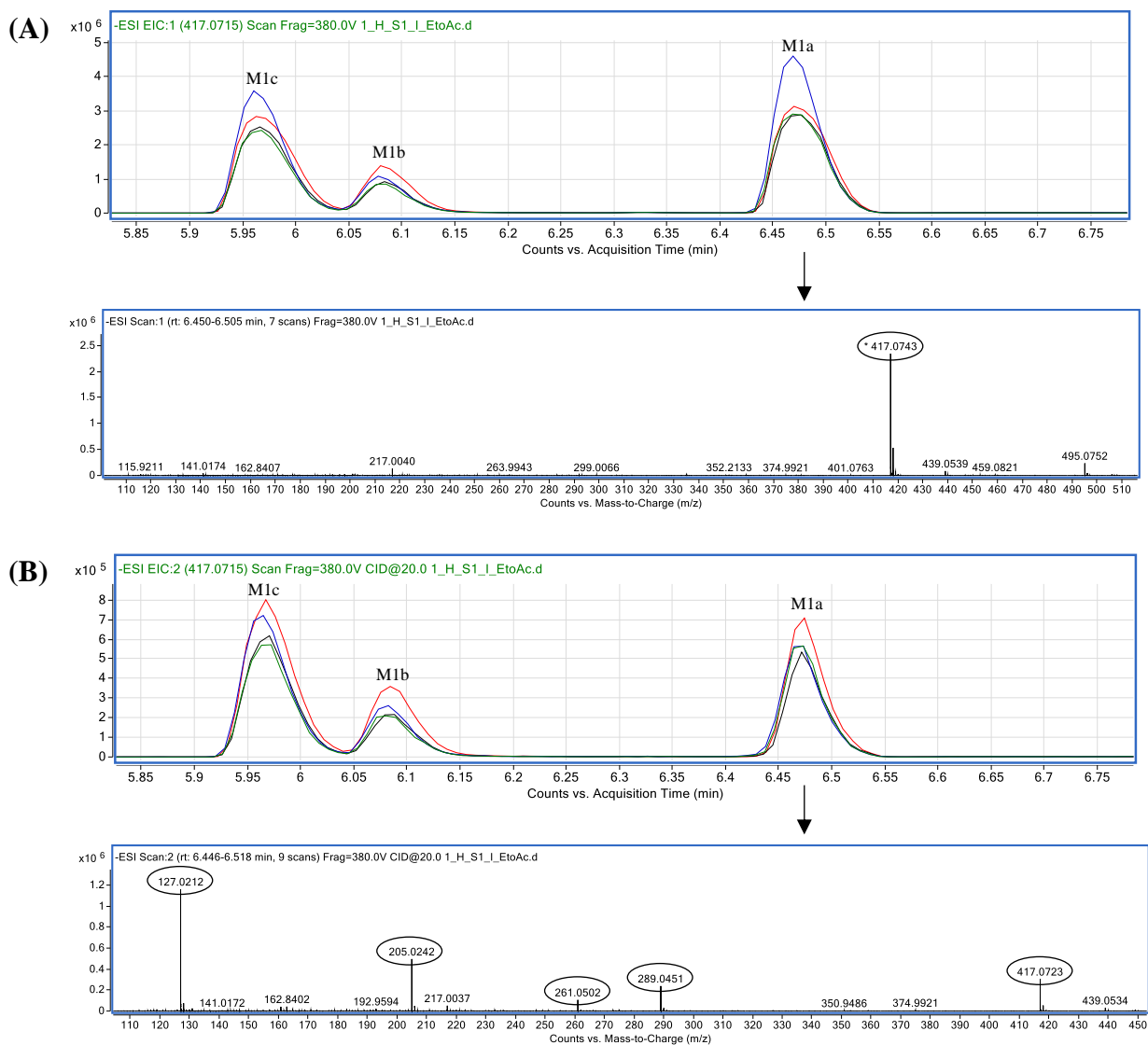
Figure 2.8 Representative chromatograms and mass spectra: Extracted ion chromatograms of *m/z* 593.1036 (M6a-c) from incubations of S-1 with S9 fractions, (black trace), homogenates (green trace) or crude homogenates (blue trace). Mass spectra were extracted from the green trace of M6c. **(A)** Segment 1 with 0 V and **(B)** segment 2 with 20 V collision energy.
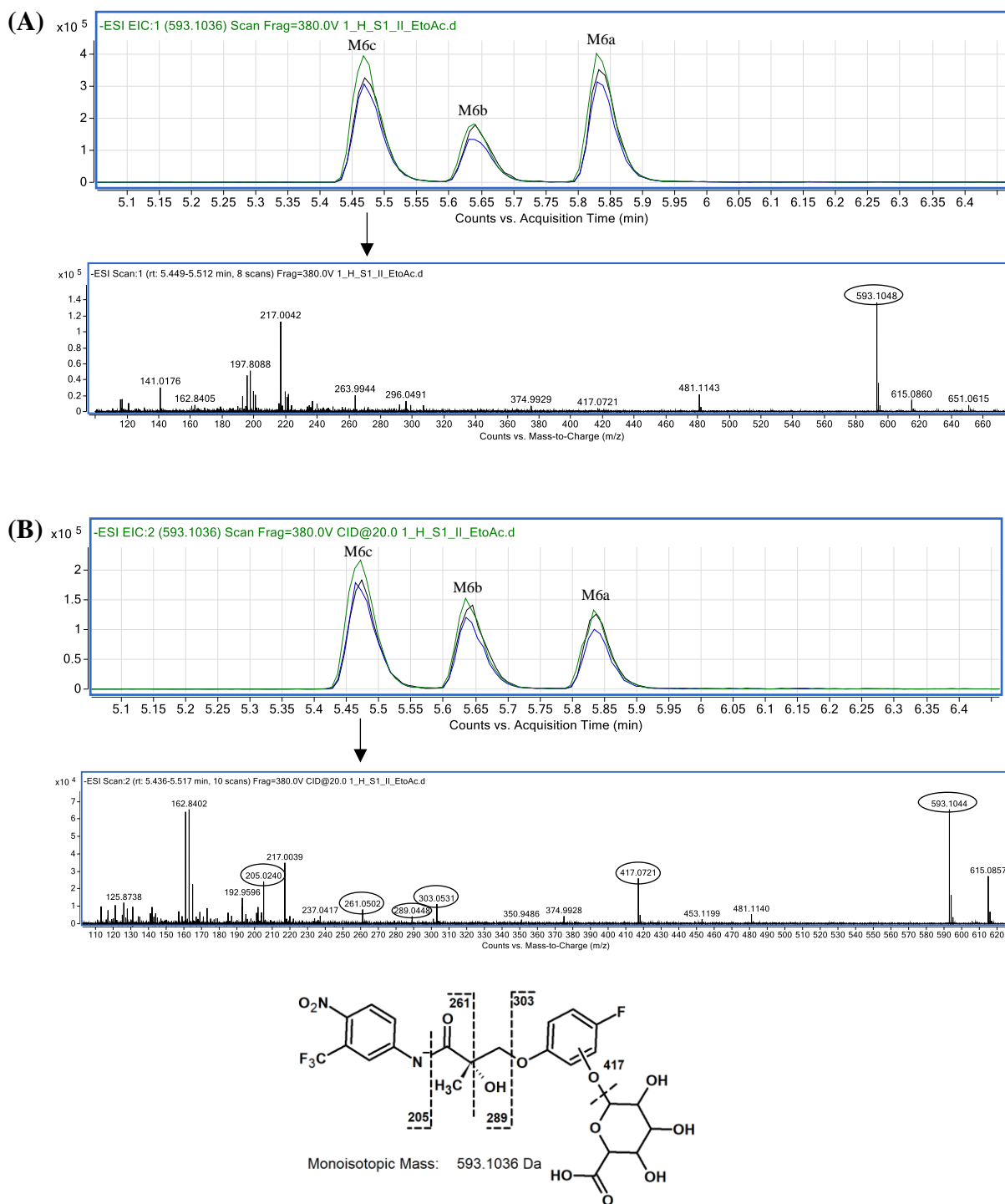
Table 2.6 Summary of the *in vitro* metabolites of ostarine, andarine, and S-1 found after incubations with crude homogenates (cH), homogenates (H), S9 fractions (S9), or microsomes (M – phase I only, phase II not applicable (N/A)).

Compound/Metabolite	cH	H	S9	M
Ostarine	✓	✓	✓	✓
Phase I				
Ostarine-M1a (Hydroxy-)	✓	✓	✓	✓
Ostarine-M1b (Hydroxy-)	✓	✓	✓	✓
Ostarine-M2a (Bishydroxy-)	✓	✓	✓	✓
Ostarine-M2b (Bishydroxy-)	✓	✓	✓	✓
Ostarine-M3 (*O*-Dephenyl-)	✓	✓	✓	✓
Phase II				
Ostarine-M4 (Glucuronide-)	✓	✓	✓	N/A
Ostarine-M5 (Hydroxy-sulfate)	✓	✓	✓	N/A
Ostarine-M6 (Hydroxy-glucuronide)	✓	✓	✓	N/A
Ostarine-M7 (Bishydroxy- glucuronide)	✓	✓	✓	N/A
Andarine	✓	✓	✓	✓
Phase I				
Andarine-M2 (Hydroxy-)	✓	✓	✓	✓
Andarine-M3 (Demethyl-hydroxy-)	✓	✓	✓	✓
Andarine-M4 (Dephenyl-)	✓	✓	✓	✓
Andarine-M5 (Deacetyl-)	✓	✓	✓	✓
Phase II				
Andarine-M6 (Glucuronide)	✓	✓	✓	N/A
Andarine-M7 (Hydroxy-glucuronide)	✓	✓	✓	N/A
Andarine-M8 (Dephenyl-glucuronide)	✓	✓	✓	N/A
S-1	✓	✓	✓	✓
Phase I				
S-1-M1a (Hydroxy-)	✓	✓	✓	✓
S-1-M1b (Hydroxy-)	✓	✓	✓	✓
S-1-M2a (Bishydroxy-)	✓	✓	✓	✓
S-1-M1c (Hydroxy-)	✓	✓	✓	✓
S-1-M2b (Bishydroxy-)	✓	✓	✓	✓
S-1-M3 (*O*-Dephenyl-)	✓	✓	✓	✓
Phase II				
S-1-M4 (Glucuronide-)	✓	✓	✓	N/A
S-1-M5a (Hydroxy-sulfate)	✓	✓	✓	N/A
S-1-M6a (Hydroxy-glucuronide)	✓	✓	✓	N/A
S-1-M6b (Hydroxy-glucuronide)	✓	✓	✓	N/A
S-1-M5b (Hydroxy-sulfate)	✓	✓	✓	N/A
S-1-M6c (Hydroxy-glucuronide)	✓	✓	✓	N/A

2.4   Conclusions

Microsomal or S9 fractions are typically used to produce drug metabolites by preliminary *in vitro* metabolism investigations for use in the development of analytical MS-based approaches. However, liver microsomes or S9 fractions are not readily available for many species such as cattle and the production thereof is laborious, time-consuming, and requires specialized equipment. This study demonstrates the potential for using bovine liver homogenates as a simple, rapid, and cost-effective *in vitro* strategy in lieu of microsomes and/or S9 fractions helping to provide material which can be used to promptly adapt analytical techniques towards reactive monitoring of emerging anabolic drug use in livestock. All prepared bovine liver fractions (including crude homogenates, homogenates, or S9 fractions for generation of phase I or II metabolites, or microsomes for producing phase I metabolites) were demonstrated to be capable of producing metabolites of SARM compounds ostarine, andarine, and S-1 that are of importance as potential analyte targets for MS analytical monitoring in biofluid matrices such as urine and/or plasma. While SARMs were used as model compounds in this study, the approach is anticipated to be equally applicable to other compounds. Observed differences in metabolite formation of investigated SARM compounds between various liver fractions were not of a qualitative nature as observed metabolites were produced by all investigated fractions but were rather quantitative. All described metabolites were produced and detected after incubations with crude homogenates, homogenates, or S9 fractions for generation of phase I or II metabolites, or microsomes for producing phase I metabolites. Certified reference materials for generated metabolites were not commercially available and thus could not be absolutely quantified. Microsomes were shown to produce phase I metabolites of investigated SARMs at relative higher abundances than by S9 fractions or homogenates, which may be due to the higher content of P450 and cytochrome b_5 and NADPH-cytochrome P450 reductase activity of microsomes that also resulted in a higher P450-mediated generation of 7-hydroxycoumarin relative to S9 fractions, homogenates, or crude homogenates. Therefore, whilst the use of microsomes could prove advantageous in the generation and subsequent detection of metabolites produced at low levels, typically for drug monitoring purposes the more abundant metabolites are preferentially chosen as target analytes. S9 fractions and homogenates offer the advantage of possessing a full set of phase I and II enzymes and consequently some metabolites (e.g. deriving from conjugation with sulfate) may be missed through only using microsomes, and therefore a combination of both microsomes and S9

fractions is commonly employed for such investigations.[184,185] In contrast to the current study where the same number of metabolites was formed by all investigated fractions, Wong et al. observed that equine liver homogenates typically generated more phase I metabolites of anabolic steroids than equine liver microsomes.[369] Wong et al. also reported the formation of phase I and II metabolites by equine liver homogenates without addition of cofactors[368], whereas in the present study phase I and II metabolite formation was reliant on addition of relevant cofactors (NADPH, UDPGA, PAPS). These different observations could be attributed to a variety of factors such as species differences between cattle and horses (discussed in detail in **Chapter 3**) or relate to differences in the preparation of homogenates. In this study homogenates were prepared by homogenisation of fresh livers, with optional low-speed centrifugation and freezing of aliquoted samples until use, whereas Wong et al. first froze and stored liver pieces, which were then thawed and homogenised prior to use.[368–370] The current approach is advantageous as it allows for characterisation of batches of prepared homogenates (**Section 2.3.1**) and offers greater consistency between individual aliquots.

Bovine liver homogenates were shown to be a promising *in vitro* system that can be used in place of microsomes and S9 fractions to rapidly produce metabolites and accelerate implementation of emerging anabolic drugs such as SARMs and metabolites thereof in LC-MS routine control regimes for the livestock sector. The use of homogenates instead of microsomes and/or S9 fractions offers several advantages with this current work demonstrating the technique to be an accessible alternative approach that does not require specialised equipment such as an ultracentrifuge and resulting short preparation times - crucial considerations for monitoring laboratories. It is envisaged that the use of homogenates as an *in vitro* tool is equally applicable for additional species and classes of drugs alongside those presented herein. For example, the Hong Kong Jockey Club Racing Laboratory has expanded their use of equine liver homogenates to several classes of drugs.[368–370] Future work in **Chapter 3** will compare the *in vitro* metabolite profiles of SARMs between several sport, food producing, and laboratory animals and assess how well the *in vitro* formed metabolites reflect actual *in vivo* metabolism of SARMs.

Chapter 3: Interspecies Comparative Profiling of *in vitro* and *in vivo* Generated SARM Metabolites by UHPLC-ion mobility-QTOF MS

3.1 Introduction

Selective androgen receptor modulators (SARMs) are a class of orally active small molecule compounds with tissue-selective ligand binding to the androgen receptor that have emerged from therapeutic drug development.[11] While they act as full androgen receptor agonists in muscle and bone, they act as partial agonists or antagonists in the prostate and seminal vesicles.[33,427,428] Metabolic amplification via 5-α-reductase as observed for testosterone does not occur for non-steroidal SARMs[429], therefore their use results in reduced side-effects compared to those of anabolic androgenic steroids such as risk of prostate cancer in men and virilization in women, while still maintaining advantageous anabolic effects on skeletal muscle and bone mass.[6,427] An array of SARM compounds based on different pharmacophores has emerged over the last two decades[405] following the first non-steroidal SARMs which were based on an aryl-propionamide core structure.[4] From this group of compounds, ostarine (S-22, MK-2866, enobosarm, GTx-024) has advanced as one of the lead compounds and has been tested in several clinical trials on muscle wasting in cancer cachexia, breast cancer, and stress urinary incontinence.[61,64,75,76] Another clinically promising SARM candidate is LGD-4033 (VK5211, ligandrol), which is based on a pyrrolidinyl-benzonitrile pharmacophore[49] and has been found to increase muscle mass without altering prostate-specific antigen[81]. Clinical application of LGD-4033 in patients with acute hip fracture has been evaluated in a phase II trial.[82] Yet another structurally distinguished SARM with clinical potential is the phenyl-oxadiazole RAD140 (testolone) which has been enrolled in a phase I clinical trial in patients with breast cancer.[53,104] Overall, SARM compounds have demonstrated efficacy and favourable safety profiles in various clinical trials, however, to date they have not gained approval for clinical application.

Although SARMs are investigational drug candidates for research purposes, many SARM compounds such as ostarine, LGD-4033, and RAD140 can be easily sourced over the Internet from non-reputable sources making them widely available around the globe.[123,124] Such ease of availability combined with their anabolic properties make them prone to abuse and like other anabolic agents, SARMs may be used in sports to enhance performance and in livestock farming to increase animal productivity. The World Anti-Doping Agency (WADA), International Federation of Horseracing Authorities (IFHA), and the European Commission have banned the use of SARMs in human sports, horse racing, and food producing animals respectively.[109,112,117] In athletes, the WADA testing figures

have shown an increasing numbers of test samples reporting positive for ostarine, LGD-4033, and RAD140, with more than doubling from 32 positive samples in 2015 to 65 reported in 2017.[137,139] Moreover, in equestrian sports the SARM compound andarine has been detected in equine blood samples [131], and the increasing number of reported cases on illegal SARM use underlines the threat SARMs pose to sports and food integrity.

Knowledge of the metabolism of SARMs is crucial to monitoring programs that aim to determine the absence or presence of these illegal drugs.[184] SARMs may be (ab)used in several species and although there can be similarities, differences in drug metabolism between species are numerous and unpredictable.[265] Several studies have investigated the metabolites formed following administration of ostarine in humans[175,176], rats[19], dogs[177], cattle[141,142], and horses[164,165]. Furthermore, the *in vitro* generated metabolites of ostarine in cattle (phase I)[141] and humans (phase I and II)[177] using liver S9 fractions have been studied. For LGD-4033, human urinary metabolites following LGD-4033 administration[132,178,179] and metabolites produced by incubations of LGD-4033 with liver microsomes or S9 fractions (phase I and glucuronidations)[127] were reported. Moreover, LGD-4033 was administered to horses and its metabolites in plasma and urine were elucidated.[180] To date, only the metabolites of RAD140 in human urine and produced by human liver microsomes (phase I) have been described[181]; the metabolism of RAD140 in other relevant species such as equine, bovine, or porcine has not been investigated. Most knowledge on biotransformation is known regarding human and laboratory animals through safety efforts in drug development and toxicity studies. Whilst information on drug metabolising enzymes in sports and food producing animals is limited, it has become evident that these species may be increasingly exposed to xenobiotics, and concerns surrounding consumer health and animal welfare have fuelled endeavours to gather information on species-relevant biotransformation and limit exposures. *In vitro* strategies such as the use of liver fractions represent a rapid and cost-effective method to draw initial conclusions about the metabolic fate of a drug and potential target analytes for use within drug surveillance, particularly when *in vivo* drug administration studies are ethically and financially hard to justify for an ever-increasing range of emerging drugs. These strategies help elucidate tentative metabolite structures as well as identify potential targets for control analysis facilitating further method development. For equine doping control applications, metabolites generated from *in vitro* incubations with liver fractions are accepted as reference materials since a revision of the ILAC-G7 guidelines in 2009.[116] Despite increased research efforts,

in vitro systems including liver fractions are still not readily available commercially for sports and food-producing animals possibly due to low demand.

For drug metabolism studies liquid chromatography (LC) coupled to high resolution (HR)-mass spectrometry (MS) is a commonly employed analytical technique to analyse complex samples obtained from *in vitro* incubations or acquired following *in vivo* administration.[430] Compared to low resolution MS (**Chapter 4**) that determines the *m/z* for each ion as nominal mass, high resolution MS features high resolution and mass accuracy and therefore measures to several decimal places allowing for determination of exact masses. By additionally coupling LC-HR-MS to ion mobility spectrometry (IMS), isomeric (i.e. identical molecular formula but distinct structure) and isobaric (i.e. same nominal mass but different molecular formula) compounds can be separated, and background noise can be reduced. While there are several IMS technologies such as travelling wave ion mobility spectrometry (TWIMS), differential mobility analyzer (DMA), and trapped ion mobility spectrometry (TIMS), drift tube ion mobility spectrometry (DTIMS) was the first designed form of IMS[431] and nowadays allows for reproducible collision cross section (CCS) determinations.[432] In DTIMS, the measured drift time, which is the time the ionized molecule takes to pass the ion mobility cell or drift tube and determined by the experimental parameters (drift tube length, temperature, drift gas pressure, drift voltages, mass of buffer gas species, and analyte molecule), can be converted to the CCS using the Mason-Schamp equation.[433] TWIMS, DMA, and TIMS measurements can also provide CCS values, however, generally indirectly after instrument calibration with compounds of known CCS.[434,435] The CCS value is a fundamental property of the analyte that represents the area of the interaction between ions and drift gas which is determined by the size and shape of the molecules. Therefore, CCS values can be used as additional identifiers for analyte characterisation[436,437] and/or to derive structural information from the separation of isomers in this third dimension by comparison with authentic reference standards and/or theoretical CCS values from molecular modelling that cannot be achieved with LC-MS alone.[438–440] Moreover, the added dimension of ion mobility enhances the selectivity and sensitivity of measurements by reducing background noise resulting in greater signal to noise ratios and separating the analyte signals and co-eluting matrix compounds.[441] In drug metabolism studies, this makes it easier to find the analytes of interest and cleans up product ion spectra, particularly from all-ion-fragmentation data where full scan and MS/MS of all incoming ions are recorded, thus improving the quality of obtained mass spectra.

Identifying *in vitro* generated metabolites of SARM compounds in a variety of relevant species can provide insights into shared and species-specific mammalian metabolism pathways and provides for comparison to *in vivo* metabolite profiles characterising the correlation between findings from *in vitro* and *in vivo* experiments. This provides a framework of appropriate species-specific metabolites to screen for aiding the development or improvement of analytical methods seeking to detect SARM compounds administration in various species of interest by identifying which metabolites are formed and including them into the methods, providing indisputable proof of ingestion and potentially extending detection windows. In this study, the comparative metabolite profiles of *in vitro* and *in vivo* generated metabolites of the SARM compounds ostarine, LGD-4033, and RAD140 chosen based on their distribution in black market products, supplements, and documented illegal use in humans, are reported for the first time. Liver microsomes and S9 fractions of major livestock species (i.e. cattle and pig), sport animals (horse), and laboratory species (rat) were prepared and characterised in terms of total protein, cytochrome b_5, and P450 levels, as well as by NADPH-cytochrome P450 reductase and 7-ethoxycoumarin *O*-deethylation activity. Microsomes alone were used for generation of phase I metabolites and also in combination with S9 fractions for generation of phase II metabolites and were selected over tissue homogenates as *in vitro* systems to ensure observation of very low abundant metabolites. Subsequently, *in vitro* profiles of SARM metabolites generated by various microsome and S9 preparations were assessed and compared across species, assessing the potential of such *in vitro* systems to accurately reflect *in vivo* metabolism observed using a rat administration model. Metabolite analyses were performed on an UHPLC-ion mobility-QTOF MS system to provide CCS values from drift tube IMS using nitrogen drift gas ($^{DT}CCS_{N2}$) as an additional identifier of SARM metabolites in addition to information on retention times and accurate masses of precursor and fragment ions. Such findings contribute to comprehensively clarifying the differences and similarities amongst *in vitro* generated SARM compound metabolites in different species by using species-specific liver fractions and assessing relevance to actual *in vivo* drug metabolites excreted in urine following SARM administrations.

3.2 Experimental

3.2.1 Materials and reagents

Tris, EDTA, Pierce BCA Protein Assay Kit, and micro-centrifugal filters (750 µL, PTFE, 0.2 µm pore size) were sourced from Thermo Fisher Scientific (Hemel Hempstead, UK). Sodium hydroxide pellets GPR RECTAPUR® were purchased from VWR (Dublin, Ireland). NADPH and β-glucuronidase (EC 3.2.1.31)/arylsulfatase (EC 3.1.6.1) from *Helix pomatia* were from Roche Diagnostics (Mannheim, Germany) and PAPS from Merck (Darmstadt, Germany). UDPGA trisodium salt, alamethicin from *Trichoderma viride*, cytochrome c from bovine heart, NADH, oxalyl chloride, potassium cyanide, sodium cholate hydrate, Triton N-101, glycerol, potassium phosphate monobasic and dibasic, magnesium chloride ($MgCl_2$) hexahydrate, umbelliferone (7-hydroxycoumarin), 7-ethoxyoumarin, chloroform HPLC Plus grade, dimethyl sulfoxide (DMSO) LiChrosol® for LC, polyethylene glycol (PEG) 300, ethanol (puriss. p.a., ACS reagent, absolute alcohol, without additive, ≥99.8%), and acetic acid eluent additive for LC-MS were bought from Sigma-Aldrich (Gillingham, UK). Methanol and acetonitrile Chromasolv™ for LC-MS were from Honeywell Riedel-de Haën (Seelze, Germany). Ultrapure water was prepared by a Milli-Q water system from Merck (Darmstadt, Germany). The analytical standard for ostarine was purchased from Sigma-Aldrich (Gillingham, UK), for LGD-4033 from Cayman Chemical supplied by Cambridge Bioscience (Cambridge, UK), for RAD140 from BOC Sciences (New York, USA), and for S-1-d4 from Toronto Research Chemicals (Toronto, Canada). All other chemicals and reagents used were from Sigma-Aldrich (Gillingham, UK).

3.2.2 *In vivo* SARM administration study

32 Sprague Dawley rats (Charles River Laboratories, Wilmington, MA, USA) were randomly distributed to four study groups ($n = 8$ per group; one control group and three treatment groups) and administered daily orally by gavage 1 mL of PEG300:ethanol 80:20 *v/v* without drug (control group), with ostarine (3 mg/kg body weight), with LGD-4033 (3 mg/kg body weight), or with RAD140 (3 mg/kg body weight) for 17 days. Urine sample collection was initiated two hours after the initial administration and took one hour to perform. A second batch of urine was collected following administration on day 9. Urine samples were also collected prior to drug administration to check for interfering matrix components. Animals were exsanguinated under terminal general anaesthesia 24 hours after the last administration and liver tissues recovered immediately, frozen on dry ice, and stored

at -80°C. All procedures were conducted under regulations as outlined within the UK Animals (Scientific Procedures) Act 1986, reviewed and approved by the Animal Welfare and Ethical Review Body (AWERB) ethical review procedures at Queen's University Belfast.

3.2.3   Preparation of species-specific subcellular liver fractions

Information on animals from which liver tissues were sourced including number of pooled livers, breed, and age is summarised in **Table 3.1**. Bovine, equine, and porcine liver samples were collected from commercial processing abattoirs and transported on ice to the laboratory, perfused with ice-cold PBS, finely minced and frozen at -80 °C. Rat liver samples were obtained from the control group animals of the described *in vivo* SARM administration study (**Section 3.2.2**). All liver samples were thawed simultaneously and preparations performed at 4 °C in a cold room. Livers from several individuals were pooled to reduce individual polymorphisms, and furthermore, only livers from male animals were included to negate potential gender differences. The procedure for isolation of S9 fractions and microsomes (**Figure 3.1**) was adapted from Pearce et al.[375] Briefly, after pooling liver pieces to obtain a representative sample, 3 volumes (36 mL) of ice-cold homogenization buffer consisting of 50 mM Tris-HCl, 150 mM KCl, and 2 mM EDTA pH 7.4 at 4 °C were added and the mixture homogenized in five x 45 second intervals at 2000 rpm with a Silverson L5M homogenizer with a vertical slotted head in a 50 mL tube. This was repeated twice, once to prepare the S9 fractions and again to isolate microsomes. Subsequently, samples were centrifuged at 15 700 × g_{max} (4 °C) for 20 min, the pellet discarded, and the supernatant (S9 fractions) either aliquoted and frozen at -80 °C, or transferred to a fresh tube and centrifuged at 105 000 × g_{max} (4 °C) for 60 min. The subsequently obtained microsomal pellet was resuspended in 14 mL of ice-cold resuspension buffer consisting of 150 mM KCl and 2 mM EDTA followed by another centrifugation step at 105 000 × g_{max} (4 °C) for 60 min. The resuspension buffer was then discarded, and the pellet resuspended in 3 mL of ice-cold storage buffer (250 mM sucrose), aliquoted and frozen at -80 °C. The protein concentration, P450 content, cytochrome b_5 content, NADPH-cytochrome P450 reductase activity and 7-ethoxycoumarin *O*-deethylation activity of S9 and microsomal fractions were determined as described in **Chapter 2 Section 2.2.3**. For the P450 assay, the carbon monoxide was produced by the reaction of oxalyl chloride with sodium hydroxide.[442] The DT-difference method was used as described in **Chapter 2 Section 2.2.3.2** for measurements.[443]

Table 3.1 Specifications of animal livers used for preparation of species-specific subcellular fractions (microsomal/S9)

Species	No.	Gender	Type	Breed	Age
Bovine	1	Male	Steer	Limousin	30 months 3 days
	2	Male	Steer	Limousin cross	29 months 25 days
	3	Male	Steer	Limousin cross	32 months 8 days
	4	Male	Steer	Limousin cross	36 months 9 days
Equine	1	Male	Gelding	Thoroughbred, Chestnut Colt	114 months 29 days
	2	Male	Gelding	Thoroughbred, Bay Colt	44 months 13 days
	3	Male	Gelding	Thoroughbred, Bay Colt	79 months
	4	Male	Gelding	Thoroughbred, Bay Colt	82 months 26 days
	5	Male	Gelding	Thoroughbred, Bay Colt	108 months
	6	Male	Gelding	Thoroughbred, Bay Colt	136 months 20 days
	7	Male	Gelding	Thoroughbred, Bay Colt	151 months 20 days
Murine	1	Male	Sire	Sprague-Dawley	2 months 16 days
	2	Male	Sire	Sprague-Dawley	2 months 16 days
	3	Male	Sire	Sprague-Dawley	2 months 16 days
	4	Male	Sire	Sprague-Dawley	2 months 16 days
	5	Male	Sire	Sprague-Dawley	2 months 16 days
	6	Male	Sire	Sprague-Dawley	2 months 16 days
	7	Male	Sire	Sprague-Dawley	2 months 16 days
	8	Male	Sire	Sprague-Dawley	2 months 16 days
Porcine	1	Male	Boar	Large white Landrace Duroc cross	23-24 weeks
	2	Male	Boar	Large white Landrace Duroc cross	23-24 weeks
	3	Male	Boar	Large white Landrace Duroc cross	23-24 weeks
	4	Male	Boar	Large white Landrace Duroc cross	23-24 weeks
	5	Male	Boar	Large white Landrace Duroc cross	23-24 weeks

(A)

Homogenised livers
from cattle, horse, pig, or rat

$15\,700 \times g_{max}$ (4 °C) for 20 min

Pellet
Red blood cells,
nuclei, mitochondria

**Supernatant
S9 fraction**

(B)

Homogenised livers
from cattle, horse, pig, or rat

$15\,700 \times g_{max}$ (4 °C) for 20 min

Pellet
Red blood cells,
nuclei, mitochondria

Supernatant
S9 fraction

$105\,000 \times g_{max}$ (4 °C) for 20 min

Pellet
Microsomes
+ Resuspension buffer

Supernatant
Cytosol

$105\,000 \times g_{max}$ (4 °C) for 20 min

Washed microsomal pellet
+ Storage buffer

Resuspended **microsomal fraction**

Figure 3.1 Scheme of preparation of species-specific **(A)** S9 fractions and **(B)** microsomes by differential (ultra)centrifugation.

3.2.4 *In vitro* generation of phase I and II SARM metabolites

10 mM stock solutions of SARM compounds were prepared - ostarine was dissolved in acetonitrile, LGD-4033 in ethanol, and RAD140 in DMSO - with 250 µM working stocks derived through dilution with incubation buffer (50 mM potassium phosphate buffer and 5 mM $MgCl_2$, pH 7.4). For generation of phase I metabolites, the total volume of incubation samples was 100 µL. 20 µL of 250 µM SARM compound (ostarine, LGD-4033, or RAD140; final concentration of 50 µM) were added to 40 µL of incubation buffer. Then, 20 µL of 5 mg/mL pooled liver microsomes (bovine, equine, murine, or porcine: final concentration of 1 mg/mL) in incubation buffer were added. After pre-incubation for 5 min at 37 °C in a shaking (300 rpm) Thermomixer comfort (Eppendorf, Stevenage, UK), phase I reactions were initiated upon addition of 20 µL of 50 mM NADPH (final concentration of 10 mM) as cofactor in incubation buffer. All samples were incubated for two hours at 37 °C (300 rpm).

To generate the phase II metabolites, it was first necessary to produce phase I metabolites. Therefore, the phase I assay preceded a phase II assay. Briefly, 10 µL of 250 µM of SARM compound (ostarine, LGD-4033, or RAD140) were added to 20 µL of incubation buffer. Further, 10 µL of 5 mg/mL pooled liver microsomes (bovine, equine, murine, or porcine) were added and the mixtures were pre-incubated for 5 min at 37 °C (300 rpm). The phase I reactions were started by adding 10 µL of 50 mM NADPH and phase I metabolites were generated for two hours at 37 °C (300 rpm). Imminently before the addition of further reagents, alamethicin and liver S9 fractions were pre-incubated on ice for 10 min. To initiate the production of phase II metabolites, 10 µL of 250 µg/mL alamethicin with 10 µL of 5 mg/mL liver S9 fractions (bovine, equine, murine, or porcine) in incubation buffer (final concentrations 25 µg/mL and 0.5 mg/mL), 10 µL of 250 µM PAPS (final concentration of 25 µM) diluted in incubation buffer, 10 µL of 50 mM UDPGA (final concentration of 5 mM) dissolved in incubation buffer, and 10 µL of 250 µM SARM compound (final concentration of 50 µM) were added. The samples were incubated for another two hours at 37 °C (300 rpm). The total volume for phase II incubation samples was 100 µL.

Phase I and II reactions were stopped upon addition of one equal volume (100 µL) of ice-cold methanol spiked with S-1-d4 at a concentration of 5 µg/mL. Subsequently, the samples were put on ice for 15 min and centrifuged at 12 000 × g (10 °C) for 15 min. 150 µL of the supernatant were transferred into an HPLC vial with insert. A 5 µL aliquot of the sample solution was injected onto the UHPLC-IM-QTOF MS system. Control samples in the absence of cofactor, test compound, or tissue fraction for respective were included as

blanks to reveal non-cofactor dependent enzymatic degradation, distinguish any interfering components originating from the matrix, or compensate for chemical instability of the drug.

3.2.5   Urine profiling of *in vivo* generated SARM metabolites

Rat urine samples (**Section 3.2.2**) were adjusted to pH 5.2 with 1 M acetic acid, and two 100 µL of aliquots transferred to 1.5 mL tubes. For detection of phase I and II metabolites, 100 µL of methanol spiked with 0.5 µg/mL S-1-d4 were added to 100 µL of rat urine. For cleavage of phase II metabolites, 2 µL of a mixture of β-glucuronidase (EC 3.2.1.31) and arylsulfatase (EC 3.1.6.1) from *Helix pomatia* were added to 100 µL of urine sample, incubated at 50 °C for 90 min in a heat block followed by addition of 100 µL methanol with 0.5 µg/mL S-1-d4. Afterwards, all samples were vortexed, cooled at -20 °C for 10 min and centrifuged for 15 min at 12 000 × g for precipitation. 150 µL of the supernatant was transferred into centrifugal filters and centrifuged at 10 400 × g for 5 min. The filtrate was directly transferred into an HPLC vial with insert, and 5 µL injected onto the UHPLC-IM-QTOF MS system.

3.2.6   UHPLC-IM-QTOF MS profiling of *in vitro* and *in vivo* formed metabolites of SARM compounds

To determine the profiles of *in vitro* (**Section 3.2.4**) and *in vivo* (**Section 3.2.5**) formed SARM metabolites an Agilent 1290 Infinity UHPLC system coupled to a 6560 drift tube (DT) ion mobility quadrupole time of flight (QTOF) mass spectrometer equipped with a dual Agilent jet stream electrospray ionisation source (Dual AJS ESI) was used (Agilent Technologies, Santa Clara, CA, USA). Chromatographic separation utilised a reversed-phase Acquity UPLC BEH C18 (dimensions 2.1 x 100 mm, particle size 1.7 µm) column from Waters (Milford, MA, USA) maintained at 45 °C. Gradient elution was performed using ultrapure water with 0.1 % acetic acid (*v/v*) as mobile phase A and methanol with 0.1 % acetic acid (*v/v*) as mobile phase B. Gradient and flow rate were programmed as follows: 0-0.5 min at 97 % A, 0.5-7.0 min 97 % A to 1 % A, 7-10 min hold 1 % A, and 10-12 min hold 97 % A, constantly at 0.4 mL/min. Autosampler temperature was held at 10 °C. The ESI source was operated in negative ionisation mode with a nitrogen sheath gas temperature at 400 °C, and nitrogen drying gas temperature at 150 °C, both at a flow rate of 12 L/min. The nebulizer gas pressure was 25 psi, the capillary voltage was 4500 V, the nozzle voltage 1600 V and the fragmentor was set at 380 V. The ion mobility trapping funnel operated with

a trap fill time of 8400 µs and a trap release time of 150 µs. The ion mobility drift tube entrance voltage was set to 1700 V and the exit voltage at 250 V with a gas pressure of 3.95 Torr and temperature at 26 °C using high purity nitrogen as collision gas. The rear funnel entrance voltage was set at 240 V and the rear funnel exit at 43 V. For acquisition 1 frame/sec and 13 transients/frame were recorded. The QTOF mass spectrometer was tuned and mass calibrated prior to analyses in extended dynamic range (2 GHz) with a low mass range (1700 *m/z*) using an Agilent ESI-L low concentration tune mix. During analysis the MS was operated in a mass range 100-1100 *m/z* in alternating frames (0 and 20 V). For single field calibration the tune mix was infused for 0.5 min between every ten samples using the same ion mobility and MS settings as for the analyte samples. Agilent MassHunter Workstation version B08.00 was used for data acquisition. Firstly, collected data were submitted to the Agilent IM-MS Reprocessor for accurate mass recalibration using reference masses of calibrant ions (negative mode: purine 119.0363 *m/z* and HP-0921 acetate ion 980.0163 *m/z*). Secondly, using the single field CCS calibration function in the Agilent IM-MS Browser B.08.00 slope (beta) and intercept (tfix) were deduced from measurements of calibrant ions from the tune mix with standardised $^{DT}CCS_{N2}$ values.[432] Three calibrants in negative mode at *m/z* 301.9981, 601.9784, and 1033.9881 were used. Subsequently, beta and tfix values were linked to sample files and used for automatic $^{DT}CCS_{N2}$ calculations from measured drift times. Agilent IM-MS Browser B.08.00 was used for feature extractions and data analysis. Chromatograms (**Figure 3.5**) were produced using Skyline daily[444] version 4.2.1.19095 applying the following descriptors for SARM metabolites: molecular formula, "adduct description" (singly deprotonated [M-H]), retention time, drift time, and CCS values.

3.3 Results and discussion

3.3.1. Characterisation of species-specific liver microsomes and S9 fractions

It is well documented that enzyme content and activity can vary among species, and whilst laboratory animals have been examined thoroughly, studies that provide specification data on liver microsomes and S9 fractions from food producing species in a direct comparison under the same conditions are rare.[271] The cytochrome b_5 content, P450 content, NADPH-cytochrome P450 reductase activity, and 7-ethoxycoumarin-O-deethylation activity determined in the different species and based on protein concentration are given in **Table 3.2**. Besides the P450 monooxygenases, the haemprotein cytochrome b_5 and the flavoprotein NADPH-cytochrome P450 reductase are main components of the electron transfer system that mediates P450 drug metabolism.[445] Furthermore, 7-ethoxycoumarin O-deethylation has been used in this study as to assess P450-mediated drug-metabolising activity. The substrate 7-ethoxycoumarin is deethylated by multiple CYP enzymes.[418] Yet, it has not been established which CYP enzymes are involved in the reaction in all investigated species and the involvement of CYP enzymes may differ across species. On the one hand characterisation of the prepared fractions was a necessary step to ensure the quality (i.e. enzymatic activity and ability to produce drug metabolites) of the prepared fractions and on the other hand enabled a direct comparison across species.

Table 3.2 shows that the highest cytochrome b_5 content was observed in bovine liver microsomes, whereas the highest P450 content and NADPH-cytochrome P450 reductase activity was observed in rat liver microsomes. Although porcine liver microsomes showed a lower P450 content and NADPH-cytochrome P450 reductase activity than rat liver microsomes, they had the highest rate of 7-ethoxycoumarin O-deethylation. Previously, Nebbia et al. have determined the NADPH-cytochrome P450 reductase activity, P450 and cytochrome b_5 content and in bovine, equine, porcine, and murine liver microsomes.[271] In accordance with the current study, bovine liver microsomes had the highest cytochrome b_5 content and rat liver microsomes showed the highest P450 content amongst these species. In both studies, cattle and horses showed a relatively low NADPH-cytochrome P450 reductase activity compared to pigs and rats. It should be noted that differences not only exist between species but also within species depending on breed or gender.[262,263]

For S9 fractions the contents and activities determined were three to nine-fold lower than that for corresponding microsomal fractions. P450, NADPH-cytochrome P450 reductase and cytochrome b_5 are enriched in microsomes as they are integral membrane proteins

primarily anchored to the cytoplasmic surface of the endoplasmic reticulum of eukaryotic cells.[197,203–205] As they are primarily linked to microsomes, their measurements in S9 fractions are less reported. Murine and equine liver S9 fractions had the highest P450 content, whilst murine liver S9 also showed the highest NADPH-cytochrome P450 reductase, deethylation activity, and cytochrome b_5 content. Similar to microsomes, bovine and equine liver S9 showed a lower NADPH-cytochrome P450 reductase activity than in porcine and murine liver S9.

To summarise, the P450 content did not correlate with the rate of deethylation indicating that other factors such as the expression levels of isoenzymes and their involvement towards the substrate metabolism may play a more decisive role than the overall amount of P450 enzymes. Moreover, the cytochrome b_5 content and NADPH-cytochrome P450 reductase activity was not seemingly correlated to the rate of the probe substrate metabolism. However, previously reported studies with cytochrome b_5 and NADPH-cytochrome P450 reductase knock-out mice have shown that they affect CYP enzyme activities and drug metabolism.[202,446]

Table 3.2 Characterisation of prepared species-specific liver S9 fractions and microsomes. Data were expressed as mean ± standard error of the mean (n = 3-8). Microsomes or S9 fractions were statistically analysed between species for each characterisation assay. Rows with different superscripts are statistically significant different ($p < 0.05$).

Liver fraction	Protein concentration mg/mL $n = 3$	Cytochrome b5 content pmol/mg protein $n = 3$	P450 content pmol/mg protein $n = 3$	NADPH-cytochrome P450 reductase activity nmol/mg protein/min $n = 8$	7-Ethoxycoumarin O-deethylation activity nmol/mg protein/min $n = 3$
Bovine microsomes	25.60 ± 0.23	722.56 ± 32.16[b]	571.80 ± 17.68[a]	95.49 ± 1.81[b]	568.05 ± 7.80[b]
Equine microsomes	32.27 ± 0.23	595.55 ± 22.69[a]	844.02 ± 10.89[c]	81.45 ± 2.04[a]	505.59 ± 9.70[a]
Murine microsomes	28.90 ± 0.22	640.84 ± 5.39[ab]	896.60 ± 8.54[d]	172.15 ± 2.47[d]	603.78 ± 5.49[c]
Porcine microsomes	24.42 ± 0.03	676.04 ± 14.89[ab]	765.38 ± 8.07[b]	130.87 ± 1.94[c]	990.64 ± 12.77[d]
Bovine S9 fractions	27.00 ± 0.17	80.71 ± 4.86[a]	104.46 ± 2.37[a]	26.20 ± 0.61[a]	67.47 ± 1.73[a]
Equine S9 fractions	31.88 ± 0.87	118.08 ± 5.37[bc]	198.82 ± 1.97[c]	24.50 ± 0.94[a]	73.23 ± 2.13[a]
Murine S9 fractions	27.75 ± 0.83	132.65 ± 12.17[c]	198.55 ± 2.44[c]	49.12 ± 1.03[c]	171.38 ± 4.51[c]
Porcine S9 fractions	17.00 ± 0.10	95.75 ± 1.71[ab]	144.23 ± 5.98[b]	36.62 ± 1.04[b]	148.92 ± 2.11[b]

3.3.2. Characterisation of species-specific *in vitro* generated SARM compound metabolites

An objective of this study was to provide a direct comparison between the metabolites of the SARM compounds ostarine, LGD-4033, and RAD140 formed *in vitro* by sports, food producing, and laboratory animals. By analysing generated metabolites using UHPLC-ion mobility-QTOF MS with alternating voltages (0 V and 20 V), partial structural characterisation was enabled through accurate mass measurement of precursor and product ions including acquired information on tentative fragmentation ("pseudo MS/MS"). Using this data-independent mode full MS unfragmented data and fragments of all ions are obtained with a single injection. By using ion mobility interfering background noise was removed and cleaned-up product ion spectra ions were obtained. CCS values were calculated from measured ion mobility drift times to serve as additional compound identifiers.

3.3.2.1. *In vitro* generated metabolites of ostarine

All observed *in vitro* metabolites of ostarine produced by bovine, equine, porcine, and murine liver microsomes alone (phase I) or in combination with S9 fractions (phase II) are listed in **Table 3.3** and the proposed metabolic pathway with tentative chemical structures is illustrated in **Figure 3.2**. Mass spectrometric fragmentation of ostarine and associated metabolites has previously been closely described by Thevis et al.[175,177]

In this study hydroxylation on the cyanophenyl ring (B-ring) with a shift + 16 Da from *m/z* 118 to *m/z* 134 was observed in two metabolites M1a and M1b. M1a was detected in all species, whereas M1b was not detected in porcine. Another hydroxylated metabolite M2 with unmodified rings *m/z* 118 and *m/z* 185 but a hydroxylated methyl group was found in bovine, equine, and murine liver microsomal samples, however, not in porcine. Previously, Thevis et al. described three monohydroxylated metabolites after incubation of ostarine with human liver S9 fractions and in a dog urine sample following ostarine administration.[177] Furthermore, two out of these three metabolites (M1a or M1b and M2) could be verified in human urine samples after ostarine intake.[175] In bovine, Rijke et al.[141] described two monohydroxylated metabolites excreted in urine following ostarine administration and formed by liver S9 fractions compared to three formed by bovine liver microsomes in the current study.

Three metabolites M3a, M3b, and M3c were formed by bishydroxylation on the B-ring with a shift of + 32 Da of *m/z* 118 to *m/z* 150. M3a was formed by bovine, equine and murine

liver microsomes, whereas M3b only in murine liver microsomal samples and M3c was detected in all investigated species. In earlier studies by Thevis et al., two bishydroxylated metabolites were detected in human liver S9 and in a dog urine sample[177], but could not be detected in human urine[175].

Additionally, *O*-dephenylation (M4), amide hydrolysis (M5) of ostarine, and subsequent hydroxylation of M5 (M6) were generated from *in vitro* preparations in all investigated species. Previously, the ostarine metabolite formed by *O*-dephenylation has also been observed in bovine[141], and human liver S9[177] incubation samples, as well as canine[177], bovine[141] and human[175] urine samples. A dephenlyated and carboxylated metabolite with *m/z* 301 was found in human[175] and bovine urine samples[141,142] and produced by bovine liver S9 incubations[141], but could not be detected in any of the current study samples. The presence of M5 has also been described in equine urine samples.[164] M6 has been described to be generated from *in vitro* preparations using bovine liver S9 fractions[141] and was observed in bovine[142] as well as rat[19] urine samples following *in vivo* administration. Besides the amide hydrolysis products M5 and M6, 3-(4-cyanophenoxy)-2-hydroxy-2-methylpropanoic acid with *m/z* 220 was initially described by Kim et al. in rat urine samples[19] and later also found in bovine urine samples[142], however, this metabolite could not be detected in this study.

Glucuronidation of ostarine (M7) was produced by *in vitro* incubations with liver microsomes in combination with S9 fractions from all species. A loss of cyanophenol *m/z* 119 yielded the glucuronic acid analogue of *m/z* 269 at *m/z* 445. Moreover, this metabolite has been previously found in bovine[141], rat[19], canine[177] and human[175,176] urine samples, and was generated by human liver S9 incubations[177]. Sulfation of a hydroxylated B-ring metabolite (M8) was observed after incubations with bovine liver microsomes and S9 fractions. Previously, M8 was found in bovine[141], rat[19], canine[177], and human[175] urine samples, and generated by human liver S9[177]. Two metabolites M9a and M9b formed by glucuronidations of hydroxylated B-ring metabolites were derived from *in vitro* preparations. M9a was generated by bovine and M9b was generated by murine, equine, and porcine liver microsomes in combination with S9 fractions. The glucuronidation of M9a and M9b could be assigned to the hydroxylated B-ring due to the molecular ion at *m/z* 310 which corresponds to the glucuronic acid conjugate of the deprotonated hydroxy-4-cyanophenol (*m/z* 176 + *m/z* 134). Other studies reported one glucuronide-conjugated monohydroxylated metabolite of ostarine following *in vivo* administration in bovine[141], rat[19], and canine[177] urine samples, and *in vitro* generated by human liver S9[177], whereas two *in vivo* formed

metabolites were reported in human urine samples[175]. A glucuronidated bishydroxylated metabolite (M10) was produced from *in vitro* incubation samples with liver microsomes in combination with S9 fractions from all investigated species. The glucuronidation of M10 could be assigned to the bishydroxylated B-ring due to the molecular ion at *m/z* 326 which corresponds to the glucuronic acid conjugate of the deprotonated bishydroxy-4-cyanophenol (*m/z* 176 + *m/z* 150). The formation of this metabolite has been previously observed by human liver S9[177] and in a human urine sample[175]. M11 and M12 were formed by sulfation and glucuronidation of M6 respectively. M11 was *in vitro* generated by all investigated species, whereas M12 was only present after *in vitro* incubations of equine and porcine liver microsomes in combination with S9 fractions. Previously, ostarine metabolite M11 formed by sulfation of M6 was reported as in *vivo*-derived metabolite in rat urine samples[19] as well as equine plasma[165] and urine[164] samples, whereas ostarine metabolite M12 formed by glucuronidation of M6 has only been previously reported in equine plasma[165] and urine[164] following *in vivo* administration. Hansson et al. described an *in vivo* formed ostarine metabolite from amide hydrolysis followed by bishydroxylation and sulfation in equine urine[164] and plasma[165] samples, but this metabolite was not detected in the current study.

To summarise, after incubations with liver fractions, ostarine was extensively metabolised in all species, with in total 13 metabolites identified from bovine, equine, and murine incubations and ten from porcine. Most metabolites (M1a, M3c, M4, M5, M6, M7, M10, and M11) were observed in all species examined in this study, with M1b, M2, and M3a generated by bovine, equine and murine liver microsomes, but not by porcine. M9b was produced by equine, porcine and murine liver microsomes in combination with S9, whereas the positional isomer M9a and the sulfated equivalent M8 was only found in incubations with bovine liver microsomes in combination with S9 fractions, with M3b exclusive to rats.

Table 3.3 Elemental compositions, observed masses in negative mode, retention times (RT), and CCS values of ostarine and metabolites found in bovine (B), equine (E), porcine (P), and rats (R) after incubations with microsomes (phase I) and S9 fractions (phase II) and in rat urine (RU) after 1-2 h after administration on day 1 (D1) and day 9 (D9). Collision energy at 20 V for fragment ions (FI), 0 V for precursor ions (PI). Comparison with metabolites found in post-administration rat urine samples with (phase I) and without (phase II) enzymatic hydrolysis. *In vivo* metabolites were ranked by abundance (1 = most abundant).

| Compound/ Metabolic reaction(s) | Negative mode (deprotonated ions) | | | RT min | $^{DT}CCS_{N2}$ Å² | In vitro | | | | In vivo | |
	Elemental composition	Observed PI/FI ions m/z	Error ppm			B	E	P	R	RU D1	D9
Ostarine[α]	$C_{19}H_{13}F_3N_3O_3$	388.0892	-5.7	6.04	193.6	✓	✓	✓	✓	✓	✓
	$C_{12}H_8F_3N_2O_2$	269.0552	3.3								
	$C_{11}H_8F_3N_2O$	241.0576	-7.5								
	$C_8H_4F_3N_2$	185.0330	-1.1								
	C_7H_4NO	118.0307	7.6								
Phase I											
M1a Hydroxylation[α]	$C_{19}H_{13}F_3N_3O_4$	404.0871	1.7	5.95	191.0	✓	✓	✓	✓	✓[3]	✓[3]
	$C_{12}H_8F_3N_2O_2$	269.0542	-0.4								
	$C_8H_4F_3N_2$	185.0336	2.2								
	$C_7H_4NO_2$	134.0255	5.2								
M1b Hydroxylation[α]	$C_{19}H_{13}F_3N_3O_4$	404.0868	1.0	5.79	195.3	✓	✓		✓		✓[5]
	$C_{12}H_8F_3N_2O_2$	269.0557	5.2								
	$C_8H_4F_3N_2$	185.0339	3.8								
	$C_7H_4NO_2$	134.0254	4.5								
M2 Hydroxylation	$C_{19}H_{13}F_3N_3O_4$	404.0850	-3.5	5.70	194.4	✓	✓		✓		
	$C_{11}H_6F_3N_2O_2$	255.0401	5.5								
	$C_8H_4F_3N_2$	185.0344	6.5								
	C_7H_4NO	118.0302	3.4								
M3a Bishydroxylation	$C_{19}H_{13}F_3N_3O_5$	420.0832	4.5	5.75	193.4	✓	✓		✓		
	$C_7H_4NO_3$	150.0202	3.3								
M3b Bishydroxylation	$C_{19}H_{13}F_3N_3O_5$	420.0811	-0.5	5.65	191.9				✓		
	$C_7H_4NO_3$	150.0200	1.3								
M3c Bishydroxylation	$C_{19}H_{13}F_3N_3O_5S$	420.0837	5.7	5.50	194.0	✓	✓	✓	✓		✓[4]
	$C_{12}H_8F_3N_2O_2$	269.0526	-6.3								
	$C_7H_4NO_3$	150.0196	4.0								
M4 *O*-Dephenylation[β]	$C_{12}H_{10}F_3N_2O_3$	287.0642	-2.4	5.04	159.0	✓	✓	✓	✓	✓[2]	✓[2]
	$C_8H_4F_3N_2$	185.0333	0.5								
M5 Amide hydrolysis	$C_8H_4F_3N_2$	185.0338	3.2	4.76	127.0	✓	✓	✓	✓		✓[6]

Table 3.3 *continued*

Compound/ Metabolic reaction(s)	Negative mode (deprotonated ions)			RT min	$^{DT}CCS_{N2}$ Å²	In vitro				In vivo	
	Elemental composition	Observed PI/FI ions *m/z*	Error ppm			B	E	P	R	RU D1	D9
M6 Amide hydrolysis + hydroxylation	$C_8H_4F_3N_2O$	201.0291	5.0	4.72	131.2	✓	✓	✓	✓	✓[1]	✓[1]
	-	181.0226	-								
Phase II											
M7 Glucuronidation	$C_{25}H_{21}F_3N_3O_9$	564.1255	3.5	5.81	225.7	✓	✓	✓	✓	✓[2]	✓[3]
	$C_{18}H_{16}F_3N_2O_8$	445.0871	1.6								
	$C_{19}H_{13}F_3N_3O_3$	388.0908	-1.5								
	$C_{12}H_{10}F_3N_2O_3$	287.0651	0.7								
	$C_{12}H_8F_3N_2O_2$	269.0541	-0.7								
	$C_8H_4F_3N_2$	185.0341	4.9								
	C_7H_4NO	118.0306	6.8								
M8 Hydroxylation + sulfation	$C_{19}H_{13}F_3N_3O_7S$	484.0435	0.6	5.62	199.7	✓				✓[3]	✓[2]
	$C_{19}H_{13}F_3N_3O_4$	404.0870	1.7								
	$C_{12}H_8F_3N_2O_2$	269.0529	-5.2								
	$C_8H_4F_3N_2$	134.0243	-3.7								
M9a Hydroxylation + glucuronidation	$C_{25}H_{21}F_3N_3O_{10}$	580.1202	2.9	5.37	225.8	✓					✓[6]
	$C_{19}H_{13}F_3N_3O_4$	404.0870	1.7								
	$C_{13}H_{12}NO_8$	310.0592	7.7								
	$C_{12}H_8F_3N_2O_2$	269.0538	-1.9								
	$C_7H_4NO_2$	134.0254	4.5								
M9b Hydroxylation + glucuronidation	$C_{25}H_{21}F_3N_3O_{10}$	580.1187	0.3	5.32	223.6		✓	✓	✓		
	$C_{19}H_{13}F_3N_3O_4$	404.0864	0.2								
	$C_{13}H_{12}NO_8$	310.0592	7.7								
	$C_7H_4NO_2$	134.0243	-3.7								
M10 Bishydroxylation + glucuronidation	$C_{25}H_{21}F_3N_3O_{11}$	596.1144	1.7	5.01	227.6	✓	✓	✓	✓		✓[5]
	$C_{19}H_{13}F_3N_3O_5$	420.0817	1.0								
	$C_{13}H_{12}NO_9$	326.0516	-0.6								
	$C_7H_4NO_3$	150.0188	-6.0								
M11 Amide hydrolysis + hydroxylation + sulfation	$C_8H_4F_3N_2O_4S$	280.9868	6.8	4.15	148.8	✓	✓	✓	✓	✓[1]	✓[1]
	$C_8H_4F_3N_2O$	201.0270	-5.5								
	-	181.0214	-								
M12 Amide hydrolysis + hydroxylation + glucuronidation	$C_{14}H_{12}F_3N_2O_7$	377.0611	2.4	3.97	178.3		✓	✓			✓[4]
	$C_8H_4F_3N_2O$	201.0274	-3.5								

[α] Adduct ions formed: Ostarine [M+Cl]⁻ 424.0698 CCS 271.6; M1a [M2-H]⁻ 809.1788 CCS 262.1; M1b [M2-H]⁻ 809.1795 CCS 271.1

[β] Also detected in lower intensity in absence of cofactor NADPH and in absence of tissue fractions
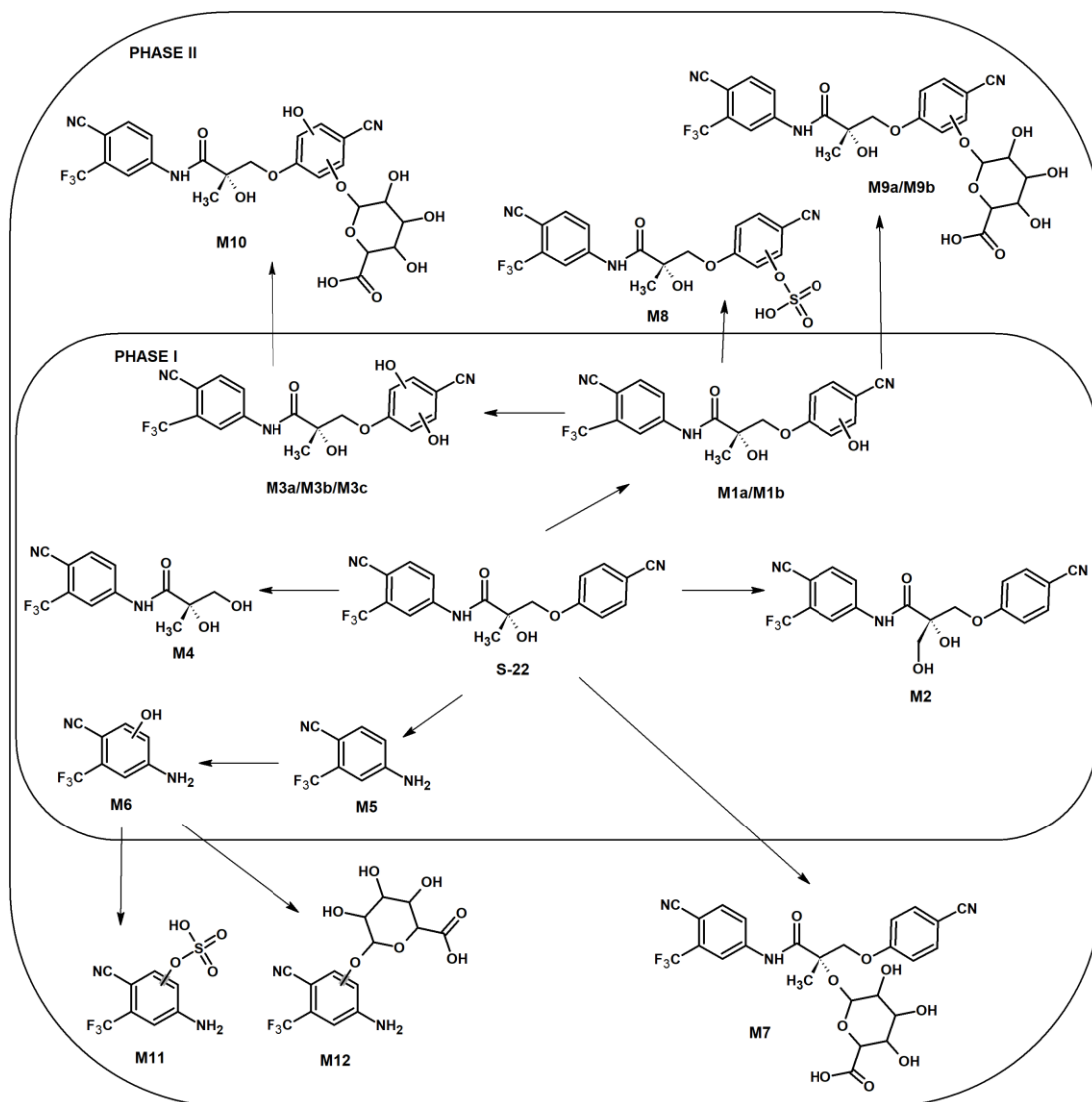
Figure 3.2 Proposed chemical structures of *in vitro* and/or *in vivo* formed phase I and II metabolites of ostarine. Metabolite numbers refer to **Table 3.3**. Arrows indicate tentative metabolic pathways.

3.3.2.2. *In vitro* generated metabolites of LGD-4033

The produced *in vitro* metabolites for LGD-4033 are listed in **Table 3.4** and the proposed metabolic pathway with tentative chemical structures is illustrated in **Figure 3.3**. Mass spectrometric fragmentation of LGD-4033 and its metabolites has previously been described using LC-MS in positive ESI and samples derived from incubations with human liver microsomes or S9 fractions[127], and an athlete's urine sample[132] as well as in negative ESI using an electrochemical synthesis approach and human liver microsomes[49]. Furthermore, studies on LGD-4033 metabolism with human liver microsomes[178], in human urine[178,180], and equine urine and plasma[180] with samples acquired following administration have been conducted.

LGD-4033 was mainly detected as an adduct ion with acetic acid to *m/z* 397 and also as a deprotonated molecular ion at *m/z* 337. LGD-4033 has two asymmetric centres resulting in four stereoisomers. Chiral centres of LGD-4033 are marked with an asterisk * in **Figure 3.3**. Whilst the epimers cannot be seperated, the diastereomers were seperated chromatographically at 6.48 min with a CCS of 179.4 Å² and at 6.34 min with a CCS of 182.8 Å². Two peaks for LGD-4033 were also observed in the study by Fragkaki et al.[179]

M1a was observed after incubations with liver microsomes from all investigated species and is suggested to arise from *N*-oxidation as it elutes at 6.38 min slightly after the main peak for LGD-4033 at 6.34 min. Alternatively, it could be formed from hydroxylation of the LGD-4033 diastereomer at 6.48 min. Due to lack of fragmentation, site of hydroxylation for M1a could not be assigned. Moreover, three hydroxylated metabolites (M1b-d) of LGD-4033 were produced by incubation with bovine, equine, porcine, and murine liver microsomes. Fragments at *m/z* 199, 185, and 170 showed that the trifluoromethyl-benzonitrile moiety stayed intact. Therefore, hydroxlyation of the pyrrolidine moiety is proposed for M1b-d. Additionally, abundant acetate adduct formation for M1c and M1d was observed. Cox et al.[132] reported three *in vivo*-derived metabolites from monohydroxylations on the pyrrolidine ring in a human urine sample that tested positive for LGD-4033, whereas only one was detected in human urine following administration of LGD-4033 to a volunteer by Fragkaki et al.[179]. In comparison, Thevis et al. reported two monohydroxylations on the pyrrolidine moiety produced by human liver microsomal incubations[49]. In the current study monohydroxylation of the benzonitrile aromatic ring was not observed, however, formation of this metabolite was previously described *in vitro* by preparations with human liver

microsomes[49,178] and *in vivo* as it was detected within human urine from a positive doping sample[132].

M2 was generated *in vitro* by microsomal samples from all investigated species. For M2 the fragment ion at *m/z* 253 suggests a hydroxylation on the pyrrolidine part followed by an oxidation to a carbonyl. These metabolic reactions previously yielded one metabolite in samples from incubations with human liver microsomes or S9 fractions[127], four metabolites in a hydrolysed human urine sample[132], and three in another human urine sample after hydrolysis[179].

LGD-4033 metabolite M3a formed by bishydroxylation of the pyrrolidine ring was *in vitro* generated by incubations of liver microsomes from all investigated species. Furthermore, another ostarine metabolite M3b formed by bishydroxylation of the pyrrolidine ring was produced by incubation with equine liver microsomes. One bishydroxylated pyrrolidine moiety metabolite has also been described by previous *in vitro* studies in human[49,127,178] and equine[180], whereas, two metabolites were detected in further studies with human urine samples[132,179]. Formation of an ostarine metabolite derived from monohydroxylation on both aromatic rings has been described *in vitro* using human liver microsomes[49] and *in vivo* in human urine from a positive doping sample [132], but this metabolite was not found in this study.

Previous studies of equine urine samples acquired following LGD-4033 administration detected a trihydroxylated metabolite.[180] Moreover, two trihydroxylated metabolites were found to be excreted in human urine following administration of LGD-4033 to a volunteer.[179] In this study, one trihydroxylation for LGD-4033 was generated for the first time *in vitro* by equine liver microsomes (M4a). Due to the presence of *m/z* 185 (M4a) suggesting that the benzonitrile ring remained unchanged, hydroxylations can be assigned to the pyrrolidine part. LGD-4033 metabolite M5a formed by hydroxylation with subsequent pyrrolidine cleavage (M5a) was observed *in vitro* in all investigates species. Moreover, this metabolite was also observed once in human samples *in vitro*[127] and *in vivo*[132,178,179].

M6 was formed from LGD-4033 after a loss of the pyrrolidine ring with subsequent hydroxylation of M6 leading to M7, both metabolites were *in vitro* generated by all investigated species. While this metabolic reaction (loss of the pyrrolidine ring) has been observed in the metabolism of other compounds with a pyrrolidine ring such as the synthetic cathinones α-pyrrolidinovalerophenone (α-PVP)[447] and methylenedioxy-pyrovalerone (MDPV)[447,448], the current study is the first to observe it for LGD-4033. Furthermore, metabolites with the accurate mass of *m/z* 185.0332 and *m/z* 201.0281 were also formed from

ostarine (**Section 3.3.2.1 Table 3.3**). Therefore, in forensic testing it should be differentiated if these metabolites originate from LGD-4033 or ostarine.

Two metabolites (M8a-b) were formed by glucuronidation of LGD-4033 that could arise from N^+- and O-glucuronidation. M8a was only generated by equine liver S9, whereas M8b was formed by all investigated species. M8a was only formed to a minor degree and chromatographically not well separated from M8b, which could explain why its CCS value was not reported in the feature list. A previous *in vivo* administration study in equine by Hansson et al. supports these findings by describing two glucuronides in urine and plasma with one potentially corresponding to an N^+-glucuronide of LGD-4033.[180] Several other studies analysing human urine samples following LGD-4033 intake only report one glucuronide of LGD-4033.[178–180]

Moreover, four metabolites (M9a-d) were formed through further glucuronidation of hydroxylated LGD-4033 metabolites. M9a was formed *in vitro* by all investigated species, whilst M9b was generated by murine, M9c by murine and equine, and M9d only by equine liver fractions. In accordance with these results, three metabolites formed by glucuronidation and hydroxylation of LGD-4033 were found in equine urine and plasma samples following LGD-4033 administration by Hansson et al.[180].

M10 represents a methoxylated metabolite that was produced by liver microsomes and S9 fractions of all investigated species. Previously, the methylation of hydroxylated LGD-4033 was described for two metabolites formed by human liver microsomes or S9 fractions[127] and one metabolite found in human urine following LGD-4033 intake[179]. A bishydroxylated glucuronated metabolite (M11b) was *in vitro* generated by incubation with rat liver microsomes in combination with S9 fractions, a metabolite which was previously found in equine urine samples[180], but in this study was not produced *in vitro* by equine. Furthermore, all investigated species *in vitro* generated M12 (formed by glucuronidation of M5) and M13 (formed by sulfation of M7). M13 is described for the first time herein as metabolite of LGD-4033, however, it is not a unique metabolite of LGD-4033 as it has also been formed *in vitro* and *in vivo* from ostarine (**Section 3.3.2.1 Table 3.3, Section 3.3.3 Figure 3.6**).

To conclude, a total of 15 metabolites of LGD-4033 was generated by bovine and porcine *in vitro* systems, 19 and 18 were formed by equine and murine respectively; 15 metabolites thereof were produced by all investigated species. One *in vitro*-derived metabolite was shared by two species (M9c in horses and rats), three *in vitro*-derived metabolites (M3b, M4a, M9d) were exclusive to horses and two (M9b, M11b) were exclusively formed by rats.

Table 3.4 Elemental compositions, observed masses in negative mode, retention times, and CCS values of LGD-4033 and metabolites found in bovine (B), equine (E), porcine (P), and rats (R) after incubations with microsomes (phase I) and/or S9 fractions (phase II) and in rat urine (RU) after 1-2 h after administration on day 1 (D1) and day 9 (D9). Collision energy at 20 V for fragment ions (FI), 0 V for precursor ions (PI). Comparison with metabolites found in post-administration rat urine samples with (phase I) and without (phase II) enzymatic hydrolysis. *In vivo* metabolites were ranked by abundance (1 = most abundant).

| Compound/ Metabolic reaction(s) | Negative mode (deprotonated ions) | | | RT min | $^{DT}CCS_{N2}$ Å² | *In vitro* | | | | *In vivo* | |
	Elemental composition	Observed PI/FI ions *m/z*	Error ppm			B	E	P	R	RU D1	D9
LGD-4033[α]	$C_{16}H_{15}F_6N_2O_3$[α]	397.0993[α]	0.3	6.48	179.4	✓	✓	✓	✓		
	$C_{14}H_{11}F_6N_2O$	337.0785	1.2								
	$C_{13}H_{10}F_3N_2O$	267.0757[γ,δ]	2.2								
	$C_{11}H_6F_3N_2O$	239.0437	-0.4								
	$C_8H_3F_4N$	170.0218	-2.9								
LGD-4033[α]	$C_{16}H_{15}F_6N_2O_3$[α]	397.0993[α]	0.3	6.34	182.8	✓	✓	✓	✓	✓	✓
	$C_{14}H_{11}F_6N_2O$	337.0764	-5.0								
	$C_{13}H_{10}F_3N_2O$	267.0742	-3.4								
	$C_{11}H_6F_3N_2O$	239.0449	4.6								
	$C_8H_3F_3N$	170.0231	4.1								
Phase I											
M1a *N*-Oxide/ Hydroxylation	$C_{14}H_{11}F_6N_2O_2$	353.0710	5.7	6.38	167.6	✓	✓	✓	✓	✓[3]	✓[4]
	$C_{13}H_{10}F_3N_2O_2$	283.0720	7.1								
M1b Hydroxylation[α]	$C_{14}H_{11}F_6N_2O_2$	353.0756	7.4	5.85	168.2	✓	✓	✓	✓		
	$C_{10}H_6F_3N_2O$	227.0448	4.4								
	$C_9H_6F_3N_2$	199.0503	7.0								
	$C_8H_4F_3N_2$	185.0331	-0.5								
	$C_8H_3F_3N$	170.0222	-0.6								
M1c Hydroxylation[α]	$C_{16}H_{15}F_6N_2O_4$[α]	413.0970[α]	6.8	5.59	184.6	✓	✓	✓	✓		
	$C_{14}H_{11}F_6N_2O_2$	353.0743	3.7								
	$C_{13}H_{10}F_3N_2O_2$	283.0702	0.7								
	$C_{10}H_6F_3N_2O$	227.0435	-1.3								
	$C_8H_4F_3N_2$	185.0348	8.6								
M1d Hydroxylation[α]	$C_{16}H_{15}F_6N_2O_4$[α]	413.0936[α]	-1.5	5.35	183.7	✓	✓	✓	✓		
	$C_{14}H_{11}F_6N_2O_2$	353.0716	-4.0								
	$C_{10}H_6F_3N_2O$	227.0449	4.8								

Table 3.4 *continued*

Compound/ Metabolic reaction(s)	Negative mode (deprotonated ions)			RT min	$^{DT}CCS_{N2}$ Å^2	In vitro				In vivo	
	Elemental composition	Observed PI/FI ions *m/z*	Error ppm			B	E	P	R	RU D1	D9
M2 Hydroxylation + double bond $^{\alpha}$	$C_{14}H_9F_6N_2O_2$	351.0580	-0.3	5.46	169.0	✓	✓	✓	✓	✓[6]	✓[7]
	$C_{13}H_8F_3N_2O_2$	281.0543 $^{\gamma,\delta}$	2.1								
	$C_{13}H_6F_3N_2O$	263.0441	-3.4								
	$C_{11}H_4F_3N_2O_2$	253.0236	2.4								
	$C_{12}H_8F_3N_2$	237.0656	4.6								
	$C_8H_3F_3N$	170.0236	7.6								
M3a Bishydroxylation	$C_{14}H_{11}F_6N_2O_3$	369.0699	5.4	5.48	174.6	✓	✓	✓	✓	✓[1]	✓[1]
	$C_{13}H_8F_3N_2O_3$	281.0553	3.2								
	$C_{13}H_6F_3N_2O$	263.0436	1.5								
	$C_{12}H_8F_3N_2$	237.0655	4.2								
	$C_8H_4F_3N_2$	185.0339	3.8								
M3b Bishydroxylation	$C_{14}H_{11}F_6N_2O_3$	369.0702	6.2	5.04	170.2		✓				
	$C_{10}H_6F_3N_2O$	227.0455	7.5								
	$C_9H_6F_3N_2$	199.0495	3.0								
	$C_8H_3F_3N$	170.0233	5.9								
M4a Trihydroxylation	$C_{14}H_{11}F_6N_2O_4$	385.0647	4.7	5.35	173.9		✓			✓[8]	✓[5]
	$C_{12}H_6F_3N_2O$	251.0453	6.0								
	$C_{10}H_6F_3N_2O$	227.0452	6.2								
	$C_9H_6F_3N_2$	199.0481	-4.0								
	$C_8H_3F_3N$	170.0228	2.9								
M4b Trihydroxylation	$C_{14}H_{11}F_6N_2O_4$	385.0651	5.7	5.27	175.2					✓[4]	✓[3]
	$C_{11}H_7F_6N_2O$	297.0493	8.4								
	$C_{12}H_8F_3N_2O_2$	269.0551	3.0								
	$C_{12}H_6F_3N_2O$	251.0427	-4.4								
	$C_{11}H_8F_3N_2O$	241.0607	5.4								
	$C_8H_4F_3N_2$	185.0349	9.2								
M5a Hydroxylation + pyrrolidine ring cleavage	$C_{14}H_{13}F_6N_2O_2$	355.0897	2.8	5.71	172.1	✓	✓	✓	✓		
	$C_{13}H_{12}F_3N_2O_2$	285.0858	0.7								
	$C_{12}H_8F_3N_2O$	253.0593	-0.4								
	$C_{10}H_6F_3N_2O$	227.0440	0.9								
	$C_8H_4F_3N_2$	185.0341	4.9								

Table 3.4 *continued*

| Compound/ Metabolic reaction(s) | Negative mode (deprotonated ions) | | | RT min | $^{DT}CCS_{N2}$ Å² | In vitro | | | | In vivo RU | |
	Elemental composition	Observed PI/FI ions *m/z*	Error ppm			B	E	P	R	D1	D9
M5b	$C_{14}H_{13}F_6N_2O_2$	355.0915	7.9	5.55	170.2	✓	✓	✓	✓	✓[5]	✓[8]
Hydroxylation	$C_{13}H_{12}F_3N_2O_2$	285.0872	5.6								
+ pyrrolidine ring	$C_{12}H_{12}F_3N_2O$	257.0921	7.8								
cleavage	$C_{10}H_5F_3N_2O$	226.0369	1.8								
	$C_9H_6F_3N_2$	199.0497	4.0								
	$C_8H_4F_3N_2$	185.0350	9.7								
	$C_8H_3F_3N$	170.0235	7.1								
M6 Loss of pyrrolidine	$C_8H_4F_3N_2$	185.0336	2.2	4.76	126.9	✓	✓	✓	✓	✓[7]	✓[6]
M7 Loss of	$C_8H_4F_3N_2O$	201.0276	-2.5	4.73	131.4	✓	✓	✓	✓	✓[2]	✓[2]
pyrrolidine	-	181.0256	-								
+ hydroxylation	-	154.0144	-								
Phase II											
M8a	$C_{20}H_{19}F_6N_2O_7$	513.1105	0.6	6.03	-		✓				
Glucuronidation	$C_{13}H_{10}F_3N_2O$	267.0763	1.9								
	$C_5H_5O_3$	113.0244	0.0								
M8b	$C_{20}H_{19}F_6N_2O_7$	513.1094	-1.6	5.94	201.8	✓	✓	✓	✓	✓[3]	✓[5]
Glucuronidation	$C_{14}H_{11}F_6N_2O$	337.0763	-5.3								
	$C_{13}H_{10}F_3N_2O$	267.0737	-5.2								
	$C_6H_7O_6$	175.0248	0.0								
M9a Hydroxylation + glucuronidation	$C_{20}H_{19}F_6N_2O_8$	529.1061	1.9	5.87	204.4	✓	✓	✓	✓	✓[2]	✓[2]
M9b	$C_{20}H_{19}F_6N_2O_8$	529.1054	0.4	5.41	210.7				✓		
Hydroxylation	$C_{14}H_{11}F_6N_2O_2$	353.0734	1.1								
+ glucuronidation	$C_{10}H_6F_3N_2O$	227.0452	6.2								
	$C_5H_5O_3$	113.0244	8.8								
M9c	$C_{20}H_{19}F_6N_2O_8$	529.1035	-3.0	5.06	208.1		✓		✓		
Hydroxylation	$C_6H_9O_7$	193.0348	-3.1								
+ glucuronidation	$C_5H_5O_3$	113.0235	-8.0								
M9d	$C_{20}H_{19}F_6N_2O_8$	529.1047	-0.8	4.85	210.4		✓				
Hydroxylation + glucuronidation	$C_6H_9O_7$	193.0339	-7.8								

Table 3.4 *continued*

Compound/ Metabolic reaction(s)	Negative mode (deprotonated ions)			RT min	$^{DT}CCS_{N2}$ Å²	In vitro				In vivo RU	
	Elemental composition	Observed PI/FI ions *m/z*	Error ppm			B	E	P	R	D1	D9
M10 Hydroxylation + methylation[α β]	$C_{17}H_{17}F_6N_2O_4$[α]	427.1093 [α]	-1.4	6.16	188.6	✓	✓	✓	✓		
	$C_{15}H_{14}F_6N_2O_2$	367.0910	6.3								
	$C_{14}H_{12}F_3N_2O_2$	297.0866 [γ,δ]	3.4								
	$C_{13}H_8F_3N_2O$	265.0614	7.5								
	$C_{12}H_8F_3N_2$	237.0664	8.0								
M11a Bishydroxylation + glucuronidation	$C_{20}H_{19}F_6N_2O_9$	545.0978	-4.0	5.12	203.9						✓[3]
	$C_{14}H_{11}F_6N_2O_3$	369.0663	-4.3								
	$C_5H_5O_3$	113.0251	6.2								
M11b Bishydroxylation + glucuronidation	$C_{20}H_{19}F_6N_2O_9$	545.1003	0.6	4.94	205.3				✓		✓[4]
	$C_{14}H_{11}F_6N_2O_3$	369.0691	3.3								
	$C_6H_9O_7$	193.0347	-3.6								
	$C_5H_5O_3$	113.0248	3.5								
M12 Hydroxylation + pyrrolidine ring cleavage + glucuronidation	$C_{20}H_{21}F_6N_2O_8$	531.1193	-2.8	5.26	209.7	✓	✓	✓	✓		
M13 Loss of pyrrolidine + hydroxylation + sulfation	$C_8H_4F_3N_2O_4S$	280.9858	3.2	4.15	148.6	✓	✓	✓	✓	✓[1]	✓[1]
	$C_8H_4F_3N_2O$	201.0294	6.5								
	-	181.0226	-								

[α] Adduct ions formed: LGD-4033 [M-H+CH₃CO₂H]⁻ 397.0993 CCS 182.8 (RT 6.34) and 179.4 (RT 6.48)

M1b [M+Cl]⁻ 389.0514 CCS 174.9, [M-H+CH₃CO₂Na]⁻ 435.0739 CCS 187.3, [2M-H]⁻ 707.1532 CCS 237.1

M1c [M-H +CH₃CO₂H]⁻ 413.0970 CCS 184.6

M1d [M-H +CH₃CO₂H]⁻ 413.0980 CCS 183.7

M2 [M+Cl]⁻ 387.0357 CCS 174, [M-H +CH₃CO₂H]⁻ 411.0794 CCS 182.3

M5a [M+Cl]⁻ 391.0646 CCS 179.8

M5b [M+Cl]⁻ 391.0650 CCS 177.6, [2M-H]⁻ 711.1827 CCS 253.6

M10 [M-H+CH₃CO₂H]⁻ 427.1093 CCS 188.6

[β] Also detected in lower intensity in absence of cofactor NADPH

[γ] post-source fragmentation

[δ] in-source fragmentation
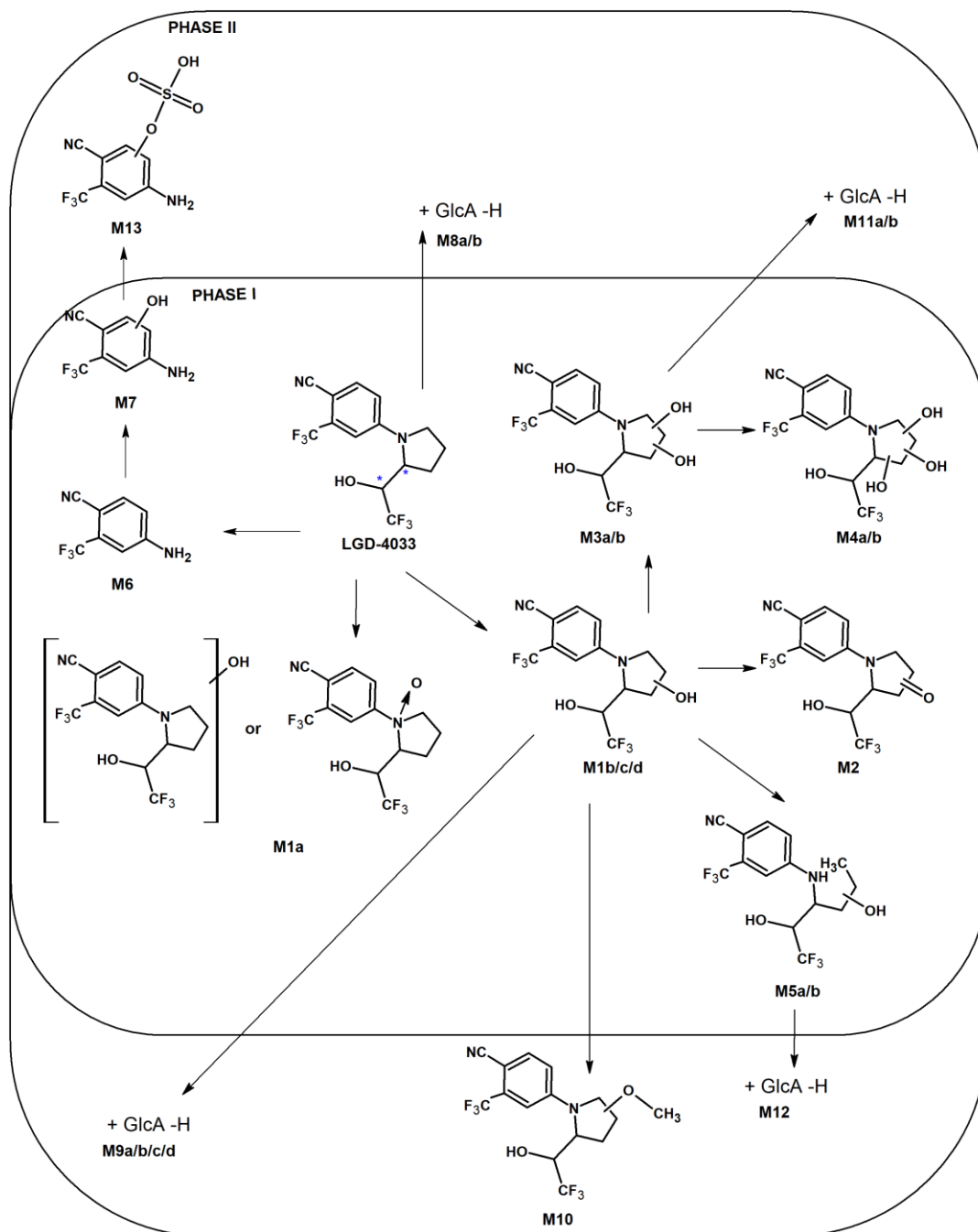
Figure 3.3 Proposed chemical structures of *in vitro* and *in vivo* formed phase I and II metabolites of LGD-4033. Metabolite numbers refer to **Table 3.4**. Arrows indicate tentative metabolic pathways.

3.3.2.3. *In vitro* generated metabolites of RAD140

RAD140 was found to be poorly metabolised in all species with observed metabolites listed in **Table 3.5** and corresponding proposed metabolic pathway with tentative chemical structures illustrated in **Figure 3.4**.

The molecular ion of RAD140 at *m/z* 392 could not be detected with RAD140 principally reported as a chloride adduct at *m/z* 428. Additionally, in-source fragmentation of RAD140 was seen to lead to the loss of an acetaldehyde group (- 44 Da) resulting in a fragment ion at *m/z* 348 - this mass spectrometric fragmentation of RAD140 has been previously described by Sobolevsky et al.[181]

Three monohydroxylated metabolites M1a, M1b, and M1c were observed. The detected fragment ion at *m/z* 193.0174 for M1a and M1c corresponds to a + 16 Da shift of the 2-chloro-3-methylbenzonitrile moiety, and hence hydroxylation is proposed on this residue. Due to a lack of fragmentation, the site of hydroxylation for M1b cannot be elucidated. M1a and M1b were exclusively produced by bovine liver microsomes, whereas M1c was *in vitro* generated by all studied species. A study by Sobolevsky et al.[181] has also previously described two hydroxy-metabolites in human urine samples after RAD140 administration and the formation of one hydroxy- and one bishydroxy-metabolite after incubation of RAD140 with human liver microsomes. However, in the current study a bishydroxy-metabolite was not formed by *in vitro* incubation samples.

Glucuronidation of RAD140 (M2) was observed to be formed *in vitro* in all studied species, and moreover two metabolites, M3a-b, were formed through hydroxylation and glucuronidation. M3a was produced by bovine and porcine *in vitro* preparations with the fragment ion at *m/z* 193.0174 pointing at hydroxylation of the 2-chloro-3-methylbenzonitrile residue. M3b was generated by bovine, equine, and murine liver microsomes and could not be further structurally elucidated due to a lack of fragmentation, and it could not be determined if these metabolites (M2, M3a-b) are *N*- or *O*-glucuronides. In accordance with this study, previous investigations by Sobolevsky et al. of human urine samples acquired following RAD140 intake have reported conjugation of RAD140 and two of its hydroxy metabolites with glucuronic acid.[181]

Table 3.5 Elemental compositions, observed masses in negative mode, retention times, and CCS values of RAD140 and metabolites found in bovine (B), equine (E), porcine (P), and rats (R) after incubations with microsomes (phase I) and/or S9 fractions (phase II) and in rat urine (RU) after 1-2 h after administration on day 1 (D1) and day 9 (D9). Collision energy at 20 V for fragment ions (FI), 0 V for precursor ions (PI). Comparison with metabolites found in post-administration rat urine samples with (phase I) and without (phase II) enzymatic hydrolysis.

| Compound/ Metabolic reaction(s) | Negative mode (deprotonated ions) | | | RT min | $^{DT}CCS_{N2}$ Å² | In vitro | | | | In vivo RU | |
	Elemental composition	Observed PI/FI ions *m/z*	Error ppm			B	E	P	R	D1	D9
RAD140[α]	$C_{20}H_{15}ClN_5O_2$[α]	428.0708[α]	4.9	5.89	204.4	✓	✓	✓	✓	✓	✓
	$C_{18}H_{11}ClN_5O$	348.0657[γ]	-0.3								
	$C_{17}H_{10}ClN_4O$	321.0551	0.9								
	$C_8H_5N_2O$	145.0411	2.8								
	$C_8H_3N_2$	127.0305	2.4								
RAD140 - acetaldehyde[δ]	$C_{18}H_{11}ClN_5O$	348.0667	2.6	5.89	195.1	✓	✓	✓	✓		✓
	$C_8H_3N_2$	127.0306	3.1								
Phase I											
M1a Hydroxylation	$C_{20}H_{15}ClN_5O_3$	408.0886	4.2	5.85	191.2	✓					
	$C_{18}H_{11}ClN_5O_2$	364.0619[γ]	3.3								
M1a Hydroxylation - acetaldehyde[δ]	$C_{18}H_{11}ClN_5O_2$	364.0626	5.2	5.85	182.3	✓					
	$C_9H_6ClN_2O$	193.0174	0.0								
	$C_8H_5ClN_2O$	180.0109	4.4								
	$C_8H_5N_2O$	145.0413	4.1								
M1b Hydroxylation	$C_{20}H_{15}ClN_5O_3$	408.0904	8.6	5.62	201.4	✓					
	$C_{18}H_{11}ClN_5O_2$	364.0631[γ]	6.6								
M1c Hydroxylation[α]	$C_{20}H_{16}ClN_5O_3$[α]	444.0665[α]	6.5	5.35	204.7	✓	✓	✓	✓		
	$C_{20}H_{15}ClN_5O_3$	408.0883	3.4								
	$C_{18}H_{11}ClN_5O_2$	364.0611[γ]	1.1								
	$C_9H_6ClN_2O$	193.0175	0.5								
	$C_9H_4N_3O$	170.0370	5.9								
M1c Hydroxylation - acetaldehyde[δ]	$C_{18}H_{11}ClN_5O_2$	364.0617	2.7	5.35	189.7	✓	✓	✓	✓	✓	✓
	$C_9H_4N_3O$	170.0366	3.5								
Phase II											
M2 Glucuronidation	$C_{26}H_{23}ClN_5O_8$	568.1245	0.7	5.52	230.2	✓	✓	✓	✓		
	$C_9H_9O_7$	193.0354	0.0								

Table 3.5 *continued*

| Compound/ Metabolic reaction(s) | Negative mode (deprotonated ions) | | | RT min | $^{DT}CCS_{N2}$ Å² | In vitro | | | | In vivo | |
	Elemental composition	Observed PI/FI ions *m/z*	Error ppm			B	E	P	R	RU D1	D9
M3a Hydroxylation + glucuronidation	$C_{26}H_{23}ClN_5O_9$	584.1223	5.6	5.37	228.3	✓		✓			
	$C_{24}H_{19}ClN_5O_8$	540.0931	0.6								
	$C_{18}H_{11}ClN_5O_2$	364.0628	5.8								
	$C_9H_6ClN_2O$	193.0181	3.6								
	$C_9H_4N_3O$	170.0365	2.9								
	$C_8H_5N_2O$	145.0414	4.8								
	$C_{18}H_{11}ClN_5O_2$	364.0619 [γ]	3.3								
M3b Hydroxylation + glucuronidation	$C_{26}H_{23}ClN_5O_9$	584.1195	0.9	5.02	230.3	✓	✓		✓		
	$C_{24}H_{19}ClN_5O_8$	540.0935	1.3								
	$C_{18}H_{11}ClN_5O_2$	364.0607	0.0								
	$C_9H_9O_7$	193.0356	1.0								

[α] Adduct ions formed: RAD140 [M+Cl]⁻ 428.0708 CCS 204.4

M1c [M+Cl]⁻ 444.0665 CCS 204.7

[γ] post-source fragmentation

[δ] in-source fragmentation
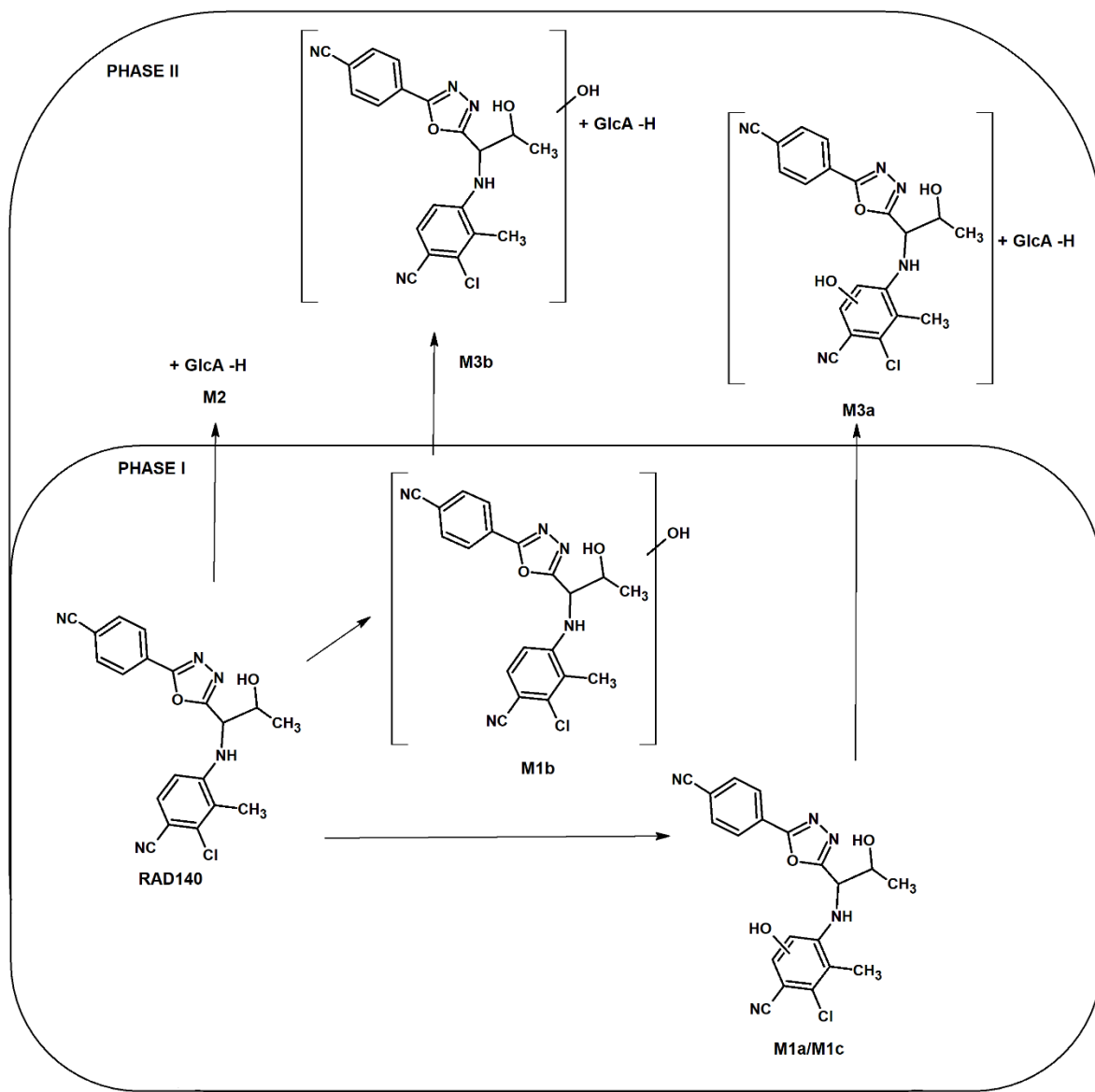
GlcA ... Glucuronic acid

Figure 3.4 Proposed chemical structures of *in vitro* and/or *in vivo* formed phase I and II metabolites of RAD140. Metabolite numbers refer to **Table 3.5**. Arrows indicate tentative metabolic pathways.

3.3.3. Comparison of *in vitro* and *in vivo* formed SARM compound metabolite profiles

In order to assess how accurately *in vitro* generated metabolites reflect *in vivo* formed metabolites of SARMs, urine obtained from Sprague-Dawley rats that were administered different SARM compounds was investigated. After two hours of initial oral drug administration urine samples were collected over the duration of an hour, this was repeated following daily SARM administration on day nine. Urine samples were either directly analysed for detection of phase II metabolites or hydrolysed with β-glucuronidase/arylsulfatase for detection of phase I metabolites. Observed urinary metabolites are summarised within **Table 3.3** (ostarine), **Table 3.4** (LGD-4033), and **Table 3.5** (RAD140) - Phase I and II metabolites are ranked by abundance separately (1 = most abundant). As observed for *in vitro* metabolism, ostarine and LGD-4033 were extensively metabolised and produced several *in vivo* metabolites whereas RAD140 was metabolically stable and only one *in vivo* formed phase I metabolite was observed. Several *in vivo* formed metabolites were observed in rat urine samples collected after initial administration of ostarine and LGD-4033, with further metabolites found in the samples collected following nine days of repeated compound administrations.

For ostarine, the unchanged parent compound was observed in samples derived from *in vitro* incubations of rat microsomes/S9 fractions and in rat urine samples from the *in vivo* administration study. The majority of metabolites observed in rat urine samples were produced by rat liver microsomal/S9 fractions including M1a, M1b, M3c, M4, M5, M6, and M7. Formation of one monohydroxylated (M2), two bishydroxylated (M3a and M3b), and one hydroxylated glucuronide metabolite (M9b) by rat liver microsomes could not be confirmed within rat urine samples. Conversely, a structural isomer of M9b (M9a) was observed exclusively in rat urine following ostarine administration, and likewise two phase II metabolites (M8 and M12) were found in rat urine samples, but not within *in vitro* preparations.

LGD-4033 was observed to be excreted unmodified in rat urine to a minor extent with the intact compound also present following incubations with rat liver microsomes/S9. Several metabolites (M1b-d, M5a, M9b-c, M10, M12) were limited to detection within *in vitro* preparations in rats. Previously, the formation of M10 has been reported in human liver S9 fractions[127], however, in the current study it has not been detected within *in vivo* samples. Conversely, M11a was found to be excreted in rat urine but was not generated via *in vitro*

preparations, with trihydroxyltions (M4a-b) similarly only present in rat urine samples following LGD-4033 administration but not produced by rat liver microsomes. However, a number of observed metabolites (M1a, M2, M3a, M5b, M6, M7, M8b, M9a, M11b, M13) in rats were formed *in vitro* by liver micrsosomes alone (phase I) or in combination with S9 fractions (phase II) and *in vivo* following LGD-4033 administration with subsequent excretion into urine. This is the first study to describe the loss of the pyrrolidine ring as a pathway for LGD-4033 metabolism, with associated metabolites M6, M7 and M13 all found to be formed by *in vitro* incubations and following *in vivo* administration (**Figure 3.5**). As these metabolites were also seen to be formed post ostarine administration (**Figure 3.6**), monitoring of the parent compounds and/or further metabolites should be used to discriminate intake of these two SARMs. Moreover, 4-amino-2-(trifluoromethyl)benzonitrile (ostarine M5, LGD-4033 M6) is also an impurity defined by the European Pharmacopoeia and a reported *in vitro* formed rat metabolite of the anti-prostate cancer drug bicalutamide (Casodex).[426] The pyrrolidine ring within LGD-4033 makes it highly suceptible to metabolism[449], and in the current study, the bishydroxy metabolite M3a was the main phase I metabolite observed in rat urine samples following LGD-4033 administration. This is in accordance with Sobolevsky et al. who recommended the bishydroxlyated metabolite for monitoring of LGD-4033 in human urine[178], which was subsequently supported by the case report of detection of LGD-4033 in an athlete's urine [132].

As observed during *in vitro* metabolite investigations, RAD140 was metabolically stable following *in vivo* administration. Besides the parent compound detected as a chloride adduct and/or as an in-source fragment (cleavage of acetaldehyde) in rat urine, one hydroxylated metabolite was detected after in-source cleavage of acetaldehyde (M1c) within both *in vitro* prepared samples and rat urine samples following RAD140 administration. Phase II metabolites were not detected within rat urine after RAD140 treatment, whilst a glucuronide of RAD140 and the hydroxylated metabolite were produced by rat liver microsomes in combination with S9 fractions. This is in accordance with observations of the high metabolic stability of RAD140 in previous experiments with rat, monkey, and human liver microsomes.[53] By introducing a 4'-blocking group to the phenyl ring, Miller et al. avoided P450-mediated hydroxylation of this moiety yielding a high metabolically stable SARM.[53] Sobolevsky et al. suggest that monitoring of the unchanged compound RAD140 is sufficient[181], which is supported by the current study taking in-source fragmentation and adduct formation into account.
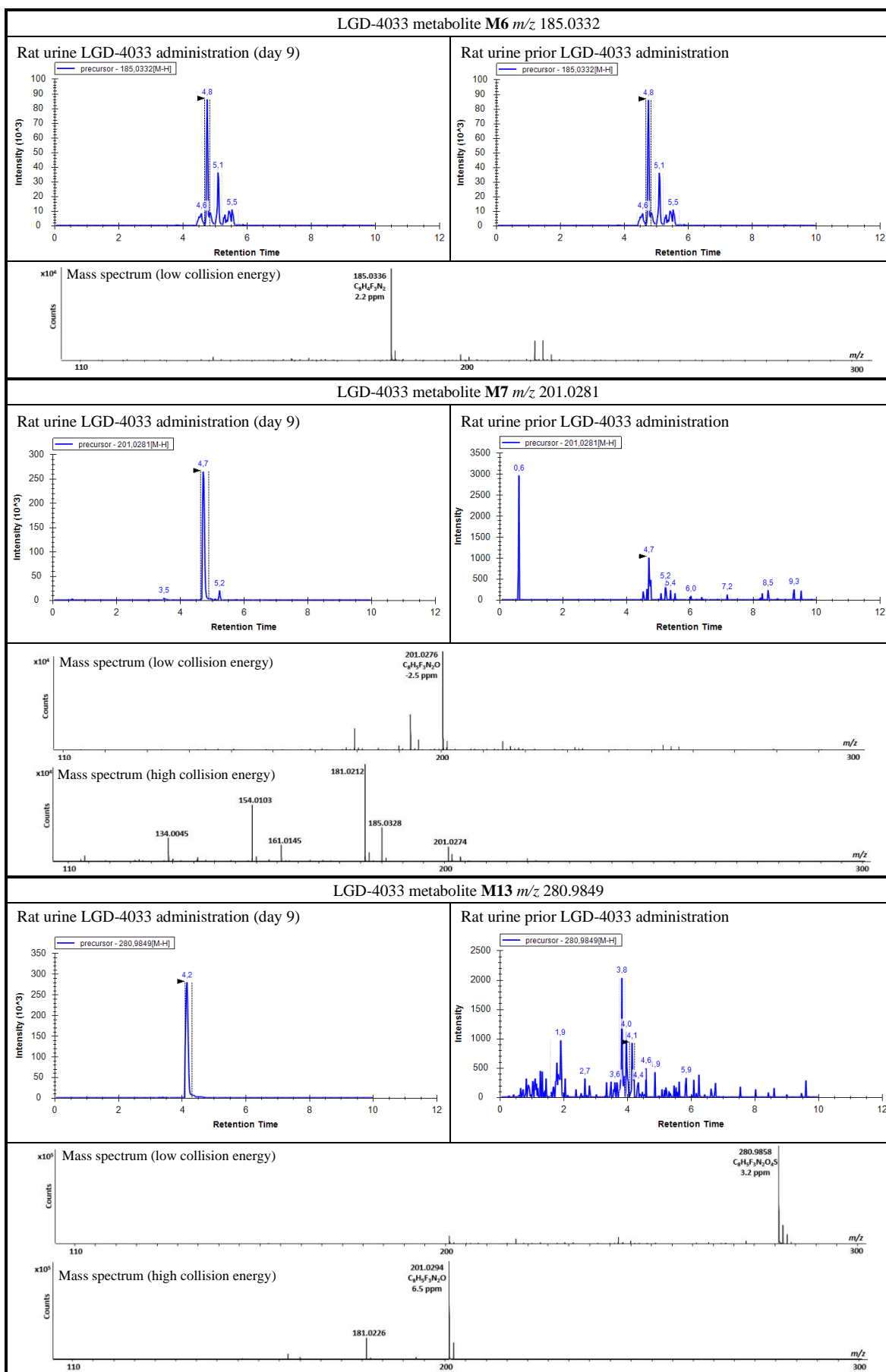
Figure 3.5 EICs of LGD-4033 metabolites M6, M7, and M13 from rat urine following administration (left) and prior to administration (right). Mass spectra with low and high collision energy shown below.
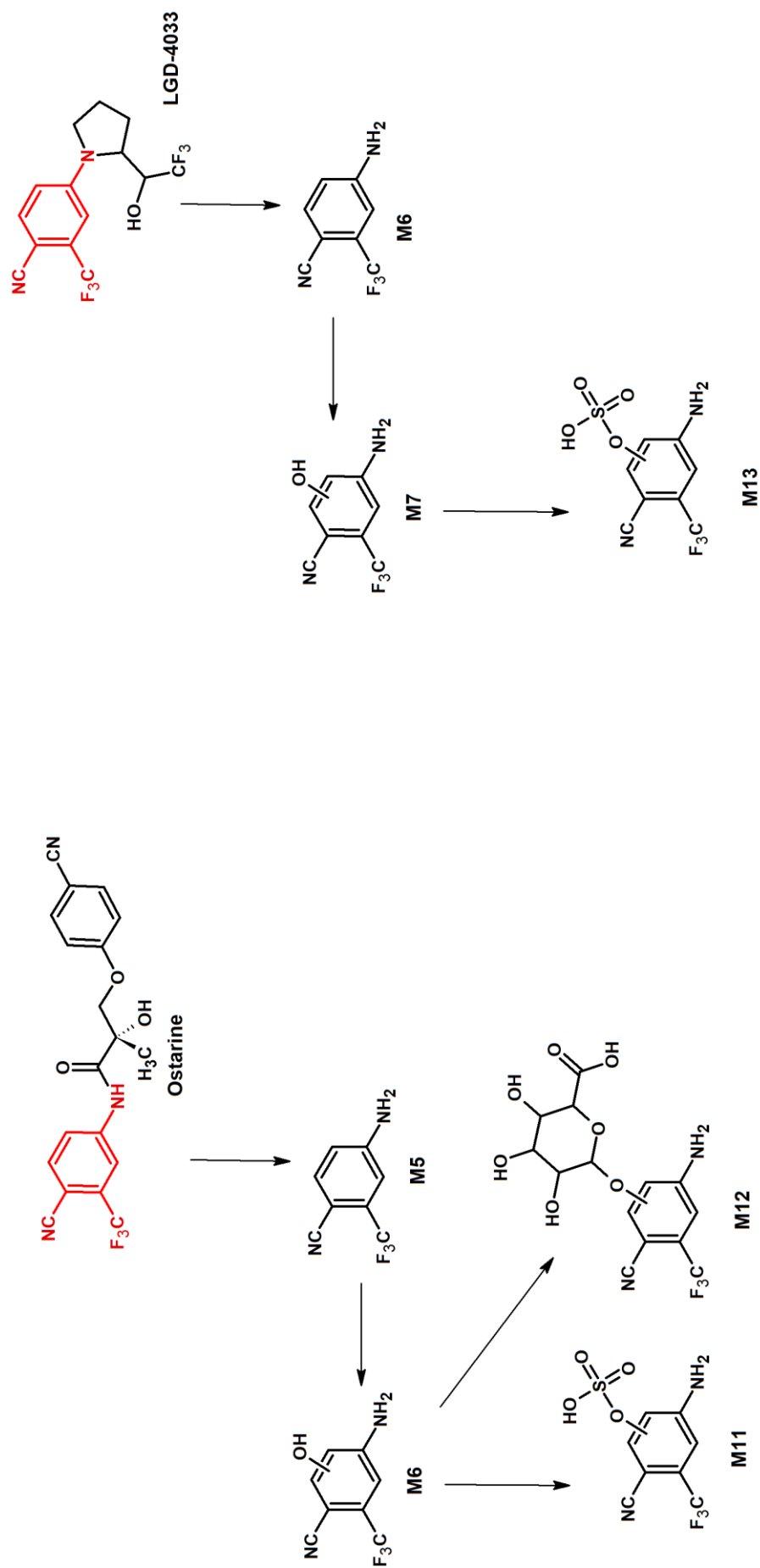
Figure 3.6 Conversion of ostarine and LGD-4033 to 4-amino-2-(trifluoromethyl)benzonitrile, M5 and M6 respectively, subsequent hydroxylation (ostarine M6, LGD-4033 M7) followed by sulfation (ostarine M11, LGD-4033 M13) or glucuronidation (ostarine M12). Numbers of metabolites (M) have been retained from **Table 3.3** for ostarine and **Table 3.4** for LGD-4033.

Table 3.6 Summary of *in vitro* and *in vivo* metabolites of ostarine, LGD-4033, and RAD140 found after incubations with bovine (B), equine (E), porcine (P), rat (R) microsomes (phase I metabolites) plus S9 fractions (phase II metabolites) and in rat urine after administration.

Compound/Metabolic reaction(s)	*In vitro*				*In vivo* RU	
	B	E	P	R	D1	D9
Ostarine	✓	✓	✓	✓	✓	✓
M1a Hydroxylation	✓	✓	✓	✓	✓	✓
M1b Hydroxylation	✓	✓		✓		✓
M2 Hydroxylation	✓	✓		✓		
M3a Bishydroxylation	✓	✓		✓		
M3b Bishydroxylation				✓		
M3c Bishydroxylation	✓	✓	✓	✓		✓
M4 *O*-Dephenylation	✓	✓	✓	✓	✓	✓
M5 Amide hydrolysis	✓	✓	✓	✓		✓
M6 Amide hydrolysis + hydroxylation	✓	✓	✓	✓	✓	✓
M7 Glucuronidation	✓	✓	✓	✓	✓	✓
M8 Hydroxylation + sulfation	✓				✓	✓
M9a Hydroxylation + glucuronidation	✓					✓
M9b Hydroxylation + glucuronidation		✓	✓	✓		
M10 Bishydroxylation + glucuronidation	✓	✓	✓	✓		✓
M11 Amide hydrolysis + hydroxylation + sulfation	✓	✓	✓	✓	✓	✓
M12 Amide hydrolysis + hydroxylation + glucuronidation		✓	✓			✓
LGD-4033 (RT 6.48 min)	✓	✓	✓	✓		
LGD-4033 (RT 6.34 min)	✓	✓	✓	✓	✓	✓
M1a *N*-Oxide/ Hydroxylation	✓	✓	✓	✓	✓	✓
M1b Hydroxylation	✓	✓	✓	✓		
M1c Hydroxylation	✓	✓	✓	✓		
M1d Hydroxylation	✓	✓	✓	✓		
M2 Hydroxylation + double bond	✓	✓	✓	✓	✓	✓
M3a Bishydroxylation	✓	✓	✓	✓	✓	✓
M3b Bishydroxylation		✓				
M4a Trihydroxylation		✓			✓	✓
M4b Trihydroxylation					✓	✓
M5a Hydroxylation + pyrrolidine ring cleavage	✓	✓	✓	✓		
M5b Hydroxylation + pyrrolidine ring cleavage	✓	✓	✓	✓	✓	✓
M6 Loss of pyrrolidine	✓	✓	✓	✓	✓	✓
M7 Loss of pyrrolidine + hydroxylation	✓	✓	✓	✓	✓	✓
M8a Glucuronidation		✓				
M8b Glucuronidation	✓	✓	✓	✓	✓	✓
M9a Hydroxylation + glucuronidation	✓	✓	✓	✓	✓	✓
M9b Hydroxylation + glucuronidation				✓		
M9c Hydroxylation + glucuronidation		✓		✓		
M9d Hydroxylation + glucuronidation		✓				
M10 Hydroxylation + methylation	✓	✓	✓	✓		
M11a Bishydroxylation + glucuronidation						✓
M11b Bishydroxylation + glucuronidation				✓		✓
M12 Hydroxylation + pyrrolidine ring cleavage + glucuronidation	✓	✓	✓	✓		
M13 Loss of pyrrolidine + hydroxylation + sulfation	✓	✓	✓	✓	✓	✓

Table 3.6 *continued*

Compound/Metabolic reaction(s)	*In vitro*				*In vivo*	
					RU	
	B	E	P	R	D1	D9
RAD140	✓	✓	✓	✓	✓	✓
RAD140 - acetaldehyde	✓	✓	✓	✓		✓
M1a Hydroxylation	✓					
M1a Hydroxylation - acetaldehyde	✓					
M1b Hydroxylation	✓					
M1c Hydroxylation	✓	✓	✓	✓		
M1c Hydroxylation - acetaldehyde	✓	✓	✓	✓	✓	✓
M2 Glucuronidation	✓	✓	✓	✓		
M3a Hydroxylation + glucuronidation	✓		✓			
M3b Hydroxylation + glucuronidation	✓	✓		✓		

3.4 Conclusions

In-house prepared liver microsomes and S9 fractions from cattle, horses, pigs, and rats were used to generate species-specific metabolites of SARM compounds ostarine, LGD-4033, and RAD140. Whilst characterisation of isolated liver fractions revealed significant differences with regards to the total P450 content, cytochrome b_5 content, and NADPH-cytochrome P450 reductase activity between species (**Section 3.3.1**), no generalisations could be made in relation to the complexity of drug metabolism between these species. For example, whilst murine liver microsomes were shown to contain the highest amount of P450, which intuitively points to a higher level of enzymatic activity, porcine liver microsomes however exhibited the highest activity towards P450-mediated 7-ethoxycoumarin *O*-dealkylation.

Comparative investigations of *in vitro* formed metabolites of SARM compounds between species were performed by UHPLC-IM-QTOF MS analyses. Although in this study structural isomers such as hydroxylated metabolites were already well separated by reversed-phase chromatography, IM-MS enabled further distinguishing of metabolites based on determined CCS values with observed differences in the range of 0.14 % to 4.06 %. The comparison of theoretical CCS values to experimental CCS values typically produces relatively large errors (e.g. MOBCAL trajectory method[450] root mean square error 15.05 %[451], MetCCS Predictor[452] median relative error of ~ 3 %[453], ISiCLE (based on refactoring MOBCAL code for trajectory method calculations) average error 3.2 %[454], DeepCCS median relative error 2.7 %[455]) which may hinder further structural characterisation of isomers in the current study. Therefore, the possibility of using a computational approach to gain additional structural insights was not explored. As CCS values are largely independent of sample matrix, analyte concentration, and chromatography, the CCS values of SARM metabolites calculated herein can be used as additional identifiers for compound identification by other laboratories. Drift time alignment aided removal of interfering ions from high and low energy mass spectra, improving the quality of data generated.

Although adduct formation depends on solvent types, mobile phase additives, and source conditions, it plays a significant role in the monitoring of SARMs with the adduct of LGD-4033 been previously shown to extend the detection time in equine plasma and lower the limit of detection (LOD) in equine plasma and urine.[180] In the present study, extensive acetate adduct formation was observed for LGD-4033 and the associated metabolites M1c-

d and M10. The deprotonated molecule of RAD140 and its hydroxylated metabolite M1c could not be detected, the compounds either formed chloride adducts or were fragmented in-source by cleavage of acetaldehyde.

As summarised in **Table 3.6** interspecies differences within determined *in vitro* metabolite profiles were observed, highlighting the need to study the metabolism of emerging anabolic agents such as SARMs specifically within the species of interest. Although, numerous *in vitro* formed metabolites for ostarine (eight out of 16 *in vitro*-derived metabolites), LGD-4033 (15 out of 22) and RAD140 (two out of six) were demonstrated to be shared by all species, several *in vitro* generated metabolites were seen to be exclusively associated to individual species e.g. equine (M3b, M4a, M8a, and M9d from LGD-4033), bovine (M8 and M9a from ostarine, M1a-b from RAD140) or rodent (M3b from ostarine, M9b and M11b from LGD-4033), with no distinctive *in vitro*-derived metabolites observable for porcine. Other metabolites were formed *in vitro* by three species (M1b, M2, and M3 from ostarine and M3b from RAD140 in bovine, equine, and murine as well as M9b from ostarine in equine, porcine, and murine) or two species (M12 from ostarine in equine and porcine, M9c from LGD-4033 in equine and murine, M3a from RAD140 in bovine and porcine) with no observed predictable pattern. Although sulfation has been reported to be absent or reduced in pigs than in other species[456], pig liver microsomes in combination with S9 fractions produced two metabolites (M11 from ostarine, M13 from LGD-4033) that were formed by sulfate conjugation to the hydroxylated 4-amino-2-(trifluoromethyl)benzonitrile metabolite. Three distinct metabolites with identical chemical structures (same RT, precursor and fragment ions, and CCS values) were formed from both ostarine (M5, M6, M11) and LGD-4033 (M6, M7, M13) in all investigated species by *in vitro* incubations and following *in vivo* administration. These metabolites were described for LGD-4033 for the first time in this study.

For rats the *in vitro* approach using liver microsomes alone (phase I metabolites) or in combination with S9 fractions (phase II metabolites) from rats, was seen to generate the majority of *in vivo* formed urinary metabolites as summarised in **Table 3.6**. For RAD140 only one *in vivo* formed metabolite by hydroxylation was found in urine, which was also generated by incubations with rat liver microsomes. Nine out of the 12 observed rat urinary metabolites for ostarine were also generated by *in vitro* incubation of this SARM compound with rat liver fractions, with only three phase II metabolites (M8, M9a, M12) detected in rat urine that were not produced *in vitro*. Similarly, ten out of 13 *in vivo* formed LGD-4033 metabolites were observed following *in vitro* incubations, with three metabolites (two phase

I metabolites M4a-b and one phase II metabolite M11a) observed exclusively in urine. Conversely, several metabolites (M2, M3a-b, and M9b for ostarine; M1b-d, M5a, M9b-c, M10, and M12 for LGD-4033; and M2 and M3b for RAD140) were generated *in vitro*, with analysis of rat urine samples could not confirm their formation following respective *in vivo* administrations. In accordance with findings from the current study, Scarth et al. compared the *in vitro* and *in vivo* metabolism of eight drugs relevant to equine sports testing (acepromazine, azaperone, celecoxib, fentanyl, fluphenazine, mepivacaine, methylphenidate, and tripelennamine), concluding that at least two *in vivo* produced major metabolites were also formed *in vitro,* with several metabolites found *in vitro* not previously been described *in vivo*.[366] These observed differences between *in vitro* and *in vivo* generated metabolite profiles may be a consequence of several factors (including concentration of protein, substrate, cofactors, and incubation time) which can impact the variety and abundance of metabolites formed *in vitro*. Moreover, liver subcellular fractions do not account for extrahepatic metabolism pathways and fail to replicate the precise cellular conditions. It is a simplified model to study drug metabolism acting to provide a snapshot of the dynamic and complex system that comprises a cell.

The present study has shown that the *in vitro* formed metabolites of the SARM compounds ostarine, LGD-4033, and RAD140 differ amongst the investigated species (cattle, horse, pig, rat). Considering the complexity of *in vivo* drug metabolism, *in vitro* and *in vivo* generated profiles of formed SARM metabolites were in good agreement as the majority of metabolites were present in both. Therefore, in the absence of *in vivo* samples or controlled studies liver microsomes and S9 fractions of the species of interest are a valuable tool to initially identify potential target analytes for SARMs and improve/facilitate the development of screening methods. Observed metabolites could be used for screening of SARM compounds in biological matrices of sports and food producing animals with additional identification based on RT, precursor ions, product ions, and CCS values. Future research is needed to determine the quantitative differences in SARM metabolite formation across species and identify which isoenzymes catalyse various metabolic pathway reactions (**Chapter 4**).

Chapter 4: CYP Reaction Phenotyping of *in vitro* Generated SARM Metabolites by UHPLC-MS/MS

4.1. Introduction

In mammalian tissues cytochrome P450 enzymes (CYPs) play a key role in the metabolism of many xenobiotics and drugs.[457] On the basis of gene sequence CYPs are assigned a family number and a subfamily letter, and then differentiated by a number for the isoenzyme. There are 18 mammalian CYP enzyme families with only CYP families 1, 2, and 3 responsible for drug metabolism.[458] Animals differ from humans with regards to elimination pathways and CYP-mediated catalytic activities, CYP isoform composition, and expression.[374,459] CYP isoenzymes belonging to families 1-3 in human, rat, horse, pig, and cattle are summarised in **Table 4.1**. CYP1A and CYP2E are seen to be well conserved across species, whereas species-specific isoforms of CYP2C, CYP3D, and CYP3A show considerable differences.[374] Enzyme mapping in veterinary species is still in its early stages with early research focused on western blot analysis to determine the expression of drug metabolising enzymes immuno-related to human variants, quantification of P450 content, and measurement of the catalytic activities of substrates selective for human isoenzymes.[271,460] Developments in molecular methods have allowed for cheaper and more accessible gene sequencing, which has since led to an increased although not yet complete characterisation of CYPs in various species.[382,461]

CYPs are a fundamental and complex component of drug metabolism with several internal (e.g. genetic polymorphisms, sex) and external (e.g. drug administration) factors affecting their activities (**Chapter 1 Sections 1.2.1.1** and **1.2.3**). Whenever several drugs are taken concurrently drug-drug interactions can occur because they share metabolic pathways and/or certain drugs can selectively induce or inhibit CYPs. Besides clinical relevance drug-drug interactions have become of concern to anti-doping laboratories. Drugs that can inhibit CYPs and are not prohibited by the WADA such as the antifungal agents ketoconazole or miconazole were shown to decrease the production of metabolites normally selected as target analytes for intake of prohibited drugs such as toremifene[462] and stanozolol[463]. Co-administration of a prohibited drug with a non-prohibited drug that modulates the pathways of the former can be a doping masking strategy.[462–465] Therefore, it is important to know which isoenzymes catalyse the metabolite formation of a drug to further investigate the potential for drug-drug interactions to occur.

The U.S. Food and Drug Administration encourages the investigation of drug metabolism and potential drug-drug interactions using *in vitro* approaches[307] with CYP reaction phenotyping experiments capable of identifying the CYP isoenzyme(s) largely

responsible for the formation of individual metabolites.[466,467] Such experimental approaches centre on the incubation of the drug of interest with complementary DNA (cDNA) expressed CYPs, i.e. particular selectively expressed CYP isoenzymes (see **Section 1.3.2.5**), and/or incubations with liver microsomes and CYP selective inhibitors. The expressed enzyme approach can establish if a metabolite is produced by a certain CYP, but cDNA expressed CYPs are not commercially available for sports and food producing animals. The alternative inhibitor-based approach focuses on the decreased formation of metabolites within incubations performed with CYP selective inhibitors as compared to inhibitor-free controls.

Within drug metabolism studies high resolution-mass spectrometry (HR-MS) based approaches (as used in **Chapter 2** and **3**) are a pivotal tool seeking to obtain exact masses, derive elemental compositions and extract structural information on known and unknown metabolites.[162,163,468] Besides HR-MS, unit resolutions mass spectrometers such as triple quadrupole instruments can be used for metabolite screening and identification.[469] When it comes to quantification of drugs and their metabolites, targeted LC-MS/MS methods in multiple reaction monitoring (MRM) mode offer especially high levels of specificity and sensitivity. However, several injections in different scan modes such as product ion and precursor ion scanning are necessary to scout MS/MS transitions and optimise MRM transitions of drug metabolites.[470] Each type of mass spectrometer has its advantages and disadvantages and a more comprehensive understanding can be gained by combining information from different instruments.

SARM compounds ostarine and LGD-4033 have been shown to be extensively metabolised and their *in vitro* species-specific metabolite profiles have been established (**Chapter 3**). By using a CYP reaction phenotyping approach based on selective CYP inhibitors the present study aims to investigate the CYP isoenzyme(s) responsible for *in vitro* formation of phase I metabolites of ostarine and LGD-4033 in bovine, equine, murine, and porcine. This information can then be used to highlight the potential for drug-drug interactions to occur that may alter the metabolite profiles and mask SARM administration. Due to the low number of phase I metabolites identified for RAD140 in **Chapter 3** and the herein applied more laborious LC-MS/MS approach, RAD140 was not included for investigation in this study. Samples were prepared by incubations of ostarine or LGD-4033 with liver microsomes from respective species with and without CYP selective inhibitors. A necessary aim of this study that preceded the analysis of the samples was therefore the establishment of a targeted MRM UHPLC-MS/MS method to detect previously identified

(in **Chapter 3** by UHPLC-IM-QTOF MS) phase I *in vitro* metabolites of ostarine and LGD-4033. A systematic multistep approach based on full scan, precursor and product ion screening was used to develop the MRM UHPLC-MS/MS method. The presented approach and MRM method herein can be adopted by control laboratories for sports and food producing animals to improve targeted methods by inclusion of not only SARM compounds, but also their associated metabolites. The data-dependant MRM approach is particularly of interest for metabolites present at trace levels due to increased selectivity and sensitivity compared to data-independent approaches.[471] Relative abundances of formed phase I metabolites from incubations without inhibitors were used to assess differences with regards to major and minor *in vitro* formed metabolites within investigated species and compared to incubations with a range of selected inhibitors (one at a time) to identify CYP isoenzymes participating in phase I SARM metabolism pathways in studied species based on decreased formation of metabolites. Reaction phenotyping enabled identification of CYP isoenzymes that are likely to be involved in the metabolism of ostarine or LGD-4033.

Table 4.1 Isoenzymes of the major drug metabolising CYP families in human, rat, horse, pig, and cattle. Isoenzymes in bold are mainly responsible for drug metabolism in the human liver.

Family	Subfamily	Human[374,472]	Rat[374,472]	Horse[378–382,473]	Pig[220]	Cattle[461,474]
CYP1	A	1A1,**1A2**	1A1, 1A2		1A2	1A1, 1A2
	B	1B1	1B1			
CYP2	A	**2A6**, 2A7,2A13	2A1, 2A2, 2A3	2A13	2A19	
	B	**2B6**, 2B7	2B1, 2B2, 2B3	2B6		2B22
	C	**2C8**, **2C9**, 2C18, **2C19**	2C6, 2C7, 2C11, 2C12, 2C13, 2C22, 2C23	2C92	2C49, 2C33v4	2C87, 2C88, 2C31
	D	**2D6**, 2D7, 2D8	2D1, 2D2, 2D3, 2D4, 2D5, 2D18	2D50	2D25	2D6
	E	**2E1**	2E1	2E1	2E1	2E1
CYP3	A	**3A4**, 3A5, 3A7, 3A43	3A1, 3A23, 3A2, 3A9, 3A18, 3A62	3A89, 3A93, 3A94, 3A95, 3A96, 3A97	3A29, 3A39	3A28, 3A48, 3A38

4.2.   Experimental

Materials, reagents, preparation of species-specific subcellular liver fractions, and *in vitro* generation of phase I SARM metabolites are described in **Chapter 3 Sections 3.2.1, 3.2.3, and 3.2.4**. Moreover, α-naphthoflavone, 8-methoxypsoralen, sertraline hydrochloride, quercetin, sulfaphenazole, ticlopidine hydrochloride, quinidine, chlormethiazole, and ketoconazole were purchased from Sigma-Aldrich (Gillingham, UK).

4.2.1   Preparation of samples for CYP reaction phenotyping

As described by Scarth et al.[294], incubations with addition of chemicals that inhibit certain human CYP isoforms were performed in order to provide preliminary information on which isoenzymes may be responsible for phase I metabolism reactions of SARMs ostarine or LGD-4033 in bovine, equine, porcine, and murine species. Inhibitor solutions were prepared at a concentration of 10 mM in ultrapure water (ticlopidine, chlormethiazole) or DMSO. Chemical inhibitors of specific human CYP isoforms added are summarised in **Table 4.2.** Selection of inhibitors and inhibitor concentrations were based on the literature (see references in **Table 4.2**). Briefly, 10 µL of 50 mM phosphate buffer with 5 mM $MgCl_2$ at pH 7.4, 10 µL of 5 mg/mL bovine/equine/murine or porcine pooled liver microsomes, 10 µL of 5 mM NADPH and 10 µL of the inhibitor solution (inhibitor B, C, D, E, F, G, H, I, or J; see **Table 4.2** for letters assigned to inhibitors)were mixed and preincubated at 37 °C 300 rpm for 15 min. Then, 10 µL of 250 µM SARM compound (ostarine or LGD-4033) were added to a total volume of 50 µL and samples were incubated at 37 °C for 30 min in a shaking (300 rpm) incubator. Control samples without addition of inhibitors were included (assigned letter A) and also used for estimation of relative abundances of *in vitro* metabolites. All samples were prepared in triplicates. Reactions were stopped by adding 50 µL of ice-cold methanol spiked with 1 µg/mL S-1-d4. Samples were centrifuged at 12 000 × g (10 °C) for 15 min and 60 µL of the supernatant were transferred into an HPLC vial with insert. A 5 µL aliquot of the sample solution was injected onto the UHPLC-MS/MS system. Based on the metabolite formation in control samples, which was set to 100 %, the percentage of metabolite formation in samples with inhibitors was calculated. Significance of reduced metabolite formation and hence inhibition was tested by two-tailed unpaired t-test using GraphPad Prism.

Table 4.2 Chemical inhibitors for human CYP isoenzymes, assigned letters used in the results section for simplicity, final assay concentrations and references.

Inhibitor	Human CYP	Assigned letter	Final assay concentration (μM)	References
α-Naphthoflavone	1A2	B	1	[223,294]
8-Methoxypsoralen	2A6	C	10	[294,475]
Sertraline	2B6	D	10	[294,476,477]
Quercetin	2C8	E	20	[223,294,478]
Sulfaphenazole	2C9	F	5	[223,294,478–480]
Ticlopidine	2C19	G	10	[223,294]
Quinidine	2D6	H	1	[223,294,479,480]
Chlormethiazole	2E1	I	10	[223,294,481]
Ketoconazole	3A4	J	1	[223,294,478–480]

4.2.2 UHPLC-MS/MS MRM method development for CYP reaction phenotyping

For analyses of the CYP inhibition samples (**Section 4.2.1**) an Acquity UPLC I-Class system (Waters, Milford, MA) coupled to a Xevo triple quadrupole mass spectrometer (TQ-MS; Waters, Manchester, UK) equipped with an electrospray ionisation source was employed. The LC conditions were as follows: Cortecs UPLC C18 (dimensions 2.1 x 100 mm, particle size 1.6 µm) column (Waters, Milford, MA, USA) maintained at 45 °C, and gradient elution with ultrapure water containing 0.1 % acetic acid (*v/v*) as mobile phase A and methanol containing 0.1 % acetic acid (*v/v*) as mobile phase B. The gradient and flow rate were programmed as follows: 0-1 min at 97 % A, 1-7 min 97 % A to 1 % A, 7-8 min hold 1 % A, and 8-10 min hold 97 % A, constantly at 0.4 mL/min. The temperature in the autosampler was kept at 10 °C. The MS instrument was operated in negative ESI mode. Reference standards of ostarine and LGD-4033 (1 µg/mL) were infused for manual tuning to determine the MS ion (parent or adduct), optimise source conditions (capillary and cone voltage, desolvation temperature, gas flows) and scout MS/MS transitions. The optimised ESI source conditions for sample analysis were as follows: desolvation temperature at 500 °C, desolvation nitrogen gas flow 1000 L/h, source temperature at 150 °C, and cone nitrogen gas flow 100 L/h. The capillary voltage was set at 1 eV and the cone voltage at 25 V. Argon was used as a collision gas with a flow rate of 0.15 mL/min. Initially, incubations samples (prepared as described in **Chapter 3 Section 3.2.4**) were injected and the MS acquisition was performed at a collision energy (CE) of 5 eV (*m/z* 50-1000) in full or precursor ion scan mode, followed by product ion scans (CE at 5, 10, 15, 20, 25, or 30 V) to establish retention times, fragment ions, and collision energies. Selected ions and experimental settings for precursor and product ion scanning are presented in **Table 4.3**. Based on these initial experiments and results from the UHPLC-IM-QTOF MS analysis (**Chapter 3 Sections 3.3.2.1-2**) a targeted MRM method for the two most abundant transitions was established for the measurement of the CYP inhibition samples (**Section 4.2.1**). Waters MassLynx software version 4.1 was used for data acquisition and analysis. This approach was also used for the estimation of relative abundances of *in vitro* metabolites in the absence of synthetic reference materials that would allow for accurate quantification.

Table 4.3 Selected ions for precursor and product ion scanning for SARM metabolites of ostarine and LGD-4033 and experimental settings including collision energy (CE), retention times (RT), mass range (m/z), and scan time (sec). Cone voltage was set at 25 V.

Precursor ion scanning

Compound	Precursor ions of m/z	CE (V)	RT (min)	m/z	Scan time (sec)
Ostarine	269.05	15	0-10	100-500	0.5
	185.03	30			
	118.03	20			
LGD-4033	267.10	10			
	239.05	20			
	185.03	20			
	170.02	25			

Product ion scanning

Compound	Product ions of m/z	CE (V)	RT (min)	m/z	Scan time (sec)
Ostarine	420.08	*	4.51-6.30	50-500	0.225
	404.09		4.96-6.30		
	287.06		4.51-4.75		
	257.05		4.76-4.95		
	201.03		4.00-4.50		
	185.03		4.20-4.50		
LGD-4033	385.06		4.50-6.00		
	369.09		4.50-5.50		
	367.09		5.51-6.00		
	355.09		4.50-6.30		
	353.07		4.50-6.30		
	351.06		4.50-6.30		

*CE 5, 10, 15, 20, 25, or 30 V

4.3.   Results and discussion

4.3.1   UHPLC-MS/MS MRM method development for CYP reaction phenotyping

To enable targeted analysis of samples for CYP reaction phenotyping (**Section 4.2.1**) a UHPLC-MS/MS MRM method to detect phase I *in vitro* metabolites of ostarine and LGD-4033 was established using a systematic multistep approach based on full scan, precursor and product ion screening. Incubation samples of ostarine or LGD-4033 with liver microsomes (prepared as described in **Chapter 3 Section 3.2.4**) were analysed in full scan mode to initially screen for metabolites by extracting ion chromatograms of metabolites of ostarine[19,141,164,165,175,177] and LGD-4033[49,127,132,178–180] previously described in the literature and identified in previous **Chapters 2** and **3**. Reference standards of ostarine and LGD-4033 were tuned manually by direct infusion, with fragment ions at *m/z* 118, 185, and 269 for ostarine and *m/z* 267, 239, 185, and 170 for LGD-4033 identified (**Table 4.3**). Subsequently, identified fragment ions from tuning were used for precursor ion scanning to look for expected and unexpected metabolites. Finally, multiple injections of incubation samples in product ion scan mode using precursor masses of tentative metabolites (**Table 4.3**) with alternating collision energies (5, 10, 15, 20. 25, or 30 V) were carried out. Subsequently, the two major transitions and ideal collision energies were established for the MRM methods for ostarine and LGD-4033 and their respective metabolites. Transitions and total ion chromatograms for ostarine and metabolites are summarised in **Table 4.4**, and for LGD-4033 and metabolites in **Table 4.5**.

Metabolites and their interspecies differences have been described in **Chapter 3 Sections 3.3.2.1-2** and numbers assigned in **Chapter 3** have been retained for simplicity. The LGD-4033 metabolite M1a as described in **Chapter 3** was not observed potentially due to a shorter incubation time used for the samples for CYP reaction phenotyping (**Section 4.2.1**) in this study (30 min as compared to two hours in **Chapter 3**). Although the same reference standard for LGD-4033 was used in the previous chapter and herein, LGD-4033 was observed to only produce one peak in this study as opposed to two in **Chapter 3** which was attributed to diastereomers of LGD-4033. A possible explanation for this is that different LC-MS systems were used in this chapter (**Section 4.2.2**) and **Chapter 3** (**Section 3.2.6**). Furthermore, LGD-4033 metabolites M6 and M7 described in **Chapter 3 Section 3.3.2.2** were not included here, as they were only found after measurements for this chapter were completed.

Table 4.4 Monitored transitions of S-1-d4, ostarine, and associated metabolites during LC–MS/MS analysis with chromatographic traces (presented in the respective row). Transitions with asterisk were employed as quantifiers.

Compound	Molecular ion, [M-H]⁻ *m/z*	Fragment ions, [M-H]⁻ *m/z*	CE, V	RT window, min	Total ion chromatogram (TIC) trace
S-1-d4	405.10	261.05*	20	5.94-6.34	
		289.04	20		
Ostarine	388.09	118.03*	20	5.42-5.82	
		269.05	15		
M1a	404.09	201.03	20	5.55-5.95	
		285.05*	15		
M1b	404.09	134.02*	20	5.36-5.76	
		269.05	20		
M2	404.09	118.03	20	5.11-5.51	
		255.04*	20		
M3a	420.08	150.02*	25	5.16- 5.56	
		206.05	20		
M3b	420.08	150.02*	20	4.93-5.33	
		269.05	25		
M3c	420.08	150.02*	25	5.05-5.46	
		185.03	20		
M4	287.06	185.03*	25	4.46-4.86	
		257.05	15		
M5	185.03			4.18-4.58	
M6	201.03	154.01	25	4.13-4.54	
		181.02*	20		

Table 4.5 Monitored transitions of S-1-d4, LGD-4033, and its metabolites during LC–MS/MS analysis with chromatographic traces (presented in the respective row). Transitions with asterisk were employed as quantifiers.

Compound	Molecular ion, [M-H]⁻ m/z	Fragment ions, [M-H]⁻ m/z	CE, V	RT window, min	Total ion chromatogram (TIC) trace
S-1-d4	405.10	261.05*	20	5.94-6.34	
		289.04	20		
LGD-4033	337.08	170.02	25	5.70-6.10	
		267.08*	10		
M1b	353.07	199.05*	20	5.23-5.63	
		227.004	25		
M1c	353.07	185.03	20	4.97-5.37	
		283.07*	10		
M1d	353.07	170.02	30	4.75-5.15	
		227.04*	20		
M2	351.06	237.06	20	4.84-5.24	
		281.05*	15		
M3a	369.07	237.06	25	4.86-5.26	
		281.05*	15		
M3b	369.07	170.02	20	4.45-4.85	
		227.04*	15		
M4a	385.06	170.02*	30	4.75-5.15	
		227.04	15		
M5a/b	355.09	185.03	25	4.94-5 .34	
		285.08*	15		

4.3.2   *In vitro* generated SARM metabolites identified by UHPLC-MS/MS

To identify major and minor *in vitro* generated metabolites of ostarine or LGD-4033, the relative contribution of each metabolite to the sum of measured metabolites was determined. Due to a lack of reference compounds for the metabolites absolute quantification was not possible. Peak areas of quantifier ion (*) traces from chromatograms of ostarine (**Table 4.4**) or LGD-4033 (**Table 4.5**) metabolites generated by bovine, equine, porcine, or murine liver microsomes without inhibitor (A, **Section 4.2.1**) were integrated by Waters MassLynx software, averages calculated (samples were prepared in triplicates), summed up and set to 100 %. Percentages for each metabolite were calculated and relative contributions of ostarine (**Figure 4.1**) and LGD-4033 (**Figure 4.2**) metabolites illustrate major and minor *in vitro* metabolites generated by bovine, equine, porcine, and murine liver microsomes. It should be noted that in the previous chapter metabolites generated by rat liver microsomes *in vitro* did not fully reflect the actual *in vivo* metabolites observed within rat urine samples (discussed in **Chapter 3 Section 3.3.3**). Therefore, in this study the abundances of the *in vitro* metabolites do not necessarily reflect their presence and/or abundance in *in vivo* samples.

For ostarine (**Figure 4.1**), M1a was shown to be the major *in vitro* metabolite in bovine (44 %), equine (44 %), and murine (52 %), whereas M4 (64 %) was the most abundant metabolite in porcine (64 %) followed by M1a (22 %). M4 was also considerably produced by bovine (15 %), equine (15 %), and rat (16 %) liver microsomes. M1b (23 %) was another main metabolite in bovine, whereas it was a minor metabolite in equine (<1 %) and murine (1.4 %). M3c was also significantly formed in bovine (15 %) and murine (13 %) and a rather insignificant metabolite in porcine (2 %) and equine (<1 %). M5 was an important metabolite in equine (24 %) as well as in porcine and murine (each 10 %), and relatively less abundant in bovine (3 %).

Relative contributions of LGD-4033 metabolites (**Figure 4.2**) showed that hydroxylations of LGD-4033 were primarily generated in bovine, equine, and murine liver microsomes. Whereas M1b was the most abundant *in vitro* metabolite in bovine, M1d was the major metabolite produced by equine liver microsomes. After incubations with murine liver microsomes, M1c was primarily generated followed by M1b and M1d. Porcine liver microsomes generated mainly the metabolites formed by hydroxylation and pyrrolidine ring cleavage M5a and M5b, which were only formed to a minor extent in the other species. M3b and M4a were only produced by equine liver microsomes to a minimal extent.
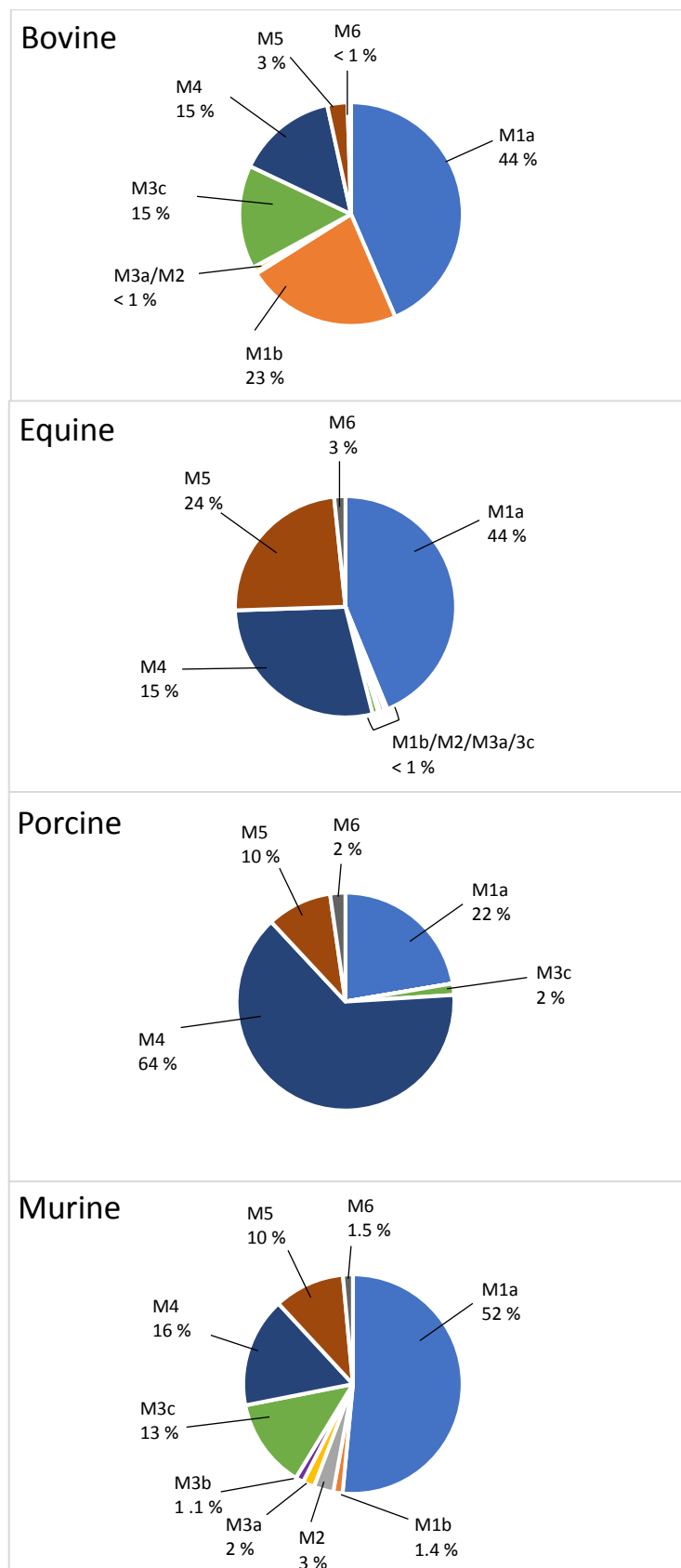
Figure 4.1 *In vitro* generated ostarine phase I metabolites. Relative contributions of each metabolite were expressed as a percentage of the sum of measured metabolites based on mean integrated peak areas of quantifier ion traces ($n = 3$).
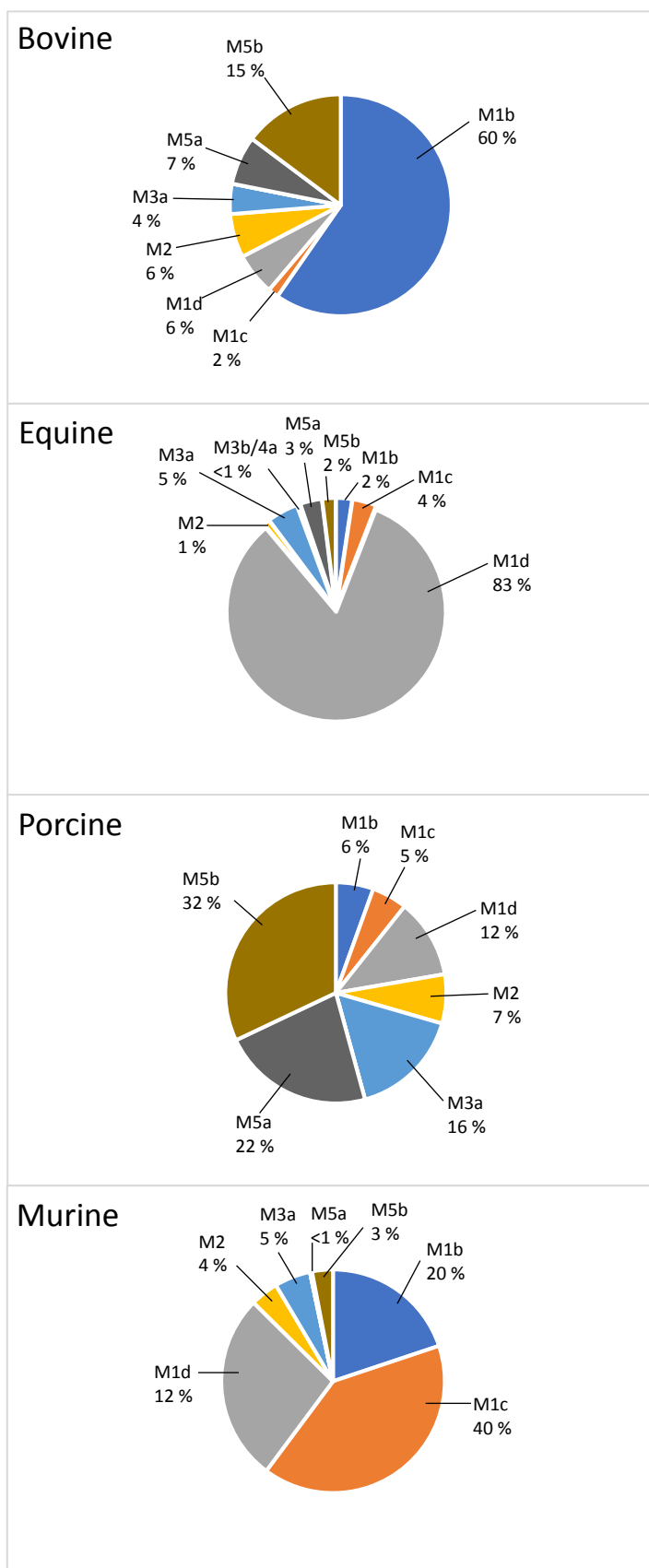
Figure 4.2 *In vitro* generated LGD-4033 phase I metabolites. Relative contributions of each metabolite were expressed as a percentage of the sum of measured metabolites based on mean integrated peak areas of quantifier ion traces (*n* = 3).

4.3.3　　CYP selective inhibition for reaction phenotyping

Using a CYP inhibitor based *in vitro* approach reaction phenotyping experiments were carried out to identify which CYP isoform(s) is/are involved in the formation of metabolites of ostarine and LGD-4033. Human CYP selective inhibitors were added to incubations with bovine, equine, porcine, or murine liver microsomes with ostarine or LGD-4033 to determine if they affected metabolite formation (**Section 4.2.1**). Samples were prepared in triplicates and inhibition was determined by comparing the extent of metabolite formation in the presence of human CYP selective inhibitors for 30 min to the extent of generated metabolites in comparable incubations without inhibitors. The most abundant ions were used as quantifiers as shown in **Table 4.4** and **Table 4.5**. Peak areas were corrected for internal standard responses and the mean of integrated peak areas ± standard error of the mean (SEM) as a measure for metabolite formation was calculated. Metabolite formation observed in inhibitor-free incubations was designated as 100 %, and percentage of metabolite formation in samples with added inhibitors was calculated. Inhibition of metabolite formation confirms that the CYP is involved in this metabolite pathway. The incubation of *in vitro* liver microsomal samples together with ostarine or LGD-4033 and human CYP specific inhibitors was an attempt to initially establish which isoenzymes of each species are involved in the formation of the metabolites. Scarth et al. have previously used the CYP reaction phenotyping approach to study the formation of hydroxy-stanozolol in equine.[294]

4.3.3.1　　CYP selective inhibition for reaction phenotyping of ostarine metabolites

The effects of human CYP inhibitors on the formation of ostarine metabolites in bovine, equine, porcine, and murine liver microsomes are illustrated in **Figure 4.3**. The structural isomers M1a, M1b, M3a, M3b, and M3c show similar inhibition profiles in each investigated species. Human CYP2A6, CYP2B6, CYP2C8, CYP2C9, and CYP3A4 inhibitors caused at least a 40% inhibition of hydroxylations (M1a and M1b) and bishydroxylations (M3a, M3b, and M3c) in all species. Quinidine, (a selective inhibitor of human CYP2D6), decreased the formation of all reported metabolites by two-thirds in rats. It also decreased metabolite formation of M1a (bovine, porcine), M1b (bovine, equine), M3a (bovine, equine) and M3c (bovine, equine, porcine) to a minor degree (24-39 % inhibition). M2 formation was mainly reduced by the human CYP2A6 inhibitor, but also by the human CYP2B6, CYP2C8, and CYP2C19 inhibitors in bovine, equine, and murine samples. The metabolite M6 was

inhibited by over 20 % in equine and porcine samples and by 48 % in bovine samples when the human CYP2A6 inhibitor 8-methoxypsoralen was added. Contrary the compound did not affect formation of M6 in rats. CYP may play a minor role in the formation of M5 as liver amidase can hydrolyse the amide bond.[190] M4 formation was only affected by inhibitors to a small extent, which suggests M4 is mainly formed by other non-CYP mediated pathways. For ostarine metabolism the involvement of human orthologous isoenzymes CYP2A6, CYP2B6, CYP2C8, CYP2C9, and CYP3A4 can be concluded. Other orthologous enzymes corresponding to human CYP1A2 and CYP2D6 may be involved to a minor extent.

4.3.3.2 CYP selective inhibition for reaction phenotyping of LGD-4033 metabolites

The effects of human CYP inhibitors on the formation of LGD-4033 metabolites in bovine, equine, porcine, and murine liver microsomes are illustrated in **Figure 4.4**. The human CYP2A6 inhibitor 8-methoxysporalen inhibited formation of M1b, M1c, and M1d in all investigated species as well as of M3b and M4a in equine. Moreover, in porcine samples M1b was decreased by over half by the CYP2B6 and CYP2C19 inhibitor. Additionally, in porcine and bovine samples M1d was reduced by the CYP2C8 inhibitor. The CYP3A4 inhibitor ketoconazole diminished the formation of M2, M3a, and M5b suggesting that the metabolites are formed by CYP3A4. On the other hand, in bovine 8-methoxypsoralen greatly induced formation of M2, M3a and M5b, which might be explained by 8-methoxypsoralen caused induction of CYP3A4.[482] A similar trend was observed for M5a in rats where elevated levels of M5a in samples with 8-methoxyspsoralen may be caused by induction of CYP3A4. Human CYP2A6, CYP2B6, CYP2C8, and CYP3A4 inhibitors decreased the formation of M2 (except in bovine) and M3a. The equine exclusive *in vitro* metabolite M3b was significantly reduced upon addition of the human CYP2A6 inhibitor and M4a by human CYP2A6, CYP2C8 and CYP3A4 inhibitors. To conclude, LGD-4033 seems to be mainly metabolised by human orthologous isoenzymes of CYP2A6, CYP2B6, CYP2C8, and CYP3A4. In the metabolism of LGD-4033 human orthologous isoenzymes of CYP1A2, CYP2C9, CYP2C19, CYP2D6, and CYP2E1 may play a minor role as addition of selective human inhibitors did not greatly diminish metabolite formation.

Figure 4.3 CYP selective inhibition for reaction phenotyping of ostarine. Y-axis: Metabolite formed in %. X-axis: A without inhibitor - concentration designated to 100 % - were compared to B-J with inhibitors and tested for significance (* $p < 0.05$, ** $p < 0.01$, *** $p < 0.001$). Bars present the means of the integrated peak areas of three incubations ± SEM

144
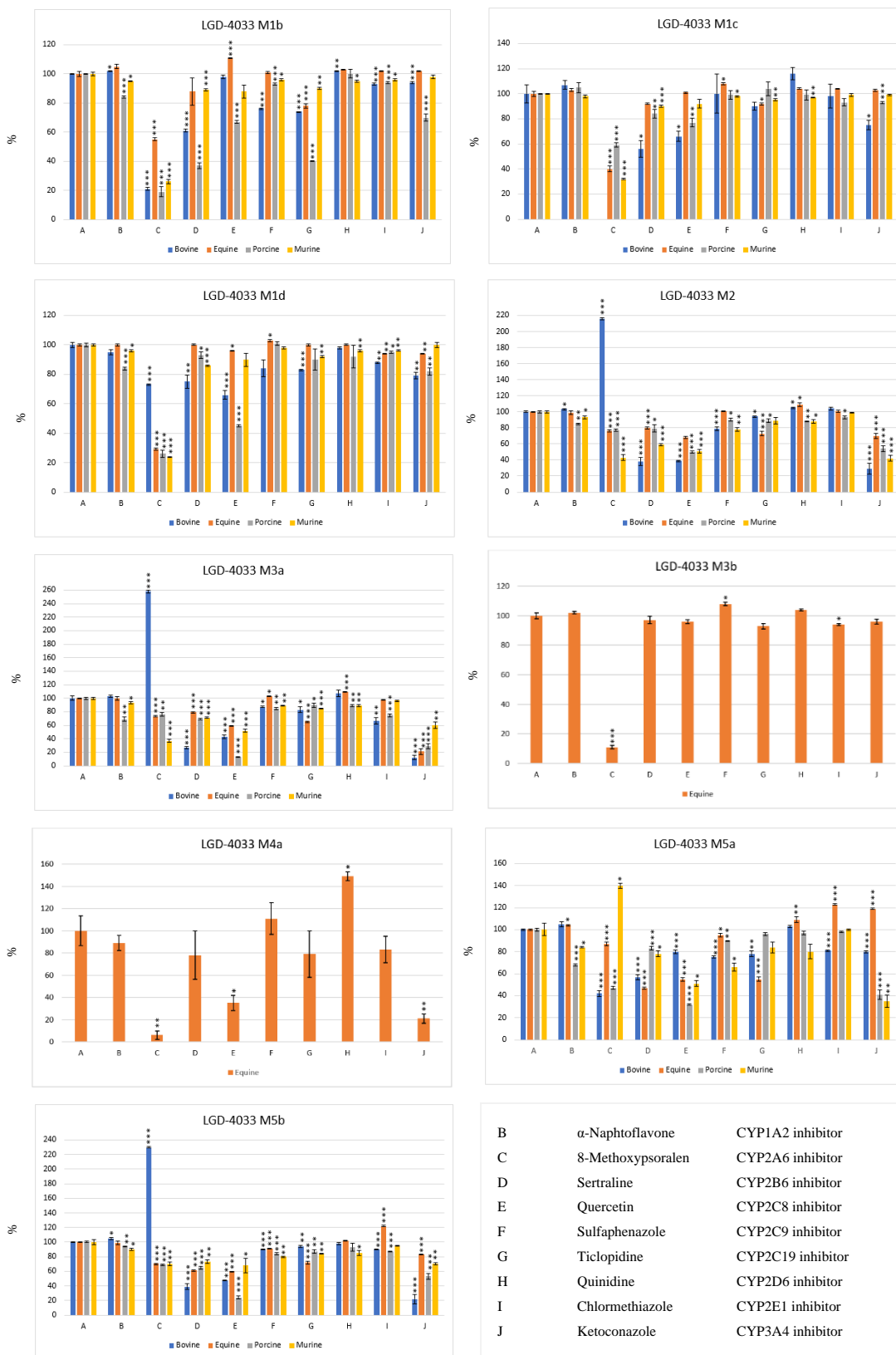
Figure 4.4 CYP selective inhibition for reaction phenotyping of LGD-4033. Y-axis: Metabolite formed in %. X-axis: A without inhibitor - concentration designated to 100 % - were compared to B-J with inhibitors and tested for significance (* $p < 0.05$, ** $p < 0.01$, *** $p < 0.001$). Bars present the means of the peak areas of three incubations ± SEM.

4.4.   Conclusions

CYP isoenzymes likely involved in the metabolism of the SARM compounds ostarine and LGD-4033 were determined (CYP reaction phenotyping) by using an *in vitro* approach with human CYP selective inhibitors. This entailed using liver microsomes to generate phase I metabolites and the development of a targeted MRM UHPLC-MS/MS method for the detection of ostarine, LGD-4033, and associated metabolites. Initially, full scan, precursor and product ion scanning experiments were carried out to scout for metabolites previously described in **Chapter 3**. Transitions of the precursor ions of phase I metabolite target analytes to the two most abundant product ions formed at optimised collision energies were selected to establish a targeted MRM method. Although this process was more time and resource-consuming than the previously employed untargeted HR-MS approach utilised within **Chapter 3**, the resulting MRM method offers advantages in terms of sensitivity and selectivity due to selective ion transmission of defined transitions for target analytes. The presented approach and MRM method herein can be adopted to improve targeted methods by inclusion of not only SARM compounds, but also their associated metabolites. For control laboratories, the monitoring of SARM metabolites can have several advantages as they can be detectable over a more prolonged time than the unchanged compounds since biotransformation can occur faster than elimination. For example, in human hydrolysed urine samples LGD-4033 was detectable for three to six days whereas its dihydroxylated metabolite was found for up to 20 days after ingestion.[179] Additionally, the monitoring of SARM metabolites is of particular interest as detection of metabolites delivers proof of ingestion and cannot arise from contamination of the sample.

By plotting relative abundances of the generated ostarine and LGD-4033 metabolites, interspecies differences were shown to be not only qualitative (**Chapter 3**) but also quantitative in nature. Relative abundances of SARM metabolites revealed appreciable differences between mammalian species in the distribution of *in vitro* formed metabolites. In cattle, horses, and rats the main *in vitro* generated metabolite for ostarine was a hydroxylated metabolite M1a, whereas in pigs it was the *O*-dephenyl-metabolite M4. Moreover, the hydroxylated ostarine metabolite M1b was a main *in vitro* metabolite formed by cattle liver microsomes, whilst it was only formed to a minor extent by equine and rat liver microsomes and not at all by pig liver microsomes. For LGD-4033, positional isomers of hydroxylated LGD-4033 were produced at varying levels in investigated species. For example, the most abundant *in vitro* LGD-4033 metabolite in cattle was the hydroxylated

metabolite M1b, which was also a major metabolite in rats but a minor metabolite in horses and pigs. Furthermore, in equine, and rats the hydroxylated LGD-4033 metabolites M1d and M1c were the most abundant respectively. The most abundant LGD-4033 metabolite formed by pig liver microsomes was through pyrrolidine ring cleavage and hydroxylation (M5b), which also constituted a major metabolite in cattle but only a minor one in horses and rats. These observed variations in product selectivity can be due to differences in CYP isoenzymes orthologues.[483]

CYP isoenzymes that catalyse ostarine and LGD-4033 phase I metabolite formation were identified by CYP reaction phenotyping by assessing the impact of specific CYP inhibitors on the metabolism of LGD-4033 and ostarine by liver microsomal incubations. This strategy can shed some insight into which orthologous CYP isoenzymes in the species of interest may be involved. An obstacle to this method is that the potential of added substances to specifically inhibit isoenzymes has been established in humans but not in the other species, e.g. differences in the response to selective human CYP inhibitors in rat and human liver microsomes have been noted.[484] Therefore, human CYP selective inhibitors may not exhibit the same selectivity or response towards orthologous enzymes in sports and food producing animal species. For example, in the present study the human CYP2E1 inhibitor chlormethiazole does not inhibit but rather induce the formation of the bishydroxylated ostarine metabolite M3c in equine. Moreover, the human CYP2A6 inhibitor 8-methoxypsoralen also induces the hydrolysis of the amide bond in ostarine to M5 in bovine and porcine. In addition, the concentrations of inhibitors that were used in the assays were added in an excess of their published human IC_{50} to compensate for differences in affinities that may occur between species. However, when CYP specific inhibitors are used at higher concentrations they may also inhibit other CYP enzymes, e.g. the human CYP3A4 inhibitor ketoconazole also inhibits human CYP2D8 at concentrations over $10\,\mu M$.[485] If and at which concentrations the used substances inhibit isoenzymes in bovine, equine, and porcine has not been established yet. A lack of P450 identification across species makes it difficult to assign the observed reactions to single orthologous isoenzymes.

Changes to metabolite levels in response to the presence/absence of CYP inhibitors revealed nuanced patterns between species. CYP2A, 2B, 2C, and 3A families of all species were primarily observed to be involved in the metabolism of ostarine and LGD-4033. Additionally, these findings indicate that the majority of the metabolites of ostarine and LGD-4033 were formed by several CYP isoenzymes. For example, CYP2A6, CYP2B6, CYP2C8, CYP2C, and CYP3A4 orthologous enzymes catalysed formation of hydroxylated

(M1a-b) and bishydroxlated (M3a-c) ostarine metabolites in all investigated species. Where multiple CYPs are involved in the formation of a metabolite, other CYPs may compensate for metabolite generation for a CYP that is inhibited. On the other hand, metabolites may be formed by only one specific CYP as was shown by the inhibition of equine-exclusive bishydroxylated metabolite M3b in incubations with the CYP2A6 inhibitor 8-methoxypsoralen. Non-CYP mediated pathways may also play a role in the formation of SARM metabolites, e.g. ostarine metabolites M4 formed by *O*-dephenylation and M5 formed by amide hydrolysis. Additional studies with recombinant single CYPs are needed to further improve the understanding of interspecies differences and variations in SARM metabolism.

Orthologous CYP isoenzymes to human CYP2A6, CYP2B6, CYP2C8, CYP2C9 (only ostarine), and CYP3A4 were mainly involved in the metabolism of ostarine and LGD-4033, therefore co-administered veterinary drugs that inhibit or induce these can potentially alter the metabolite profiles of ostarine and LGD-4033 which should be considered by monitoring laboratories. The results show that veterinary drugs that are inhibitors for CYPs involved in SARM metabolism, such as the antifungal agent ketoconazole (which inhibits human CYP3A4), can decrease the formation of certain ostarine and LGD-4033 metabolites. This demonstrates that drug-drug interactions can occur between banned SARMs and non-prohibited veterinary drugs. Although drug-drug interactions may not be clinically relevant as ostarine and LGD-4033 were metabolised by several CYPs and pathways, they may be relevant to monitoring laboratories by altering metabolite profiles and potentially masking SARM administration. In order to avoid false-negative samples the analysis should be expanded as much as possible and not only include the unchanged compounds and major, relatively high abundant metabolites but also minor, relatively low abundant metabolites as well as non-prohibited drugs that may alter metabolite formation of other drugs by CYP interactions and mask SARM administration.

Chapter 5: Profiling of *in vitro* Generated Metabolites of SARM Compounds by Equine Tissues

5.1.   Introduction

Horse racing is a multibillion dollar industry[486] and similar to human sports, guidelines have been established in equestrian sports that ban the in- and out-of-competition use of specified drugs to prevent unfair advantages and because of animal welfare concerns. Administering SARMs, a class of anabolic agents, to horses has been prohibited since 2015 as outlined in the International Agreement on Breeding, Racing and Wagering (IABRW).[112,113] SARMs increase lean muscle mass and bone density with similar anabolic effects to anabolic androgenic steroids (AAS), but with reduced side effects in androgenic tissues such as the prostate.[11,487,488] Their tissue-selective effects make them promising drug candidates to treat diseases associated with muscle mass and bone density loss, e.g. cachexia or sarcopenia.[54] Although, several SARM compounds such as ostarine[61,64,75,76], LGD-4033[82], and RAD140[53,104] have advanced into clinical testing, none has gained clinical approval yet. The anabolic properties of SARMs make them prone to abuse in sports to gain muscle mass with the goal of enhancing performance, and the illegal use of the SARM andarine in race horses illustrates the importance of equestrian anti-doping control schemes enforcing established guidelines.[131]

Illicit administration of banned compounds such as SARMs to horses could threaten the integrity of the food supply chain. In certain European countries, horses have also gained importance as minor food producing animals. Although not bred for food purposes, sport performance horses are often sold for food processing at the end of their racing careers. However, many of these horses will frequently have received drugs prohibited for use in animals entering the food chain. National residue control plans stipulate testing of animal-derived products for drug residues.[118] In the European Union, growth promoters such as SARMs have been banned in food producing animals.[117] For example, administration of the non-steroidal anti-inflammatory drug phenylbutazone to Thoroughbred race horses that are subsequently sold for slaughter for human consumption has been identified as a particular public health risk due to bone marrow suppression caused by phenylbutazone in humans.[489] To help prevent such drugs entering the food-chain, animal therapeutic treatments must be recorded and documented within a horse passport, but various compliance issues have been identified with this process.[490]

Establishing methods for detection of SARM (ab)use requires prerequisite knowledge on drug compound metabolism, as often traces of the original administered parent compound may no longer be present or detectable, in which case the only option for reliable detection

is to monitor associated formed metabolites. There are numerous examples where metabolites have been demonstrated to be detectable for a more prolonged period relative to initially administered unchanged compounds.[396,491] The detection of metabolites can also corroborate that a drug has been metabolised by the horse and rule out the possibility of a false positive which may for example arise from sample contamination. The metabolic fate of a drug depends on both hepatic and extra-hepatic biotransformation, and whilst the liver plays a dominant role in the first pass metabolism of ingested xenobiotics, the small intestine, lung and kidney also express drug metabolising enzymes.[492] In the horse, expression of CYP3A isoenzymes has previously been studied in liver, lung, and intestine[493,494], and differential expression profiling of drug metabolising enzymes has shown that CYP1A and CYP2C have the highest expression in equine intestines whereas CYP2E and CYP2A are highest in equine liver.[219]

As SARM compounds such as ostarine, LGD-4033, and RAD140 can be orally administered[19,53,81], small intestinal epithelial cells (enterocytes) are the first site where drug metabolism can occur. Most drugs are transformed in the liver into more hydrophilic metabolites, with generated metabolites and/or unchanged compounds further metabolised and/or directly eliminated by the kidneys into urine but can also enter the bile and be excreted into the small intestine and duodenum. Here, compounds can either be reabsorbed (enterohepatic recycling) or can pass through the large intestine and be excreted in the faeces. Moreover, compounds may be excreted via secondary routes through the lungs, sweat, tears, saliva, or hair. SARMs and associated metabolites have been previously detected in several matrices including urine, plasma, faeces and hair.[19,142,159,164,165,180,183]

Conventional *in vitro* studies on metabolite formation have focused primarily on the use of liver-based strategies[495] as liver is the major site of drug metabolism. This study seeks to investigate and evaluate the *in vitro* metabolism of selected SARM compounds by microsomes alone (to generate phase I metabolites) and in combination with S9 fractions (to generate phase II metabolites) from various equine tissues including liver, lungs, kidneys, and small intestine. The SARM compounds ostarine, LGD-4033, and RAD140 have been selected for investigation based on their ease of availability and reported use in equines.[124,128,129] Observing the *in vitro* metabolites produced by multiple organs allows us to determine potential sites of SARM metabolite formation and compare the profile of metabolites generated. Whilst other studies have employed equine lung alongside liver S9 fractions and confirmed liver as the major site of drug metabolism[294,367], the current investigation will expand the approach by additionally examining kidney and small intestinal

fractions to investigate if and to what extent SARM metabolites can be formed by other tissues. This will provide a snapshot of the similarities and differences in metabolite production in a range of different metabolic tissues and elucidate whether other metabolic tissues such as kidneys, lungs or intestines produce the same range of SARM metabolites as liver. As such, this study will serve to inform whether metabolite formation in minor metabolic tissues merits further study. A specific case where this could prove useful is in the development of MS methods requiring information on target analytes to monitor for prohibited substances such as SARMs in specific tissues. Furthermore, identification of SARM-derived metabolites in equines using this approach of this study may provide an insight into actual *in vivo* metabolism thereby improving upon the current knowledge of where SARMs metabolism occurs and identify the main sites of metabolism.

5.2. Experimental

Materials and reagents have been described in **Chapter 2 Section 2.2.1**. LGD-4033 was purchased from Cayman Chemical supplied by Cambridge Bioscience (Cambridge, UK) and RAD140 was from BOC Sciences (New York, USA).

5.2.1 Preparation of equine tissue microsomes and S9 fractions

Equine tissue samples were collected at a commercial abattoir facility from five animals as shown in **Table 5.1**, including one Thoroughbred bay filly, one Thoroughbred chestnut filly, two Thoroughbred chestnut mares, and one Thoroughbred bay gelding. Tissues collected from each animal were liver, kidney, lung and small intestine and were immediately cooled on ice. Upon arrival in the laboratory, tissue samples were washed with ice-cold PBS (with SIGMA*FAST* protease inhibitor tablets for intestines) and finely minced. All work was carried out in a cold room at 4 °C. The procedure for isolation was adapted from Pearce et al.[375] and Damre et al.[496] for handling of intestines. Mucosal cells were scraped from the intestinal tissue. After pooling pieces of each tissue separately from several animals to obtain a representative sample, 3 volumes of ice-cold homogenization buffer (50 mM Tris, 150 mM KCl, and 2 mM EDTA pH 7.4 at 4 °C) were added and the mixture was homogenized at 4 °C in five x 45 seconds intervals at 2000 rpm with a Silverson L5M homogenizer with a vertical slotted head in a 50 mL tube. The tubes were centrifuged at 10 400 × g$_{max}$ (4 °C) for 20 min. The pellet was discarded, and an aliquot of the supernatant (S9 fractions) was collected and frozen at -80 °C. The remaining supernatant was transferred to a fresh tube and centrifuged at 105 000 × g$_{max}$ (4 °C) for 60 min. The pellet was resuspended in 10 mL ice-cold resuspension buffer (150 mM KCl, 2 mM EDTA) followed by another centrifugation step at 105 000 × g$_{max}$ (4 °C) for 60 min. The resuspension buffer was then discarded, and the pellet was resuspended in 3 mL ice-cold storage buffer (250 mM sucrose), aliquoted and frozen at -80 °C. In summary, S9 fractions and microsomes were prepared from liver, lung, kidney, and small intestine.

Table 5.1 Information on horses, which tissues were included in the study, including gender, breed, and age at the time of slaughter

No.	Gender	Type	Breed	Age
1	Female	Filly	Thoroughbred, Bay	7 years
2	Female	Filly	Thoroughbred, Chestnut	8 years
3	Female	Mare	Thoroughbred, Chestnut	9 years
4	Female	Mare	Thoroughbred, Chestnut	11 years
5	Male	Gelding	Thoroughbred, Bay	14 years

5.2.2 Characterisation of equine tissue microsomes and S9 fractions

Protein concentration, P450 content, cytochrome b_5 content, NADPH-cytochrome P450 reductase activity, and 7-ethoxycoumarin *O*-dealkylation were determined as described in **Chapter 2 Section 2.2.3** with the following changes:

5.2.2.1 Cytochrome P450 content determination

In **Chapter 2 Section 2.2.3.2** the CO for the P450 assay was from a gas cylinder. In this chapter the CO was produced by the reaction of oxalyl chloride with sodium hydroxide.[442] For the measurements the DT-difference method as described in **Chapter 2 Section 2.2.3.2** was used.[443]

5.2.2.2 Cytochrome b₅ content determination

The sample volume used for equine liver and lung microsomes was 25 µL as used in **Chapter 2 Section 2.2.3.3**. 100 µL of equine kidney microsomes and liver S9 and 200 µL of equine intestinal microsomes and S9 fractions were used for measurements. Addition of respective volumes of 100 mM potassium buffer pH 7.4 and 5 µL of 20 mM NADH resulted in a total assay volume of 1 mL.

5.2.2.3 NADPH-cytochrome P450 reductase activity measurements

The total assay volume of 250 µL stayed the same. The following sample volumes and final concentrations were used for a linear response curve over three minutes:

- 12.5 µL of 0.4 mg/mL (final concentration 0.02 mg/mL) equine liver microsomes or S9 fractions (as used in **Chapter 2 Section 2.2.3.4**)
- 25 µL of 0.4 mg/mL (final concentration 0.04 mg/mL) equine lung or kidney microsomes
- 90 µL of 0.4 mg/mL (final concentration 0.14 mg/mL) equine intestinal microsomes
- 90 µL of 1 mg/mL (final concentration 0.36 mg/mL) equine lung, kidney, or intestinal S9 fractions

5.2.2.4 7-Ethoxycoumarin *O*-deethylation activity measurements

Different concentrations of 7-hydroxycoumarin for the calibration curves were used. To measure 7-hydroxycoumarin formation in tissue S9 fractions, 4 µL of the metabolite

reference standard at concentrations of 250, 100, 50, 10, 5, and 1 µM (final concentrations 5, 2, 1, 0.2, 0.1, and 0.02 µM) were added. For tissue microsomes, 4 µL of 7-hydroxycoumarin at concentrations of 1000, 750, 500, 250, 50 and 5 µM (final concentrations 20, 15, 10, 5, 1, and 0.1 µM) were added. The activity in lung microsomes was unexpectedly high, and an additional calibrant for 7-hydroxycoumarin at 40 µM end concentration was needed.

5.2.3   *In vitro* generation of phase I and II SARM metabolites

Assay conditions for generation of phase I and II SARM metabolites using microsomes and S9 fractions were described in **Chapter 2 Section 2.2.4**. For clarity, the pipetting scheme is presented in **Table 5.2**.

Table 5.2 *In vitro* assays conditions for generation of phase I and II SARM metabolites

Compound	Concentration	Volume added (µL)	End concentration
50 mM phosphate buffer + 5 mM MgCl$_2$	-	20	-
SARM compound (Ostarine, LGD-4033, or RAD140)	250 µM	10	50 µM
Equine microsomes from liver, lung, kidney, or small intestine	5 mg/mL	10	1 mg/mL
NADPH	50 mM	10	10 mM
Total volume incubation samples		50	

Incubation for 2 hours at 37 °C.

Phase I reactions stopped upon addition of 150 µL ice-cold acetonitrile.

Phase II reactions added the following:

S9 fractions from liver, lung, kidney, or small intestine	5 mg/mL	10	0.5 mg/mL
Alamethicin	250 µg/mL	10	25 µg/mL
UDPGA	50 mM	10	5 mM
PAPS	250 µM	10	25 µM
SARM compound (Ostarine, LGD-4033, or RAD140)	250 µM	10	50 µM
Total volume incubation samples		100	

Incubation for 2 hours at 37 °C.

Phase II reactions stopped upon addition of 100 µL ice-cold acetonitrile.

5.2.4 UHPLC-QTOF MS profiling of *in vitro* generated SARM metabolites

Analysis of *in vitro* samples was performed on a UHPLC-QTOF MS system as described in **Chapter 2 Section 2.2.5**. However, instead of full scan MS mode data acquisition was performed in auto MS/MS mode with a list preferred of precursor ions for ostarine, LGD-4033, or RAD140 phase I or II metabolites. The list shown in **Table 5.3** includes expected metabolites based on a literature search. Spectral parameters were set as follows: mass range 100-1000 m/z (MS) and 50-1000 *m/z* (MS/MS), acquisition rate 5 spectra/sec (MS) and 20 spectra/sec (MS/MS), acquisition time 200 ms/spectrum (MS) and 50 ms/spectrum (MS/MS), transients/spectrum 1597 (MS) and 259 (MS/MS) with a narrow (~1.3 m/z) isolation width in MS/MS. The collision energy was fixed at 20 V. Maximum five precursors per cycle were selected with an absolute threshold of 200 and a relative threshold of 0.01 %.

Table 5.3 List of preferred precursor ions in auto MS/MS data acquisition mode for ostarine, LGD-4033, or RAD140 phase I or II metabolites. References (Ref.) are provided for metabolites previously described in the literature.

Compound	Phase I	Preferred precursor ions *m/z*	Ref.	Phase II	Preferred precursor ions *m/z*	Ref.
Ostarine		388.0914		+ Glucuronidation	564.1235	[19,141,164,175–177,497]
	Hydroxylation	404.0864	[19,141,142,175–177]	+ Glucuronidation	580.1185	[19,141,142,175–177,497]
				+ Sulfation	484.0432	[19,141,142,175,177]
	Bishydroxylation	420.0813	[177]	+ Glucuronidation	596.1135	[175,177]
				+ Sulfation	500.0382	[177]
	O-Dephenylation	287.0649	[141,164,175,177]	+ Glucuronidation	463.0969	[175]
	O-Dephenylation + carboxylation	301.0442	[141,142,175]			
	Amide hydrolysis + hydroxylation A-ring	201.0281	[19,141]	+ Glucuronidation	377.0602	[164,165]
				+ Sulfation	280.9849	[19,164,165]
	Amide hydrolysis A-ring	185.0332	[164]			
LGD-4033		337.0781		+ Glucuronidation	513.1102	[178–180]
				+ Sulfation	417.0349	
	Hydroxylation	353.0730	[49,132,178,179]	+ Glucuronidation	529.1051	[179,180]
				+ Sulfation	433.0298	
	Hydroxylation + double-bond	351.0574	[127,132,179]			
	Bishydroxylation	369.0679	[49,127,132,178–180]	+ Glucuronidation	545.1000	
				+ Sulfation	449.0248	
	Hydroxylation + pyrrolidine ring cleavage	355.0887	[127,132,178,179]	+ Glucuronidation	531.1208	[179]
				+ Sulfation	435.0455	
	Hydroxylation + methylation	367.0887	[127]			
	Trihydroxylation	385.0629	[179,180]			
RAD140	(-acetaldehyde)	392.0920 (348.0658)		+ Glucuronidation	568.1241	
				+ Sulfation	472.0488	
	Hydroxylation (-acetaldehyde)	408.0869 (364.0607)	[181]	+ Glucuronidation	584.1190	
				+ Sulfation	488.8815	
	Bishydroxylation (-acetaldehyde)	424.0818 (380.0556)		+ Glucuronidation	600.1139	
				+ Sulfation	504.0386	

5.3. Results and discussion

5.3.1 Characterisation of equine tissue microsomes and S9 fractions

In-house prepared equine microsomes and S9 fractions from livers, lungs, kidneys, and small intestines were characterised by measuring their protein concentration, cytochrome b_5, P450 content, NADPH-cytochrome P450 reductase and 7-ethoxycoumarin O-dealkylation activity (**Table 5.4**). For microsomes, cytochrome b_5 content, P450 content, and NADPH-cytochrome P450 reductase activity were highest in liver followed by lung, kidney and small intestine. The P450 content in lung was three-fold lower than in liver. A study by Lakritz et al. supports this observation, reporting a three-fold greater equine hepatic P450 content than in lung microsomes. In comparison the P450 content in murine lung microsomes has been reported 20-40 fold lower than in murine liver microsomes.[213] Another study showed seven to 14-fold lower P450 contents in lung than in liver microsomes of the investigated species namely rat, rabbit, mouse, hamster, and guinea pig.[498] This suggests that horses have a higher lung/liver ratio of total P450 and may have higher P450 activity in lung tissues in comparison to other species. The highest 7-ethoxycoumarin O-dealkylation rate was measured in lung microsomes potentially due to the increased presence of CYP enzymes with high affinity to the substrate. For example, in horses all seven CYP3A isoenzymes are present in the lung whereas only four CYP3A isoenzymes were identified in liver.[493,494] Experiments with recombinant human CYP isoenzymes have shown that besides CYP1 and CYP2, CYP3 isoenzymes are also involved in the dealkylation of 7-ethoxycoumarin.[499]

In this study, the P450 content of intestinal microsomes and S9 fractions as well as kidney S9 fractions could not be determined. This was likely caused by an insufficient level of sensitivity in the employed method for the detection of very low levels of P450. However, a study by Tydén et al. reported the P450 content and CYP3A isoenzyme expression levels in equine intestinal microsomes.[493] Furthermore, in this study the cytochrome b_5 content could not be determined in lung and kidney S9 fractions most likely due to obstructing spectrometric absorbances from the sample matrices. Schmitz et al. have previously observed unusual spectrometric patterns in equine lung microsomes that prevented the determination of the P450 content.[500]

Table 5.4 Characterisation of prepared equine liver, lung, kidney, and small intestinal S9 fractions and microsomes. Data are expressed as mean ± standard error of the mean ($n = 3$-8). Rows with different superscripts are statistically significant different ($p < 0.05$).

Tissue fraction	Protein concentration mg/mL $n = 3$	Cytochrome b$_5$ content pmol/mg protein $n = 3$	P450 content pmol/mg protein $n = 3$	NADPH-cytochrome P450 reductase activity nmol/mg protein/min $n = 8$	7-Ethoxycoumarin O-deethylation activity nmol/mg protein/min $n = 3$
Liver microsomes	16.83 ± 0.38	826.32 ± 6.22^d	1193.44 ± 5.16^c	79.33 ± 0.80^d	498.60 ± 5.71^c
Lung microsomes	4.98 ± 0.05	131.52 ± 9.14^c	384.62 ± 15.70^b	50.15 ± 0.86^c	1196.41 ± 22.59^d
Kidney microsomes	7.71 ± 0.02	48.42 ± 1.59^b	117.19 ± 1.73^a	5.74 ± 0.14^b	14.87 ± 0.59^b
Intestinal microsomes	3.42 ± 0.02	18.07 ± 0.89^a	n.d.	4.14 ± 0.11^a	0.81 ± 0.43^a
Liver S9 fractions	21.65 ± 0.96	126.95 ± 4.63^b	307.04 ± 3.73^b	22.16 ± 0.96^d	101.83 ± 1.78^d
Lung S9 fractions	13.00 ± 0.74	n.d.	49.88 ± 5.06^a	3.09 ± 0.13^c	84.84 ± 1.00^c
Kidney S9 fractions	13.82 ± 0.35	n.d.	n.d.	2.17 ± 0.07^b	3.72 ± 0.05^b
Intestinal S9 fractions	8.15 ± 0.25	7.27 ± 1.69^a	n.d.	1.34 ± 0.05^a	0.56 ± 0.02^a

5.3.2 *In vitro* equine tissue generated SARM metabolites

SARM compounds ostarine, LGD-4033, or RAD140 were incubated with microsomes and S9 fractions prepared from equine liver, lung, kidney, or small intestinal tissues with derived samples subsequently analysed by UHPLC-QTOF MS in auto MS/MS mode. Microsomes alone were used for generation of phase I metabolites and also in combination with S9 fractions for generation of phase II metabolites and were selected over tissue homogenates as *in vitro* systems to ensure observation of very low abundant metabolites. Identification of tentative metabolic pathways/metabolites were based on accurate masses of the precursor ions and fragmentation thereof as shown in **Table 5.5** (ostarine), **Table 5.6** (LGD-4033), and **Table 5.7** (RAD140). Assigned numbers have been retained from **Chapter 3 Section 3.3.2** for simplicity. Moreover, mass spectrometric fragmentation has been discussed in **Chapter 3 Section 3.3.2**. All identified metabolites are summarised in **Table 5.8** presented at the end of **Section 5.3**.

5.3.2.1. *In vitro* equine tissue generated metabolites of ostarine

As previously described in **Chapter 3 Section 3.3.2.1**, three hydroxylated metabolites (M1a>M1c>M1b) were produced by equine liver microsomes. Additionally, M1a was generated after incubations with microsomes derived from equine small intestines. Bishydroxylation of ostarine was only observed in equine liver microsomes. Ostarine metabolite M4 resulting from *O*-dephenylation was found in incubations from liver, lung, kidney, and small intestinal microsomes. However, this metabolite was also found in control samples without NADPH as cofactor and without tissue fractions, showing that it can result from non-CYP mediated or non-enzymatic reactions. Ostarine metabolite M5 resulting from amide hydrolysis was produced by liver, kidney, and small intestinal microsomes. Furthermore, M5 was observed in control samples without NADPH also suggesting non-CYP mediated metabolism. M5 was found hydroxylated (M6) in **Chapter 3**, however, in this study, no distinct peak for M6 was observed, most likely due to the high background noise for the EIC of *m/z* 201. Ostarine was conjugated with glucuronic acid (M7) after incubation with liver and kidney fractions. Representative chromatograms and mass spectra including MS and MS/MS traces of M7 are shown in **Figure 5.1**. Glucuronidation of a hydroxylated and bishydroxylated ostarine metabolite were only observed after incubations with liver fractions. Whereas conjugation of M6 with sulfate (M11) was found in samples with liver and kidney fractions. M4, M5, and M11 have been previously detected in in equine

urine after administration of ostarine.[164] Moreover, M11 was found in equine plasma.[165] Additionally, glucuronidation of M5 and dihydroxylation followed by sulfation of M5 were detected in equine urine and plasma[164,165], however, these metabolites were not produced by *in vitro* incubation samples in the current study.

Table 5.5 Detected metabolites after incubation of ostarine with equine liver (Li), lung (Lu), kidney (K), or small intestinal (Int) microsomes (phase I) and in combination with S9 fractions (phase II). Precursor ions (PI) were observed in MS mode and fragment ions (FI) in MS/MS.

Compound/ Metabolic reactions phase I	Elemental composition	Observed PI/FI ions m/z (error ppm)	RT min	Li	Lu	K	Int	Compound/ Metabolic reactions phase II	Elemental composition	Observed PI/FI ions m/z (error ppm)	RT min	Li	Lu	K	Int
Ostarine	$C_{19}H_{13}F_3N_3O_3$	388.0930 (4.1)	6.04	✓	✓	✓	✓	M7 Glucuronidation	$C_{25}H_{21}F_3N_3O_9$	564.1238 (0.5)	5.81	✓			✓
	$C_{12}H_8F_3N_2O_2$	269.0552 (3.3)							$C_{18}H_{16}F_3N_2O_8$	445.0841 (-5.2)					
	$C_{11}H_8F_3N_2O$	241.0607 (5.4)							$C_{19}H_{13}F_3N_3O_3$	388.0920 (1.3)					
	$C_8H_4F_3N_2$	185.0334 (1.1)							$C_{12}H_{10}F_3N_2O_3$	287.0652 (1.0)					
	C_7H_4NO	118.0302 (3.4)							$C_{12}H_8F_3N_3O_2$	269.0524 (-7.1)					
									$C_8H_4F_3N_2$	185.0334 (1.1)					
									C_7H_4NO	118.0295 (-2.5)					
M1a Hydroxylation	$C_{19}H_{13}F_3N_3O_4$	404.0871 (1.7)	5.95	✓				M9b Hydroxylation + glucuronidation	$C_{25}H_{21}F_3N_3O_{10}$	580.1185 (0.0)	5.32	✓			
	$C_{12}H_8F_3N_2O_2$	269.0553 (3.7)							$C_{19}H_{13}F_3N_3O_4$	404.0862 (-0.2)					
	$C_{11}H_8F_3N_2O$	241.0604 (4.1)							$C_{13}H_{12}N_3O_8$	310.0574 (1.9)					
	$C_8H_4F_3N_2$	185.0327 (-2.7)							$C_7H_4NO_2$	134.0245 (-2.2)					
	$C_7H_4NO_2$	134.0254 (4.5)													
M1b Hydroxylation	$C_{19}H_{13}F_3N_3O_4$	404.0859 (-1.2)	5.79	✓											
	$C_{12}H_8F_3N_2O_2$	269.0530 (-4.8)													
	$C_7H_4NO_2$	134.0238 (-7.5)													
M2 Hydroxylation	$C_{19}H_{13}F_3N_3O_4$	404.0858 (-1.5)	5.70	✓											
	$C_8H_4F_3N_2$	185.0322 (-5.4)													
	C_7H_4NO	118.0297 (-0.8)													
M3a Bishydroxylation	$C_{19}H_{13}F_3N_3O_5$	420.0815 (0.5)	5.75	✓				M10 Bishydroxylation + glucuronidation	$C_{25}H_{21}F_3N_3O_{11}$	596.1091 (-7.2)	5.01	✓			
	$C_7H_4NO_3$	150.0186 (-7.3)							$C_{19}H_{13}F_3N_3O_5$	420.0793 (-4.8)					
									$C_{13}H_{12}NO_9$	326.0508 (-3.1)					
									$C_7H_4NO_3$	150.0185 (-8.0)					
M4 O-Dephenylation	$C_{12}H_{10}F_3N_2O_3$	287.0642 (-2.4)	5.04	✓	✓	✓	✓							
	$C_8H_4F_3N_2$	185.0333 (0.5)													
M5 Amide hydrolysis	$C_8H_4F_3N_2$	185.0338 (3.2)	4.76	✓		✓	✓	M11 Amide hydrolysis + hydroxylation + sulfation	$C_8H_4F_3N_2O_4S$	280.9854 (1.8)	4.08	✓		✓	
									$C_8H_4F_3N_2O$	201.0278 (-1.5)					
									$C_8H_3F_2N_2O$	181.0219 (0.0)					

163
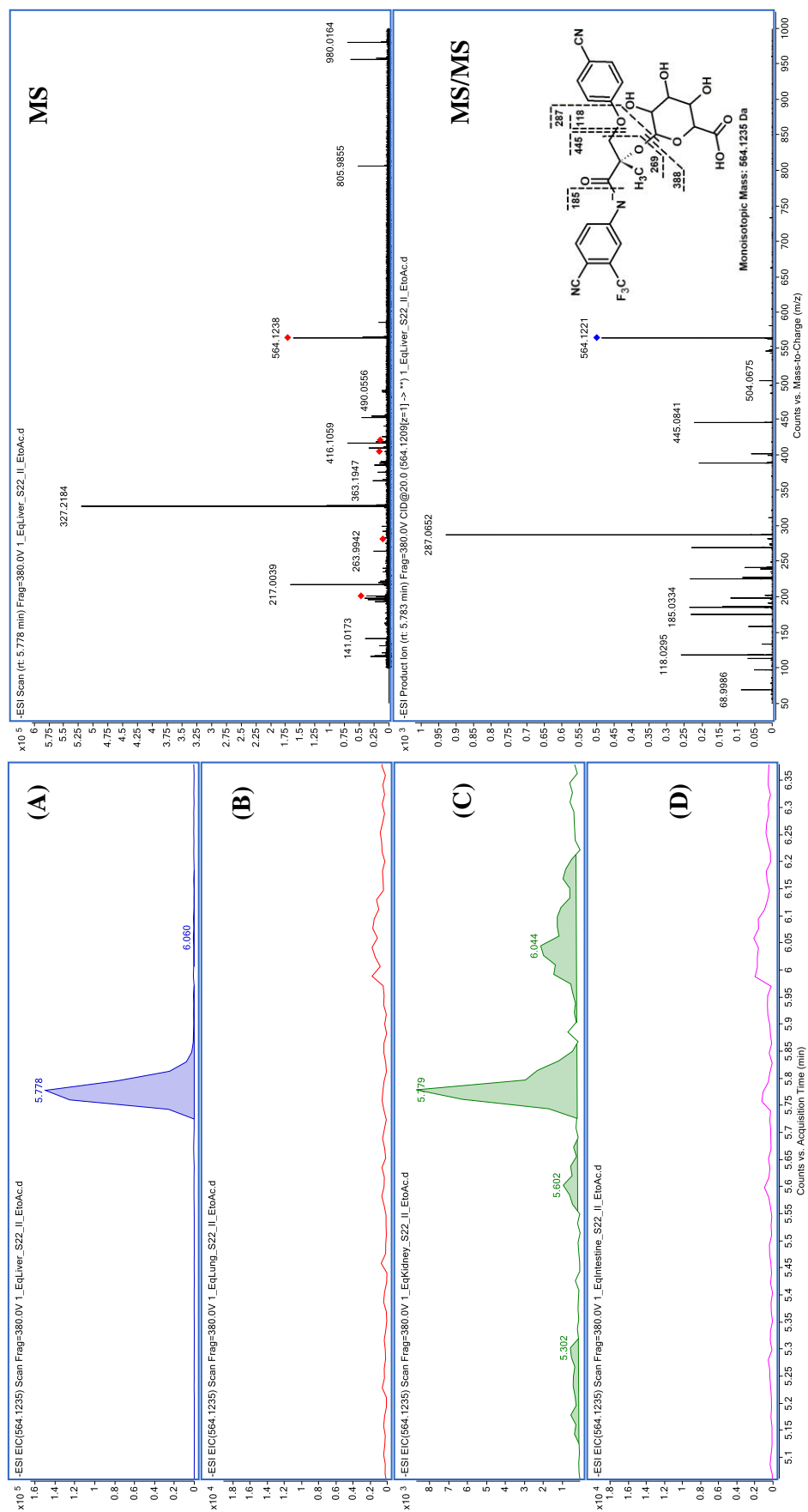
Figure 5.1 Representative chromatograms of glucuronidated ostarine M7 are represented on the left side. M7 was generated mainly by (**A**) liver and to a minor extent by (**C**) kidney, however, not by (**B**) lung or (**D**) small intestines. The mass spectra (MS top and MS/MS bottom) with the chemical structure of M7 are shown on the right.

5.3.2.2. *In vitro* equine tissue generated metabolites of LGD-4033

Out of the four hydroxylated LGD-4033 metabolites (M1a-d) produced by equine liver microsomes, two were also generated by kidney (M1a and M1b) and one by lung (M1a) microsomes. LGD-4033 metabolites M2, M3a-b, M4a, and M5a were exclusively found in incubation samples with equine liver microsomes. Besides liver microsomes LGD-4033 metabolite M5b was found after incubation with equine lung microsomes. Loss of the pyrrolidine moiety resulting in M6 and hydroxylated M6 were only observed to be formed by equine liver microsomes. Conjugation of LGD-4033 with glucuronic acid resulted in two metabolites M8a-b in liver incubation samples as described in **Chapter 3 Section 3.3.2.2**. Metabolite M8b was also found in lung, kidney and intestinal incubation samples. Chromatograms of LGD-4033 and its glucuronidated metabolite(s) are shown in **Figure 5.2**. Hydroxylation followed by methylation of LGD-4033 (M10) was formed by equine liver, kidney, and small intestinal fractions. However, its formation was also observed in control samples without cofactors or tissue fractions indicating non-CYP-mediated and non-enzymatic formation. Formation of M9c-d, M12 and M13 were exclusive to liver fractions.

Phase I and II urinary and plasma metabolites of LGD-4033 in horses have been described by Hansson et al.[180] In accordance with the results presented herein, M3a-b, M4a (only in urine samples), M8a-b, and M9c-d were detected. Moreover, a bishydroxylated glucuronidated metabolite in urine was previously described, despite not been formed within *in vitro* samples in this study. Hansson et al. did not detect the unchanged compound in equine urine after administration of LGD-4033, corroborating its extensive metabolism that has been observed *in vitro* by the formation of several metabolites herein.

5.3.2.3. *In vitro* equine tissue generated metabolites of RAD140

Only one phase I metabolite and two phase II metabolites for RAD140 were produced by liver samples in accordance with data from **Chapter 3 Section 3.3.2.3**. Besides liver, hydroxylation of RAD140 was also observed in lung microsomal samples. Furthermore, conjugation of RAD140 with glucuronic acid occurred not only in the liver but also in the kidney.

Table 5.6 Detected metabolites after incubation of LGD-4033 with equine liver (Li), lung (Lu), kidney (K), or small intestinal (Int) microsomes (phase I) and in combination with S9 fractions (phase II). Precursor ions (PI) were observed in MS mode and fragment ions (FI) in MS/MS.

Compound/ Metabolic reactions phase I	Elemental composition	Observed PI/FI ions m/z (error ppm)	RT min	Li	Lu	K	Int
LGD-4033 Acetate adduct	$C_{16}H_{15}F_6N_2O_3$	397.0996 (1.0)	6.48	✓	✓	✓	✓
	$C_{14}H_{11}F_6N_2O$	337.0787 (1.8)					
	$C_{13}H_{10}F_3N_2O$	267.0758 (2.6)					
	$C_{11}H_6F_3N_2O$	239.0435 (-1.3)					
	$C_8H_3F_4N$	170.0222 (-0.6)					
LGD-4033 Acetate adduct	$C_{16}H_{15}F_6N_2O_3$	397.1010 (4.5)	6.34	✓	✓	✓	✓
	$C_{14}H_{11}F_6N_2O$	337.0794 (3.9)					
	$C_{13}H_{10}F_3N_2O$	267.0754 (1.1)					
	$C_{11}H_6F_3N_2O$	239.0447 (3.8)					
	$C_8H_3F_4N$	170.0224 (0.6)					
M1a N-Oxidation/ Hydroxylation	$C_{14}H_{11}F_6N_2O_2$	353.0707 (-6.5)	6.38	✓	✓	✓	
	$C_{13}H_{10}F_3N_2O_2$	283.0675 (-8.8)					
M1b Hydroxylation	$C_{14}H_{11}F_6N_2O_2$	353.0740 (2.8)	5.83	✓		✓	
	$C_{10}H_6F_3N_2O$	227.0438 (0.0)					
	$C_9H_6F_3N_2$	199.0492 (1.5)					
	$C_8H_4F_3N_2$	185.0339 (3.8)					
M1c Hydroxylation	$C_{16}H_{15}F_6N_2O_4$	413.0946 (1.0)	5.56	✓			
	$C_{14}H_{11}F_6N_2O_2$	353.0738 (2.3)					
	$C_{13}H_{10}F_3N_2O_2$	283.0698 (-0.7)					
	$C_8H_4F_3N_2$	185.0335 (1.6)					
M1d Hydroxylation	$C_{16}H_{15}F_6N_2O_4$	413.0964 (5.3)	5.33	✓			
	$C_{14}H_{11}F_6N_2O_2$	353.0758 (7.9)					
	$C_{10}H_6F_3N_2O$	227.0448 (4.8)					
	$C_8H_4F_4N$	170.0227 (2.4)					

Compound/ Metabolic reactions phase II	Elemental composition	Observed PI/FI ions m/z (error ppm)	RT min	Li	Lu	K	Int
M8a Glucuronidation	$C_{20}H_{19}F_6N_2O_7$	513.1108 (1.2)	6.03	✓			
	$C_{13}H_{10}F_3N_2O$	267.0737 (3.7)					
	$C_6H_7O_6$	175.0236 (-6.9)					
	$C_5H_5O_3$	113.0246 (1.8)					
M8b Glucuronidation	$C_{20}H_{19}F_6N_2O_7$	513.1110 (1.6)	5.92	✓	✓	✓	✓
	$C_{14}H_{11}F_6N_2O$	337.0794 (3.9)					
	$C_{13}H_{10}F_3N_2O$	267.0740 (-4.1)					
	$C_6H_7O_6$	175.0247 (-0.6)					
	$C_5H_5O_3$	113.0240 (-3.5)					
M9c Hydroxylation + glucuronidation	$C_{20}H_{19}F_6N_2O_8$	529.1055 (0.8)	5.04	✓			
	$C_{10}H_6F_3N_2O$	227.0460 (9.7)					
M9d Hydroxylation + glucuronidation	$C_{20}H_{19}F_6N_2O_8$	529.1057 (1.1)	4.81	✓			
	$C_{13}H_8F_3N_2O$	265.0609 (5.7)					
	$C_{10}H_6F_3N_2O$	227.0423 (-6.6)					
	$C_6H_9O_7$	193.0357 (1.6)					
M10 Hydroxylation + methylation	$C_{17}H_{17}F_6N_2O_4$	427.1108 (2.3)	6.20	✓	✓		✓
	$C_{15}H_{14}F_6N_2O_2$	367.0895 (2.2)					
	$C_{14}H_{12}F_3N_2O_2$	297.0863 (2.4)					
	$C_{13}H_8F_3N_2O$	265.0599 (1.9)					
	$C_{12}H_8F_3N_2$	237.0664 (8.0)					

Table 5.6 *continued*

Compound/ Metabolic reactions phase I	Elemental composition	Observed PI/FI ions *m/z* (error ppm)	RT min	Li	Lu	K	Int	Compound/ Metabolic reactions phase II	Elemental composition	Observed PI/FI ions *m/z* (error ppm)	RT min	Li	Lu	K	Int
M2 Hydroxylation + double bond	$C_{14}H_9F_6N_2O_2$	351.0582 (2.3)	5.46	✓											
	$C_{13}H_8F_3N_2O_2$	281.0550 (2.5)													
	$C_{13}H_6F_3N_2O$	263.0418 (-7.6)													
	$C_{11}H_4F_3N_2O_2$	253.0210 (-7.9)													
	$C_{12}H_8F_3N_2$	237.0661 (6.7)													
M3a Bishydroxylation	$C_{14}H_{11}F_6N_2O_3$	369.0692 (3.5)	5.46	✓											
	$C_{13}H_8F_3N_2O_3$	281.0545 (0.7)													
	$C_{13}H_6F_3N_2O$	263.0448 (3.8)													
	$C_{12}H_8F_3N_2$	237.0644 (-0.4)													
	$C_8H_4F_3N_2$	185.0330 (-1.1)													
M3b Bishydroxylation	$C_{14}H_{11}F_6N_2O_3$	369.0681 (0.5)	5.04	✓											
	$C_{10}H_6F_3N_2O$	227.0439 (0.4)													
	$C_8H_4F_3N_2$	185.0325 (-3.8)													
M4a Trihydroxylation	$C_{14}H_{11}F_6N_2O_4$	385.0640 (2.9)	5.35	✓											
	$C_{12}H_6F_3N_2O$	251.0438 (0.0)													
	$C_{10}H_6F_3N_2O$	227.0436 (-0.9)													
	$C_8H_4F_3N_2$	185.0343 (5.9)													
	$C_8H_3F_4N$	170.0235 (7.1)													
M5a Hydroxylation + pyrrolidine ring cleavage	$C_{14}H_{13}F_6N_2O_2$	355.0884 (-0.8)	5.71	✓				M12 Hydroxylation + pyrrolidine ring cleavage + glucuronidation	$C_{20}H_{21}F_6N_2O_8$	531.1204 (-0.8)	5.25	✓			
	$C_{13}H_{12}F_3N_2O_2$	285.0864 (2.8)							$C_{14}H_{13}F_6N_2O_2$	355.0899 (3.4)					
	$C_8H_4F_3N_2$	185.0335 (1.6)							$C_{13}H_{12}F_3N_2O_2$	285.0851 (-1.8)					
	$C_8H_3F_4N$	170.0221 (-1.2)													

Table 5.6 *continued*

Compound/ Metabolic reactions phase I	Elemental composition	Observed PI/FI ions m/z (error ppm)	RT min	Li	Lu	K	Int	Compound/ Metabolic reactions phase II	Elemental composition	Observed PI/FI ions m/z (error ppm)	RT min	Li	Lu	K	Int
M5b Hydroxylation + pyrrolidine ring cleavage	$C_{14}H_{13}F_6N_2O_2$	355.0898 (3.1)	5.55	✓										✓	✓
	$C_{13}H_{12}F_3N_2O_2$	285.0858 (0.7)													
	$C_{12}H_{12}F_3N_2O$	257.0906 (−0.4)													
	$C_{10}H_5F_3N_2O$	226.0358 (1.8)													
	$C_9H_6F_3N_2$	199.0494 (2.5)													
	$C_8H_4F_3N_2$	185.0327 (−2.7)													
	$C_8H_3NF_4$	170.0225 (1.2)													
M6 Loss of pyrrolidine	$C_8H_4F_3N_2$	185.0339 (3.8)	4.75	✓											
M7 Loss of pyrrolidine + hydroxylation	$C_8H_4F_3N_2O$	201.0283 (1.0)	4.71	✓				M13 Loss of pyrrolidine + hydroxylation + sulfation	$C_8H_4F_3N_2O_4S$	280.0853 (1.4)	4.09	✓			
		181.0208							$C_8H_4F_3N_2O$	201.0286 (2.5)					
		154.0140							$C_8H_3F_2N_2O$	181.0214 (−2.8)					
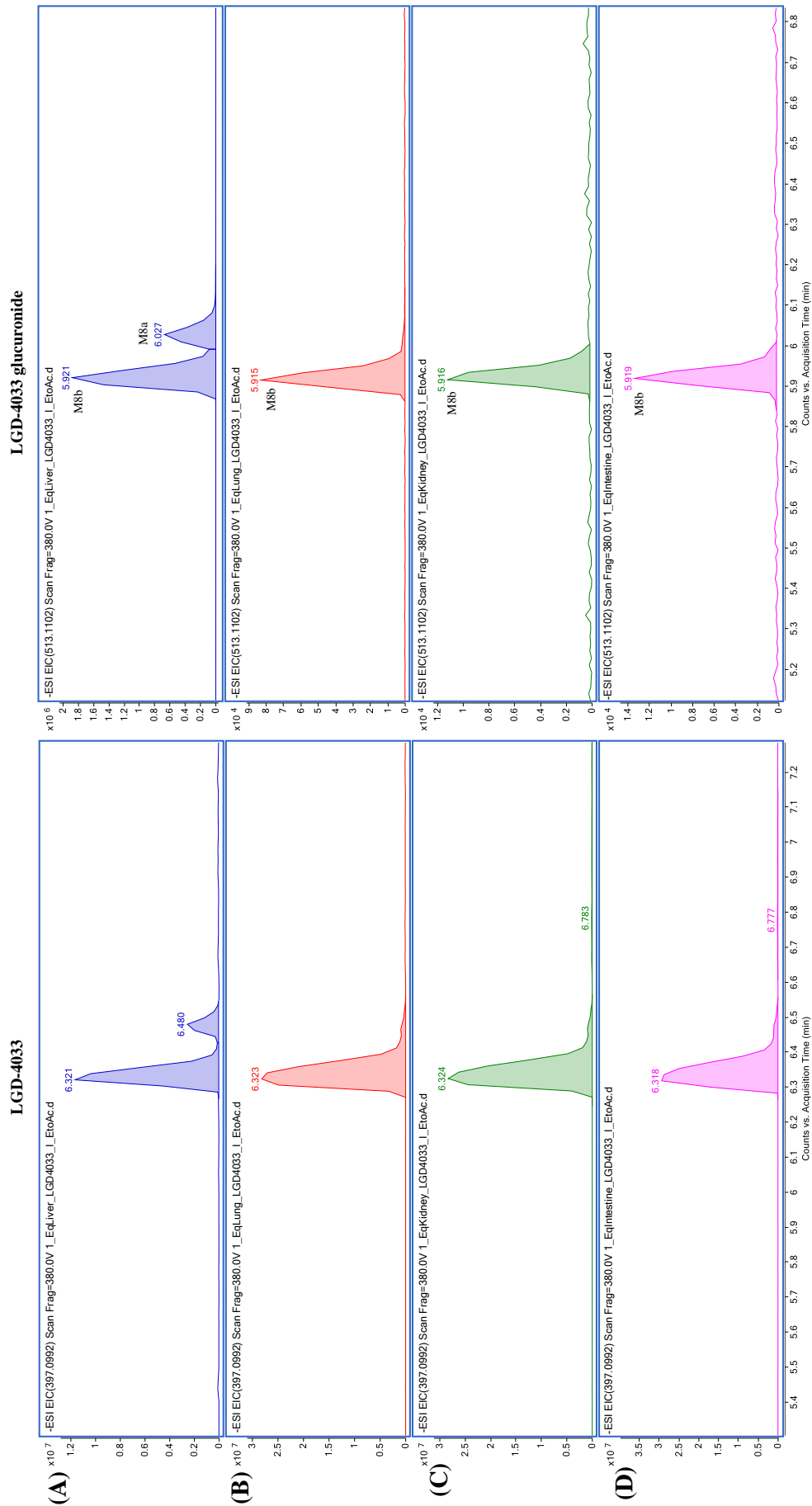
Figure 5.2 Chromatograms of LGD-4033 (left) and LGD-4033 glucuronide M8a and M8b (right) generated from (**A**) equine liver, (**B**) lung, (**C**) kidney, and (**D**) small intestinal fractions.

Table 5.7 Detected metabolites after incubation of RAD140 with equine liver (Li), lung (Lu), kidney (K), or small intestinal (Int) microsomes (phase I) and in combination with S9 fractions (phase II). Precursor ions (PI) were observed in MS mode and fragment ions (FI) in MS/MS.

Compound/ Metabolic reactions phase I	Elemental composition	Observed PI/FI ions m/z (error ppm)	RT min	Li	Lu	K	Int	Compound/ Metabolic reactions phase II	Elemental composition	Observed PI/FI ions m/z (error ppm)	RT min	Li	Lu	K	Int
RAD140 Chloride adduct	$C_{20}H_{15}ClN_5O_2$ $C_{18}H_{11}ClN_5O$ $C_{17}H_{10}ClN_4O$ $C_8H_5N_2O$ $C_8H_3N_2$	428.0693 (1.4) 348.0661 (0.9) 321.0553 (1.6) 145.0420 (9.0) 127.0312 (7.9)	5.89	✓	✓	✓	✓	M2 Glucuronidation	$C_{26}H_{23}ClN_5O_8$ $C_9H_9O_7$	568.1246 (0.9) 193.0354 (-7.3)	5.50	✓		✓	
RAD140 -acetaldehyde	$C_{18}H_{11}ClN_5O$ $C_{17}H_{10}ClN_4O$ $C_8H_6ClN_2$ $C_8H_3N_2$	348.0676 (5.2) 321.0536 (-3.7) 165.0226 (0.6) 127.0312 (7.9)	5.89	✓	✓	✓	✓								
M1c Hydroxylation Chloride adduct	$C_{20}H_{16}ClN_5O_3$ $C_{20}H_{15}ClN_5O_3$ $C_{18}H_{11}ClN_5O_2$ $C_9H_6ClN_2O$ $C_9H_4N_3O$	444.0633 (-0.7) 408.0863 (-1.5) 364.0611 (1.1) 193.0170 (-2.1) 170.0351 (-2.4)	5.35	✓	✓			M3b Hydroxylation + glucuronidation	$C_{26}H_{23}ClN_5O_9$ $C_{24}H_{19}ClN_5O_8$ $C_{18}H_{11}ClN_5O_2$ $C_9H_9O_7$	584.1199 (1.5) 540.0902 (-4.8) 364.0621 (3.8) 193.0359 (2.6)	5.00	✓			
M1c Hydroxylation - acetaldehyde	$C_{18}H_{11}ClN_5O_2$ $C_9H_4N_3O$	364.0613 (1.6) 170.0356 (-2.4)	5.35	✓	✓										

Table 5.8 Summary of *in vitro* metabolites of ostarine, LGD-4033, and RAD140 found after incubations with equine liver (Li), lung (Lu), kidney (K), and small intestinal (Int) microsomes (phase I metabolites) and in combination with S9 fractions (phase II metabolites).

Compound/Metabolic reaction(s)	Li	Lu	K	Int
Ostarine	✓	✓	✓	✓
M1a Hydroxylation	✓			✓
M1b Hydroxylation	✓			
M2 Hydroxylation	✓			
M3a Bishydroxylation	✓			
M3b Bishydroxylation				✓
M4 *O*-Dephenylation	✓	✓	✓	✓
M5 Amide hydrolysis	✓		✓	✓
M7 Glucuronidation	✓		✓	
M9b Hydroxylation + glucuronidation	✓			
M10 Bishydroxylation + glucuronidation	✓			
M11 Amide hydrolysis + hydroxylation + sulfation	✓		✓	
LGD-4033 (RT 6.48 min)	✓	✓	✓	✓
LGD-4033 (RT 6.34 min)	✓	✓	✓	✓
M1a *N*-Oxide/ Hydroxylation	✓	✓	✓	
M1b Hydroxylation	✓		✓	
M1c Hydroxylation	✓			
M1d Hydroxylation	✓			
M2 Hydroxylation + double bond	✓			
M3a Bishydroxylation	✓			
M3b Bishydroxylation	✓			
M4a Trihydroxylation	✓			
M5a Hydroxylation + pyrrolidine ring cleavage	✓			
M5b Hydroxylation + pyrrolidine ring cleavage	✓		✓	
M6 Loss of pyrrolidine	✓			
M7 Loss of pyrrolidine + hydroxylation	✓			
M8a Glucuronidation	✓			
M8b Glucuronidation	✓	✓	✓	✓
M9c Hydroxylation + glucuronidation	✓			
M9d Hydroxylation + glucuronidation	✓			
M10 Hydroxylation + methylation	✓		✓	✓
M12 Hydroxylation + pyrrolidine ring cleavage + glucuronidation	✓			
M13 Loss of pyrrolidine + hydroxylation + sulfation	✓			
RAD140	✓	✓	✓	✓
RAD140 - acetaldehyde	✓	✓	✓	✓
M1c Hydroxylation	✓	✓		
M1c Hydroxylation - acetaldehyde	✓	✓		
M2 Glucuronidation	✓		✓	
M3b Glucuronidation + Hydroxylation	✓			

5.4. Conclusions

While *in vivo* drug metabolism studies may show the most representative picture of possible biotransformations of a drug, *in vitro* based studies do not involve animal experimentation and can be tailored to study mechanistic aspects of metabolite formation. Liver-based *in vitro* systems are the most popular, as liver is recognised as the main organ responsible for drug metabolism. In this study, kidney, lung, and small intestine *in vitro* systems were included alongside a liver *in vitro* system to investigate SARM compound metabolism. The aim was to determine the sites of biotransformation of selected SARM agents (ostarine, LGD-4033, and RAD140) in equines and to expand on the current knowledge of their *in vitro* metabolism by studying several tissue-based *in vitro* systems. Although the *in vivo* generated metabolites of ostarine and LGD-4033 been previously characterised[164,165,180], nevertheless due to the innate advantages of using *in vitro* over *in vivo* methods (**Chapter 1 Section 1.3**), it is worthwhile studying metabolites produced by *in vitro* incubations of liver which are acceptable for use as reference material by horse racing laboratories.[116].

SARM metabolites (summarised in **Table 5.8**) were produced by liver, lung, kidney and small intestinal microsomes alone (phase I) and in combination with S9 fractions (phase II). Comparison of SARM-generated metabolites by various tissues using UHPLC-QTOF MS confirmed liver to be the major site of SARM metabolism. The majority of metabolites were exclusively formed by liver using microsomes for generation of phase I metabolites (M1b, M2, and M3a from ostarine, M1c-d, M2, M3a-b, M4a, M5a, M6, and M7 from LGD-4033) or in combination with S9 fractions for generation of phase II metabolites (M9a and M10 from ostarine, M9c-d, M12, and M13 from LGD-4033, and M3b from RAD140). Moreover, liver microsomes and S9 fractions possessed the highest NADPH-cytochrome P450 activity, P450 and cytochrome b_5 content relative to other investigated tissues. Several SARM metabolites formed by CYP- and UGT-catalysed reactions were not only produced by liver but also to a minor extent by lung, kidney, and small intestinal microsomes and S9 fractions. Ostarine metabolite M4 (*O*-dephenylation) was shown to be formed by microsomes from all investigated tissues. Similarly, LGD-4033 metabolite M8b (glucuronidation) was generated by microsomes/S9 fractions from all investigated tissues. Besides liver, lung and kidney microsomes also generated LGD-4033 metabolite M1a by hydroxylation or *N*-oxide formation. Hydroxylation of ostarine (M1a) was formed by liver and small intestinal microsomes, whereas hydroxylation of RAD140 (M1c) and LGD-4033 (M1b) was observed

by liver and lung microsomes. Kidney was found to be the second most metabolically active tissue after liver based on the number of phase I (M5 from ostarine, M1b and M5b from LGD-4033) and phase II (M7 and M11 from ostarine, M10 from LGD-4033, M2 from RAD140) metabolites formed using microsomes and S9 fractions that were also observed using fractions from livers. However, P450 content, cytochrome b_5 content, NADPH-cytochrome P450 reductase and 7-ethoxycoumarin O-dealkylation activities were higher in lung microsomes and S9 fractions than kidney, suggesting different CYP isoforms to be present at varying levels in lung and kidney. Ostarine metabolite M5 formed by amide hydrolysis was also produced by *in vitro* incubations with intestinal microsomes, with the LGD-4033 metabolite M10 formed by addition of a methoxy group by intestinal microsomes/S9 fractions. These observations show that lungs, kidneys, and small intestines produce a limited range of metabolites compared to liver, thus they are minor sites of *in vitro* SARM metabolite formation and may potentially form these metabolites *in vivo*.

The results presented herein suggest that besides liver, CYP and UGT are also present in equine lungs, kidneys, and small intestine. Moreover, one sulfation of an ostarine metabolite (M11) was observed in liver and kidney fractions suggesting the presence of SULT in equine liver and kidney. Molecular analysis of CYPs in equine liver, lungs, kidneys, and intestine has been described[219,271,378–380,493,494], but expression of phase II metabolising enzymes such as UGTs and SULTs has not yet been fully elucidated. In equine liver microsomes expression of a UGT1A isoform was previously detected by immunoblotting with antibodies.[501] Recently, expression levels of equine orthologous to human UGT1A6 and UGT3A2 were shown to be higher in liver compared to kidneys and lungs (which exhibited similar levels).[502] In horses individual SULT isoforms have not yet been explicitly described but gene family expansion analysis has inferred several equine SULT proteins.[503] By observing glucuronidations and sulfations of SARMs and/or derived metabolites this is the first *in vitro* equine study to report UGT activities in small intestine and SULT activities in kidney. Although there is limited information on phase II DMEs in the horse, glucuronidation and sulfation are important biotransformation pathways, with for example AAS and respective metabolites being extensively conjugated with glucuronic acid and sulfate.[504] For SARM compounds and metabolites thereof, glucuronidation was shown to be a major pathway by this study, and therefore detection of phase II conjugates or sample hydrolysis prior to analysis are important considerations in equine sports drug surveillance.[367,505]

This study describes potential sites of SARM metabolite formation in horses within multiple *in vitro* organ tissue models reflecting possible *in vivo* metabolism processes, demonstrating that not only hepatic but also extrahepatic phase I and II DMEs may be involved in SARM metabolism. This study confirmed liver to be the major site of *in vitro* SARM metabolite generation. As no additional metabolites were identified by kidney, lung, intestinal *in vitro* systems further to liver, it is sufficient to investigate drug metabolism by liver-based systems unless specific target analytes in specific tissues e.g. kidney are needed for monitoring purposes. Future research focusing on recombinant expression and characterisation of DMEs in horses is needed to gain a better mechanistic understanding of the involved isoenzymes that metabolise drugs in different tissues. Work in **Chapter 4** applied a CYP reaction phenotyping approach to evaluate which CYP isoenzymes are involved in catalysing SARM metabolite formation in liver microsomes, and with the present study demonstrating SARMs to be metabolised primarily in the liver, forthcoming **Chapters 6** and **7** will seek to investigate the *in vivo* responses of relative protein levels in liver to SARM compound administrations.

Chapter 6: Characterisation of *in vivo* Hepatic Protein Responses to SARM Compounds

6.1 Introduction

Selective androgen receptor modulators (SARMs) are a group of small molecule synthetic compounds that tissue-selectively bind to the androgen receptor (AR).[5] The AR is a member of the steroid hormone nuclear receptors and is widely expressed in numerous tissues.[506] Given its important role in many biological processes including the reproductive, musculoskeletal, cardiovascular, immune, neural, and haemopoietic system but also in cancer, the AR is a versatile drug target.[507] The AR is closely linked with several hormone-related diseases such as prostate, breast, ovarian, and pancreatic cancer as well as anabolic deficiencies such as muscle atrophy and osteoporosis. AR ligands can act as antagonists, agonists, or selective modulators and are considered as potential therapeutics. Upon agonist binding the AR can translocate from the cytoplasm to the nucleus and functions as transcription factor or it can directly initiate cellular events in the cytoplasm.[508] Testosterone, its more potent metabolite dihydrotestosterone (DHT), and structurally derived synthetic anabolic androgenic steroids (AAS) are AR agonists that exert anabolic (increased muscle mass, bone density) and androgenic (impaired libido, virilisation, acne) effects with many clinical applications.[509] SARMs can act as AR agonists in muscle and bone with similar anabolic effects to AAS, but as partial agonists or antagonists in androgenic tissues (e.g. prostate and seminal vesicles) thereby separating the anabolic from the androgenic activities.[510] They are not substrates for 5α-reductases and aromatases and therefore the metabolic amplification of androgenic or estrogenic functions of AAS, notably the conversion of testosterone to DHT and estradiol, is eliminated.[429] The underlying molecular mechanisms of SARM tissue selectivity are not fully elucidated, but ligand-specific conformational AR changes and subsequent different coregulator recruitment as well as tissue-specific expression of coregulators may play a role.[7–9,39] SARMs mode of action is not limited to the genomic level and also affects several non-genomic pathways.[10]

Due to their tissue-specific effects, SARMs present potential targeted therapy options to address certain medical conditions while reducing off-target side effects. Moreover, good oral bioavailability and a pharmacokinetic profile that is consistent with daily dosing make SARMs a promising class of therapeutic drugs.[511] The first SARMs have been structurally derived from the AR antagonist bicalutamide and further optimisations led to SARMs with an aryl-propionamide core structure including ostarine (S-22, GTx-024) as one of the lead drug candidates licensed by GTx Inc.[4,18] Ostarine improved lean body mass and physical function in a phase II trial with healthy participants.[55] Moreover, it showed promise to treat

AR positive triple negative (tested negative for estrogen receptors, progesterone receptors, and excess HER2 protein) breast cancer by inhibiting tumour-related gene expression and paracrine factors. Subsequently, it has entered clinical trials for cachexia[64], muscle wasting in patients with non-small cell lung cancer[72], stress urinary incontinence[75], and breast cancer[62,79,512]. Other promising candidates include LGD-4033 with a pyrrolidinyl-benzonitrile pharmacophore by Viking Therapeutics (VK5221), which has been tested in a phase II clinical trial for hip fractures.[81,82] Moreover, RAD140 developed by Radius Pharmaceuticals was shown to be a potent AR agonist in breast cancer cells but not in prostate cells leading to AR-mediated repression of estrogen receptor 1 gene expression and has entered a phase I clinical trial with hormone receptor positive breast cancer patients.[53,104,513] Despite not yet been approved for therapeutic use, SARMs can be obtained online[129] and have also been found as unlabelled substances in nutritional supplements[514].

The illegal use of investigational SARM compounds such as ostarine, LGD-4033, and RAD140 by athletes has increased significantly in recent years[139], particularly in non-athletes striving to look more lean and muscular with as yet unknown long-term health consequences.[515] As these non-approved SARMs are taken orally and liver is the main organ of metabolism, it is important to gain more information on the effects of SARMs on liver tissues. AAS use has been associated with several adverse effects on the liver ranging from reversible elevations in liver functions tests such as transaminases to pathophysiological changes such as tumours.[3] A superior safety profile of SARMs over AAS has been evaluated with only transient elevated alanine aminotransferase levels observed in 8.3 % of patients treated with ostarine.[6,55] The AR is also expressed in the liver[516], thus, SARMs may also exert liver-specific actions that have not yet been unravelled.

Complex perturbations in biological systems in response to drug administration can be studied by a range of omics-focused approaches.[517] Proteomics sits at the interface of transcriptomics and metabolomics and can be applied to highlight actual changes in functional protein levels. Proteins are central to most major cellular processes and responses at the protein level can provide important information towards deciphering the molecular mechanisms of drug activity and effect.[518] This study investigates the alterations to the proteome within the rat liver following recurrent sub-toxic oral administration of the SARM compounds ostarine, LGD-4033, and RAD140. A comprehensive knowledge of tissue-selective molecular action mechanisms and responses triggered by such SARM compounds with different pharmacophores can aid the design of more effective SARM compounds and

guide new therapeutic strategies. Livers from control and SARM-treated animals were homogenised and lysates analysed using comparative proteomic analysis combining two-dimensional difference gel electrophoresis (2-D DIGE) to determine differential abundances of hepatic proteins resulting from SARM treatment, with subsequent matrix-assisted laser desorption/ionization-time of flight (MALDI-TOF) protein identification. Findings presented herein provide a deeper understanding into the biological and molecular effects of responses to different SARM compound administrations in the liver, a defined drug target which also acts as a key metabolic tissue.

6.2 Experimental

6.2.1 Materials and reagents

Urea, thiourea, 3-[(3-cholamidopropyl)dimethylammonio]-1-propanesulfonate (CHAPS), Tris, glycine, sodium dodecyl sulfate (SDS), Triton X-100, DL-dithiothreitol (DTT), acrylamide/bis-acrylamide 30 % solution, ammonium persulfate (APS), L-lysine monohydrochloride, ammonium bicarbonate, ammonium sulfate, Coomassie brilliant blue G-250, PEG 300, ethanol (puriss. p.a., ACS reagent, absolute alcohol, without additive, ≥99.8%), acetonitrile (LC-MS grade), α-cyano-4-hydroxycinnamic acid (CHCA), trifluoroacetic acid (TFA), and formic acid (LC-MS grade) were purchased from Sigma-Aldrich (Gillingham, UK). Phosphoric acid 85 wt. % solution in water as well as iodoacetamide were from Acros Organics (Loughborough, UK). Dimethylformamide (labelling grade) and cyanine dyes (Cy2, Cy3, Cy5 N-hydroxysuccinimide (NHS) ester minimal dyes) were obtained from Lumiprobe (Hannover, Germany). PlusOne tetramethylethylenediamine (TEMED), Immobiline DryStrips pH 3-10 non-linear (NL) 24 cm, immobilised pH gradient (IPG) buffer pH 3-10 NL, and DeStreak Rehydration Solution were from GE Healthcare Life Sciences (Amersham, UK). Ultrapure water was prepared by a Milli-Q water system from Merck (Darmstadt, Germany). Sequencing grade modified porcine trypsin (lyophilized) was purchased from Promega (Southampton, UK) and peptide calibration standard II for mass spectrometry with a covered mass range 700-3500 Da was from Bruker Daltonics Inc. (Bremen, Germany).

6.2.2 *In vivo* SARM administration study

32 Sprague Dawley rats (Charles River Laboratories Wilmington, MA, USA) were randomly distributed to four study groups ($n = 8$ per group) and administered daily orally by gavage 1 mL of PEG 300:ethanol 80:20 *v/v* without drug, with ostarine (3 mg/kg body weight), with LGD-4033 (3 mg/kg body weight), or with RAD140 (3 mg/kg body weight) for 17 days. Animals were exsanguinated under terminal general anaesthesia 24 hours after the last administration. Then, liver tissues were recovered immediately, frozen on dry ice and stored at -80 °C. All procedures were conducted under regulations as outlined within the UK Animals (Scientific Procedures) Act 1986, reviewed and approved by the Animal Welfare and Ethical Review Body (AWERB) ethical review procedures at Queen's University Belfast.

6.2.3 Preparation of liver lysates

Liver samples from individual animals (approximately 50 µg) were homogenised in 800 µL of DIGE lysis buffer (7 M urea, 2 M thiourea, 2 % CHAPS, 30 mM Tris) using BeadBug prefilled tubes, 2.0 mL capacity with 3.0 mm Zirconium beads, from Sigma-Aldrich (Gillingham, UK) with a Precellys 24 homogeniser (Montigny-le-Bretonneux, France). Samples were processed at 6000 rpm for 30 seconds, cooled on ice for 1 min, centrifuged at $1000 \times g$ (4 °C) and placed on ice again. The homogenisation was repeated three more times and samples were then centrifuged at 16 000 x g (4 °C) for 15 min. The resulting supernatant was aliquoted and stored at -80 °C.

6.2.4 Minimal fluorescent reciprocal labelling

The preliminary protein concentration was determined using a 2-D Quant kit following manufacturer's instructions (GE Healthcare Life Sciences, Amersham, UK) and adjusted to 5-10 mg/mL. The pH of samples was then adjusted to 8.5 at 4 °C with 250 mM NaOH in DIGE lysis buffer and the 2-D Quant assay repeated to determine the final protein concentration of the samples. Protein samples were differentially labelled with fluorescent, spectrally distinct cyanine dyes (Cy2, Cy3, and Cy5 NHS ester minimal dyes). 5 nmol of Cy2, Cy3, and Cy5 were each dissolved in 12.5 µL anhydrous dimethylformamide resulting in a concentration of 400 pmol/µL. Subsequently, 50 µg protein of each sample were labelled with 1 µL of this Cy3 or Cy5 dye solution. Samples were labelled using a reciprocal labelling approach, in which half of each experimental group is labelled with Cy3 and the other half with Cy5 to eliminate inconsistencies in spot intensities due to preferential labelling.[519] 25 µg protein of each sample were combined to create a pooled sample comprised of an equal quantity of protein from each sample serving as internal standard for normalisation of protein levels - this pooled internal sample was labelled with 4 µL of Cy2 dye solution. Labelling was performed on ice for 50 min in the dark, and reactions were quenched under addition of 1 µL 20 mM lysine to individual samples and 4 µL to pooled samples. Before labelled samples were combined, they were left on ice for 10 min in the dark. Quenched Cy3 and Cy5 labelled samples were diluted with 10 µL of DIGE lysis buffer and combined as outlined in **Table 6.1**. The quenched Cy2 labelling pool was diluted with 40 µL of DIGE lysis buffer and added in equal amounts to the combined samples resulting in a total amount of 150 µg protein per combined sample. Additionally, 450 µg unlabelled pooled lysate protein were added to each combined sample for Coomassie staining and spot picking.

6.2.5   2-D DIGE

4.5 µL of 1 M DTT were added to each combined sample and placed on ice for 15 min. 1.25 µL of IPG buffer (pH 3-10) was further added and the total sample volumes were adjusted to 450 µL with DeStreak rehydration solution. Samples were added to the sample tray of the Bio-Rad (Hemel Hempstead, UK) Multiphor II system (strips 1-12 **Table 6.1**) or PROTEAN i12 IEF system (strips 13-20 **Table 6.1**) and overlaid with 24 cm Immobiline DryStrips pH 3-10 NL (gel side down) for overnight rehydration (13 hours) at 100 V and 20 °C. Following rehydration, strips were subjected to isoelectric focusing (IEF) using the following Bio-Rad protocol (24 cm pH 3-10 NL G) at 20 °C: 250 V for 30 min, gradient of 250 V to 10 000 V over two hours, 10 000 V for six hours. Focused strips were stored at -80 ºC overnight. At room temperature focused strips were placed in equilibration buffer (50 mM Tris-HCl pH 8.8, 6 M urea, 30 % glycerol, 2 % SDS, 0.002 % bromophenol blue) containing 1 % DTT for 15 min and equilibration buffer containing 2.5% iodoacetamide for another 15 min. Equilibrated strips were placed onto 12.5 % lab-cast SDS-polyacrylamide gels (low fluorescent glass plates) and overcasted with 0.5 % agarose in Laemmli electrophoresis running buffer (25 mM Tris, 192 mM glycine, 0.1 % SDS). An Ettan DALTsix electrophoresis unit from GE Healthcare Life Sciences (Amersham, UK) filled with Laemmli electrophoresis running buffer was used for second dimension gel electrophoresis for up to six gels at a time (**Table 6.1**). 12 mL of 10 % SDS were added in the upper chamber. The first step of electrophoresis was performed at 80 V, 10 mA per gel and 1 W per gel for one hour at 500 V, the second step at 40 mA per gel and 13 W per gel for six hours.

Table 6.1 Experimental set-up for 2-D DIGE analysis of liver lysates. Four or six gels were run at a time with eight replicates (1-8) in each of the four study groups (control, ostarine, LGD-4033, RAD140). A normalisation pool of all samples was labelled with Cy2. Individual samples were labelled with Cy3 and Cy5.

Strip/Gel	Sample
1	Cy2 Pool/ Cy3 Control 1/ Cy5 RAD140 1
2	Cy2 Pool/ Cy3 RAD140 2/ Cy5 Control 6
3	Cy2 Pool/ Cy3 RAD140 3/ Cy5 Ostarine 1
4	Cy2 Pool/ Cy3 Control 2/ Cy5 Ostarine 2
5	Cy2 Pool/ Cy3 RAD140 4/ Cy5 Ostarine 3
6	Cy2 Pool/ Cy3 RAD140 5/ Cy5 Control 7
7	Cy2 Pool/ Cy3 Ostarine 4/ Cy5 RAD140 6
8	Cy2 Pool/ Cy3 Ostarine 5/Cy5 Ostarine 6
9	Cy2 Pool/ Cy3 Control 3/ Cy5 Ostarine 7
10	Cy2 Pool/ Cy3 Control 4/ Cy5 RAD140 7
11	Cy2 Pool/ Cy3 Ostarine 8/ Cy5 Control 8
12	Cy2 Pool/ Cy3 Control 5/ Cy5 RAD140 8
13	Cy2 Pool/ Cy3 Control 1/ Cy5 LGD-4033 5
14	Cy2 Pool/ Cy3 Control 2/Cy5 LGD-4033 6
15	Cy2 Pool/ Cy3 LGD-4033 3/ Cy5 Control 5
16	Cy2 Pool/ Cy3 LGD-4033 4/ Cy5 Control 6
17	Cy2 Pool/ Cy3 Control 3/ Cy5 LGD-4033 7
18	Cy2 Pool/ Cy3 Control 4/ Cy5 LGD-4033 8
19	Cy2 Pool/ Cy3 LGD-4033 1/ Cy5 Control 7
20	Cy2 Pool/ Cy3 LGD-4033 2/ Cy5 Control 8

6.2.6 DIGE imaging and spot analysis

Gel plates were cleaned using 70 % ethanol and placed onto black anti-reflective plastic screens prior to imaging using a G:BOX Chemi XX9 gel documentation system with an edge lighting unit plus Cy2, Cy3, and Cy5 emission filters (Syngene, Cambridge, UK). Gel images were acquired with an aperture of f/4.0, automatic exposure with no pixel binning and manual adjustment of the focus in 16-bit TIF using GeneSys software version 1.5.6.0 (Syngene, Cambridge, UK). Acquired images were uploaded to SameSpots version 4.6.1.218 (TotalLab, Newcastle upon Tyne, UK) for differential protein abundance analysis between treatment and non-treatment groups. A reference image for alignment was selected and warping vectors applied both automatically and manually. Background subtraction, Cy2 internal standard normalization and spot detection were processed by the software. For the experimental design control versus treated, images were grouped into respective conditions (ostarine, LGD-4033, RAD140, non-treated control) and spots were selected based on relative-fold-changes and significance ($p < 0.05$, ANOVA). Relative fold-changes were calculated as ratio treated/control of average normalized spot volumes.

6.2.7 Spot picking and in-gel digestion

Gels were fixed overnight in 50% methanol and 3% phosphoric acid, and then stained with a colloidal Coomassie brilliant blue solution (17% ammonium sulfate, 34% methanol, 3% phosphoric acid, and 0.035 % Coomassie brilliant blue G-250) for 4 days and destained with ultrapure water. Gels were placed onto a white screen light converter and scanned using the G:BOX Chemi XX9 gel documentation system equipped with a UV transluminator from Syngene (Cambridge, UK). Images were recorded using GeneSys software. The scanned preparative gels were matched with the Cy2 reference image using SameSpots software to pick protein spots with differential abundances in livers of SARM treated animals relative to non-treated animals (**Section 6.3.2**). Protein spots of interest were excised manually from preparative gels using a clean scalpel. 50 μL of 1:1 acetonitrile: 100 mM ammonium bicarbonate were added to the gel pieces to destain them at 37 ℃ for one hour in a shaking (700 rpm) Thermomixer comfort (Eppendorf, Stevenage, UK) followed by dehydration for 30 min at room temperature with 500 μL of acetonitrile. Tubes were centrifuged at 5000 × g for 1 min, the supernatant removed, and gel pieces stored at -80 ℃. Approximately 10 μL of 13 ng/μL modified trypsin in 10 mM ammonium bicarbonate/10 % acetonitrile were used to completely rehydrate the gel pieces while keeping them on ice for two hours. For trypsin

digestion of the proteins, they were subsequently incubated overnight at 37 ℃ in a heat block. The condensate was removed from the tube lid, effectively desalting the sample. 10 µL of 0.1 % TFA were added to stop digestion and rehydrate the gel pieces. Approximately 15 µL (twice the volume of the gel piece) of acetonitrile with 0.1 % TFA were added to rehydrated gel pieces and samples were sonicated for 15 min to extract tryptic digests for MALDI analysis.

6.2.8 MALDI-TOF analysis and peptide mass fingerprinting

1 µL of tryptic digest was spotted onto a polished steel 384 plate MALDI target plate (Bruker, Billerica, MA, USA) and mixed with 1 µL of saturated CHCA in 30:70 acetonitrile: 0.1% TFA (*v/v*). External calibration was performed prior to sample acquisition and every five spots using peptide calibration standard II 700-3500 Da (Bruker working stock diluted 1:10 with saturated CHCA in 30:70 acetonitrile: 0.1% TFA (*v/v*)). Analysis was performed using a Bruker AutoFlex speed MALDI-TOF (Bruker, Billerica, MA, USA) in positive ionization reflective mode with Smartbeam 6 ultra-laser using FlexControl version 3.4 operating software (Bruker, Billerica, USA). The following conditions were used: ion source 1, 19.14 kV; ion source 2, 16.79 kV; lens voltage, 8.09 kV, reflector 1, 21.14 kV; reflector 2, 9.67 kV; pulsed ion extraction, 120 ns; gain factor, 10 x and 30 x, and matrix suppression mass cut-off, 450 Da. Acquisitions were based on an average of 2000 shots at 1000 Hz using random walk sample carrier (800 µm) over the mass range 700-4000 Da. Smoothing and background subtraction were automatically employed using FlexAnalysis version 3.4 (Bruker, Billerica, MA, USA). Trypsin autodigestion fragments (842.509 Da, 1045.5637 Da, and 2211.1040 Da) were used as internal calibrants. Peptide mass fingerprinting (PMF) was performed using the Mascot Server version 2.5 (www.matrixscience.com) with masses with S/N > 10 searched against SwissProt or NCBIprot with Rattus taxonomy. Contaminant masses were removed via search against the contaminants database and blank spot measurements resulting in a filtered peak list. Search parameters were as follows: trypsin specificity with 1 missed cleavage, monoisotopic mass, carbamidomethylation of all cysteine residues set as fixed modification, methionine oxidation set as variable modification, and a peptide mass tolerance of 100 ppm. Searches were performed using the raw and the filtered peak list with reported scores resulting from the filtered peak list. Furthermore, where applicable the theoretical relative molecular mass (M_r) and isoelectric

point (pI) of the identified proteins were checked against their gel position to confirm identities.

6.2.9 Bioinformatics analysis of proteomics data

Accession numbers and gene names were added to identified proteins (**Table 6.3**) using UniProt (https://www.uniprot.org/).[520] Subsequently, the list of UniProt accession numbers was submitted to PANTHER Version 14.1 (http://www.pantherdb.org/)[521] to assign Gene Ontology (GO) biological processes, molecular functions, and cell compartments to identified proteins (**Table 6.3**).

To explore the involvement of identified proteins in biological pathways, gene names were submitted to Reactome Version 68 (https://reactome.org/).[522] Gene names from liver were automatically converted to human homologues and mapped to pathways. Statistical tests for over-representation were performed resulting in p-values and false discovery rates (FDR) presenting corrected over-representation probability (**Table 6.4**).

6.3 Results and discussion

6.3.1 SARM compound administration study

SARM compounds ostarine, LGD-4033, and RAD140 were administered daily (9.00 am) at a dose of 3 mg/kg body weight to rats ($n = 8$ per group) for 17 days. During the animal study, no adverse effects were observed in control nor SARM-treated groups. Body weight was measured before the study, on days five, eight, and eleven of the treatment, and after the last administration on day 17 - No significant change in body weight was observed between study groups over the study period.

6.3.2 2-D DIGE comparative proteomic profiling and MALDI-TOF protein identification

Proteomic analysis of rat livers ($n = 8$ per group) from SARM treated (ostarine, LGD-4033 or RAD140) and non-treated (control) groups was performed using 2-D DIGE. An average of 1478 protein spots were detected on 2-D DIGE gel images using SameSpots software. Based on relative fold-change and significance ($p < 0.05$), eleven protein spots were found to be altered in response to SARMs treatments relative to non-treated controls (**Table 6.2**). Ostarine, LGD-4033, and RAD140 each led to distinct protein changes. Seven protein spots were uniquely altered in response to LGD-4033 (4 decreased, 3 increased),

three to RAD140 (1 decreased, 2 increased) and one decreased in response to ostarine. SameSpots analysis was performed separately for ostarine/RAD140/control (gels 1-12) and LGD-4033/control (13-20) as gels did not perfectly align, which leads to missing values (N/A not applicable) in **Table 6.2** for non-significant protein spots. This variation was probably due to two different IEF systems (Multiphor II for strips 1-12 and PROTEAN i12 for strips 13-20) that had to be used as the Multiphor II stopped working mid-study.

Figure 6.1 illustrates a representative Coomassie-stained gel with assigned spot numbers of selected protein spots that displayed modified abundances in livers following SARM treatments relative to non-treated controls. For identification, protein spots were manually excised from Coomassie-stained gels and trypsin-digested extracts were analysed with MALDI-TOF. After submission of a list of detected peptides to the Mascot Server, six protein spots were successfully identified, corresponding to five unique proteins: protein disulfide-isomerase A1 (P4HB) altered in response to RAD140, and 3-alpha-hydroxysteroid dehydrogenase (AKRCR14), alpha-soluble NSF attachment protein (NAPA), serum paraoxonase/lactonase 3 (PON3), and glyceraldehyde-3-phosphate dehydrogenase (GAPDH) altered in response to LGD-4033. Treatment with ostarine led to decreased relative hepatic levels of a single protein spot (spot no. 1212), which could not be identified. In total, five protein spots with differential abundances in treated groups relative to the non-treated group could not be identified by MALDI-TOF. This potentially may be due to an insufficient protein quantity or insufficient trypsin digestion obstructing protein spot identification, or it could also be that the associated protein sequence has not yet been registered within a reference database.
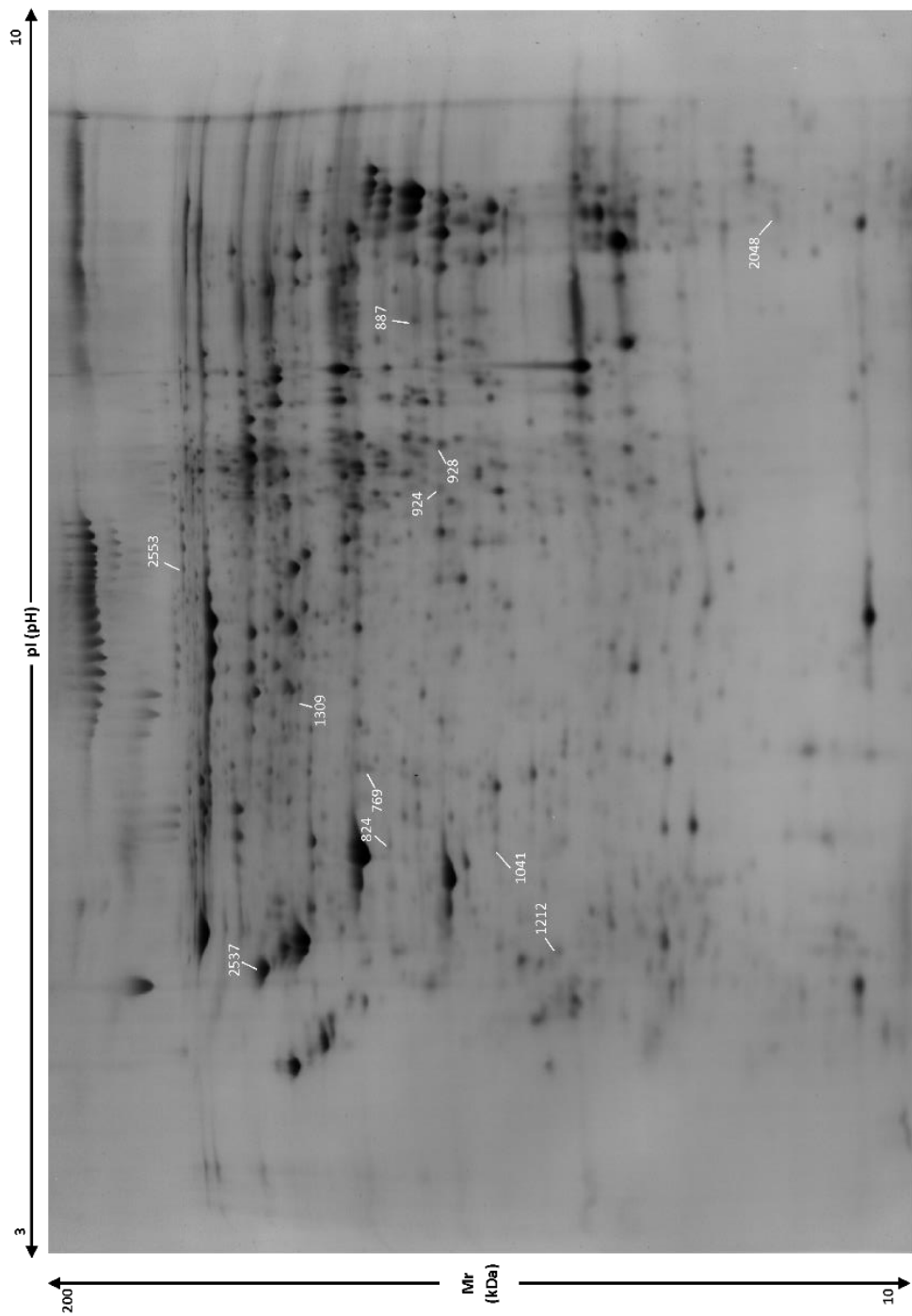
Figure 6.1 Representative Coomassie-stained gel image (450 µg of pooled liver lysate protein) with assigned spot numbers of selected proteins in rat liver lysates following 17 days of ostarine, LGD-4033, or RAD140 administration.

187

Table 6.2 Protein spots with relative fold-changes and significance (NS, not significant; $*$ $p < 0.05$; $**$ $p < 0.01$; $***$ $p < 0.005$) in rat liver lysates following 17 days of ostarine (three protein spots), LGD-4033 (seven protein spots), or RAD140 (one protein spot) administration versus non-treated group. Six protein spots corresponding to five unique proteins were identified by Mascot search of SwissProt or NCBIprot databases. N/A not applicable.

Protein name	Spot No.	Relative fold-change			Protein spot Mascot identification						
		Ostarine	LGD-4033	RAD140	SwissProt Entry Name	M_r (kDa)	pI	Sequence coverage (%)	No. of peptides matched	Score	Expectation value
3-Alpha-hydroxysteroid dehydrogenase	924	N/A	0.85**	N/A	DIDH_RAT	37.517	6.67	50	15	199	1.00E-16
	928	N/A	0.84***	N/A	DIDH_RAT	37.517	6.67	55	16	187	1.60E-15
Alpha-soluble NSF attachment protein	1041	N/A	1.18*	N/A	SNAA_RAT	33.627	5.30	44	10	103	4.00E-07
Glyceraldehyde-3-phosphate dehydrogenase	887	N/A	0.80*	N/A	G3P_RAT	36.090	8.14	32	9	60	7.70E-03
	824	N/A	1.22*	N/A							
	2048	N/A	1.24**	N/A							
Not identified	1212	0.82*	N/A	0.90^{NS}							
	1309	1.20^{NS}	N/A	1.25*							
	2553	0.95^{NS}	N/A	0.75*							
Protein disulfide-isomerase A1	2537	1.17^{NS}	N/A	1.16*	PDIA1_RAT	57.315	4.82	55	25	253	4.00E-22
Serum paraoxonase/lactonase 3	769	N/A	0.87*	N/A	PON3_RAT	39.604	5.49	38	11	97	1.50E-06

6.3.3 Functional annotation and pathway analysis of identified proteins

The proteins which exhibited altered abundances following SARM administration were further investigated using bioinformatics in an effort to gain an insight into their functions and the pathways affected by these SARMs.

Following submission of the protein list to PANTHER (**Section 6.2.9**), the proteins were determined to be involved in the following biological processes: cellular processes (NAPA, GAPDH, P4HB, and AKR1C14), biological regulation and cellular localisation (NAPA), response to stimulus (P4HB and PON3), and metabolic processes (GAPDH and AKR1C14) (**Table 6.3**). The majority of these proteins are primarily catalytic (GAPDH, P4HB, and AKR1C14) in function with the exception of NAPA which is involved in protein complex formation (**Table 6.3**). In terms of location, proteins were associated with cytosol (GAPDH and AKR1C14), ER (P4HB), plasma membrane (NAPA and P4HB), the extracellular space and intracellular membrane-bound organelles (PON3).

Reactome (**Section 6.2.9**) was used to assign pathways to the identified proteins. They are involved in several pathways (**Table 6.4**), primarily metabolism (PON3, GAPDH, AKR1C14). PON3 (decreased by LGD-4003) is a high-density lipoprotein-associated protein primarily expressed in the liver and participates in the prevention of low-density lipoprotein oxidation[523]. AAS are known to induce changes in lipid profiles and exogenous testosterone administration was shown to increase PON3.[6,524] Therefore, similar to testosterone, LGD-4033 may play a role in PON3 regulation affecting lipid profiles. Another protein involved in metabolism pathways is GAPDH (also found decreased by LGD-4033), a multifunctional enzyme that can translocate within the cell compartments manifesting pleiotropic effects.[525] The AR can be coactivated by GAPDH, forming a protein complex that translocates from the cytoplasm to the nucleus, thereby enhancing transcriptional activity of the AR.[526] Cytosolic GAPDH is known to be inactivated to counteract oxidative stress [527] and depressed GAPDH levels could be a cellular response to oxidative stress related to LGD-4033 administration. Moreover, AKR1C14 (decreased by LGD-4033) is associated with metabolism; it catalyses the conversion of DHT to its less active 3-β-diol metabolite. Additionally, NAPA (decreased by LGD-4033) is involved in vesicle-mediated transport, whilst the protein di-sulfide isomerase (PDI) P4HB (increased by RAD140) plays a role in the metabolism of proteins, cellular response to stimuli, signal transduction, transport of small molecules, extracellular matrix organisation, and immune system. Upregulation of PDIs can be caused by an activation of the unfolded protein response (UPR)

under conditions of ER stress.[528] Upon accumulation of misfolded proteins, PDIs act as chaperones and target terminally misfolded proteins for ER-associated degradation (ERAD).[529] Initially, UPR asserts a protective and adaptive mechanism but can shift to apoptosis under sustained chronic ER stress. Oxidative protein folding produces reactive oxygen species that can cause an imbalance in the redox status of the ER leading to oxidative stress.[530] Therefore, increased levels of P4HB following RAD140 administration may be linked to oxidative stress.

Table 6.3 Identified proteins in rat liver following SARMs treatment in alphabetical order with UniProt Accession number, gene name, their involvement in biological processes, assignment of molecular functions, and cellular compartments.

Protein name	UniProt Accession No.	Gene name	Panther GO-slim Biological process	Panther GO-slim Molecular function	GO Cellular compartment
3-Alpha-hydroxysteroid dehydrogenase	P23457	*Akr1c14*	Alcohol metabolic process Ammonium ion metabolic process Carbohydrate derivative metabolic process Cellular aromatic compound metabolic process Cofactor metabolic process Drug metabolic process Hormone metabolic process Prostaglandin metabolic process Secondary metabolic process Steroid metabolic process	Oxidoreductase activity acting on the CH-OH group of donors, NAD or NADP as acceptor	Cytosol
Alpha-soluble NSF attachment protein	P54921	*Napa*	Cellular protein complex disassembly Cellular protein-containing complex assembly Intracellular protein transport Modulation of chemical synaptic transmission Regulation of exocytosis Regulation of protein complex assembly Synaptic transmission, glutamatergic Synaptic vesicle exocytosis Vesicle fusion to plasma membrane	Syntaxin binding	SNARE complex Plasma membrane region
Glyceraldehyde-3-phosphate dehydrogenase	P04797	*Gapdh*	ATP biosynthetic process Carbohydrate metabolic process Carboxylic acid biosynthetic process Coenzyme biosynthetic process Generation of precursor metabolites and energy Nucleotide catabolic process Nucleotide phosphorylation Pyruvate metabolic process	Hydro-lyase activity Intramolecular transferase activity Kinase activity Oxidoreductase activity Phosphotransferase activity, alcohol group as acceptor	Cytosol
Protein di-sulfide isomerase A1	P04785	*P4hb*	Protein folding Response to endoplasmic reticulum stress	Catalytic activity, acting on a protein	Endoplasmic reticulum Plasma membrane
Serum paraoxonase/lactonase 3	Q68FP2	*Pon3*	Response to toxic substance	Carboxylic ester hydrolase activity	Extracellular space, intracellular membrane-bounded organelle

Table 6.4 Reactome analysis (see **Section 6.2.9**) of identified proteins with differentially altered levels in rat livers following SARMs administration relative to non-treated controls. For protein names corresponding to gene names see **Table 6.3**.

Pathway name	No. Entities found	No. Entities total	Entities p-value	Entities FDR	Submitted gene entities found
Cellular responses to external stimuli	1	505	0.243	0.243	*P4hb*
Cellular responses to stress	1	408	0.201	0.201	*P4hb*
Detoxification of reactive oxygen species	1	39	0.021	0.054	*P4hb*
Extracellular matrix organisation	1	301	0.151	0.151	*P4hb*
Collagen formation	1	90	0.047	0.054	*P4hb*
Collagen biosynthesis & modifying enzymes	1	67	0.036	0.054	*P4hb*
Immune system	1	2233	0.739	0.739	*P4hb*
Cytokine signalling in immune system	1	777	0.352	0.352	*P4hb*
Signalling by interleukins	1	458	0.223	0.223	*P4hb*
Interleukin-12-family signalling	1	56	0.030	0.054	*P4hb*
Metabolism	3	2132	0.088	0.088	*Pon3, Gapdh, Akr1c14*
Metabolism of carbohydrates	1	300	0.151	0.151	*Gapdh*
Glucose metabolism	1	98	0.052	0.054	*Gapdh*
Metabolism of lipids	2	746	0.056	0.056	*Pon3, Akr1c14*
Fatty acid metabolism	1	179	0.093	0.093	*Pon3*
Arachidonic acid metabolism	1	59	0.031	0.054	*Pon3*
Metabolism of steroids	1	152	0.079	0.079	*Akr1c14*
Bile acid & bile salt metabolism	1	43	0.023	0.054	*Akr1c14*
Metabolism of vitamins and cofactors	1	192	0.099	0.099	*Akr1c14*
Metabolism of fat-soluble vitamins	1	48	0.026	0.054	*Akr1c14*
Retinoid metabolism & transport	1	44	0.023	0.054	*Akr1c14*
Metabolism of proteins	1	2010	0.076	0.076	*P4hb*
Regulation of insulin-like growth factor transport & uptake by insulin-like growth factor binding proteins	1	124	0.065	0.065	*P4hb*
Signal transduction	2	2758	0.460	0.460	*Akr1c14, P4hb*
Signalling by Hedgehog	1	150	0.078	0.078	*P4hb*
Hedgehog ligand biogenesis	1	65	0.034	0.054	*P4hb*
Transport of small molecules	1	731	0.334	0.334	*P4hb*
Plasma lipoprotein assembly, remodelling & clearance	1	72	0.038	0.054	*P4hb*
Plasma lipoprotein assembly	1	19	0.010	0.054	*P4hb*
VLDL assembly	1	5	0.003	0.054	*P4hb*
Vesicle-mediated transport	1	761	0.346	0.346	*Napa*
Membrane trafficking	1	635	0.297	0.297	*Napa*
ER to Golgi anterograde transport	1	155	0.081	0.081	*Napa*
COPI-mediated anterograde transport	1	102	0.054	0.054	*Napa*
COPII-mediated vesicle transport	1	68	0.036	0.054	*Napa*
Intra-golgi- & retrograde golgi-to-ER-traffic	1	206	0.106	0.106	*Napa*

6.4   Conclusions

This study investigated the effects of SARM compound (ostarine, LGD-4033, and RAD140) administration on the rat liver proteome using 2-D DIGE methodologies. Comparative analysis of relative hepatic protein profiles provided a holistic overview of protein abundance changes following SARM treatments. Whilst the effects of SARM GSK212A on skeletal muscle proteins have been reported previously[531], this is the first reported study that has investigated the proteomic responses in liver post-SARM administrations. Key findings of the present study were that even after a relatively short treatment period of 17 days with daily dosing (3 mg/kg body weight), relative levels of 11 protein spots were altered in livers of SARM-treated animals compared to control non-treated group, with five significantly decreased and six increased. Ostarine, LGD-4033, and RAD140 each exerted distinct effects as reflected in the comparative liver protein profiles. Six protein spots corresponding to five unique proteins were identified by MALDI-TOF and play a role in a number of biological pathways. Levels of three proteins (PON3, GAPDH, and AKR1C14) that play a role in metabolism were decreased and one protein (NAPA) with functions in vesicle-mediated transport was increased in response to LGD-4033 administrations. Relative levels of P4HB which is involved in several biological pathways including the ER stress response were increased upon RAD140 treatment. In the current study, two identified proteins (GAPDH and P4HB) could be linked to oxidative stress. Use of AAS such as stanozolol[532], nandrolone[533], or testosterone[534] is already known to disrupt oxidative homeostasis and causes an oxidative stress response in rat liver, and further research is needed to investigate if SARM compounds can mediate an oxidative stress response.

Additional investigations on the tissue-selective effects of SARM compounds in liver (**Chapter 7**) will further investigate the proteomic response by employing subcellular fractionation to isolate subcellular compartments such as nuclei, mitochondria, cytosol, and microsomes (derived from ER artefacts). Subcellular fractionation enriches proteins by localisation and helps to assign proteins to their subcellular compartment which is important for interpretation of protein function. Proteomic analysis of subcellular fractions is anticipated to achieve greater proteome coverage and aid characterisation of low-level relative protein abundance changes due to enrichment and assign protein functions more clearly due to knowledge of protein subcellular localisation.

Chapter 7: Subcellular Proteomic Profiling of Hepatic Responses to SARMs

7.1　　　Introduction

Previous work (**Chapter 6**) has reported the differential protein response in liver to treatment with SARMs (ostarine, LGD-4033 or RAD140) compared to vehicle-treated control group animals. Liver tissue total protein lysates were analysed by comparative proteomic analysis (2-D DIGE) followed by MALDI-TOF protein identification with distinct changes in the protein profile to each investigated SARM compound revealed. Liver is the most metabolically active tissue, the whole liver proteome consists of over 10,000 proteins[535] and many of which are unique to this tissue[516]. 2-D DIGE allowed for highly sensitive protein labelling and separation of complex protein mixtures in liver based on molecular weight and isoelectric point. However, due to the high dynamic range of protein concentrations, low abundant proteins can be masked by high abundant proteins. A dynamic range of almost seven orders of magnitude for liver proteins has been described[536], and the classical approach of analysing the proteome of whole liver lysates may dilute or mask specific cellular responses by presenting average levels of a blend of proteins from different cell compartments. Specific proteins can be major components of an organelle but present a minority when the whole liver proteome is considered.

Subcellular proteomics provides an alternative strategy to the traditional approach of analysing whole tissue samples by combining biochemical fractionation techniques with proteomic-based approaches.[537] Prior to proteomic analysis, tissue cells are disrupted and organelles can be fractionated by different methods such as density gradient centrifugation or differential ultracentrifugation.[538] This strategy offers several advantages as each subcellular compartment has a varied set of proteins and subcellular proteomics can be used to localise proteins within each cell compartment.[539] Moreover, it provides functional context for identified proteins by organelle localisation. Proteins can be present in multiple organelles and their subcellular localisation governs their functions.[540] The proteome is dynamic; protein levels and subcellular localisation can change in response to stimuli. Additionally, fractionation enriches target organelles and their proteins, which leads to better resolution and detection in 2-D gel electrophoresis, especially for low abundant proteins. Using enriched subcellular fractions for protein extraction reduces the complexity of the sample by displaying a subset of proteins in cells.

In the present study, a subcellular proteomics approach was employed to enrich proteins and gain further insights into liver-specific proteomic signatures in response to different SARM compound administrations. For this purpose, livers from three animal SARM

compound (ostarine, LGD-4033, or RAD140) treatment groups and a control group ($n = 8$ per group) were processed simultaneously, with livers pooled, homogenised, and fractionated into their major intracellular components (cytosol, mitochondria, nuclei) and microsomes (derived from ER artefacts) by differential (ultra)centrifugation. Extracted proteins from subcellular samples were subjected to 2-D DIGE followed by comparative profiling of spots with differentially altered abundances and subsequent protein identification. Relevance of the proteome response and identified proteins in various molecular pathways was subsequently investigated with a view to determining the molecular effects of SARM compound action and to provide information on the potential mechanisms by which different SARMs mediate their tissue-selective effects in liver.

7.2 Experimental

7.2.1 Materials and reagents

Methods described here used the same materials and reagents as outlined in **Chapter 6 Section 6.2.1**. Additionally, Pierce EDTA-free protease inhibitor mini tablets from Thermo Fisher Scientific and trichloroacetic acid (TCA) were purchased from Sigma-Aldrich (Gillingham, UK) and EASYstrainer cell sieves for 50 mL tubes with a mesh size of 100 µm were from Greiner Bio-One (Stonehouse, UK).

7.2.2 *In vivo* SARM administration study

Liver samples were collected from the *in vivo* SARM administration study as described in **Chapter 6 Section 6.2.2**.

7.2.3 Preparation of subcellular liver fractions

The method for differential centrifugation used to isolate subcellular fractions (**Figure 7.1**) was modified from a protocol by Cox and Emili[541]. The preparation was mainly performed in a cold room (4 °C) and samples were kept on ice. Livers ($n = 8$ per treatment group; 1.5 g each) were pooled, finely minced with scissors and transferred into a 50 mL test tube. As a wash step 30 mL of PBS was added, samples were centrifuged at $100 \times g$ (4 °C) for 1 min and the supernatant discarded. This wash step was repeated four more times. Shortly before use, homogenisation buffer consisting of 50 mM Tris-HCl, 150 mM KCl, 250 mM sucrose, 5 mM $MgCl_2$, and 1 mM EDTA pH 7.4 at 4 °C was supplemented with protease inhibitors (1 EDTA-free mini tablet/ 100 mL). To rinse the livers one more time, 30 mL of homogenisation buffer was added, the samples were centrifuged at $100 \times g$ (4 °C) for 1 min and the supernatant discarded. Subsequently, 3 volumes (36 mL) of homogenisation buffer were added and the samples were homogenised manually with a Wheaton Potter-Elvehjem tissue grinder (PTFE pestle and glass tube with 50 mL capacity, chamber clearance 0.1 - 0.15 mm). Homogenates were transferred to a 50 mL tube with a cell sieve (100 µm mesh size) on top and centrifuged at $250 \times g$ (4 °C) for 5 min to remove red blood cells and cell debris. The pellet was discarded, and the supernatant transferred to a fresh test tube. Centrifugation at $250 \times g$ was repeated once more followed by centrifugation at $800 \times g$ (4 °C) for 15 min, and 20 mL of homogenisation buffer added to the resulting supernatant. The pellet (nuclei) was resuspended in 5 volumes (35 mL) of homogenisation buffer and centrifuged at $1000 \times g$ (4 °C) for 15 min. The nuclear pellet was saved, and the supernatant

transferred to a fresh test tube. Supernatants were centrifuged at $1000 \times g$ (4 °C) for 15 min for three and four more times respectively, whereby the resulting nuclear pellet was always saved, and the supernatant used for the next centrifugation. Nuclear pellets were combined and 44 mL of nuclei buffer consisting of 2 M sucrose, 50 mM Tris-HCl, 150 mM KCl, 5 mM $MgCl_2$, 1 mM EDTA, 1 mM DTT, and protease inhibitors (1 EDTA-free mini tablet/ 100 mL) pH 7.4 at 4 °C were added. Samples were centrifuged at $80\,000 \times g_{max}$ (4 °C) for one hour, resulting supernatant discarded, and the nuclear pellets resuspended in 3 mL of homogenisation buffer without protease inhibitor tablets, aliquoted and stored at -80 °C. Supernatants for isolation of mitochondria, cytosol, and microsomes were combined and centrifuged at $12\,000 \times g_{max}$ (4 °C) for 20 min. The supernatant was saved and the pellet (mitochondria) was resuspended in 50 mL of homogenisation buffer and repeatedly centrifuged at $12\,000 \times g_{max}$ (4 °C) for 20 min. This time the supernatant was discarded, and the mitochondrial pellet was resuspended in 3 mL of homogenisation buffer without protease inhibitor tablets, aliquoted and stored at -80 °C. The saved supernatant was repeatedly centrifuged at $12\,000 \times g_{max}$ (4 °C) for 20 min as well, whereby the pellet was discarded, and the resulting supernatant for isolation of cytosol and microsomes was centrifuged at $105\,000 \times g_{max}$ (4 °C) for one hour. The supernatant (cytosol) was transferred to a fresh test tube, aliquoted and frozen at -80 °C. The microsomal pellet was resuspended in 50 mL of washing buffer consisting of 150 mM KCl, and 1 mM EDTA pH 7.4 at 4 °C and centrifuged at $105\,000 \times g_{max}$ (4 °C) for one hour. The supernatant was discarded, and the microsomal pellet resuspended in 2 mL of homogenisation buffer without protease inhibitor tablets, aliquoted, and stored at -80 °C.

To summarise, the following subcellular fractions were isolated from rat livers ($n = 8$ per group) of untreated (control group) and SARM treated groups (ostarine, LGD-4033, and RAD140) by homogenisation and (ultra)centrifugation: nuclei (NUC), mitochondria (MIT), cytosol (CYT), and microsomes (MIC).

Rat liver homogenate

2 x │ 250 × g (4 °C) for 5 min

Pellet
Red blood cells

Supernatant

800 × g (4 °C) for 5 min

Pellet
Nuclei
+ Homogenisation buffer

Supernatant

4 x │ 1000 × g (4 °C) for 5 min

4 x │ 1000 × g (4 °C) for 5 min

Pellet
Nuclei

Supernatant

Supernatant

Pellet
Nuclei

Combined nuclear pellet
+ Nuclei buffer

80 00 × g (4 °C) for 60 min

2 x │ 12 000 × g (4 °C) for 20 min

Washed nuclear pellet

Pellet
Mitochondria
+ Homogenisation buffer

Supernatant

105 000 × g (4 °C) for 60 min

12 000 × g (4 °C) for 20 min

Washed mitochondrial pellet

Pellet
Microsomes
+ Wash buffer

**Supernatant
Cytosol**

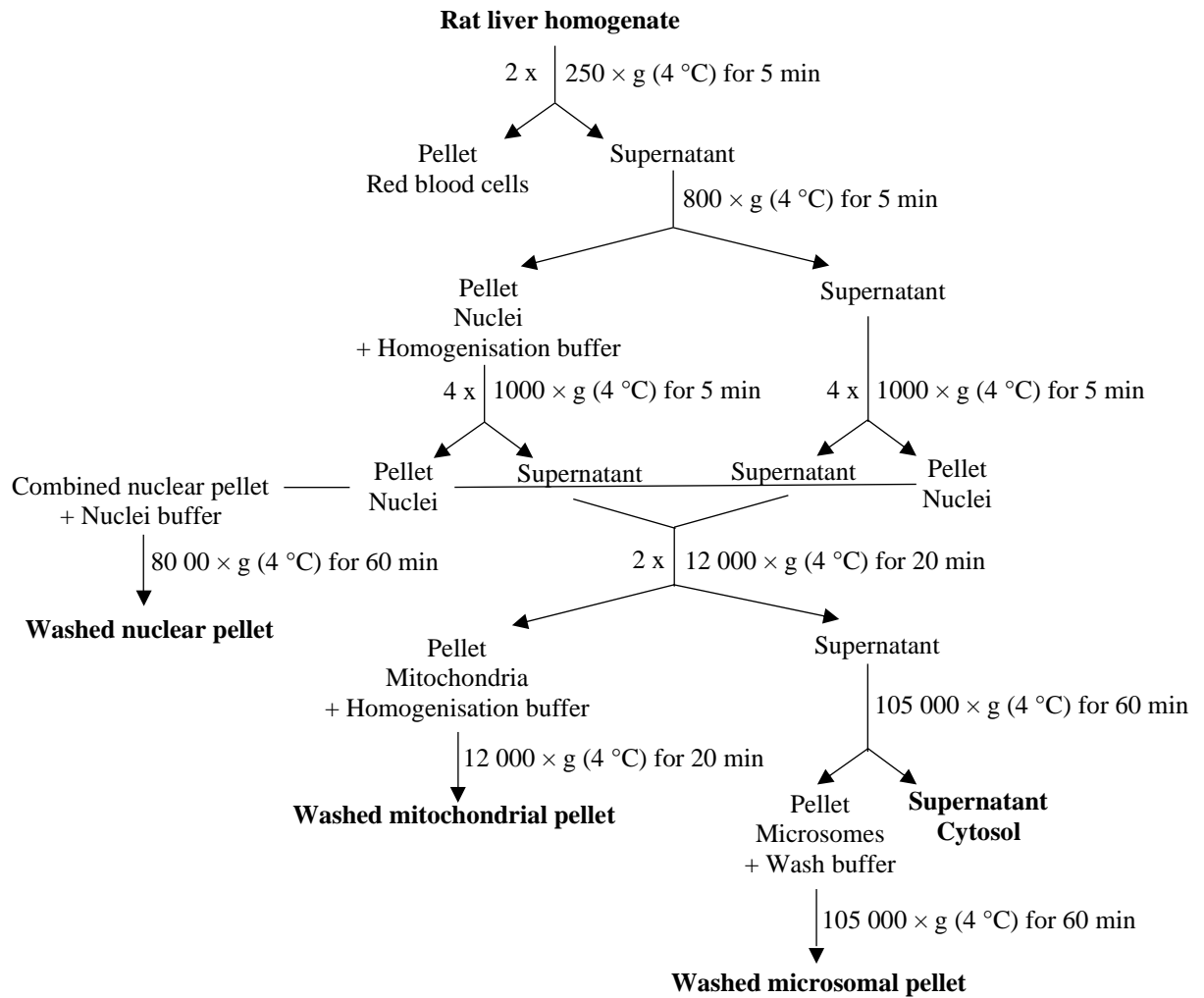105 000 × g (4 °C) for 60 min

Washed microsomal pellet

Figure 7.1 Scheme of subcellular fractionation by differential ultracentrifugation. Four fractions were isolated: nuclei, mitochondria, cytosol, and microsomes. Pellets were washed by resuspension followed by centrifugation and ultimately resuspended in homogenisation buffer without protease inhibitor tablets.

199

7.2.4   Subcellular protein extraction

75 µL of homogenisation buffer (50 mM Tris, 150 mM KCl, 250 mM sucrose, 5 mM $MgCl_2$, 1 mM EDTA supplemented with 1 EDTA-free protease inhibitor mini-tablet/ 100 mL) and 2 % Triton were added to an equal volume of each isolated fraction. Then, samples were incubated at 4 °C for one hour in a shaking (400 rpm) Thermomixer comfort (Eppendorf, Stevenage, UK). To shear DNA, samples of nuclear and mitochondrial fractions were passed 10 times through a 21 gauge needle. Lysed fractions were centrifuged at 10 000 $\times$ g (4 °C) for 10 min and 100 µL of the supernatant were transferred into a fresh 1.5 mL tube. For protein precipitation, 800 µL of acetone and 100 µL of TCA were added, vortexed and left at -20 °C overnight. Samples were centrifuged at 10 000 $\times$ g (4 °C) for 10 min and the supernatant discarded. The pellet was resuspended in 1 mL of acetone by vortexing and sonication and stored at -20 ° C for one hour. This acetone wash was repeated two more times and the cleaned-up pellet resuspended in lysis buffer.

7.2.5   Minimal fluorescent reciprocal labelling

Procedures for minimal fluorescent labelling were followed as described previously in **Chapter 6 Section 6.2.4**. Subcellular samples were labelled in duplicate using a reciprocal labelling approach to eliminate inconsistencies in spot intensities due to preferential labelling and combined (**Table 7.1** strip/gel 1-4). Instead of adding unlabelled protein to the fluorescent labelled samples as for lysates in **Chapter 6**, preparative gels with 400 µg or 600 µg of unlabelled protein were run on separate IEF strips (**Table 7.1** strip/gel 5-6).

7.2.6   2-D DIGE comparative subcellular profiling and MALDI-TOF protein spot identification

Comparative 2-D DIGE and MALDI-TOF analysis of protein spots with differential abundances were performed as previously described (**Chapter 6 Sections 6.2.5-6.2.8**). The workflow for preparation and analysis of analytical gels and preparative gels is illustrated in **Figure 7.2**. Analytical gels using 2-D DIGE were used for comparative proteomic profiling, whilst preparative gels using 2-D gel electrophoresis (GE) with Coomassie staining were subsequently used for protein spot identification by MALDI-TOF and PMF.

Table 7.1 Experimental set-up for 2-D DIGE analysis of subcellular fractions (NUC - nuclei, MIT - mitochondria, CYT - cytosol, MIC - microsomes). Six gels including four analytical DIGE gels with each sample of the four groups (ostarine, LGD-4033, RAD140, control) in duplicate (1, 2) and two preparative gels (400 µg or 600 µg protein) were run at a time. A normalisation pool of all samples was labelled with Cy2. Individual samples were labelled with Cy3 and Cy5.

Strip/Gel	Sample
1	Cy2 Pool NUC/ Cy3 NUC Control 1/ Cy5 NUC LGD-4033 1
2	Cy2 Pool NUC/ Cy3 NUC Ostarine 1/Cy5 NUC RAD140 1
3	Cy2 Pool NUC/ Cy3 NUC LGD-4033 2/ Cy5 NUC Ostarine 2
4	Cy2 Pool NUC/ Cy3 NUC RAD140 2/ Cy5 NUC Control 2
5	400 µg NUC
6	600 µg NUC
1	Cy2 Pool MIT/ Cy3 MIT Control 1/ Cy5 MIT LGD-4033 1
2	Cy2 Pool MIT/ Cy3 MIT Ostarine 1/Cy5 MIT RAD-140 1
3	Cy2 Pool MIT/ Cy3 MIT LGD-4033 2/ Cy5 MIT Ostarine 2
4	Cy2 Pool MIT/ Cy3 MIT RAD-140 2/ Cy5 MIT Control 2
5	400 µg MIT
6	600 µg MIT
1	Cy2 Pool CYT/ Cy3 CYT Control 1/ Cy5 CYT LGD-4033 1
2	Cy2 Pool CYT/ Cy3 CYT Ostarine 1/Cy5 CYT RAD140 1
3	Cy2 Pool CYT/ Cy3 CYT LGD-4033 2/ Cy5 CYT Ostarine 2
4	Cy2 Pool CYT/ Cy3 CYT RAD140 2/ Cy5 CYT Control 2
5	400 µg CYT
6	600 µg CYT
1	Cy2 Pool MIC/ Cy3 MIC Control 1/ Cy5 MIC LGD-4033 1
2	Cy2 Pool MIC/ Cy3 MIC Ostarine 1/Cy5 MIC RAD140 1
3	Cy2 Pool MIC/ Cy3 MIC LGD-4033 2/ Cy5 MIC Ostarine 2
4	Cy2 Pool MIC/ Cy3 MIC RAD140 2/ Cy5 MIC Control 2
5	400 µg MIC
6	600 µg MIC
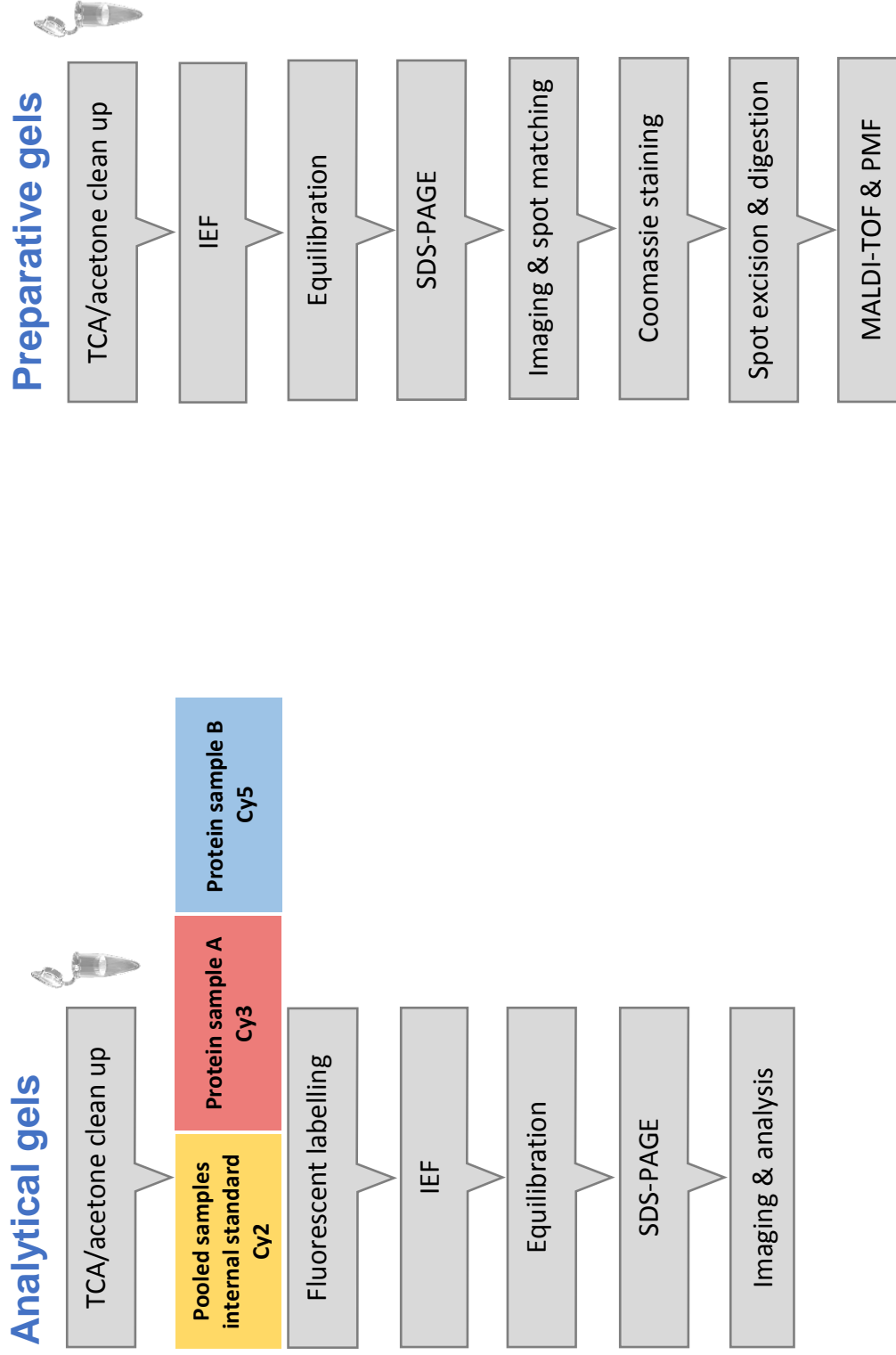
Figure 7.2 Summarised schematic workflow of 2-D DIGE for analytical gels and 2-D GE for preparative gels. Left: Workflow for 2-D DIGE of labelled protein samples. Right: Workflow for 2-D GE of unlabelled protein samples.

7.2.7   Bioinformatics analysis of proteomics data

The Kyoto Encyclopedia of Genes and Genomes Release 89.1 (KEGG, https://www.genome.jp/kegg/)[542], which is a collection of manually curated knowledge databases, was utilised to perform functional analysis. The KEGG classification was used to assign pathways and functional hierarchies to identified protein spots. Pathway enrichment analysis based on hypergeometric distribution followed by FDR correction was performed by submitting gene names for proteins to ShinyGo v060 (http://bioinformatics.sdstate.edu/go/).[543] Biological pathways that were significantly enriched in the gene lists were subsequently identified. UniProt accession numbers for the identified protein spots were submitted to the Search Tool for the Retrieval of Interacting Genes/Proteins (STRING) version 11.0 (https://string-db.org/)[544] to generate protein-protein interaction networks. STRING is a prediction software using several sources and techniques such as automated text mining, genomic context predictions, previous knowledge in databases, lab experiments, and co-expression to score this evidence and suggest a functional link.

7.3　　　　　Results

7.3.1　　　　2-D DIGE comparative subcellular proteomic profiling and MALDI-TOF protein spot identification

To enrich organelle-specific proteins and detect more subtle changes in response to SARM administration within the liver proteome, pooled rat livers were subfractionated into major cellular compartments (nuclei, mitochondria, microsomes, and cytosol) by differential (ultra)centrifugation. Proteomic analysis of rat liver subcellular fractions from SARM treated and non-treated control groups was performed using 2-D DIGE.

For gel images of each fraction, "between subject design" was used to analyse differences in protein spot abundance between treatment and control conditions. After spot detection and filtering using SameSpots software, 1437 protein spots within nuclei, 1664 within mitochondria, 1844 within microsomes, and 1796 within cytosol have been detected on 2-D DIGE images. Spot volumes were automatically normalised against Cy2 pools as internal standard and log transformed to stabilise variance. Outputs of the analysis included protein profiles of each spot with log transformed average spot volumes $\pm$ standard deviation (**Figure 7.3**). Spot volumes were normalised, and fold-changes were calculated as ratios of normalised volumes of a single spot between gels of treatment and control groups. Spots of interest between control and treatment group were selected based on relative fold-changes and significance ($p < 0.05$, ANOVA). Levels of 112 protein spots in total following treatment with SARM compounds were altered and are summarised in **Table 7.2**. Their location in representative Coomassie-stained gels with 400 µg protein of nuclei, mitochondria, microsomes, and cytosol after alignment with 2-D DIGE gels using SameSpots software is illustrated in **Figure 7.4**.

Venn diagrams were produced (**Figure 7.5**) to visualise the selected spots which exhibited increased or decreased abundances between treatment and control groups.[545] The relative abundance of 18 spots was uniquely altered in response to ostarine treatment (5 decreased, 13 increased). LGD-4033 and RAD140 uniquely altered abundances in 35 spots (five decreased, 30 increased) and in 24 spots (6 decreased, 18 increased) respectively. Eight spots had significantly altered relative levels by both ostarine and RAD140 treatment (four decreased, four increased), seven by both ostarine and LGD-4033 (one decreased, six increased), and eight by both LGD-4033 and RAD140 (five decreased, three increased). Relative abundances of 12 spots were commonly altered in response to each of the three SARM treatments. In total after ostarine administration 45 protein spots exhibited altered

levels (17 decreased, 28 increased). In response to LGD-4033 a total of 62 protein spots were modified in abundance (18 decreased, 44 increased). Upon RAD140 administration 52 protein spot levels were modified relative to the control group with an increase observed for 30 and a decrease for 22 spots. When looking at the number of spots by subcellular sample, a similar number of spots given in brackets was found to be altered by all three SARM compounds combined in cytosol (44), microsomes (40), and nuclei (41) whereas mitochondrial samples displayed the lowest number (29) of altered spots (**Figure 7.6**). Cytosol was the most impacted subcellular compartment by ostarine with 20 detected protein spots, whereas the least number of spots altered by ostarine was observed in mitochondrial samples with four spots. The largest number (21) of protein spots whose relative levels were altered by LGD-4033 were detected in samples from nuclei, with the lowest number of 12 spots found in mitochondria. In samples after RAD140 administration, spots with altered levels were relatively evenly distributed across all four compartments.

Following selection, spots of interest were manually excised from preparative Coomassie-stained gels with $400\,\mu g$ and $600\,\mu g$ protein of nuclei, mitochondria, microsomes or cytosol (**Figure 7.4)** for protein identification by tryptic in-gel digestion and MALDI-TOF analysis. Following a Mascot search using MS-acquired peak lists of peptides, 89 protein spots were identified corresponding to 58 unique proteins, and 22 spots could not be identified (**Table 7.2**). Nine identified proteins elicited a similar response in all treatment groups (increase of PDIA3, PDIA6, AIFM1A, INMT, and PCCB; decrease of DMGDH, GAPDH, NDUFS1, and NDUFS2). A representative mass spectrum from the mitochondrial spot no. 954 that has been identified as protein di-sulfide isomerase A3 is presented in **Figure 7.3**.

(A) 2-D DIGE comparative subcellular proteomic profiling using SameSpots software
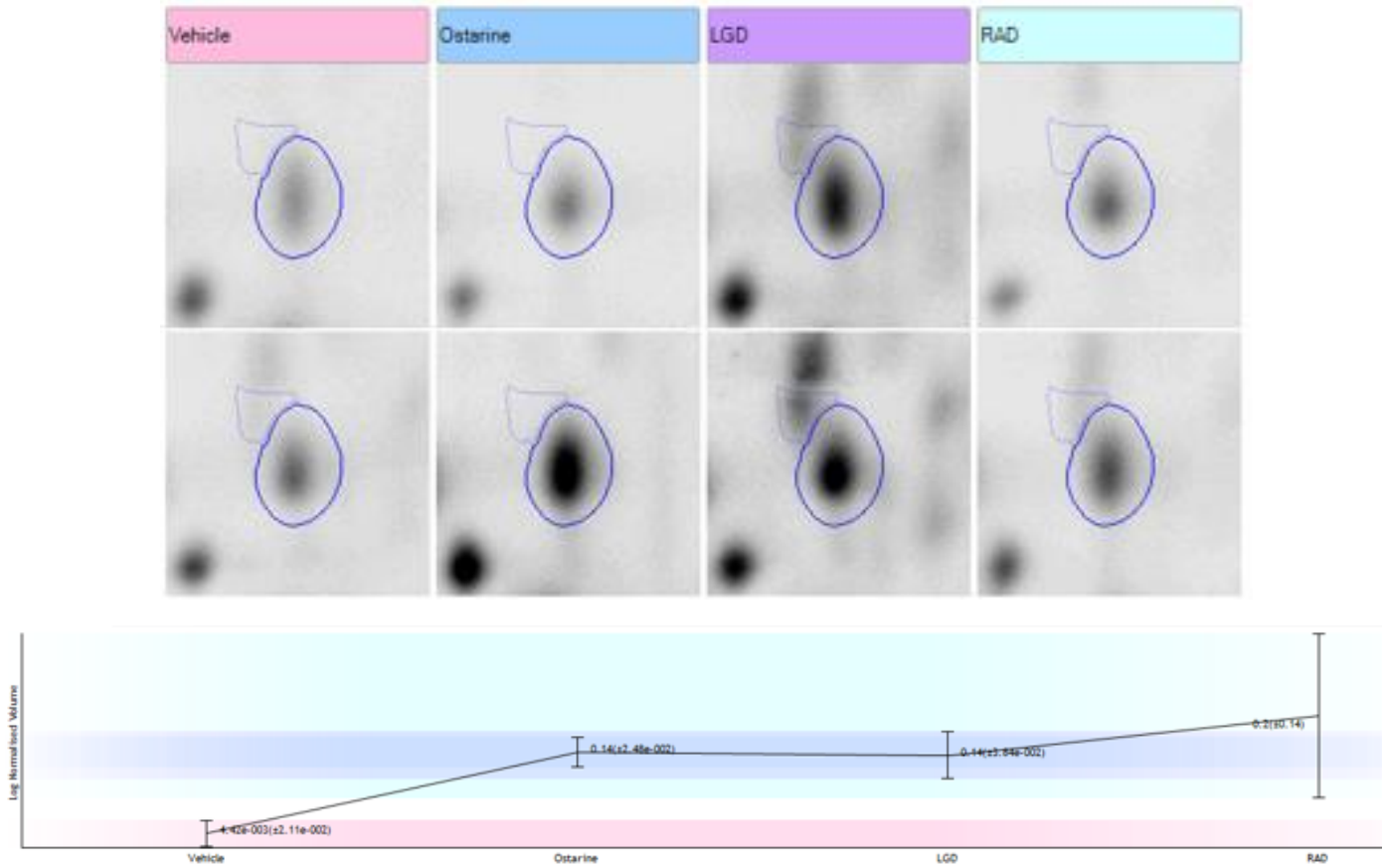
(B) Protein spot identification using MALDI-TOF analysis and Mascot server
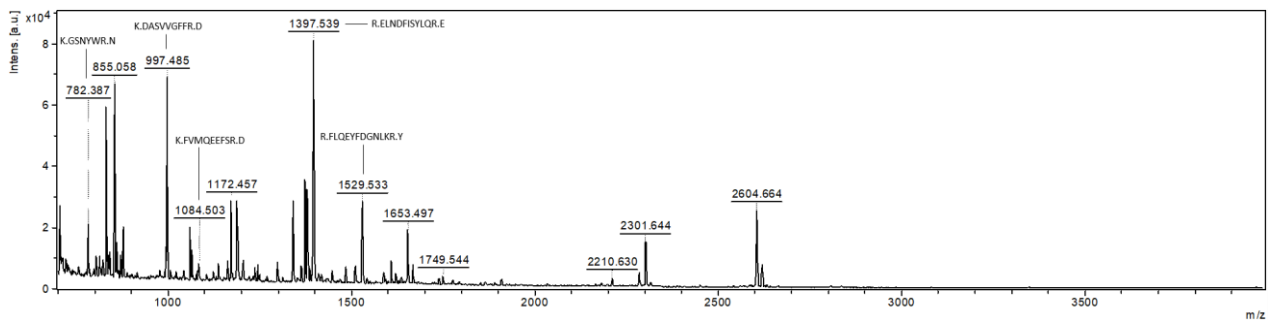
Figure 7.3 Spot no. 954 (nuclei) was selected as representative spot to illustrate the workflow. **(A)** Protein spot profile with log transformed average spot volumes ± standard deviation. The spot abundance was significantly ($p < 0.05$) increased upon treatment with ostarine, LGD-4033, or RAD140. **(B)** Representative MALDI spectrum obtained after tryptic digestion of a colloidal Coomassie-stained protein spot. Upon submission of the peptide peak list to the Mascot server, spot number 954 was identified as protein di-sulfide isomerase A3.11 peptides matched the protein sequence. Peptide sequences have been partly assigned to the observed mass fragments.
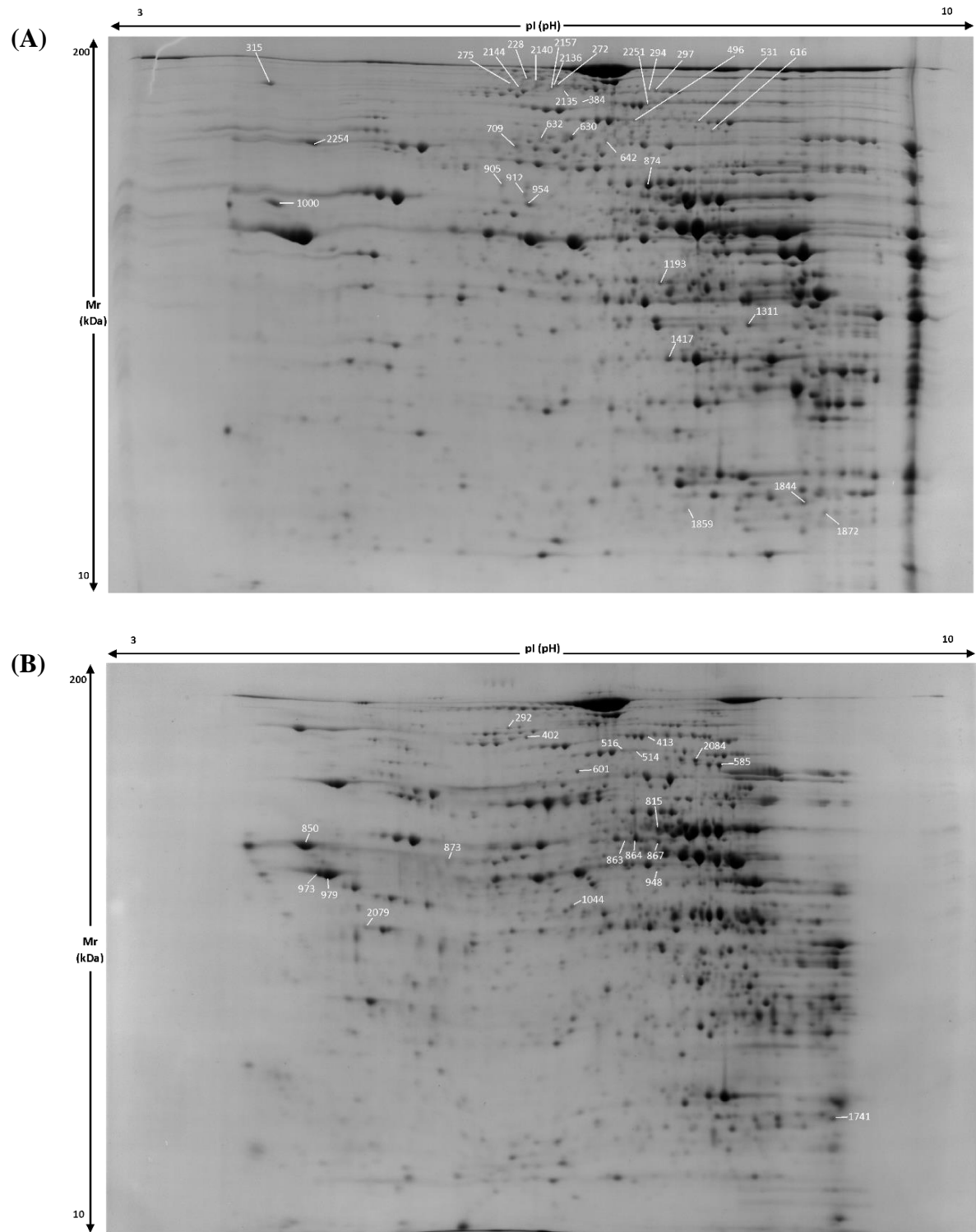
Figure 7.4 Coomassie-stained gel images used for spot picking with assigned spot numbers of selected proteins of rat liver **(A)** nuclei, **(B)** mitochondria, **(C)** microsomes, and **(D)** cytosol samples (400 μg protein).
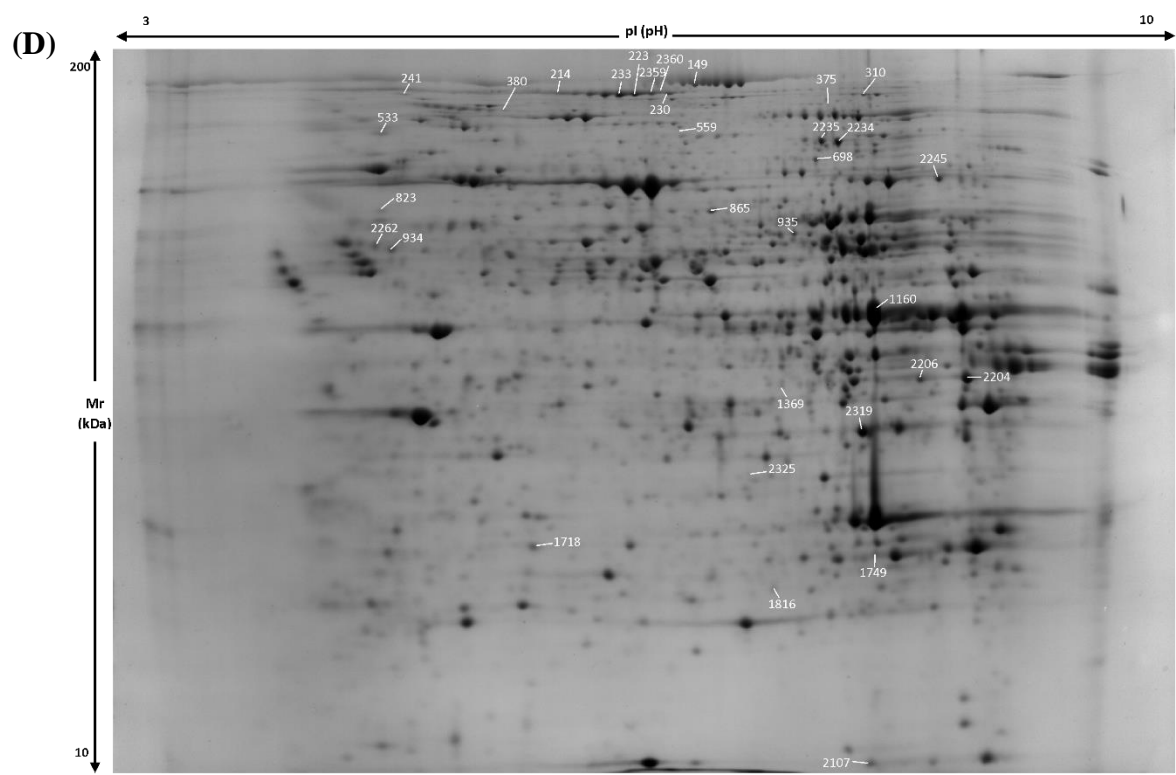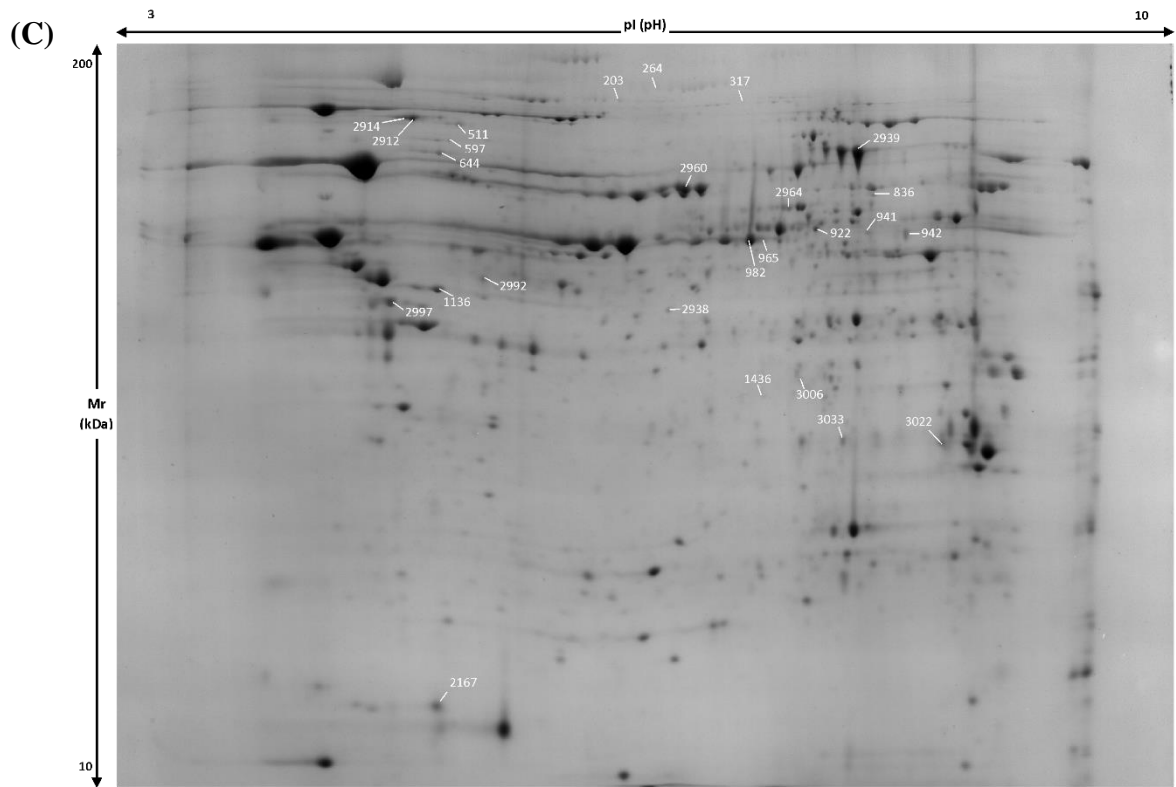
Figure 7.4 *continued* Coomassie-stained gel images used for spot picking with assigned spot numbers of selected proteins of rat liver **(A)** nuclei, **(B)** mitochondria, **(C)** microsomes, and **(D)** cytosol samples (400 µg protein).
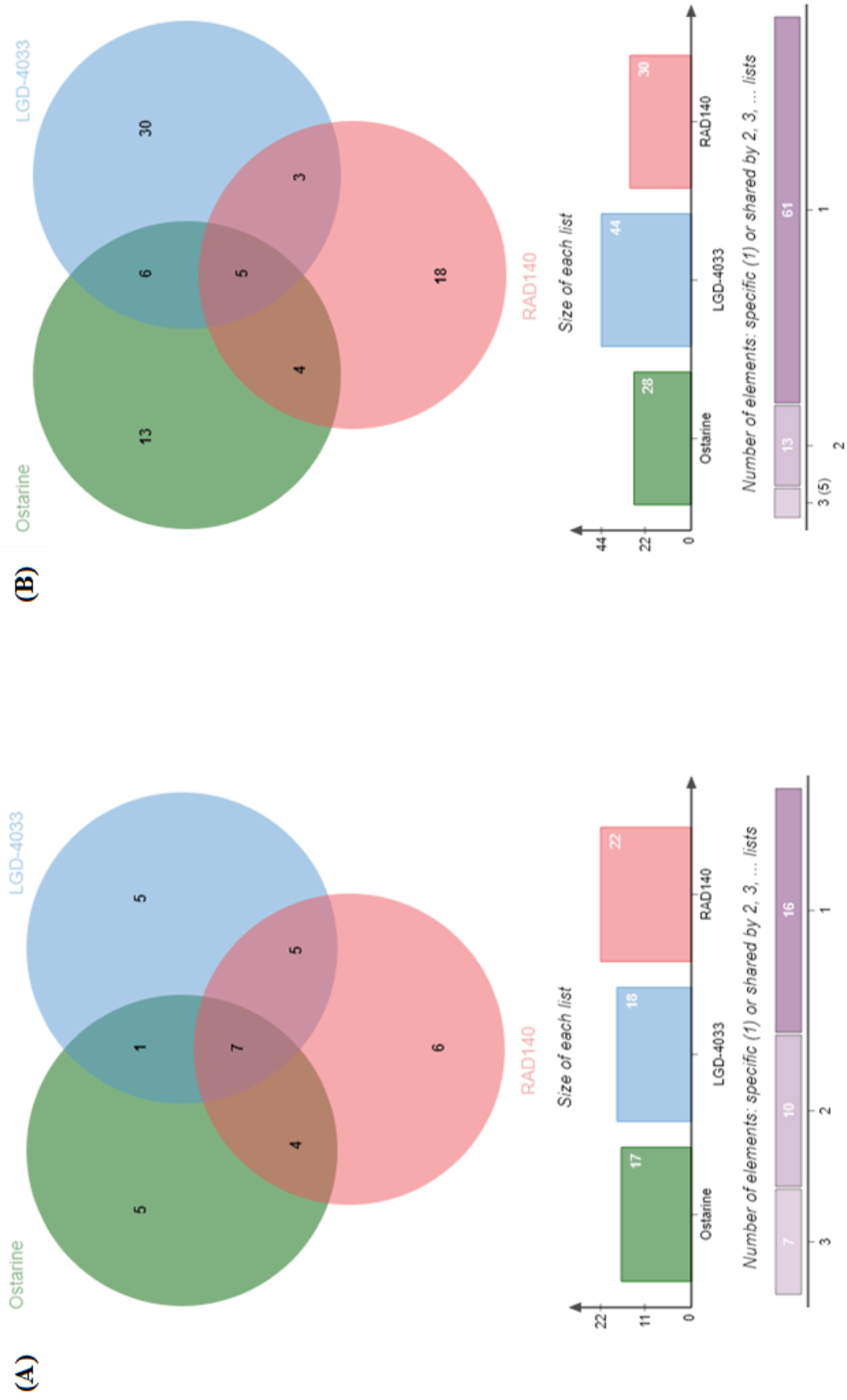
Figure 7.5 Differential protein spots with relative (**A**) decreased or (**B**) increased levels after treatment with ostarine, LGD-4033, or RAD140 compared to the control group.
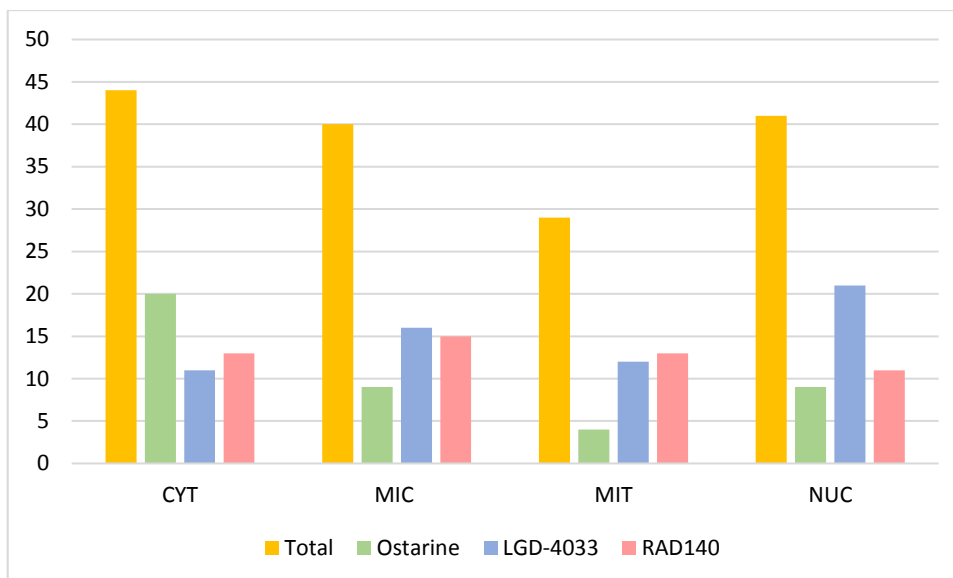
Figure 7.6 Number of spots with differential response to treatment with ostarine, LGD-4033, or RAD140 compared to the control group in subcellular samples from cytosol (CYT), microsomes (MIC), mitochondria (MIT), and nuclei (NUC). The yellow bar displays the number of spots with altered levels in response to all three SARM compounds combined per subcellular compartment.

Table 7.2 Protein spots with relative fold-changes and significance (NS, not significant; * $p < 0.05$; ** $p < 0.01$; *** $p < 0.005$) in rat liver nuclei (NUC), microsomes (MIC), mitochondria (MIT), or cytosol (CYT) following 17 days of ostarine, LGD-4033, or RAD140 administration versus non-treated group. Protein spots were identified by Mascot search of SwissProt or NCBIprot databases.

| Protein name	Spot No.	Sample	Relative fold-change			Estimated		UniProt Accession No.	SwissProt NCBIprot Entry Name	Protein spot Mascot identification					
			Ostarine	LGD-4033	RAD140	Mr (kDa)	pI			Mr (kDa)	pI	Sequence coverage (%)	No. of peptides matched	Score	Expectation value
3-Oxo-5-beta-steroid 4-dehydrogenase	1369	CYT	0.56*	0.61*	0.54NS	35.790	6.68	P31210	AK1D1_RAT	37.639	6.18	22	7	86	1.80E-05
Aconitate hydratase, mitochondrial	531	NUC	0.70*	0.82NS	0.74*	83.003	7.06	Q9ER34	ACON_RAT	86.121	7.87	16	8	65	2.50E-03
Actin, cytoplasmic 1	2079	MIT	1.19NS	1.21**	1.22NS	45.058	5.29	P60711	ACTB_RAT	42.052	5.29	26	7	49	1.10E-01
Actin, cytoplasmic 2								P63259	ACTG_RAT	42.108	5.31	26	7	49	1.10E-01
Acyl-coenzyme A synthetase ACSM1, mitochondrial isoform X4	874	NUC	0.89NS	0.85NS	0.85*	65.437	6.68		XP_008757993.1	65.854	7.25	23	10	129	1.10E-08
Aldehyde oxidase 3	230	CYT	1.38*	1.36NS	1.15NS	135.622	6.13	Q5QE80	AOXC_RAT	148.595	6.41	14	13	63	4.00E-03
	2360		1.34NS	1.33*	1.07NS	139.576	6.06	Q5QE80	AOXC_RAT	148.595	6.41	8	9	75	2.60E-04
Alpha-1-antiproteinase	934	CYT	1.15NS	1.35NS	1.65*	59.504	4.97	P17475	A1AT_RAT	46.278	5.7	44	14	110	8.00E-08
	2262	CYT	0.96NS	1.27*	1.28*	60.622	4.72	P17475	A1AT_RAT	46.278	5.7	26	9	99	9.20E-07
Alpha-1-macroglobulin	317	MIC	1.27NS	1.05NS	1.16*	-	6.48	Q63041	A1M_RAT	168.388	6.46	8	8	48	1.20E-01
Apoptosis-inducing factor 1, mitochondrial	836	MIC	1.29***	1.17***	1.19*	68.882	7.40	Q9JM53	AIFM1_RAT	66.966	9.06	25	15	127	1.60E-09
ATP-citrate synthase	310	CYT	1.03NS	0.93NS	0.83*	113.479	7.26	P16638	ACLY_RAT	121.471	6.96	11	13	110	8.00E-08
Betaine-homocysteine S-methyltransferase	1160	CYT	1.21*	1.09NS	1.05NS	44.849	8.07	O09171	BHMT1_RAT	45.404	8.02	58	20	168	1.30E-13
	228		0.77NS	2.13NS	1.19NS	149.874	6.05	P07756	CPSM_RAT	165.673	6.33	11	18	77	1.60E-04
	272		0.81NS	1.85***	1.41NS	118.276	6.17	P07756	CPSM_RAT	165.673	6.33	15	22	139	1.00E-10
	632		0.59NS	2.37*	1.35NS	77.470	6.12	P07756	CPSM_RAT	165.673	6.33	14	17	88	1.30E-05
	2136	NUC	0.68NS	1.73*	1.17NS	118.276	6.16	P07756	CPSM_RAT	165.673	6.33	15	22	114	3.20E-08
	2140		0.68NS	2.16*	1.40NS	119.856	6.10	P07756	CPSM_RAT	165.673	6.33	9	13	86	1.80E-05
	2144		0.73NS	2.54*	1.34NS	116.696	6.04	P07756	CPSM_RAT	165.673	6.33	17	26	177	1.60E-14
Carbamoyl-phosphate synthase [ammonia], mitochondrial	2251		0.83NS	0.67*	0.57***	89.785	6.67	P07756	CPSM_RAT	165.673	6.33	13	16	63	3.90E-03
	149		1.16*	0.99NS	0.96NS	159.346	6.29	P07756	CPSM_RAT	165.673	6.33	33	46	323	4.00E-29
	223	CYT	1.32*	1.15NS	1.14NS	136.413	5.98	P07756	CPSM_RAT	165.673	6.33	22	28	192	5.10E-16
	2359		1.16*	1.08NS	1.09NS	141.158	6.04	P07756	CPSM_RAT	165.679	6.33	12	18	111	6.40E-08
	203	MIC	1.32*	1.15NS	1.10NS	-	6.00	P07756	CPSM_RAT	165.673	6.33	10	12	87	1.50E-05
	264		1.37NS	1.24***	1.06NS	-	5.88	P07756	CPSM_RAT	165.673	6.33	11	14	70	8.80E-04
	233	CYT	1.39*	1.16NS	1.09NS	132.459	5.93	P07756	CPSM_RAT	165.673	6.33	25	36	239	1.00E-20
	935	CYT	1.32*	0.94NS	1.05NS	59.504	6.78	P16303	CES1D_RAT	62.393	6.10	37	13	98	1.40E-06
Carboxylesterase 1D	864	MIT	1.44***	1.36NS	1.64NS	58.532	6.94	P16303	CES1D_RAT	62.393	6.10	34	14	156	2.00E-12
	965	MIC	1.40NS	1.17NS	1.59***	59.930	6.65	P16303	CES1D_RAT	62.393	6.10	20	10	69	9.90E-04
	982		1.26NS	1.09NS	1.26*	59.252	6.51	P16303	CES1D_RAT	62.393	6.10	35	13	116	2.00E-08

211

Table 7.2 *continued*

Protein name	Spot No.	Sample	Relative fold-change			Estimated		UniProt Accession No.	SwissProt NCBIprot Entry Name	Protein spot Mascot identification					
			Ostarine	LGD-4033	RAD140	Mr (kDa)	pI			Mr (kDa)	pI	Sequence coverage (%)	No. of peptides matched	Score	Expectation value
Catalase	922	MIC	1.19^{NS}	1.13^{NS}	1.29*	61.693	6.87	P04762	CATA_RAT	60.062	7.07	27	12	159	1.00E-12
Cytochrome b-c1 complex subunit 1, mitochondrial	1136	MIC	0.84*	0.90^{NS}	0.80*	48.808	5.26	Q68FY0	QCR1_RAT	53.500	5.57	20	8	94	3.00E-06
Dimethylglycine dehydrogenase, mitochondrial	496	NUC	0.61***	0.64*	0.64*	84.431	6.56	Q63342	M2GD_RAT	96.273	6.91	14	7	50	7.70E-02
	514	MIT	0.63*	0.53*	0.54*	89.009	6.95	Q63342	M2GD_RAT	96.273	6.91	13	7	45	2.50E-01
	516	MIT	0.82^{NS}	0.62***	0.75*	88.670	6.87	Q63342	M2GD_RAT	96.273	6.91	17	9	67	1.60E-03
Electron transfer flavoprotein-ubiquinone oxidoreductase	2964	MIC	0.96^{NS}	0.85^{NS}	0.86***	66.440	6.71	Q6UPE1	ETFD_RAT	69.010	7.33	11	6	61	6.80E-03
Endoplasmic reticulum chaperone Bip	2254	NUC	1.34^{NS}	1.22^{NS}	1.65*	72.473	5.14	P06761	BIP_RAT	72.473	5.07	32	21	211	6.40E-18
endoplasmic reticulum resident protein 44 precursor	2997	MIC	0.75**	0.83^{NS}	0.83*	47.248	5.10		NP_001008318.1	47.248	5.09	40	13	157	1.70E-11
Endoplasmin	315	NUC	1.59*	1.73^{NS}	1.74*	92.998	4.70	Q66HD0	ENPL_RAT	92.998	4.72	27	16	123	4.00E-09
Fibrinogen beta chain	942	MIC	1.08^{NS}	1.16^{NS}	1.27*	60.472	7.81	P14480	FIBB_RAT	54.828	7.9	34	15	90	7.30E-06
Formimidoyltransferase-cyclodeaminase	873	MIT	1.21^{NS}	1.38^{NS}	1.42*	48.675	5.14	O88618	FTCD_RAT	59.504	5.80	28	9	67	1.50E-03
Glutaminase liver isoform, mitochondrial	867	MIT	1.24^{NS}	1.14^{NS}	1.48*	58.399	7.09	P28492	GLSL_RAT	67.060	7.07	20	10	54	3.10E-02
Glutathione S-transferase Mu 1	1844	NUC	1.01^{NS}	1.08^{NS}	1.33*	26.595	8.07	P04905	GSTM1_RAT	26.068	8.27	55	13	128	1.30E-09
	1741	MIT	1.22^{NS}	1.25*	1.27*	26.068	8.34	P04905	GSTM1_RAT	26.068	8.27	49	10	103	4.0e-07
Glutathione S-transferase Mu 2	1859	NUC	0.72*	0.97^{NS}	0.89^{NS}	26.151	6.99	P08010	GSTM2_RAT	25.857	6.9	26	4	59	1.00E-02
Glyceraldehyde-3-phosphate dehydrogenase	3009	MIC	0.75^{NS}	0.87*	0.85*	40.618	8.38	P04797	G3P_RAT	36.090	8.14	21	5	64	3.40E-03
	2204	CYT	0.47***	0.62**	0.60**	36.526	8.12	P04797	G3P_RAT	36.090	8.14	38	12	86	2.20E-05
	2206	CYT	0.49*	0.64*	0.60***	36.044	7.68	P04797	G3P_RAT	36.090	8.14	30	7	81	6.70E-05
Glycine N-methyltransferase	3033	MIC	1.29*	1.26^{NS}	1.13^{NS}	37.736	7.05	P13255	GNMT_RAT	32.298	7.10	33	6	59	1.10E-02
Heat shock protein HSP 90-beta	533	CYT	0.93^{NS}	0.75^{NS}	0.83*	87.456	4.91	P34058	HS90B_RAT	83.571	4.97	27	16	110	8.00E-08
Hydroxyacid oxidase 1	1311	NUC	1.21**	1.13^{NS}	1.2^{NS}	46.252	7.50	-	NP_001101250.1	41.227	6.92	45	14	136	2.20E-09
Indolethylamine N-methyltransferase	1718	CYT	1.54*	1.50*	1.71*	30.025	5.54	-	NP_001102492.1	29.989	5.70	57	8	104	3.40E-06
Kynurenine-oxoglutarate transaminase 3	1193	NUC	1.25*	1.17^{NS}	1.03^{NS}	51.582	6.79	Q58FK9	KAT3_RAT	51.582	8.61	45	18	174	3.20E-14
Liver carboxylesterase 4	815	MIT	1.23*	1.25**	1.36^{NS}	62.128	7.09	Q64573	EST4_RAT	62.668	6.29	29	10	83	3.80E-05
Major urinary protein	2167	MIC	0.90^{NS}	1.22*	1.09^{NS}	21.009	5.29	P02761	MUP_RAT	21.009	5.85	50	9	56	2.30E-02
Major vault protein	380	CYT	1.04^{NS}	1.29*	1.40*	96.081	5.47	Q62667	MVP_RAT	96.081	5.43	15	9	50	8.00E-02
Maleylacetoacetate isomerase	1816	CYT	0.86^{NS}	1.29*	1.09^{NS}	28.192	6.62	P57113	MAAI_RAT	24.174	7.63	62	11	98	1.20E-06

Table 7.2 *continued*

Protein name	Spot No.	Sample	Relative fold-change			Estimated		UniProt Accession No.	SwissProt *NCBIprot* Entry Name	Protein spot Mascot identification					
			Ostarine	LGD-4033	RAD140	Mr (kDa)	pI			Mr (kDa)	pI	Sequence coverage (%)	No. of peptides matched	Score	Expectation value
Methylcrotonoyl-CoA carboxylase beta chain, mitochondrial	941	MIC	1.14^NS	1.12^NS	1.43*	60.472	7.37	Q5XIT9	MCCB_RAT	61.992	8.56	20	9	72	5.60E-04
MICOS complex subunit Mic60 (Fragment)	597	MIC	0.82^NS	0.79*	0.80^NS	82.473	5.30	Q3KR86	MIC60_RAT	67.477	5.57	17	8	44	2.90E-01
NADH dehydrogenase [ubiquinone] 1 beta subcomplex subunit 10	1872	NUC	1.12^NS	1.49*	0.82^NS	25.683	8.56	-	*NP_001102913.1*	21.131	7.57	58	10	92	5.20E-05
NADH dehydrogenase [ubiquinone] iron-sulfur protein 2, mitochondrial	2938	MIC	0.70*	0.79*	0.65**	46.533	6.05	Q641Y2	NDUS2_RAT	52.927	6.52	10	4	51	6.10E-02
NADH-ubiquinone oxidoreductase 75 kDa subunit, mitochondrial	644	MIC	0.74*	0.82*	0.78*	78.241	5.27	Q66HF1	NDUS1_RAT	80.331	5.65	18	8	82	4.80E-05
Neutral alpha-glucosidase AB isoform X2	292	MIT	1.11^NS	1.33*	1.10^NS	-	6.11	-	*XP_006231039.1*	107.293	5.69	38	32	256	2.20E-21
Not identified	275	NUC	0.79^NS	1.69*	1.26^NS	116.696	5.97								
	294		0.85^NS	1.51*	1.15^NS	105.637	6.73								
	297		0.96^NS	1.23*	0.94^NS	102.477	6.67								
	384		0.69^NS	1.83*	1.15^NS	89.607	6.29								
	630		0.95^NS	1.28*	1.05^NS	79.434	7.10								
	905		0.76^NS	2.22*	1.48^NS	63.355	5.95								
	912		0.62***	2.87**	1.43^NS	62.244	6.05								
	2135		0.97^NS	2.05*	1.47^NS	92.998	6.15								
	2157		0.72^NS	1.90*	1.20^NS	102.477	6.21								
	601	MIT	0.79*	0.86^NS	0.82*	76.914	6.60								
	948		0.84^NS	0.75**	0.82*	51.472	7.09								
	1044		0.83^NS	0.87^NS	0.75*	46.235	6.55								
	1436	MIC	0.71*	0.76*	0.66*	40.509	6.60								
	2992		1.12	1.19***	1.18^NS	51.927	5.44								
	3006		1.25^NS	1.08^NS	1.20*	41.831	6.78								
	214		1.15*	1.01^NS	0.88^NS	140.367	5.66								
	559		1.05^NS	1.26*	1.06^NS	82.345	6.17								
	823		0.89^NS	1.26*	1.31*	66.586	4.87								
	1749	CYT	0.67**	0.95^NS	0.95^NS	29.414	7.31								
	2245		0.82*	0.96^NS	1.02^NS	69.940	7.88								
	2319		1.38*	1.18^NS	1.21*	34.383	7.23								
	2325		1.72*	1.64*	1.51*	32.492	6.52								
Ornithine carbamoyl-transferase, mitochondrial	1417	NUC	0.85^NS	0.87^NS	0.75*	42.753	6.85	P00481	OTC_RAT	39.918	9.12	61	18	138	1.30E-10

Table 7.2 *continued*

Protein name	Spot No.	Sample	Ostarine	LGD-4033	RAD140	Est. Mr (kDa)	Est. pI	UniProt Accession No.	SwissProt / NCBIprot Entry Name	Mascot Mr (kDa)	Mascot pI	Sequence coverage (%)	No. of peptides matched	Score	Expectation value
Peroxiredoxin-5, mitochondrial	2107	CYT	1.04^{NS}	1.10^{NS}	1.30*	22.68	7.22	Q9R063	PRDX5_RAT	22.507	8.94	40	7	84	3.60E-05
Phosphoglucomutase-1	865	CYT	1.21*	1.26*	1.18^{NS}	63.604	6.30	P38652	PGM1_RAT	61.650	6.30	24	9	86	1.90E-05
Probable 10-formyltetrahydrofolate dehydrogenase ALDH1L2	402	MIT	0.86^{NS}	0.86*	0.70*	100.182	6.22		*NP 001178707.1*	102.359	5.76	27	21	110	8.60E-07
Probable 2-oxoglutarate dehydrogenase E1 component DHKTD1, mitochondrial	413	MIT	0.81^{NS}	0.60*	0.74^{NS}	99.505	7.03	Q4KLP0	DHTK1_RAT	103.318	6.57	13	9	46	1.80E-01
Procollagen-lysine,2-oxoglutarate 5-dioxygenase 2	642	NUC	0.77^{NS}	1.63*	1.20^{NS}	76.400	6.40	Q811A3	PLOD2_RAT	85.116	6.26	16	8	65	2.40E-03
Propionyl-CoA carboxylase alpha chain, mitochondrial	709	NUC	0.82^{NS}	1.58**	1.19^{NS}	73.365	6.01	P14882	PCCA_RAT	82.198	7.59	15	10	84	2.40E-03
Propionyl-CoA carboxylase beta chain, mitochondrial	863	MIT	1.56*	1.42**	1.53**	58.532	6.89	P07633	PCCB_RAT	59.216	7.19	21	7	44	3.00E-01
Protein di-sulfide isomerase A1	1000	NUC	1.30^{NS}	1.14^{NS}	1.62*	57.068	4.92	P04785	PDIA1_RAT	57.315	4.82	49	20	221	6.40E-19
	850	MIT	1.23**	1.31^{NS}	1.50*	59.598	4.81	P04785	PDIA1_RAT	57.315	4.82	34	11	99	1.10E-06
Protein di-sulfide isomerase A3	954	NUC	1.37**	1.36*	1.59*	59.328	6.08	P11598	PDIA3_RAT	57.044	5.88	17	11	99	9.40E-07
Protein di-sulfide isomerase A6	973	MIT	1.14^{NS}	1.18*	1.25**	48.675	5.14	Q63081	PDIA6_RAT	48.542	5.00	24	7	71	6.80E-04
	979	NUC	1.22*	1.24*	1.34*	48.542	5.20	Q63081	PDIA6_RAT	48.542	5.00	23	8	82	4.60E-05
Serotransferrin	616	NUC	1.00^{NS}	1.23^{NS}	1.30**	79.434	7.17	P12346	TRFE_RAT	78.512	7.14	26	14	119	1.00E-08
	585	MIT	1.15^{NS}	1.37^{NS}	1.38^{NS}	78.512	7.54	P12346	TRFE_RAT	78.512	7.14	24	14	144	3.20E-11
	2084	MIC	1.05^{NS}	1.35*	1.16^{NS}	81.898	7.34	P12346	TRFE_RAT	78.512	7.14	22	12	137	1.60E-10
	2939	MIC	1.05^{NS}	1.16^{NS}	1.08^{NS}	78.309	7.24	P12346	TRFE_RAT	78.512	7.14	30	18	199	1.00E-16
	698	CYT	0.89^{NS}	1.25^{NS}	1.33*	74.288	6.91	P12346	TRFE_RAT	78.512	7.14	17	10	103	4.00E-07
	2235	CYT	0.80*	0.96^{NS}	0.87^{NS}	78.077	6.95	P12346	TRFE_RAT	78.512	7.14	19	10	105	2.50E-07
	2237	CYT	1.32*	1.16^{NS}	1.14^{NS}	77.829	7.07	P12346	TRFE_RAT	78.512	7.14	22	13	131	6.40E-10
Serum albumin	2960	MIC	1.37^{NS}	1.35*	1.51^{NS}	70.781	6.15	P02770	ALBU_RAT	70.682	6.09	25	13	133	4.00E-10
Spectrin alpha chain, non-erythrocytic	241	CYT	1.15*	1.01^{NS}	1.27*	130.877	5.07	P16086	SPTN1_RAT	285.261	5.20	13	29	126	2.00E-09
Staphylococcal nuclease domain-containing protein 1	375	CYT	1.06^{NS}	0.77*	0.90^{NS}	97.663	6.98	Q66X93	SND1_RAT	102.573	6.79	14	9	59	1.00E-02
Transitional endoplasmic reticulum ATPase	511	MI	1.08	1.20*	1.01^{NS}	87.892	5.34	P46462	TERA_RAT	89.977	5.14	10	9	55	2.30E-02
	2912	MI	1.35*	1.31^{NS}	1.10^{NS}	89.664	5.17	P46462	TERA_RAT	89.977	5.14	60	41	306	2.00E-27
	2914	MI	1.32*	1.26*	1.08^{NS}	89.873	5.16	P46462	TERA_RAT	89.977	5.14	30	15	143	4.00E-11
Voltage-dependent anion-selective channel protein 1	3022	MIC	0.83^{NS}	0.86***	0.83^{NS}	36.804	8.31	Q9Z2L0	VDAC1_RAT	30.851	8.62	31	5	71	6.80E-04

214

7.3.2 KEGG pathway and enrichment analysis of identified proteins

As proteins control many biological processes and can have a variety of molecular functions, MALDI-TOF identified proteins were assigned to pathways and protein families (**Table 7.3**) using the KEGG (https://www.genome.jp/kegg/)[542] databases, and classified into the following KEGG BRITE protein families: metabolism, genetic information processing, environmental information processing, cellular processes, organismal systems, and human diseases. Some of the proteins were not in the database and as such were not assigned to protein families.

Figure 7.7 illustrates the relative contribution (%) of identified proteins to each specified network, with all three SARM treatments demonstrating similar trends in terms of the protein distribution within networks, with most associated with metabolism, and principally amino acid, carbohydrate, and energy metabolism. Proteins associated with metabolism accounted for 38 %, 37 % and 30 % of all significantly regulated proteins in subcellular liver samples by ostarine, LGD-4033 and RAD140 respectively. 15 %, 18 %, and 19 % of identified proteins for ostarine, LGD-4033 and RAD140 respectively were linked to organismal systems, and similarly, 17 % (ostarine), 18 % (LGD-4033), and 19 % (RAD140) were assigned to the human diseases network. Genetic and environmental information processing, cellular responses, and unassigned networks accounted for a minority of identified proteins.

To identify specific KEGG pathways that were overrepresented, lists of gene names derived from MALDI-TOF identified proteins were submitted to ShinyGO v060 using rat as matching species and a false discovery rate (FDR) corrected p-value cut-off of 0.05. The search was limited to the 20 most significant terms (**Table 7.4**) and enrichment analysis revealed 12 pathways to be significantly impacted in response to all three SARM treatments. These were mostly related to metabolism, but also human diseases (Alzheimer's, Huntington's, Parkinson's), genetic information processing (protein processing in the ER) and organismal systems (thermogenesis). For example, the enriched pathway for protein processing in the ER included protein di-sulfide isomerase A3 (PDIA3), protein di-sulfide isomerase A6 (PDIA6), endoplasmin, protein di-sulfide isomerase A1 (P4HB), endoplasmic reticulum chaperone binding immunoglobulin protein (BIP), heat shock protein 90-beta (HSP90AB1), neutral alpha-glucosidase AB isoform X2 (GANAB), and/or transitional endoplasmic reticulum ATPase (VCP) and was mapped using KEGG as illustrated in **Figure 7.8**.

215

Table 7.3 MALDI-TOF identified protein spots in alphabetical order with sample types (NUC - nuclei, MIT- mitochondria, MIC - microsomes, CYT - cytosol), spots numbers, relative fold-change, p-values (* $p < 0.05$; ** $p < 0.01$; *** $p < 0.005$) for ostarine, LGD-4033, and RAD140, gene names, KEGG Orthology (KO) definition, their involvement in KEGG pathways and assignment to KEGG BRITE protein families.

Protein name	Sample	Spot No.	Relative fold-change			Gene name	KO definition	KEGG Pathway Rattus norvegicus [rno]	KEGG Brite Protein family
			Ostarine	LGD-4033	RAD140				
3-Oxo-5-beta-steroid 4-dehydrogenase	CYT	1369	0.56*	0.61*	0.54NS	Akr1d1		00120 Primary bile acid biosynthesis, 00140 Steroid hormone biosynthesis ,01100 Metabolic pathways	Metabolism
Aconitate hydratase, mitochondrial	NUC	531	0.70*	0.82NS	0.74*	Aco2	K01681	00020 Citrate cycle (TCA cycle), 00630 Glyoxylate and dicarboxylate metabolism, 01100 Metabolic pathways, 01200 Carbon metabolism, 01210 2-Oxocarboxylic acid metabolism, 01230 Biosynthesis of amino acids	Metabolism
Actin, cytoplasmic 1 or 2	MIT	2079	1.19NS	1.21**	1.22NS	Actb	K05692	04015 Rap1 signalling pathway , 04145 Phagosome , 04210 Apoptosis , 04390 Hippo signalling pathway, 04510 Focal adhesion , 04520 Adherens junction, 04530 Tight junction , 04611 Platelet activation, 04670 Leukocyte transendothelial migration , 04714 Thermogenesis, 04810 Regulation of actin cytoskeleton, 04919 Thyroid hormone signalling pathway, 04921 Oxytocin signalling pathway, 04971 Gastric acid secretion, 05100 Bacterial invasion of epithelial cells, 05132 Salmonella infection, 05164 Influenza A, 05205 Proteoglycans in cancer, 05225 Hepatocellular carcinoma, 05410 Hypertrophic cardiomyopathy (HCM), 05412 Arrhythmogenic right ventricular cardiomyopathy (ARVC), 05414 Dilated cardiomyopathy (DCM), 05416 Viral myocarditis, 05418 Fluid shear stress and atherosclerosis	Environmental information processing Cellular processes Organismal systems Human diseases
Acyl-coenzyme A synthetase ACSM1, mitochondrial isoform X4	NUC	874	0.89NS	0.85NS	0.85*	Acsm1	-	-	Not assigned
Aldehyde oxidase 3	CYT	230 / 2360	1.38NS / 1.34NS	1.36NS / 1.33*	1.15NS / 1.07NS	Aox3	-	00280 Valine, leucine and isoleucine degradation, 00350 Tyrosine metabolism 00380 Tryptophan metabolism, 00750 Vitamin B6 metabolism, 00760 Nicotinate and nicotinamide metabolism, 00830 Retinol metabolism, 00982 Drug metabolism - cytochrome P450, 01100 Metabolic pathways, 04630 Jak-STAT signaling pathway	Metabolism
Alpha-1-antiproteinase	CYT	934 / 2262	1.15NS / 0.96NS	1.35NS / 1.27*	1.65* / 1.28*	Serpina1	K03984	04610 Complement and coagulation cascades	Organismal systems
Alpha-1-macroglobulin	MIC	317	1.27NS	1.05NS	1.16*	Pzp	-	-	Not assigned
Apoptosis-inducing factor 1, mitochondrial	MIC	836	1.29***	1.17***	1.19*	Aifm1	K04727	04210 Apoptosis, 04217 Necroptosis	Cellular processes
ATP-citrate synthase	CYT	310	1.03NS	0.93NS	0.83*	Acly	K01648	00020 Citrate cycle (TCA cycle), 01100 Metabolic pathways	Metabolism
Betaine-homocysteine S-methyltransferase	CYT	1160	1.21*	1.09NS	1.05NS	Bhmt		00260 Glycine, serine and threonine metabolism, 00270 Cysteine and methionine metabolism, 01100 Metabolic pathways	Metabolism

Table 7.3 *continued*

Protein name	Sample	Spot No.	Relative fold-change			Gene name	KO definition	KEGG Pathway Rattus norvegicus [rno]	KEGG Brite Protein family
			Ostarine	LGD-4033	RAD140				
Carbamoyl-phosphate synthase [ammonia], mitochondrial	NUC	228	0.77^{NS}	2.13*	1.19^{NS}	Cps1	K01948	00220 Arginine biosynthesis, 00250 Alanine, aspartate and glutamate metabolism, 00910 Nitrogen metabolism, 01100 Metabolic pathways 01200 Carbon metabolism, 01230 Biosynthesis of amino acids	Metabolism
		272	0.81^{NS}	1.85****	1.41^{NS}				
		632	0.59^{NS}	2.37*	1.35^{NS}				
		2136	0.68^{NS}	1.73*	1.17^{NS}				
		2140	0.68^{NS}	2.16*	1.40^{NS}				
		2144	0.73^{NS}	2.54*	1.34^{NS}				
		2251	0.83^{NS}	0.67*	0.57***				
	MIC	203	1.32*	1.15^{NS}	1.10^{NS}				
		264	1.37^{NS}	1.24***	1.06^{NS}				
	CYT	149	1.16*	0.99^{NS}	0.96^{NS}				
		214	1.15*	1.01^{NS}	0.88^{NS}				
		233	1.39*	1.16^{NS}	1.09^{NS}				
		2359	1.16*	1.08^{NS}	1.09^{NS}				
	CYT	935	1.32*	0.94^{NS}	1.05^{NS}				
Carboxylesterase 1 D	MIT	864	1.44***	1.36^{NS}	1.64^{NS}	Ces1d	K01044	00983 Drug metabolism - other enzymes, 01100 Metabolic pathways	Metabolism
	MIC	965	1.40^{NS}	1.17^{NS}	1.59***				
		982	1.26^{NS}	1.09^{NS}	1.26*				
Catalase	MIC	922	1.19^{NS}	1.13^{NS}	1.29*	Cat	K03781	00380 Tryptophan metabolism, 00630 Glyoxylate and dicarboxylate metabolism, 01200 Carbon metabolism, 04068 FoxO signalling pathway, 04146 Peroxisome, 04211 Longevity regulating pathway, 04213 Longevity regulating pathway, 05014 Amyotrophic lateral sclerosis (ALS)	Metabolism Environmental information processing Cellular processes Organismal systems Human diseases
Cytochrome b-c1 complex subunit 1, mitochondrial	MIC	1136	0.84*	0.90^{NS}	0.80*	Uqcrc1	K00414	00190 Oxidative phosphorylation, 01100 Metabolic pathways, 04260 Cardiac muscle contraction, 04714 Thermogenesis, 04932 Non-alcoholic fatty liver disease (NAFLD), 05010 Alzheimer's disease, 05012 Parkinson's disease, 05016 Huntington's disease	Metabolism Organismal systems Human diseases
Dimethylglycine dehydrogenase, mitochondrial	NUC	496	0.61**	0.64*	0.64*	Dmgdh	K00315	00260 Glycine, serine and threonine metabolism, 01100 Metabolic pathways	Metabolism
	MIT	514	0.63*	0.53*	0.54*				
		516	0.82^{NS}	0.62***	0.75*				
Electron transfer flavoprotein-ubiquinone oxidoreductase	MIC	2964	0.96^{NS}	0.85^{NS}	0.86***	Etfdh	K00311	-	Metabolism
Endoplasmic reticulum chaperone Bip	NUC	2254	1.34^{NS}	1.22^{NS}	1.65*	Hspa5	K09490	03060 Protein export, 04141 Protein processing in endoplasmic reticulum, 04612 Antigen processing and presentation, 04918 Thyroid hormone synthesis, 05020 Prion diseases	Genetic information processing Organismal systems Human diseases
endoplasmic reticulum resident protein 44 precursor	MIC	2997	0.75**	0.83^{NS}	0.83*	Erp44	K17264	-	Genetic Information processing
Endoplasmin	NUC	315	1.59*	1.73^{NS}	1.74^{NS}	Hsp90b1	K09487	04141 Protein processing in endoplasmic reticulum, 04151 PI3K-Akt signalling pathway, 04657 IL-17 signalling pathway, 04915 Estrogen signalling pathway, 04918 Thyroid hormone synthesis, 05200 Pathways in cancer, 05215 Prostate cancer, 05418 Fluid shear stress and atherosclerosis	Genetic information processing Environmental information processing Organismal system Human diseases

Table 7.3 *continued*

Protein name	Sample	Spot No.	Relative fold-change			Gene name	KO definition	KEGG Pathway Rattus norvegicus [rno]	KEGG Brite Protein family
			Ostarine	LGD-4033	RAD140				
Fibrinogen beta chain	MIC	942	1.08^{NS}	1.16^{NS}	1.27*	Fbg	K03904	04610 Complement and coagulation cascades, 04611 Platelet activation	Organismal system
Formimidoyltransferase-cyclodeaminase	MIT	873	1.21^{NS}	1.38^{NS}	1.42*	Ftcd	K13990	00340 Histidine metabolism, 00670 One carbon pool by folate, 01100 Metabolic pathways	Metabolism
Glutaminase liver isoform, mitochondrial	MIT	867	1.24^{NS}	1.14^{NS}	1.48*	Gls2	K01425	00220 Arginine biosynthesis, 00250 Alanine, aspartate and glutamate metabolism, 00471 D-Glutamine and D-glutamate metabolism, 01100 Metabolic pathways, 04724 Glutamatergic synapse, 04727 GABAergic synapse, 04964 Proximal tubule bicarbonate reclamation, 05206 MicroRNAs in cancer, 05230 Central carbon metabolism in cancer	Metabolism Organismal systems Human diseases
Glutathione S-transferase Mu 1	NUC	1844	1.01^{NS}	1.08^{NS}	1.33*	Gstm1	K00799	00480 Glutathione metabolism, 00980 Metabolism of xenobiotics by cytochrome P450, 00982 Drug metabolism - cytochrome P450, 00983 Drug metabolism - other enzymes, 01524 Platinum drug resistance, 05204 Chemical carcinogenesis, 05225 Hepatocellular carcinoma, 05418 Fluid shear stress and atherosclerosis	Metabolism Human diseases
	MIT	1741	1.22^{NS}	1.25*	1.27*				
Glutathione S-transferase Mu 2	NUC	1859	0.72*	0.97^{NS}	0.89^{NS}	Gstm2	K00799	00480 Glutathione metabolism, 00980 Metabolism of xenobiotics by cytochrome P450, 00982 Drug metabolism - cytochrome P450, 00983 Drug metabolism - other enzymes, 01524 Platinum drug resistance, 05200 Pathways in cancer, 05204 Chemical carcinogenesis, 05225 Hepatocellular carcinoma, 05418 Fluid shear stress and atherosclerosis	Metabolism Human diseases
Glyceraldehyde-3-phosphate dehydrogenase	MIC	3009	0.75^{NS}	0.87*	0.85*	Gapdh	K00134	00010 Glycolysis / Gluconeogenesis, 01100 Metabolic pathways, 01200 Carbon metabolism, 01230 Biosynthesis of amino acids, 04066 HIF-1 signalling pathway, 05010 Alzheimer's disease	Metabolism Environmental information processing Human diseases
	CYT	2204	0.47***	0.62**	0.60**				
	CYT	2206	0.49*	0.64*	0.60***				
Glycine *N*-methyltransferase	MIC	3033	1.29*	1.26*	1.13^{NS}	Gnmt	K00552	00260 Glycine, serine and threonine metabolism	Metabolism
Heat shock protein HSP 90-beta	CYT	533	0.93^{NS}	0.75^{NS}	0.83*	Hsp90ab1	K04079	04141 Protein processing in endoplasmic reticulum, 04151 PI3K-Akt signalling pathway, 04217 Necroptosis, 04612 Antigen processing and presentation, 04621 NOD-like receptor signalling pathway, 04657 IL-17 signalling pathway, 04659 Th17 cell differentiation, 04914 Progesterone-mediated oocyte maturation, 04915 Estrogen signalling pathway, 05200 Pathways in cancer, 05215 Prostate cancer, 05418 Fluid shear stress and atherosclerosis	Genetic information processing Environmental information processing Cellular processes Organismal systems Human diseases
Hydroxyacid oxidase 1	NUC	1311	1.21**	1.13^{NS}	1.2^{NS}	Hao1	K11517	00630 Glyoxylate and dicarboxylate metabolism, 01100 Metabolic pathways, 01200 Carbon metabolism, 04146 Peroxisome (amino acid metabolism)	Metabolism Cellular processes
Indolethylamine N-methyltransferase	CYT	1718	1.54*	1.50*	1.71*	Inmt	K00562	00380 Tryptophan metabolism, 00450 Selenocompound metabolism	Metabolism
Kynurenine-oxoglutarate transaminase 3	NUC	1193	1.25*	1.17^{NS}	1.03^{NS}	Kyat3	-	-	Metabolism
Liver carboxylesterase 4	MIT	815	1.23*	1.25**	1.36^{NS}	-	-	-	Metabolism

218

Table 7.3 *continued*

Protein name	Sample	Spot No.	Relative fold-change			Gene name	KO definition	KEGG Pathway Rattus norvegicus [rno]	KEGG Brite Protein family
			Ostarine	LGD-4033	RAD140				
Major urinary protein	MIC	2167	0.90^NS	1.22*	1.09^NS	Mup5	-	-	Not assigned
Major vault protein	CYT	380	1.04^NS	1.29^NS	1.40*	Mvp	K17266	-	Not assigned
Maleylacetoacetate isomerase	CYT	1816	0.86^NS	1.29*	1.09^NS	Gstz1	-	00350 Tyrosine metabolism, 01100 Metabolic pathway	Metabolism
Methylcrotonoyl-CoA carboxylase beta chain, mitochondrial	MIC	941	1.14^NS	1.12^NS	1.43*	Mccc2	K01969	00280 Valine, leucine and isoleucine degradation, 01100 Metabolic pathways	Metabolism
MICOS complex subunit Mic60 (Fragment)	MIC	597	0.82^NS	0.79*	0.80^NS	Immt	K17785	-	Not assigned
NADH dehydrogenase [ubiquinone] 1 beta subcomplex subunit 10	NUC	1872	1.12^NS	1.49*	0.82^NS	Ndufb10	K03934	00190 Oxidative phosphorylation, 01100 Metabolic pathways, 04714 Thermogenesis, 04723 Retrograde endocannabinoid signalling, 04932 Non-alcoholic fatty liver disease (NAFLD), 05010 Alzheimer's disease, 05012 Parkinson's disease, 05016 Huntington's disease	Metabolism Organismal systems Human diseases
NADH dehydrogenase [ubiquinone] iron-sulfur protein 2, mitochondrial	MIC	2938	0.70*	0.79*	0.65**	Ndufs2	K03935	00190 Oxidative phosphorylation, 01100 Metabolic pathways, 04714 Thermogenesis, 04723 Retrograde endocannabinoid signalling, 04932 Non-alcoholic fatty liver disease (NAFLD), 05010 Alzheimer's disease, 05012 Parkinson's disease, 05016 Huntington's disease	Metabolism Organismal systems Human diseases
NADH-ubiquinone oxidoreductase 75 kDa subunit, mitochondrial	MIC	644	0.74*	0.82*	0.78*	Ndufs1	K03934	00190 Oxidative phosphorylation, 01100 Metabolic pathways, 04714 Thermogenesis, 04723 Retrograde endocannabinoid signalling, 04932 Non-alcoholic fatty liver disease (NAFLD), 05010 Alzheimer's disease, 05012 Parkinson's disease, 05016 Huntington's disease	Metabolism Organismal systems Human diseases
Neutral alpha-glucosidase AB isoform X2	MIT	292	1.11^NS	1.33*	1.10^NS	Ganab	K05546	00510 N-Glycan biosynthesis, 01100 Metabolic pathways, 04141 Protein processing in endoplasmic reticulum	Metabolism Genetic information processing
Ornithine carbamoyltransferase, mitochondrial	NUC	1417	0.85^NS	0.87^NS	0.75*	Otc	K00611	00220 Arginine biosynthesis, 01100 Metabolic pathways, 01230 Biosynthesis of amino acids	Metabolism
Peroxiredoxin-5, mitochondrial	CYT	2107	1.04^NS	1.10^NS	1.30*	Prdx5	K11187	04146 Peroxisome	Cellular process
Phosphoglucomutase-1	CYT	865	1.21*	1.26*	1.18^NS	Pgm1	K01835	00010 Glycolysis / Gluconeogenesis, 00030 Pentose phosphate pathway, 00052 Galactose metabolism, 00230 Purine metabolism, 00500 Starch and sucrose metabolism, 00520 Amino sugar and nucleotide sugar metabolism, rno01100 Metabolic pathways	Metabolism
Probable 10-formyltetrahydrofolate dehydrogenase ALDH1L2	MIT	402	0.86^NS	0.86*	0.70*	-	-	-	Metabolism
Probable 2-oxoglutarate dehydrogenase E1 component DHKTD1, mitochondrial	MIT	413	0.81^NS	0.60*	0.74^NS	Dhtkd1	K15791	-	Genetic information processing
Procollagen-lysine,2-oxoglutarate 5-dioxygenase 2	NUC	642	0.77^NS	1.63*	1.20^NS	Plod2	K13645	00310 Lysine degradation	Metabolism

Table 7.3 *continued*

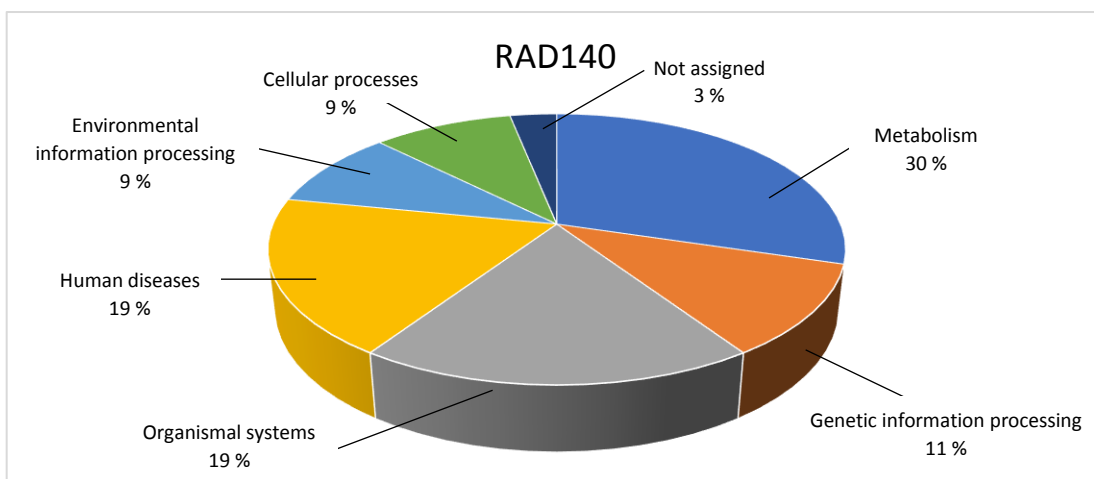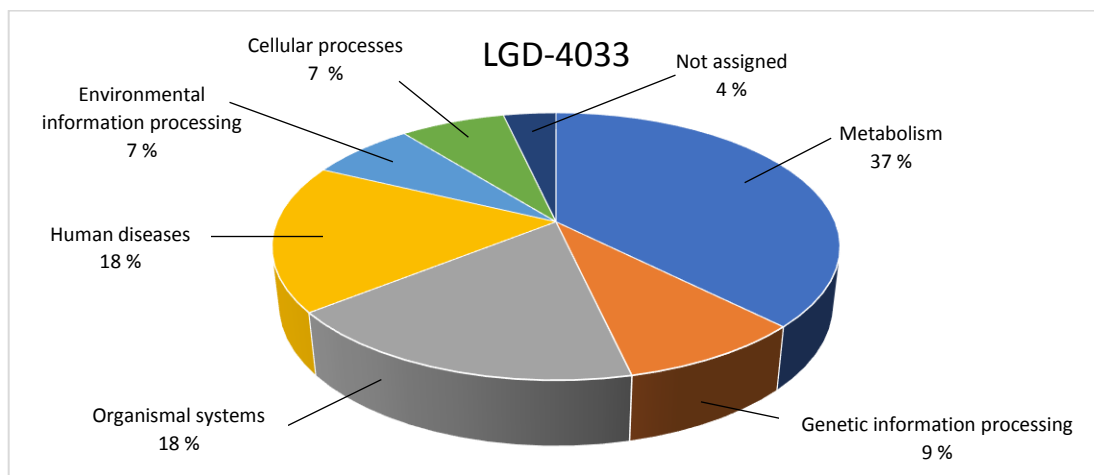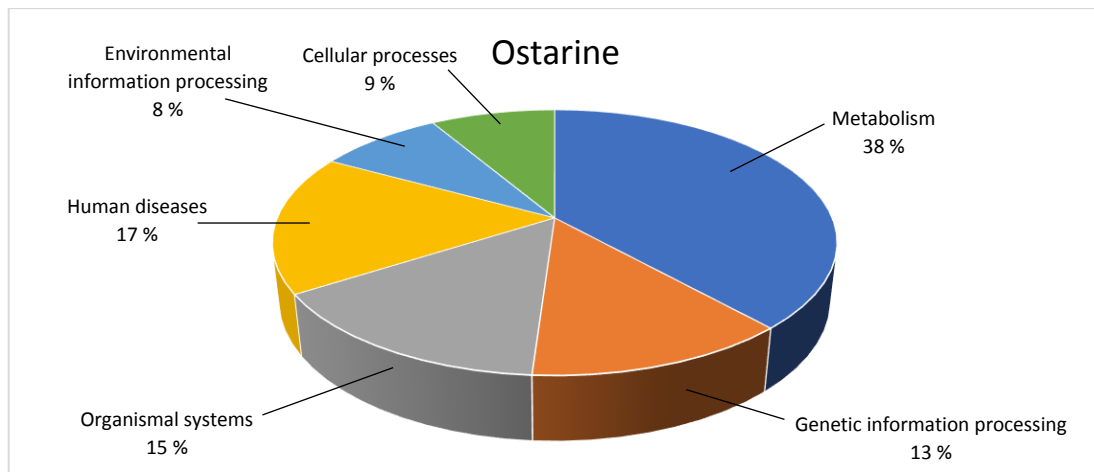| Protein name	Sample	Spot No.	Relative fold-change			Gene name	KO definition	KEGG Pathway Rattus norvegicus [rno]	KEGG Brite Protein family
			Ostarine	LGD-4033	RAD140				
Propionyl-CoA carboxylase alpha chain, mitochondrial	NUC	709	0.82^NS	1.58**	1.19^NS	Pcca	K01965	00280 Valine, leucine and isoleucine degradation, 00630 Glyoxylate and dicarboxylate metabolism, 00640 Propanoate metabolism, 01100 Metabolic pathways, 01200 Carbon metabolism	Metabolism
Propionyl-CoA carboxylase beta chain, mitochondrial	MIT	863	1.56*	1.42**	1.53**	Pccb	K01966	00280 Valine, leucine and isoleucine degradation, 00630 Glyoxylate and dicarboxylate metabolism, 00640 Propanoate metabolism, 01100 Metabolic pathways, 01200 Carbon metabolism	Metabolism
Protein di-sulfide isomerase A1	NUC	1000	1.30^NS	1.14^NS	1.62*	P4hb	K09580	04141 Protein processing in endoplasmic reticulum	Genetic information processing
	MIT	850	1.23**	1.31^NS	1.50*				
Protein di-sulfide isomerase A3	NUC	954	1.37**	1.36*	1.59*	Pdia3	K08056	04141 Protein processing in endoplasmic reticulum, 04612 Antigen processing and presentation, 05163 Human cytomegalovirus infection, 05169 Epstein-Barr virus infection, 05170 Human immunodeficiency virus 1 infection	Genetic information processing Organismal systems Human diseases
Protein di-sulfide isomerase A6	MIT	973	1.14^NS	1.18*	1.25**	Pdia6	K09584	04141 Protein processing in endoplasmic reticulum	Genetic information processing
		979	1.22*	1.24*	1.34*				
Serotransferrin	NUC	616	1.00^NS	1.23^NS	1.30**	Tf	K14736	04066 HIF-1 signalling pathway, 04216 Ferroptosis, 04978 Mineral absorption	Environmental information processing Cellular process Organismal system
	MIT	585	1.15^NS	1.37*	1.38^NS				
	MIT	2084	1.05^NS	1.35*	1.16^NS				
	MIC	2939	1.05^NS	1.16*	1.08				
		698	0.89^NS	1.25^NS	1.33*				
	CYT	2235	0.80*	0.96^NS	0.87^NS				
		2237	1.32*	1.16^NS	1.14^NS				
Serum albumin	MIC	2960	1.37^NS	1.35*	1.51^NS	Alb	K16141	04918 Thyroid hormone synthesis	Organismal systems
Spectrin alpha chain, non-erythrocytic	CYT	241	1.15*	1.01^NS	1.27*	Sptan1	K06114	04210 Apoptosis	Cellular processes
Staphylococcal nuclease domain-containing protein 1	CYT	375	1.06^NS	0.77*	0.90^NS	Snd1	K15979	05203 Viral carcinogenesis	Human diseases
Transitional endoplasmic reticulum ATPase	MIC	511	1.08	1.20*	1.01^NS	Vcp	K13525	04141 Protein processing in endoplasmic reticulum, 05134 Legionellosis	Genetic information processing Human diseases
		2912	1.35*	1.31*	1.10^NS				
		2914	1.32*	1.26*	1.08^NS				
Voltage-dependent anion-selective channel protein 1	MIC	3022	0.83^NS	0.86***	0.83^NS	Vdac1	K05862	04020 Calcium signalling pathway, 04022 cGMP-PKG signalling pathway, 04217 Necroptosis, 04218 Cellular senescence, 04621 NOD-like receptor signalling pathway, 04979 Cholesterol metabolism, 05012 Parkinson's disease, 05016 Huntington's disease, 05164 Influenza A, 05166 Human T-cell leukemia virus 1 infection	Environmental information processing Cellular processes Organismal systems Human diseases

Figure 7.7 Identified proteins were classified into the following networks as specified by the KEGG pathway database: metabolism, genetic information processing, environmental information processing, cellular processes, organismal systems, and human diseases. Some of the proteins were not in the database and as such were not assigned to protein families. The differently coloured sectors of the pie chart show the percentage.

Table 7.4 Overrepresented KEGG pathways with a false discovery rate corrected p-value of 0.05 for ostarine, LGD-4033, and RAD140 following submission of gene names derived from protein spots to ShinyGO v0.60. Pathways found to be enriched in all treatment groups are underlined.

KEGG pathway name	Genes in list	Gene names	Total genes	Enrichment FDR
Ostarine				
Metabolic pathways	13	Gapdh Akr1d1 Dmgdh Pccb Pgm1 Ndufs2 Uqcrc1 Ndufs1 Aox3 Cps1 Kyat3 Aco2 Bhmt	1251	1.77E-09
Protein processing in endoplasmic reticulum	5	Vcp P4hb Pdia6 Pdia3 Hsp90b1	162	8.77E-06
Carbon metabolism	4	Gapdh Pccb Cps1 Aco2	118	5.89E-05
Glycine, serine and threonine metabolism	3	Dmgdh Gnmt Bhmt	40	6.37E-05
Alzheimer's disease	4	Gapdh dufs2 Uqcrcr1 Ndufs1	176	1.70E-04
Biosynthesis of amino acids	3	Gapdh Cps1 Aco2	79	3.31E-04
Oxidative phosphorylation	3	Ndufs2 Uqcrc1 Ndufs1	136	1.29E-03
Glyoxylate and dicarboxylate metabolism	2	Pccb Aco2	30	1.29E-03
Parkinson's disease	3	Ndufs2 Uqcrc1 Ndufs1	144	1.29E-03
Non-alcoholic fatty liver disease (NAFLD)	3	Ndufs2 Uqcrc1 Ndufs1	154	1.42E-03
Cysteine and methionine metabolism	2	Kyat3 Bhmt	48	2.25E-03
Tryptophan metabolism	2	Aox3 Kyat3	48	2.25E-03
Huntington's disease	3	Ndufs22 Uqcrc1 Ndufs1	190	2.25E-03
Valine, leucine and isoleucine degradation	2	Pccb Aox3	53	2.37E-03
Drug metabolism	2	Gstm2 Aox3	53	2.37E-03
Glycolysis / Gluconeogenesis	2	Gapdh Pgm1	61	2.77E-03
Thermogenesis	3	Ndufs22 Uqcrc1 Ndufs1	233	2.77E-03
Drug metabolism	2	Ces1d Gstm2	72	3.43E-03
Chemical carcinogenesis	2	Gstm2 Kyat3	72	3.43E-03
HIF-1 signalling pathway	2	Gapdh Tf	101	6.33E-03
LGD-4033				
Metabolic pathways	12	Gapdh Akr1d1 Dmgdh Pccb Pgm1 Ndufs2 Ndufs1 Dhtkd1 Aox3 Cps1 Gstz1 Pcca	1251	1.14E-07
Carbon metabolism	4	Gapdh Pccb Cps1 Pcca	118	1.33E-04
Valine, leucine and isoleucine degradation	3	Pccb Aox3 Pcca	53	2.76E-04
Glyoxylate and dicarboxylate metabolism	2	Pccb Pcca	30	2.68E-03
Propanoate metabolism	2	Pccb Pcca	31	2.68E-03
Parkinson's disease	3	Ndufs2 Ndufs1 Vdac1	144	2.68E-03
Tyrosine metabolism	2	Aox3 Gstz1	36	2.83E-03
Protein processing in endoplasmic reticulum	3	Vcp Pdia6 Pdia3	162	2.83E-03
Glycine, serine and threonine metabolism	2	Dmgdh Gnmt	40	2.87E-03

Table 7.4 *continued*

KEGG pathway name	Genes in list	Gene names	Total genes	Enrichment FDR
Alzheimer's disease	3	*Gapdh Ndufs2 Ndufs*	176	2.87E-03
Tryptophan metabolism	2	*Dhtkd1 Aox3*	48	3.10E-03
Huntington's disease	3	*Ndufs2 Ndufs1 Vdac1*	190	3.10E-03
Drug metabolism	2	*Gstm1 Aox3*	53	3.48E-03
Lysine degradation	2	*Plod2 Dhtkd1*	58	3:87E-03
Glycolysis / Gluconeogenesis	2	*Gapdh Pgm1*	61	3.99E-03
Thermogenesis	3	*Ndufs2 Ndufs1 Atcb*	233	4.00E-03
Biosynthesis of amino acids	2	*Gapdh Cps1*	79	5.85E-03
HIF-1 signaling pathway	2	*Gapdh Tf*	101	8.92E-03
Oxidative phosphorylation	2	*Ndufs2 Ndufs1*	136	1.38E-02
Apoptosis	2	*Actb Aifm1*	132	1.38E-02
RAD140				
Metabolic pathways	13	*Gapdh Gls2 Acly Dmgdh Pccb Otc Ndufs2 Uqcrc1 Ndfus1 Mccc2 Cps1 Aco2 Ftcd*	1251	4.61E-08
Carbon metabolism	5	*Gapdh Cat Pccb Cps1 Aco2*	118	6.20E-06
Protein processing in endoplasmic reticulum	5	*Hspa5 Pdia6 Pdia3 Hsp90ab1 Hsp90b1*	162	1.98E-05
Biosynthesis of amino acids	4	*Gapdh Otc Cps1 Aco2*	79	2.45E-05
Glyoxylate and dicarboxylate metabolism	3	*Cat Pccb Aco2*	30	4.74E-05
Alzheimer's disease	4	*Gapdh Ndufs2 Uqcrc1 Ndufs1*	176	3.85E-04
Antigen processing and presentation	3	*Hspa5 Pdia3 Hsp90ab1*	76	5.62E-04
Arginine biosynthesis	2	*Otc Cps1*	19	1.03E-03
Citrate cycle (TCA cycle)	2	*Acly Aco2*	30	2.14E-03
Oxidative phosphorylation	3	*Ndufs2 Uqcrc1 Ndufs1*	136	2.14E-03
Parkinson's disease	3	*Ndufs2 Uqcrc1 Ndufs1*	144	2.14E-03
Fluid shear stress and atherosclerosis	3	*Gstm1 Hsp90ab1 Hsp90b1*	140	2.14E-03
Alanine, aspartate and glutamate metabolism	2	*Gls2 Cps1*	36	2.23E-03
Non-alcoholic fatty liver disease (NAFLD)	3	*Ndufs2 Uqcrc1 Ndufs1*	154	2.23E-03
Huntington's disease	3	*Ndufs2 Uqcrc1 Ndufs1*	190	3.80E-03
Valine, leucine and isoleucine degradation	2	*Pccb Mccc2*	53	4.06E-03
Thermogenesis	3	*Ndufs2 Uqcrc1 Ndufs1*	233	5.97E-03
Drug metabolism	2	*Ces1d Gstm1*	72	6.25E-03
Thyroid hormone synthesis	2	*Hspa5 Hsp90b1*	72	6.25E-03
Complement and coagulation cascades	2	*Fgb Serpina1*	80	7.30E-03

Figure 7.8 Pathway of protein processing in the endoplasmic reticulum in Rattus norvegicus (rno04141) was significantly enriched in response to SARMs following pathway enrichment analysis based on hypergeometric distribution followed by FDR correction using the ShinyGO web application (for results see **Table 7.4**). Pathway was retrieved from KEGG using the KEGG Mapper Search Pathway tool. Proteins with modified levels in response to SARMs relative to the control group are coloured in red: protein di-sulfide isomerases (PDIs) A1, A3 (ERP57) and A6, endoplasmin (GRP94, Hsp90b1, Hsp90), endoplasmic reticulum chaperone binding immunoglobulin protein (BIP), heat shock protein

7.3.3   STRING protein-protein interaction network analysis

Biological processes are often mediated by a complex network of multiple proteins. To generate protein-protein interaction networks and predict functional associations, accession numbers of identified proteins for each investigated SARM compound were submitted to the STRING database v11 (https://string-db.org/)[544]. Interaction sources included text-mining, co-expression, known interactions from databases and experimentally determined, and predicted interactions based on gene neighbourhood, fusions, and co-occurrence. The minimum required interaction score was set at 0.70 (high confidence). Networks of known and predicted protein-protein interactions were automatically generated (**Figure 7.9**). STRING did not match the following proteins: Q5QE80, Q64573, Q58FK9, NP_001178707.1, and XP_008757993.1. The nodes which are displayed in arbitrary colours represent proteins. The lines represent the interactions between proteins with line colours displaying the type of interaction evidence. Disconnected nodes were hidden from the network. Permanently accessible links are provided here:

(A) Ostarine

https://version-11-0.string-db.org/cgi/network.pl?networkId=nLoDRTZ9kzaA

(B) LGD-4033

https://version-11-0.string-db.org/cgi/network.pl?networkId=Qabcrqh5RAwB

(C) RAD140

https://version-11-0.string-db.org/cgi/network.pl?networkId=ZyqCxezUcApS

Analysis of functional protein interactions using STRING revealed several protein-protein interactions and protein clusters. One cluster which became apparent is that comprised of numerous proteins associated with oxidative phosphorylation (NDUFS2, UQCRC1, NDUFS1, NDUFB10) and metabolic pathways (ACLY, NDUFS2, UQCRC1, NDUFS1, NDUFB10, ACO2). Another cluster consists of proteins involved in protein processing in the ER (P4HB, HSPA5, PDIA6, PDIA3, HSP90AB1, HSP90B1, GANAB, VCP).
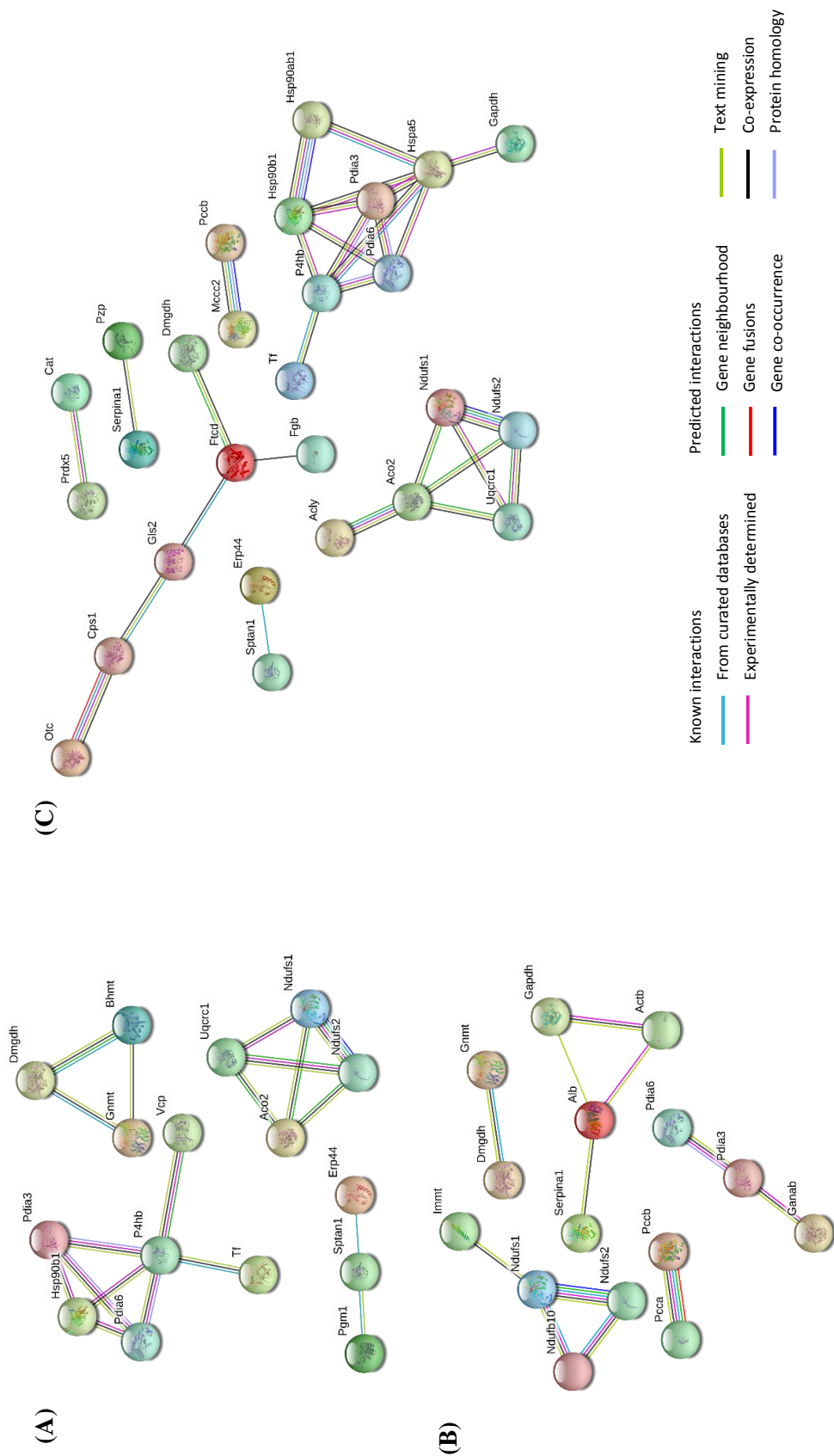
Figure 7.9 Networks of known and predicted protein-protein interactions generated by STRING v11 of proteins whose levels were modified in response to treatment with (**A**) ostarine, (**B**) LGD-4033, and (**C**) RAD140. Nodes present proteins - Line thickness indicates strength of data support.

7.4   Discussion

The effects of SARM compounds on the liver protein profile was a focus of this study as the liver is the primary site of SARM metabolism. Whilst the effects of the SARM compound GSK212A on skeletal muscle proteins[531], has been reported previously, the work detailed in **Chapter 6** was the first study to investigate the hepatic proteomic response to a range of SARM compound treatments (ostarine, LGD-4033, or RAD140). The current study continues that work by assessing proteomic response to SARM compounds in the liver within the following subcellular constituents: cytosol, mitochondria, nuclei, and endoplasmic reticulum-derived microsomes. In **Chapter 6**, SARM administrations were shown by proteomic analysis using a 2-D DIGE approach to alter relative protein levels in liver tissue. In this study, organelle-specific hepatic proteins were enriched by subcellular fractionation prior to 2-D DIGE analysis with the objective of detecting and identifying more subtle changes to the relative protein profiles than that which could be observed from analysis of whole liver tissue lysates. 58 unique proteins from 159 protein spots with altered abundances following treatment with ostarine, LGD-4033, or RAD140 compared to the control group were identified by MALDI-TOF, two of which had been previously reported in **Chapter 6** (glyceraldehyde-3-phosphate dehydrogenase and protein disulfide-isomerase A1). Three proteins described in **Chapter 6** (alpha-soluble NSF attachment protein, 3-alpha-hydroxysteroid dehydrogenase, and serum paraoxonase/lactonase 3) were not identified in this study, a possible explanation for this could be that they were differentially altered but not identified by MALDI-TOF or that they were not detected as differentially altered due to the different methodology used (pooling of liver samples followed by subcellular fractionation vs. single biological replicates of liver lysates).

In the first step, comparative analysis of proteins revealed changes in proteomic profiles between the treated and non-treated groups with observed overall changes typically heterogeneous for each SARM compound, but also including shared responses between two or all the investigated compounds. In this study it was shown that SARMs show compound specific effects on the protein profile as the majority of protein spot levels were uniquely altered in response to one SARM compound. The three investigated compounds ostarine, LGD-4033, and RAD140 all have different chemical scaffolds which may lead to variant interaction with the AR and subsequent pathways accounting for the divergence in protein responses. Despite the different responses, relative abundances of 12 spots were commonly altered in response to treatments with either ostarine, LGD-4033, or RAD140 showing that

they also exhibit common effects possibly due to their interaction with the AR. Subsequently, selected protein spots were identified following trypsin digestion and MALDI-TOF analysis and bioinformatics approaches utilised to interpret significantly enriched pathways and interaction networks. Nine out of the 12 common altered spots were identified (increase of PDIA3, PDIA6, AIFM1A, INMT, and PCCB; decrease of DMGDH, GAPDH, NDUFS1, and NDUFS2) with functions associated with metabolic pathways (GAPDH, DMGDH, PCCB, NDUFS2, NDUFS1) and protein processing in the ER (PDIA3, PDIA6).

Following enrichment analysis of proteins with KEGG as reference database, common enriched functional pathways were identified to derive a biological meaning from the proteomics data set. The identified role of amino acid metabolism is considered to be of particular interest, as several proteins whose relative levels were found to be altered by SARM compound administrations are involved in amino acid synthesis and degradation. Carbamoyl phosphate synthase (CPS1) plays a role in biosynthesis of the amino acid arginine and was identified in several protein spots due potentially to post-translational modifications and degradation products of the protein leading to a shift in pI and/or MW.[546] In most cases treatment with LGD-4033 and ostarine resulted in an increased level of CPS1 with the exception of spot 2251 that resulted in decreased levels of CPS1 after LGD-4033 and RAD140 treatments. CPS1 catalyses the formation of carbamoyl phosphate from ammonia and bicarbonate using ATP with N-acetyl glutamate as essential cofactor[547] and is the rate-limiting enzyme in the urea cycle. Increase of CPS1 levels during SARM treatment suggests promotion of the urea cycle that is associated with an irreversible loss of nitrogen through urea excretion. However, nitrogen retention and a subsequent decrease of urea are key indicators of anabolic metabolism.[548] Another enzyme in the arginine biosynthesis pathway, ornithine carbamoyltransferase which generates citrulline from the reaction between carbomoyl phosphate and ornithine to form citrulline was shown to be reduced in livers of RAD140 treated animals. A previous study has demonstrated that ornithine supplementation decreases blood ammonia through activation of the urea cycle and attenuates the feeling of physical fatigue[549] - during exercise ammonia build up and accumulation has been suggested to provoke fatigue.[550,551] Glutaminase, an additional protein also linked to this pathway and which catalyses the hydrolysis of glutamine to glutamate and ammonia, was found to be increased within RAD140 animals. Increased plasma levels of glutamine after treatment with the SARM GLPG0492 have been observed

previously[552] with glutaminase increasing levels of glutamate, and subsequently α-ketoglutarate, which in turn elevates mitochondrial oxidation and ATP generation[553].

Within the glycine, serine and threonine metabolism KEGG pathway, the relative levels of three proteins were demonstrated to be altered in response to SARM compounds. Firstly, levels of dimethylglycine dehydrogenase (DMGDH) which is involved in the catabolism of the amino acid choline and catalyses the demethylation of dimethylglycine (DMG) to sarcosine were decreased following ostarine, LGD-4033, and RAD140 administration. Decreased *Dmgdh* gene expression is linked to an increased level of DMG[554], and DMG is sold as a dietary supplement with disputed performance enhancing effects and is used widespread in horses where a reduction of blood lactate levels and increase of travelled distance have been observed during DMG intake.[555] Secondly, the relative levels of two transferases in the choline oxidation pathway were elevated - betaine-homocysteine S-methyltransferase in response to ostarine administration and glycine N-methyltransferase upon ostarine and LGD-4033 administration. Proteins whose levels were differentially altered with functions in the catabolism of essential branched-chained amino acids (BCAA) valine, leucine, and isoleucine included methylcrotonoyl-CoA carboxylase beta chain (MCCC2), propionyl-CoA carboxylase alpha (PCCA) and beta chain (PCCB), and aldehyde oxidase 3 (AOX3). MCCC2 functions as a ligase in the degradation of leucine and had increased levels within the RAD140 group relative to the control group. PCCA levels were similarly increased by LGD-4033, and PCCB also by ostarine and RAD140, with both proteins involved in the degradation of valine and isoleucine to synthesise succinyl CoA. AOX3 catalyses the oxidation of aldehydes into carboxylic acids such as in the L-valine degradation pathway and its levels were increased following ostarine or LGD-4033 treatment. Similarly, administration of testosterone was observed to increase mRNA of aldehyde oxidase in female rats.[556]

According to the KEGG classification, several proteins whose levels were differentially altered are associated with carbohydrate metabolism pathways including aconitrate hydratase (ACO2), ATP-citrate synthase (ACLY), hydroxyacid oxidase 1 (HAO1), catalase (CAT), PCCA, PCCB, phosphoglucomutase-1 (PGM1) and glyceraldehyde-3-phosphate dehydrogenase (GAPDH). ACO2 and ACLY, two proteins of the citrate cycle, were decreased by RAD140, with decreased levels of ACO2 also associated with ostarine. ACO2 interconverts isocitrate and citrate, whilst ACLY reversibly forms citrate with oxaloacetate and acetyl-CoA. SARMs have previously been linked to the citrate cycle with intermediates of the citrate cycle citrate, fumarate, and pyruvate significantly increased in plasma by

SARM GLPG0492.[552] HAO1 and CAT are part of the glyoxylate metabolism and their levels were increased in the ostarine and RAD140 treated groups. Ostarine and LGD-4033 administration elevated relative levels of PGM1 which catalyses the bi-directional interconversion of glucose-1-phosphate and glucose-6-phosphate. Another differentially altered protein in the glycolysis pathway is GAPDH which catalyses the sixth step of glycolysis to convert glyceraldehyde 3-phosphate into D-glycerate 1,3-bisphosphate. Within cytosol fractions, GAPDH protein spot abundances were decreased in the ostarine, LGD-4033, and RAD140 groups relative to the control group. GAPDH was previously identified in **Chapter 6** from a protein spot with decreased levels after LGD-4033 treatment. Cytosolic GAPDH is known to be inactivated to counteract oxidative stress [527] and depressed GAPDH levels could be a cellular response to oxidative stress related to SARM compound administration. Biphosphonates which are used as drugs in the treatment of osteoporosis, have also shown to downregulate *Gapdh*[557] and the osteoprotective effects of ostarine and LGD-4033 have been reported as potential therapeutic benefits in osteoporosis treatment[558,559]. On the other hand, a proteomics study on liver of Fathead Minnows reported an increase of GAPDH protein after treatment with the AAS 17β-trenbolone.[560] Furthermore, an increase in *Gapdh* expression was observed in a prostate cancer cell line and functioned as AR coactivator in the cytosol enhancing its transcriptional activity in the nucleus.[526] Besides its well-known glycolytic and AR coactivator function in the cytosol, GAPDH possesses multifunctional roles within several subcellular compartments and cellular processes such as nuclear membrane assembly, endocytosis, and cell death.[561] GAPDH can be imported to mitochondria through the voltage-dependent anion channel.[562] Voltage-dependent anion-selective channel protein 1 showed decreased levels upon LGD-4033 administration in this study.

Besides the citrate cycle and glycolysis, oxidative phosphorylation plays a role in cellular respiration. Oxidative phosphorylation was identified as a significantly enriched pathway in KEGG analysis. NADH dehydrogenase [ubiquinone] iron-sulfur protein 2 (NDUFS2) and NADH-ubiquinone oxidoreductase (NDUFS1) were found at decreased levels in microsomes after ostarine, LGD-4033, and RAD140 treatments suggesting reduced oxidative phosphorylation. NDUFS1 and 2 are both subunits of complex I and inhibition of complex I has been linked to anti-tumour growth.[563] In nuclei samples an increase of NADH dehydrogenase [ubiquinone] 1 beta subcomplex subunit 10 (NDUFB10) was observed by LGD-4033 and in microsomal samples cytochrome b-c1 complex subunit 1 (UQCRC1) decreased after ostarine and RAD140 treatment.

SARMs were shown to influence levels of several proteins that are involved in protein processing in the ER with protein disulfide isomerase A3 (PDIA3) and A6 (PDIA6) levels increased by all three SARMs relative to the control. Moreover, the levels of two more chaperones, protein disulfide isomerase A1 (P4HB) and endoplasmin, were increased following RAD140 and ostarine treatment. P4HB was previously found increased within liver tissue in **Chapter 6** after RAD140 treatment. Under conditions of ER stress, protein disulfide isomerase expression is upregulated to target terminally misfolded proteins for ER-associated degradation (ERAD).[564] Transitional endoplasmic reticulum ATPase, another protein involved in ERAD, was increased by ostarine and LGD-4033 administration. Its function is to segregate proteins from binding ones so they can be degraded by the proteasome.[565] Heat shock protein 90-beta (HSP90AB1) that can act as a chaperone was slightly decreased by RAD140 and also plays a role in androgen receptor (AR) signalling. In the absence of ligands it forms a complex with the AR keeping it in a high affinity ligand-binding position and hence inhibition of HSP90 blocks AR signalling.[566] Additionally, RAD140 administration elevated the levels of endoplasmic reticulum chaperone binding immunoglobulin protein (BIP). In fact, PDIA3, BIP, and endoplasmin were firstly described together as glucose-regulated proteins (GRP) as their expression increases as stress response after glucose depletion.[567] ER stress is caused by factors that disrupt protein folding such as energy deprivation, oxidative stress, disease, increased protein trafficking, and chemical triggers.[568] On accumulation of misfolded proteins, the unfolded protein response (UPR) is triggered, and the initial response is adaptive by upregulating expression of chaperones to increase folding and degradation of proteins and thus restore homeostasis.[569] If ER stress cannot be alleviated apoptosis is induced.[570] In this study only levels of two proteins that are linked to apoptosis were slightly increased, apoptosis inducing factor 1 following treatment with all investigated SARM compounds and spectrin alpha chain after ostarine or RAD140 treatment. Not only accumulation of misfolded proteins can initiate the UPR but also other factors that perturbate homeostasis such as a decrease in cellular ATP which in turn inhibits sarcoplasmic/ER Ca^{2+}-ATPase pump activity and decreases ER calcium levels.[571] The current study revealed several proteins (NDUFS1, NDUFS2, GAPDH, ACO2, and/or ACLY) involved in cellular respiration decreased by SARMs that could potentially cause a shortage in ATP and initiate UPR. Several ER stress-associated chaperones were increased by SARMs. However, it is yet to be determined which upstream processes cause the observed elevated levels.

Notably, many of the identified proteins also play roles in tumorigenesis or in the development of other diseases. For example, oxidative phosphorylation complex I enzymes were found downregulated in Alzheimer's disease[572] whilst GAPDH overexpression is reported in many cancers.[573] Cellular processes within diseased states may greatly differ from physiological conditions, and therefore, pathophysiological processes can influence drug-induced effects. As an agent targeting muscle anabolic pathways, ostarine has been previously trialled as a treatment for cachexia, a chronic muscle wasting disease, but failed to demonstrate clear functional benefits in phase III trials.[72,105] Since it has become clear that monotherapy with SARMs is unable to counteract cachectic catabolic signalling pathways, co-administration of SARMs with known anti-cachectic agents combines anabolic potential of SARMs with inhibition of catabolic signalling leading to an improved anabolic response.[574] Therefore, there is potential for this work to be expanded using animal models for human diseases to gain a better understanding of the proteomic response to SARMs within pathophysiological states.

7.5   Conclusions

The current study presents a comprehensive analysis of differentially altered proteins in liver of SARM (ostarine, LGD-4033, and RAD140)-treated rats revealing a complex response in the liver proteome with a plethora of proteins affected across multiple pathways. The coverage of proteins with differentially altered levels in the hepatic response to oral administration of SARM compounds was greatly expanded by using subcellular fractions as compared to lysates (**Chapter 6**). Subcellular fractionation was shown to enhance the detection of low-level protein abundance changes. However, subfractionation entails a certain degree of cross-contamination of organelles by other organelles or organelle disruption[575]. Ostarine, LGD-4033, and RAD140 were each observed to exert distinct effects as reflected in the observed comparative liver protein profiles. Out of 112 altered protein levels in response to SARM compounds ostarine, LGD-4033, and RAD140 12 spots were found to be altered in response to all of them, the remaining majority of protein spot abundances were only changed in response to one or two of the investigated SARMs.

Enrichment analysis highlighted several shared overrepresented pathways in response to treatment with the investigated SARM compounds. Proteins with altered abundances following SARM treatment were principally associated with metabolic processes including amino acid, energy, and carbohydrate metabolism. Furthermore, several proteins involved

in protein processing within the ER had elevated differential abundances in response to treatment with SARMs. A reason for this could be that SARM administration disrupts the redox balance potentially by altering aforementioned metabolic processes leading to perturbations of the ER and oxidative stress as has been associated with the use of AAS. This could subsequently trigger the UPR, a process that initially enables repression or upon prolonged activation induction of apoptosis and/or autophagy. Although androgens such as testosterone are known to regulate lipid and cholesterol homeostasis in the liver[576], SARMs do not seem to alter pathways in lipid metabolism.

The current study promotes an understanding of the effects of SARM compounds on the liver, identifying potentially affected biochemical pathways upon SARM administration that merit more in-depth investigations. Future work can build on this to advance drug development and clinical trial processes. Further multi-omics studies are needed to decipher the underlying molecular upstream and downstream mechanisms of SARMs considering the current findings on differentially altered relative protein profiles. Moreover, proteomics studies analysing other target tissues such as testes, breasts, bone marrow, and brain would be useful in establishing tissue-selective responses following SARM compound administration. Whilst it was shown in this study that there are immediate changes to the relative protein levels in the liver upon SARM administration, the long-term effects of SARM compound administration and their effects when administered at supraphysiologic doses have yet to be investigated.

Chapter 8: General Discussion and Future Perspectives

Over the last two decades the class of compounds known as SARMs has attracted considerable attention in drug development due to their anabolic effects and other favourable characteristics (e.g. tissue specificity, oral bioavailability, and reduced side effects) over other conventional anabolic agents such as testosterone, resulting in a chemical diverse and extensive array of compounds. Although several SARM compounds have been investigated in clinical trials and several are still on-going, they have not yet been approved for pharmaceutical use and can be easily sourced and bought for example through Internet sources. Such availability has threatened to escalate their misuse with products marketed as dietary supplements found to illegally contain SARM compounds which may constitute a risk for public health. Due to their myoanabolic properties, SARMs pose potential for abuse in sports and with a rising number of adverse analytical findings in routine testing have been banned in human sports by WADA and in equestrian sports by the FEI and IFHA. Abuse of SARM compounds in livestock animals for growth-promoting purposes also poses a threat to animal welfare and food integrity, with potential for associated dietary-related contamination putting consumers at risk. Therefore, the work of this thesis has sought to investigate the *in vitro* and *in vivo* metabolism of a number of key SARM compounds to help aid attempts to detect their administration and also to explore the potential biological effects of these emerging drugs.

A new and ever-expanding range of SARM compounds with the potential for abuse in several species including sports and food producing animals have emerged on the black market which can be used to circumvent current legislation, regulatory controls, and detection procedures in a range of fields of analysis. For control laboratories comprehensive screening procedures that include the most representative target analytes are vital to effectively detect substance abuse and trigger confirmatory analysis. Simple, reliable, rapid, and cost-effective *in vitro* strategies that can promptly respond to analytical challenges in the control of emerging illegal drug use are therefore required to predict their metabolites and ensure effective drug monitoring by implementing metabolites into test methods. Liver homogenates (**Chapter 2**) from cattle (chosen as a representative and relevant target species) were shown to be an *in vitro* tool that can be easily prepared and used to rapidly produce metabolites of SARM compounds for LC-MS characterisation. After incubation of a range of liver preparations (including crude homogenates, homogenates, or conventionally used S9 fractions or microsomes) with representative SARM compounds (ostarine, andarine, and S-1) in the presence of required co-factors (NADPH phase I, UDPGA and PAPS phase II), drug metabolite compounds were concentrated by selected protein precipitation and LLE

procedures. Metabolites generated through *in vitro* incubations were separated by UHPLC and identified by QTOF MS with collision energy switching (0 and 20 V). All prepared bovine liver fractions were capable of producing metabolites of the aryl-propionamide SARM compounds ostarine, andarine, and S-1 that are important target analytes to improve routine monitoring. SARM compounds for investigation were chosen based on their availability as certified analytical reference compounds and as black/grey-market products easily procured by potential users on the Internet. Since drug development of andarine and S-1 has come to a halt due to the favourable pharmacokinetic profile of ostarine, only ostarine has advanced to the clinical stage (**Section 1.1.1**). Although some compounds may be more relevant to clinical trials than others, they should ideally all be integrated into testing schemes as clinically less advanced compounds may still be abused in an attempt to circumvent detection, and therefore rapid and simple *in vitro* strategies are necessary to investigate their metabolism. Isolated fractions from cattle livers were characterised by determining their protein, P450, cytochrome b_5 content, and NADPH-cytochrome c reductase, 7-ethoxycoumarin *O*-dealkylation activity, which was essential for this study to ensure and demonstrate the quality of the fractions with regards to enzymatic activity and ability to produce drug metabolites. However, for routine preparation of liver homogenates only the measurement of the protein concentration is required for addition of an adequate protein amount (generally 0.5-2 mg protein/mL, with 1 mg protein/mL used in the current study). Of course, other parameters can provide a measure to monitor for batch-to-batch variability, but their determination is not essential to the use of the fractions for the production of drug metabolites. The use of homogenates was shown to be effective and efficient, offering several advantages over microsomes and/or S9 fractions such as simple preparation and use, as well as a low cost in resources and time – all key attributes that could facilitate the adoption of homogenates as an *in vitro* approach into routine workflows of monitoring laboratories on a broad scale. One prerequisite for the preparation of homogenates is a supply of liver tissues from abattoirs, preferably fresh and from healthy animals. This could present a potential bottleneck to the routine use of homogenates to rapidly produce metabolites for LC-MS characterisation. However, from the experience of the work within this thesis abattoirs supported tissue donations for research purposes. While in early drug development, drug safety and efficacy testing current trends favour the use of advanced complex *in vitro* models such as 3-D cultures, organoids, and liver-on-a-chip platforms (**Section 1.3.2**) to closer mimic physiological conditions, a simpler approach such as homogenates was proposed to facilitate the rapid identification and selection of

metabolites for incorporation into LC-MS based monitoring approaches. The large number of potential emerging drugs of abuse necessitates not a complex *in vitro* approach but one such as the proposed liver homogenate approach that is high-throughput and can be adopted for use with several species and classes of drugs by multiple laboratories.

Due to their anabolic properties, SARMs may be misused in a number of species including sports and food producing animals. Species differences in the metabolism of drugs are numerous and unpredictable (**Section 1.2.3**), this is of relevance to laboratories monitoring for drugs of abuse such as SARMs. Therefore, the phase I and phase II metabolites produced by incubations with liver microsomes alone (phase I) or in combination with S9 fractions (phase II) of several relevant species and SARM compounds ostarine, LGD-4033, and RAD140 were characterised by UHPLC-IM-QTOF MS analysis (**Chapter 3**). Simultaneous preparation of liver microsomes and S9 fractions from sports (horse), food producing (cattle, pig), and laboratory (rat) animals allowed for a direct comparison of their P450 content, cytochrome b_5 content, NADPH-cytochrome P450 reductase and 7-ethoxycoumarin *O*-dealkylation activity. As mentioned earlier this was found necessary to characterise and ensure the quality of the *in vitro* systems. Furthermore, significant inter-species differences with regards to these parameters were observed underlining the complexity of drug metabolism between species. Analysis of samples prepared from *in vitro* incubations in **Chapter 3** was performed similarly to **Chapter 2** with the optional ion mobility mode of the Agilent 6560 DT IM-QTOF mass spectrometer switched on. The utilisation of ion mobility as a third dimension in addition to retention time and *m/z* improved the quality of acquired spectral data by filtering out interferences that elute at the same time as analytes but differ in drift time. Measurement of drift times allowed for calculation of compound-specific CCS values to be used as additional identifiers thus enhancing confidence in compound identification. Additional data comes at the price of increased complexity and time required for data analysis. Despite great technical advances in IM-MS over the last decade, there are still opportunities to further improve the bioinformatics tools using ion mobility data, e.g. library support for Agilent's IM-MS browser (similar to the transition list in Skyline daily) or a function to overlay extracted ion chromatograms using Skyline daily, or to develop software applications that accurately predict CCS and structural relationships. For routine analysis IM-MS has potential to further reduce false positives by implementing CCS values of drugs and metabolites thereof into library matching besides retention times and mass spectra.

Work in **Chapter 3** focused on ostarine, LGD-4033, and RAD140 as key SARM compounds based on their availability in bulk quantities from chemical suppliers as analytical reference material and from web shops and reports of their abuse in human sports (**Section 1.1.2**) that may coincide with their likelihood to be misused in sport and food producing animals. Generally, ostarine and LGD-4033 were shown to be extensively metabolised whereas RAD140 was metabolically stable. Characterised *in vitro* metabolite profiles revealed similarities but also differences in metabolites produced as observed in comparison of the investigated species. Species-specific *in vitro* metabolites were observed in cattle, horses, and rats but not for pigs. For LGD-4033 three metabolites (formed by loss of pyrrolidine, subsequent hydroxylation and sulfation) that were produced by all investigated species were described herein for the first time and have not been reported in previous studies.[178–180] Although data mining approaches[162] (e.g. EIC, product ion filter, background subtraction, and/or control sample comparison) allow for the sensitive detection of metabolites, unexpected ones can still be missed, and data analysis is also dependent on the analyst. Besides biological variables (**Section 1.2.3**), metabolite identification is also dependent on sample preparation procedures and analytical techniques. Several minor metabolites that were produced by bovine liver microsomes/S9 fractions within this chapter (M2, M3b, M5, M6, M11, and M12) were not previously observed by work with bovine liver fractions performed in **Chapter 2**. This may be due to the increased selectivity and sensitivity provided for by the additional separation power of ion mobility, and/or differences in sample preparation procedures (protein precipitation followed by LLE in **Chapter 2** and protein precipitation in **Chapter 3**). Furthermore, the *in vitro* generated metabolites using rat liver microsomes (phase I) and in combination with S9 fractions were compared to *in vivo* formed metabolites detected in rat urine samples following administration of ostarine, LGD-4033, or RAD140. Urine samples were collected for one hour on day 1 two hours after initial SARM compound administration and on day 9 after consecutive daily administration. Similarly to *in vitro* incubations RAD140 remained metabolically stable with only one urinary metabolite formed by hydroxylation. Ostarine and LGD-4033 were not only extensively modified *in vitro* but also *in vivo* with various metabolites characterised in rat urine. While several metabolites were produced shortly after administration of ostarine and LGD-4033, additional metabolites were observed in urine collected on day 9 following a daily dosing regimen. Animals were sacrificed at the end of the study to collect livers for proteomics studies in **Chapters 6** and **7** and use livers of the non-treated control group for production of microsomes and S9 fractions subsequently used

in **Chapter 3**. Consequently, a drug excretion profile to identify long-term metabolites could therefore not be established. Considering the employed subcellular *in vitro* liver fractions represent a reductionist approach to the organism, organ, tissue, and cellular level using optimised experimental conditions, it provided a relatively good representation of actual *in vivo* formed metabolites. Only one urinary metabolite formed from RAD140 was observed, which was also formed *in vitro*. Out of 12 *in vivo* generated urinary metabolites of ostarine nine thereof were produced by rat liver microsomes/S9 fractions. Also, the majority of *in vivo* formed LGD-4033 metabolites were observed following *in vitro* incubations (ten out of 13). While this shows that only a few metabolites were observed in urine for ostarine and LGD-4033 that were not produced *in vitro*, several metabolites were also generated *in vitro* from RAD140, ostarine, and LGD-4033 with their production not confirmed *in vivo*. Therefore, when implementing metabolites from *in vitro* studies into testing procedures it is recommended to keep updated with the latest literature for information on confirmation of their formation and any newly described metabolites *in vivo* in the respective species.

To determine the distinct CYP isoenzymes involved in the formation of phase I metabolites of ostarine and LGD-4033, another *in vitro* approach centred on the incubation of species-specific liver microsomes (produced within **Chapter 3**) with ostarine or LGD-4033 together with CYP-selective inhibitors was used to measure the decrease in metabolite formation (**Chapter 4,** CYP reaction phenotyping). SARM compounds ostarine and LGD-4033 were chosen for this investigation as they produced several phase I metabolites as observed in **Chapter 3**. The development of a targeted MRM UHPLC-MS/MS for monitoring phase I metabolites of ostarine and LGD-4033 preceded the CYP reaction phenotyping experiments. A systematic multistep approach with full scan, precursor and product ion screening was used to establish a targeted method for monitoring SARM metabolites in MRM mode. Although this was not the primary aim of the study, it demonstrated how information gained from drug metabolism studies can be used for method development/improvement, especially considering that routine analyses are often performed with triple quadrupole mass spectrometers. Primary findings of the study were that bovine, equine, murine, and porcine CYP orthologues of human CYP2A6, CYP2B6, CYP2C8, CYP2C9 (only ostarine), and CYP3A4 were mainly involved in the metabolism of ostarine and LGD-4033. Consequently, co-administered veterinary drugs that inhibit or induce these CYP isoenzymes can potentially alter the metabolite profiles of ostarine and LGD-4033 which should be taken into consideration in future by monitoring laboratories as this can potentially mask an intake of these SARMs.

With regards to CYP isoenzymes, interspecies differences were less pronounced than expected. However, the chemical inhibitors used are selective towards human CYP isoenzymes, and as such selectivity towards CYP isoenzymes in other species is not well understood. CYP reaction phenotyping studies are common in human drug development being applied to investigate at an early stage the potential individual variability in drug metabolism due to CYP gene polymorphisms and potential metabolism-mediated drug-drug interactions of new chemical entities – these are two critical issues when developing new therapeutic drugs. Further research is needed to fully determine, isolate, and characterise the CYP isoenzymes in veterinary species, and to establish the selectivity of chemical inhibitors used in this study towards these species-specific CYPs in order to improve upon the employed CYP reaction phenotyping approach herein. Future studies could follow up on this work by using single cDNA expressed specific CYP isoenzymes, which are more active than liver microsomes but were not commercially available (**Section 1.3.2.5**). Using a singular species-specific CYP and monitoring the formation of metabolites by certain CYP would enable to further elucidate which isoenzymes produce specific metabolites and gain an improved understanding of how SARMs are metabolised in different species. Ideally an integrated approach using both methods, chemical inhibitors and heterologously expressed individual recombinant CYP, would be used to gain confidence in the results considering the limitations of each method.

To expand on the liver-based *in vitro* tools employed in this thesis, the metabolism of SARM compounds ostarine, LGD-4033, and RAD140 by multiple equine tissue microsomal and S9 fractions was investigated in an effort to better mimic actual *in vivo* metabolism (**Chapter 5**). In addition to liver, metabolism of SARM compounds by other relevant metabolic tissues, namely kidneys, lungs, and small intestine, was investigated. Compared to *in vivo* models, *in vitro* tools provide for the opportunity to independently study tissues and investigate the extent to which they metabolise drugs. Analysis of *in vitro* samples from incubations of equine liver, lung, kidney, or small intestinal microsomes alone (phase I) and in combination with S9 fractions (phase II) was performed on an UHPLC-QTOF MS system in auto MS/MS mode with a list of preferred ions and collision energy switching (0 V and 20 V). Compared to the data-independent acquisition ("pseudo MS/MS" mode, all-ion fragmentation) used in **Chapter 2** and **3** that fragments all ions leading to spectra that may contain fragments from co-eluting components, this data-dependent acquisition mode provided additional selectivity in recording MS/MS spectra by using a predefined list of expected metabolites. However, several metabolites described in **Chapter 3** (ostarine M3c,

M6, and M12, LGD-4033 M7) could not be detected either due to differences in the acquisition mode or sample preparation (protein precipitation followed by LLE and SPE for the aqueous phase in **Chapter 5** and protein precipitation in **Chapter 3**).This work demonstrated that whilst extrahepatic pathways can potentially contribute to the metabolism of SARM compounds, no additional metabolites were produced by extrahepatic tissues, and liver-based *in vitro* technologies can be considered sufficient for preliminary prediction of drug metabolism.

Substance abuse of SARM compounds is not only a threat to sports and food integrity but also a public health risk through intentional (e.g. doping) or unintentional, unknowing (e.g. contamination or undeclared ingredient in dietary supplements, potential dietary-related contamination of animal products) exposure. In order to elucidate physiological effects of SARM compound use, the hepatic response to ostarine, LGD-4033, and RAD140 was investigated in terms of protein profiles using 2-DIGE and MALDI-TOF (**Chapters 6** and **7**) approach. Following SARM compound administration to rats at a sub-toxic dose (3 mg/kg body weight) for 17 days mimicking a therapeutic dosing regimen (**Section 1.1.1**), differential analysis of liver lysates revealed that treatments altered levels of six protein spots following LGD-4033 exposure, four protein spots following RAD140, and one following ostarine administration (**Chapter 6**). Following Coomassie staining of gels, trypsin digestion of excised spots, MALDI-TOF analysis, and PMF six out of these 11 spots were identified corresponding to five unique proteins. Levels of three proteins (PON3, GAPDH, and AKR1C14) that play a role in metabolism were decreased and one protein (NAPA) with functions in vesicle-mediated transport was increased in response to LGD-4033 administrations. Relative levels of P4HB which is involved in several biological pathways including the ER stress response were increased upon RAD140 treatment.

Crude tissue lysates can underestimate low abundance changes and subsequently, to facilitate investigation of more subtle changes in the protein expression profiles organelle-specific proteins were enriched by subcellular fractionation (**Chapter 7**). Comparative analysis revealed that a total of 112 protein spot levels were altered following treatment with SARM compounds ostarine, LGD-4033, and RAD140. While protein levels of 12 spots were found to be altered in response to all SARM compounds, ostarine, LGD-4033, and RAD140 were each observed to exert distinct effects as shown by their uniquely altered liver protein profiles. Ostarine uniquely altered abundances in 18 spots (five decreased, 13 increased), LGD-4033 in 35 spots (five decreased, 30 increased), and RAD140 in 24 spots (six decreased, 18 increased). Eight spots had significantly altered relative levels by both ostarine

and RAD140 treatment (four decreased, four increased), seven by both ostarine and LGD-4033 (one decreased, six increased), and eight by both LGD-4033 and RAD140 (five decreased, three increased). The results show that subcellular fractionation greatly enhanced the detection of low-level protein abundance changes in comparison to the whole tissue approach (a total of 11 versus 112 protein spots). One problem with subfractionation is the cross-contamination of organelles by other organelles or organelle disruption.[575] Measures such as careful homogenisation and fractionation at cool temperatures were followed to keep cross-contamination to a minimum. Organelle assignment is further complicated by the fact that proteins can have single or multi-organelle distribution within cells or translocate between cellular compartments.[577] Another problem with subfractionation was that four samples (nuclei, mitochondria, microsomes, cytosol) were obtained from one (liver homogenate). Therefore, liver samples ($n = 8$ per group) were pooled prior to fractionation taking biological variation into account and samples were then analysed in duplicate (technical replicate).[578,579]

Functional analysis of identified proteins from **Chapter 7** highlighted several shared overrepresented pathways in response to treatment with investigated SARM compounds. Proteins with altered abundances following SARM treatment were principally associated with various metabolic processes including amino acid, energy, and carbohydrate metabolism. Levels of several proteins involved in protein processing within the ER were elevated, potentially pointing towards a stress response. The fundamental effects of a drug are reflected at the cellular level and proteomics was used to measure the effects of SARMs on functional protein levels as a product of translation. It has been observed that SARMs exhibit dose-dependent effects[559] and therefore, higher doses and/or a longer treatment period with SARMs merit further investigations. Future research into the molecular effects of SARM compounds using complimentary omics such as metabolomics (e.g. MS, NMR) or genomics (e.g. DNA sequencing, genotyping) approaches can help to identify down- and up-stream signalling processes and causality in conjunction with the proteomics data presented herein to provide a high-level systems biology perspective for affected complex and dynamic interactions. Additionally, by the development and use of novel bioinformatics approaches (e.g. deep learning and artificial intelligence) to mine various data sets, further biological meaning and interactions may be derived from the herein presented differential protein profiles.

The employed 2-D gel electrophoresis approaches in **Chapters 6** and **7** for comparative protein analysis and protein identification provided adequate protein separation and

resolution by pI and MW.[580] Horizontal streaking mainly in the basic region of the gels was observed which could be due to the electroendoosmotic flow of water from the cathode to the anode, poor solubility of proteins, and/or contaminants such as nucleic acids. Some highly abundant proteins showed vertical streaking due to protein overload. Intrinsic limitations such as poor solubility and transition into IPG strips or SDS-PAGE gels of hydrophobic proteins could be partly overcome in future studies by LC-MS approaches. Five protein spots in **Chapter 6** and 22 protein spots in **Chapter 7** could not be identified by MALDI-TOF analysis which is probably due to an insufficient protein quantity or trypsin digestion. It could also be that the protein sequence for these proteins has not yet been registered in a reference database.

Described approaches and observations in this thesis inform about the *in vitro* and *in vivo* formed metabolites of key SARM compounds that could advance analytical methods in the control and monitoring of illegal SARM use enforcing regulations and maintaining high standards for animal welfare, sports and food integrity with the accurate prediction and detection of metabolites a prerequisite to confirm that a drug has been administered. The thesis focused on a selected range of key SARM compounds including S-1, andarine, and ostarine in **Chapter 2** and ostarine, LGD-4033, and RAD140 in **Chapters 3-7.** Many more SARM compounds such as SARM 2-f and GSK2881078 (**Section 1.1.1**) are emerging as potential drugs of abuse. Therefore, the use of liver homogenates (**Chapter 2**) provides a rapid, cheap, and easy alternative approach to study the *in vitro* fate of novel emerging SARMs and thereby continuously improve upon control analyses to meet these new challenges. Testing for misuse of SARMs is relevant in a number of species and it has been shown that the metabolism of SARMs should be studied on a species-by-species basis due to interspecies differences in SARM metabolism (**Chapter 3**). Although *in vivo* SARM administration studies are favourable to study formed metabolites (**Chapter 3**), it is unlikely that all emerging SARMs will be administered to all relevant species to study their metabolism making the presented *in vitro* approaches such as use of liver homogenates (**Chapter 2**), microsomes, and S9 fractions (**Chapters 3-5**) indispensable tools to predict SARM compound metabolism. Besides the lack of authentic post-administration samples, unavailability of reference standards for metabolites is a bottleneck in drug metabolism research. Therefore, the position of functional groups, e.g. hydroxy or sulfate group, could not be fully assigned by LC-MS analyses as metabolic formation of several regioisomers is possible. Besides chemical synthesis and the use of *C. elegans*, future research could investigate the use of liver homogenates as means to produce sufficient amounts of

metabolites for purification by preparative HPLC followed by structural elucidation using NMR and/or infrared (IR) spectroscopy. UHPLC-HR-MS and UHPLC-MS/MS techniques allowed for efficient separation and detection of SARM metabolites and it is envisaged that recent developments in LC-MS such as miniaturized systems will allow for on-site drug testing using mobile laboratories in future. Comparative proteomic profiling of hepatic responses following administration of ostarine, LGD-4033, and RAD140 provided insights into the effects of SARMs at a molecular level thus providing a better understanding of the complex physiological effects of SARMs *in vivo*. Future studies measuring specific oxidative stress biomarkers, e.g. glutathione, malondialdehyde, and protein carbonyl content in liver and using high-content analysis to monitor morphological changes of hepatocytes upon addition of SARMs are needed to further evaluate if SARMs cause oxidative stress. This thesis has identified *in vitro* and *in vivo* metabolites of key SARM compounds in relevant species that can be used to advance metabolite-based forensic testing and provided a better understanding of the *in vivo* effects of key SARM compounds in liver as a key metabolic tissue using a proteomics approach.

References

[1]   N. Agrwal, M. B. Elamin, J. F. Gallegos-Orozco, A. T. Wang. Adverse effects of testosterone therapy in adult men: a systematic review and meta-analysis. *J. Clin. Endocrinol. Metab.*, **2010**, *95*, 2560–2575.

[2]   C. Maravelias, A. Dona, M. Stefanidou, C. Spiliopoulou. Adverse effects of anabolic steroids in athletes: a constant threat. *Toxicol. Lett.*, **2005**, *158*, 167–175.

[3]   C. Rolf, E. Nieschlag. Potential adverse effects of long-term testosterone therapy. *Baillieres. Clin. Endocrinol. Metab.*, **1998**, *12*, 521–534.

[4]   J. T. Dalton, A. Mukherjee, Z. Zhu, L. Kirkovsky, D. D. Miller. Discovery of nonsteroidal androgens. *Biochem. Biophys. Res. Commun.*, **1998**, *244*, 1–4.

[5]   J. O. Jones. Improving selective androgen receptor modulator discovery and preclinical evaluation. *Expert Opin. Drug Discov.*, **2009**, *4*, 981–993.

[6]   S. M. Choi, B.-M. Lee. Comparative safety evaluation of selective androgen receptor modulators and anabolic androgenic steroids. *Expert Opin. Drug Saf.*, **2015**, *14*, 1773–1785.

[7]   D. Kazmin, T. Prytkova, C. E. Cook, R. Wolfinger, T.-M. Chu, D. Beratan, J. D. Norris, C. Chang, D. P. McDonnell. Linking ligand-induced alterations in androgen receptor structure to differential gene expression: a first step in the rational design of selective androgen receptor modulators. *Mol. Endocrinol.*, **2006**, *20*, 1201–1217.

[8]   J.-H. Bebermeier, J. D. Brooks, S. E. DePrimo, R. Werner, U. Deppe, J. Demeter, O. Hiort, P.-M. Holterhus. Cell-line and tissue-specific signatures of androgen receptor-coregulator transcription. *J. Mol. Med.*, **2006**, *84*, 919–931.

[9]   C. Chang, D. P. McDonnell. Androgen receptor–cofactor interactions as targets for new drug discovery. *Trends Pharmacol. Sci.*, **2005**, *26*, 225–228.

[10]   R. Narayanan, C. C. Coss, M. Yepuru, J. D. Kearbey, D. D. Miller, J. T. Dalton. Steroidal androgens and nonsteroidal, tissue-selective androgen receptor modulator, S-22, regulate androgen receptor function through distinct genomic and nongenomic signaling pathways. *Mol. Endocrinol.*, **2008**, *22*, 2448–2465.

[11]   A. Negro-Vilar. Selective Androgen Receptor Modulators (SARMs): A Novel Approach to Androgen Therapy for the New Millennium. *J. Clin. Endocrinol. Metab.*, **1999**, *84*, 3459–3462.

[12]   D. Yin, Y. He, M. A. Perera, S. S. Hong, C. Marhefka, N. Stourman, L. Kirkovsky, D. D. Miller, J. T. Dalton. Key structural features of nonsteroidal ligands for binding and activation of the androgen receptor. *Mol. Pharmacol.*, **2003**, *63*, 211–223.

[13]   D. Yin, H. Xu, Y. He, L. I. Kirkovsky, D. D. Miller, J. T. Dalton. Pharmacology, pharmacokinetics, and metabolism of acetothiolutamide, a novel nonsteroidal agonist for the androgen receptor. *J. Pharmacol. Exp. Ther.*, **2003**, *304*, 1323–1333.

[14]   C. A. Marhefka, W. Gao, K. Chung, J. Kim, Y. He, D. Yin, C. Bohl, J. T. Dalton, D. D. Miller. Design, synthesis, and biological characterization of metabolically stable selective androgen receptor modulators. *J. Med. Chem.*, **2004**, *47*, 993–998.

[15]   D. Yin, W. Gao, J. D. Kearbey, H. Xu, K. Chung, Y. He, C. A. Marhefka, K. A. Veverka, D. D. Miller, J. T. Dalton. Pharmacodynamics of selective androgen receptor modulators. *J. Pharmacol. Exp. Ther.*, **2003**, *304*, 1334–1340.

[16]   D. Wu, Z. Wu, J. Yang, V. A. Nair, D. D. Miller, J. T. Dalton. Pharmacokinetics and metabolism of a selective androgen receptor modulator in rats: implication of molecular properties and intensive metabolic profile to investigate ideal pharmacokinetic characteristics of a propanamide in preclinical study. *Drug Metab. Dispos.*, **2006**, *34*, 483–494.

[17]   J. D. Kearbey, D. Wu, W. Gao, D. D. Miller, J. T. Dalton. Pharmacokinetics of S-3-(4-acetylamino-phenoxy)-2-hydroxy-2-methyl-N-(4-nitro-3-trifluoromethyl-phenyl)-propionamide in rats, a non-steroidal selective androgen receptor modulator. *Xenobiotica*, **2004**, *34*, 273–280.

[18]   J. Kim, D. Wu, D. J. Hwang, D. D. Miller, J. T. Dalton. The para substituent of S-3-(phenoxy)-2-hydroxy-2-methyl-N-(4-nitro-3-trifluoromethyl-phenyl)-propionamides is a major structural determinant of in vivo disposition and activity of selective androgen receptor modulators. *J. Pharmacol. Exp. Ther.*, **2005**, *315*, 230–239.

[19]   J. Kim, R. Wang, K. A. Veverka, J. T. Dalton. Absorption, distribution, metabolism and excretion of the novel SARM GTx-024 [(S)-N-(4-cyano-3-(trifluoromethyl) phenyl)-3-(4-cyanophenoxy)-2-hydroxy-2-methylpropanamide] in rats. *Xenobiotica*, **2013**, *43*, 993–1009.

[20]   A. Schmidt, D. B. Kimmel, C. Bai, A. Scafonas, S. Rutledge, R. L. Vogel, S. McElwee-Witmer, F. Chen, P. V Nantermet, V. Kasparcova. Discovery of the selective androgen receptor modulator MK-0773 using a rational development strategy based on differential transcriptional requirements for androgenic anabolism versus reproductive physiology. *J. Biol. Chem.*, **2010**, *285*, 17054–17064.

[21]   L. Min, T. Yanase, T. Tanaka, W. Fan, M. Nomura, H. Kawate, T. Okabe, R. Takayanagi, H. Nawata. A novel synthetic androgen receptor ligand, S42, works as a selective androgen receptor

modulator and possesses metabolic effects with little impact on the prostate. *Endocrinology*, **2009**, *150*, 5606–5616.

[22] Y. Kanno, R. Hikosaka, S.-Y. Zhang, Y. Inoue, T. Nakahama, K. Kato, A. Yamaguchi, N. Tominaga, S. Kohra, K. Arizono. (17α, 20E)-17, 20-[(1-Methoxyethylidene) bis (oxy)]-3-oxo-19-norpregna-4, 20-diene-21-carboxylic Acid Methyl Ester (YK11) Is a Partial Agonist of the Androgen Receptor. *Biol. Pharm. Bull.*, **2011**, *34*, 318–323.

[23] Y. Kanno, R. Ota, K. Someya, T. Kusakabe, K. Kato, Y. Inouye. Selective androgen receptor modulator, YK11, regulates myogenic differentiation of C2C12 myoblasts by follistatin expression. *Biol. Pharm. Bull.*, **2013**, *36*, 1460–1465.

[24] A. Schmidt, S.-I. Harada, D. B. Kimmel, C. Bai, F. Chen, S. J. Rutledge, R. L. Vogel, A. Scafonas, M. A. Gentile, P. V Nantermet. Identification of anabolic selective androgen receptor modulators with reduced activities in reproductive tissues and sebaceous glands. *J. Biol. Chem.*, **2009**, *284*, 36367–36376.

[25] A. Jones, J. Chen, D. J. Hwang, D. D. Miller, J. T. Dalton. Preclinical characterization of a (S)-N-(4-cyano-3-trifluoromethyl-phenyl)-3-(3-fluoro, 4-chlorophenoxy)-2-hydroxy-2-methyl-propanamide: a selective androgen receptor modulator for hormonal male contraception. *Endocrinology*, **2008**, *150*, 385–395.

[26] C. E. Bohl, Z. Wu, J. Chen, M. L. Mohler, J. Yang, D. J. Hwang, S. Mustafa, D. D. Miller, C. E. Bell, J. T. Dalton. Effect of B-ring substitution pattern on binding mode of propionamide selective androgen receptor modulators. *Bioorganic Med. Chem. Lett.*, **2008**, *18*, 5567–5570.

[27] J. Chen, D. J. Hwang, C. E. Bohl, D. D. Miller, J. T. Dalton. A selective androgen receptor modulator for hormonal male contraception. *J. Pharmacol. Exp. Ther.*, **2005**, *312*, 546–553.

[28] J. T. Dalton, R. P. Taylor, M. L. Mohler, M. S. Steiner. Selective androgen receptor modulators for the prevention and treatment of muscle wasting associated with cancer. *Curr. Opin. Support. Palliat. Care*, **2013**, *7*, 345–351.

[29] J. Ostrowski, J. E. Kuhns, J. A. Lupisella, M. C. Manfredi, B. C. Beehler, S. R. Krystek Jr, Y. Bi, C. Sun, R. Seethala, R. Golla. Pharmacological and x-ray structural characterization of a novel selective androgen receptor modulator: potent hyperanabolic stimulation of skeletal muscle with hypostimulation of prostate in rats. *Endocrinology*, **2007**, *148*, 4–12.

[30] X. Zhang, G. F. Allan, T. Sbriscia, O. Linton, S. G. Lundeen, Z. Sui. Synthesis and SAR of novel hydantoin derivatives as selective androgen receptor modulators. *Bioorg. Med. Chem. Lett.*, **2006**, *16*, 5763–5766.

[31] A. Cozzoli, R. F. Capogrosso, V. T. Sblendorio, M. M. Dinardo, C. Jagerschmidt, F. Namour, G. M. Camerino, A. De Luca. GLPG0492, a novel selective androgen receptor modulator, improves muscle performance in the exercised-mdx mouse model of muscular dystrophy. *Pharmacol. Res.*, **2013**, *72*, 9–24.

[32] I. Bhattacharya, S. Tarabar, Y. Liang, V. Pradhan, J. Owens, B. Oemar. Safety, Pharmacokinetic, and Pharmacodynamic Evaluation After Single and Multiple Ascending Doses of a Novel Selective Androgen Receptor Modulator in Healthy Subjects. *Clin. Ther.*, **2016**, *38*, 1401–1416.

[33] J. N. Miner, W. Chang, M. S. Chapman, P. D. Finn, M. H. Hong, F. J. López, K. B. Marschke, J. Rosen, W. Schrader, R. Turner. An orally active selective androgen receptor modulator is efficacious on bone, muscle, and sex function with reduced impact on prostate. *Endocrinology*, **2007**, *148*, 363–373.

[34] E. Martinborough, Y. Shen, A. van Oeveren, Y. O. Long, T. L. S. Lau, K. B. Marschke, W. Y. Chang, F. J. López, E. G. Vajda, P. J. Rix. Substituted 6-(1-pyrrolidine) quinolin-2 (1 H)-ones as novel selective androgen receptor modulators. *J. Med. Chem.*, **2007**, *50*, 5049–5052.

[35] E. G. Vajda, F. J. López, P. Rix, R. Hill, Y. Chen, K.-J. Lee, Z. O'Brien, W. Y. Chang, M. D. Meglasson, Y.-H. Lee. Pharmacokinetics and pharmacodynamics of LGD-3303 [9-chloro-2-ethyl-1-methyl-3-(2, 2, 2-trifluoroethyl)-3H-pyrrolo-[3, 2-f] quinolin-7 (6H)-one], an orally available nonsteroidal-selective androgen receptor modulator. *J. Pharmacol. Exp. Ther.*, **2009**, *328*, 663–670.

[36] L. G. Hamann, N. S. Mani, R. L. Davis, X.-N. Wang, K. B. Marschke, T. K. Jones. Discovery of a potent, orally active, nonsteroidal androgen receptor agonist: 4-ethyl-1, 2, 3, 4-tetrahydro-6-(trifluoromethyl)-8-pyridono [5, 6-g]-quinoline (LG121071). *J. Med. Chem.*, **1999**, *42*, 210–212.

[37] K. Hanada, K. Furuya, N. Yamamoto, H. Nejishima, K. Ichikawa, T. Nakamura, M. Miyakawa, S. Amano, Y. Sumita, N. Oguro. Bone anabolic effects of S-40503, a novel nonsteroidal selective androgen receptor modulator (SARM), in rat models of osteoporosis. *Biol. Pharm. Bull.*, **2003**, *26*, 1563–1569.

[38] K. Furuya, N. Yamamoto, Y. Ohyabu, A. Makino, T. Morikyu, H. Ishige, K. Kuzutani, Y. Endo. The novel non-steroidal selective androgen receptor modulator S-101479 has additive effects with bisphosphonate, selective estrogen receptor modulator, and parathyroid hormone on the bones of

osteoporotic female rats. *Biol. Pharm. Bull.*, **2012**, *35*, 1096–1104.

[39] K. Furuya, N. Yamamoto, Y. Ohyabu, T. Morikyu, H. Ishige, M. Albers, Y. Endo. Mechanism of the tissue-specific action of the selective androgen receptor modulator S-101479. *Biol. Pharm. Bull.*, **2013**, *36*, 442–51.

[40] G. Allan, T. Sbriscia, O. Linton, M.-T. Lai, D. Haynes-Johnson, S. Bhattacharjee, R. Ng, Z. Sui, S. Lundeen. A selective androgen receptor modulator with minimal prostate hypertrophic activity restores lean body mass in aged orchidectomized male rats. *J. Steroid Biochem. Mol. Biol.*, **2008**, *110*, 207–213.

[41] P. Yi, J. F. Rehmel, K. Cassidy, C. Hadden, K. Campanale, N. Patel, J. Johnson. Disposition and metabolism of LY2452473, a selective androgen receptor modulator, in humans. *Drug Metab. Dispos.*, **2012**, *40*, 2354–2364.

[42] R. V Clark, A. C. Walker, S. Andrews, P. Turnbull, J. A. Wald, M. H. Magee. Safety, Pharmacokinetics and Pharmacologic Effects of the Selective Androgen Receptor Modulator, GSK2881078, in Healthy Men and Postmenopausal Women. *Br. J. Clin. Pharmacol.*, **2017**, *83*, 2179-2194.

[43] G. Allan, M.-T. Lai, T. Sbriscia, O. Linton, D. Haynes-Johnson, S. Bhattacharjee, R. Dodds, J. Fiordeliso, J. Lanter, Z. Sui. A selective androgen receptor modulator that reduces prostate tumor size and prevents orchidectomy-induced bone loss in rats. *J. Steroid Biochem. Mol. Biol.*, **2007**, *103*, 76–83.

[44] J. C. Lanter, J. J. Fiordeliso, W. Jiang, G. F. Allan, M.-T. Lai, O. Linton, D. W. Hahn, S. G. Lundeen, Z. Sui. The discovery of a potent orally efficacious indole androgen receptor antagonist through in vivo screening. *Bioorg. Med. Chem. Lett.*, **2007**, *17*, 123–126.

[45] N. Schlienger, B. W. Lund, J. Pawlas, F. Badalassi, F. Bertozzi, R. Lewinsky, A. Fejzic, M. B. Thygesen, A. Tabatabaei, S. R. Bradley. Synthesis, structure− activity relationships, and characterization of novel nonsteroidal and selective androgen receptor modulators. *J. Med. Chem.*, **2009**, *52*, 7186–7191.

[46] F. Piu, L. R. Gardell, T. Son, N. Schlienger, B. W. Lund, H. H. Schiffer, K. E. Vanover, R. E. Davis, R. Olsson, S. R. Bradley. Pharmacological characterization of AC-262536, a novel selective androgen receptor modulator. *J. Steroid Biochem. Mol. Biol.*, **2008**, *109*, 129–137.

[47] X. Zhang, X. Li, G. F. Allan, T. Sbriscia, O. Linton, S. G. Lundeen, Z. Sui. Serendipitous discovery of novel imidazolopyrazole scaffold as selective androgen receptor modulators. *Bioorg. Med. Chem. Lett.*, **2007**, *17*, 439–443.

[48] X. Zhang, G. F. Allan, P. Tannenbaum, T. Sbriscia, O. Linton, M.-T. Lai, D. Haynes-Johnson, S. Bhattacharjee, S. G. Lundeen, Z. Sui. Pharmacological characterization of an imidazolopyrazole as novel selective androgen receptor modulator. *J. Steroid Biochem. Mol. Biol.*, **2013**, *134*, 51–58.

[49] M. Thevis, A. Lagojda, D. Kuehne, A. Thomas, J. Dib, A. Hansson, M. Hedeland, U. Bondesson, T. Wigger, U. Karst, W. Schänzer. Characterization of a non-approved selective androgen receptor modulator drug candidate sold via the Internet and identification of *in vitro* generated phase-I metabolites for human sports drug testing. *Rapid Commun. Mass Spectrom.*, **2015**, *29*, 991–999.

[50] K. Aikawa, M. Asano, K. Ono, N. Habuka, J. Yano, K. Wilson, H. Fujita, H. Kandori, T. Hara, M. Morimoto. Synthesis and biological evaluation of novel selective androgen receptor modulators (SARMs) Part III: Discovery of 4-(5-oxopyrrolidine-1-yl) benzonitrile derivative 2f as a clinical candidate. *Bioorg. Med. Chem.*, **2017**, *25*, 3330–3349.

[51] G. F. Allan, P. Tannenbaum, T. Sbriscia, O. Linton, M.-T. Lai, D. Haynes-Johnson, S. Bhattacharjee, X. Zhang, Z. Sui, S. G. Lundeen. A selective androgen receptor modulator with minimal prostate hypertrophic activity enhances lean body mass in male rats and stimulates sexual behavior in female rats. *Endocrine*, **2007**, *32*, 41–51.

[52] K. Akita, K. Harada, J. Ichihara, N. Takata, Y. Takahashi, K. Saito. A novel selective androgen receptor modulator, NEP28, is efficacious in muscle and brain without serious side effects on prostate. *Eur. J. Pharmacol.*, **2013**, *720*, 107–114.

[53] C. P. Miller, M. Shomali, C. R. Lyttle, L. S. L. O'dea, H. Herendeen, K. Gallacher, D. Paquin, D. R. Compton, B. Sahoo, S. a. Kerrigan, M. S. Burge, M. Nickels, J. L. Green, J. a. Katzenellenbogen, A. Tchesnokov, G. Hattersley. Design, synthesis, and preclinical characterization of the selective androgen receptor modulator (SARM) RAD140. *ACS Med. Chem. Lett.*, **2011**, *2*, 124–129.

[54] R. Narayanan, C. C. Coss, J. T. Dalton. Development of selective androgen receptor modulators (SARMs). *Mol. Cell. Endocrinol.*, **2018**, *465*, 134–142.

[55] J. T. Dalton, K. G. Barnette, C. E. Bohl, M. L. Hancock, D. Rodriguez, S. T. Dodson, R. A. Morton, M. S. Steiner. The selective androgen receptor modulator GTx-024 (enobosarm) improves lean body mass and physical function in healthy elderly men and postmenopausal women: results of a double-blind, placebo-controlled phase II trial. *J. Cachexia. Sarcopenia Muscle*, **2011**, *2*, 153–161.

[56]   C. C. Coss, M. Bauler, R. Narayanan, D. D. Miller, J. T. Dalton. Alanine aminotransferase regulation by androgens in non-hepatic tissues. *Pharm. Res.*, **2012**, *29*, 1046–1056.

[57]   E. E. Marcantonio, R. E. Witter, Y. Ding, Y. Xu, J. Klappenbach, Y. Wang, P. H. Wong, F. Liu, J. A. Chodakewitz, J. A. Wagner. A 12-Week Pharmacokinetic and Pharmacodynamic Study of Two Selective Androgen Receptor Modulators (SARMs) in Postmenopausal Subjects., in *Posters I*, Endocrine Society, **2010**, pp. P2-2.

[58]   R. Narayanan, J. T. Dalton. Androgen receptor: a complex therapeutic target for breast cancer. *Cancers.*, **2016**, *8*, 108.

[59]   F. E. Vera-Badillo, A. J. Templeton, P. de Gouveia, I. Diaz-Padilla, P. L. Bedard, M. Al-Mubarak, B. Seruga, I. F. Tannock, A. Ocana, E. Amir. Androgen receptor expression and outcomes in early breast cancer: a systematic review and meta-analysis. *J. Natl. Cancer Inst.*, **2014**, *106*, djt319.

[60]   N. Vontela, V. Koduri, L. S. Schwartzberg, G. A. Vidal. Selective androgen receptor modulator in a patient with hormone-positive metastatic breast cancer. *J. Natl. Compr. Cancer Netw.*, **2017**, *15*, 284–287.

[61]   B. Overmoyer, P. Sanz-Altamira, R. P. Taylor, M. L. Hancock, J. T. Dalton, M. A. Johnston, M. S. Steiner. Enobosarm: A targeted therapy for metastatic, androgen receptor positive, breast cancer. **2014**.

[62]   GTx. "Phase II Study of GTx024 in Women With Metastatic Breast Cancer," Available at: https://clinicaltrials.gov/ct2/show/NCT01616758?term=NCT01616758&rank=1, **2012**. Last accessed: 16/02/2020

[63]   M. S. Steiner, K. G. Barnette, M. L. Hancock, S. T. Dodson, D. Rodriguez, R. A. Morton. Effect of GTx-024, a selective androgen receptor modulator (SARM), on stair climb performance and quality of life (QOL) in patients with cancer cachexia. *J. Clin. Oncol.*, **2010**, *28*, 9147.

[64]   A. S. Dobs, R. V Boccia, C. C. Croot, N. Y. Gabrail, J. T. Dalton, M. L. Hancock, M. A. Johnston, M. S. Steiner. Effects of enobosarm on muscle wasting and physical function in patients with cancer: a double-blind, randomised controlled phase 2 trial. *Lancet Oncol.*, **2013**, *14*, 335–345.

[65]   GTx. "Study of GTx-024 on Muscle Wasting (Cachexia) Cancer," Available at: https://clinicaltrials.gov/ct2/show/NCT00467844?term=NCT00467844&rank=1, **2007**. Last accessed: 16/02/2020

[66]   S. W. Hayward, G. R. Cunha. The prostate: development and physiology. *Radiol. Clin. North Am.*, **2000**, *38*, 1–14.

[67]   P. M. Pierorazio, L. Ferrucci, A. Kettermann, D. L. Longo, E. J. Metter, H. B. Carter. Serum testosterone is associated with aggressive prostate cancer in older men: results from the Baltimore Longitudinal Study of Aging. *BJU Int.*, **2010**, *105*, 824–829.

[68]   F. H. Schröder, J. Hugosson, M. J. Roobol, T. L. J. Tammela, S. Ciatto, V. Nelen, M. Kwiatkowski, M. Lujan, H. Lilja, M. Zappa. Screening and prostate-cancer mortality in a randomized European study. *N. Engl. J. Med.*, **2009**, *360*, 1320–1328.

[69]   M. S. Steiner, A. Dobs, M. L. Hancock, M. A. Johnston, G. Barnette, S. Dodson. Effect of GTx-024, a selective androgen receptor modulator (SARM), on physical function in patients with non-small cell lung cancer (NSCLC) with cancer cachexia. *J. Clin. Oncol.*, **2011**, *29*, 9022.

[70]   GTx. "Phase III Study of the Effect of GTx-024 on Muscle Wasting in Patients With Non-Small Cell Lung Cancer (NSCLC)," Available at: https://clinicaltrials.gov/ct2/show/NCT01355484?term=NCT01355484&rank=1, **2011**. Last accessed: 16/02/2020

[71]   GTx. "Effect of GTx-024 on Muscle Wasting in Patients With Non-Small Cell Lung Cancer (NSCLC) on First Line Platinum," Available at: https://clinicaltrials.gov/ct2/show/NCT01355497?term=NCT01355497&rank=1, **2011**. Last accessed: 16/02/2020

[72]   J. Crawford, C. M. M. Prado, M. A. Johnston, R. J. Gralla, R. P. Taylor, M. L. Hancock, J. T. Dalton. Study design and rationale for the phase 3 clinical development program of enobosarm, a selective androgen receptor modulator, for the prevention and treatment of muscle wasting in cancer patients (POWER trials). *Curr. Oncol. Rep.*, **2016**, *18*, 37.

[73]   J. Crawford, M. A. Johnston, R. P. Taylor, J. T. Dalton, M. S. Steiner. Enobosarm and lean body mass in patients with non-small cell lung cancer. *J. Clin. Oncol.*, **2014**, *32*.

[74]   J. Crawford, J. T. Dalton, M. L. Hancock, M. A. Johnston, M. Steiner. Enobosarm, a selective androgen receptor modulator (SARM), increases lean body mass (LBM) in advanced non-small cell lung cancer patients in two pivotal, international Phase 3 trials. *J Cachexia Sarcopenia Muscle*, **2014**, *5*, 35–78.

[75]   GTx. "Study to Assess Enobosarm (GTx-024) in Postmenopausal Women With Stress Urinary Incontinence (ASTRID)," Available at: https://clinicaltrials.gov/ct2/show/NCT03241342, **2017**. Last

accessed: 16/02/2020

[76]   GTx. "GTx-024 as a Treatment for Stress Urinary Incontinence in Women," Available at:
         https://clinicaltrials.gov/ct2/show/NCT02658448?term=enobosarm&rank=1, **2016**. Last accessed:
         16/02/2020

[77]   GTx. "Durability Extension Study to Assess Clinical Activity and Safety of Enobosarm (GTx-024) in
         Stress Urinary Incontinence," Available at:
         https://clinicaltrials.gov/ct2/show/NCT03508648?term=GTx-024&rank=5, **2018**. Last accessed:
         16/02/2020

[78]   GTx. "Study to Assess Long-Term Safety/Tolerability of Enobosarm (GTx 024) in Stress Urinary
         Incontinence," Available at: https://clinicaltrials.gov/ct2/show/NCT03566290, **2018**. Last accessed:
         16/02/2020

[79]   GTx. "Efficacy and Safety of GTx-024 in Patients With ER+/AR+ Breast Cancer," Available at:
         https://clinicaltrials.gov/ct2/show/NCT02463032?term=G200802&rank=2, **2015**. Last accessed:
         16/02/2020

[80]   City of Hope Medical Center. "Pembrolizumab and Enobosarm in Treating Patients With Androgen
         Receptor Positive Metastatic Triple Negative Breast Cancer," Available at:
         https://clinicaltrials.gov/ct2/show/NCT02971761?term=enobosarm&rank=3, **2016**. Last accessed:
         16/02/2020

[81]   S. Basaria, L. Collins, E. L. Dillon, K. Orwoll, T. W. Storer, R. Miciek, J. Ulloor, A. Zhang, R. Eder,
         H. Zientek. The safety, pharmacokinetics, and effects of LGD-4033, a novel nonsteroidal oral,
         selective androgen receptor modulator, in healthy young men. *Journals Gerontol. Ser. A Biomed. Sci.
         Med. Sci.*, **2010**, *68*, 87–95.

[82]   Viking Therapeutics. "Acute Hip Fracture Study in Patients 65 Years or Greater," Available at:
         https://clinicaltrials.gov/ct2/show/study/NCT02578095?term=VK5211&rank=1, **2015**. Last accessed:
         16/02/2020

[83]   D. A. Papanicolaou, S. N. Ather, H. Zhu, Y. Zhou, J. Lutkiewicz, B. B. Scott, J. Chandler. A phase
         IIA randomized, placebo-controlled clinical trial to study the efficacy and safety of the selective
         androgen receptor modulator (SARM), MK-0773 in female participants with sarcopenia. *J. Nutr.
         Health Aging*, **2013**, *17*, 533–543.

[84]   Merck Sharp & Dohme Corp. "A Study of the Safety and Efficacy of MK-0773 in Women With
         Sarcopenia (Loss of Muscle Mass)(MK-0773-005)," Available at:
         https://clinicaltrials.gov/ct2/show/NCT00529659?term=NCT00529659&rank=1, **2007**. Last
         accessed: 16/02/2020

[85]   Pfizer. "The Bioavailability of a Spray Dried Dispersion Solid Dose Formulation of PF-06260414
         Relative to a Suspension Formulation," Available at:
         https://clinicaltrials.gov/ct2/show/NCT02393807?term=NCT02393807&rank=1, **2015**. Last
         accessed: 16/02/2020

[86]   Galapagos NV. "First-in-Human Single Ascending Dose of GLPG0492," Available at:
         https://clinicaltrials.gov/ct2/show/NCT01130818?term=NCT01130818&rank=1, **2010**. Last
         accessed: 16/02/2020

[87]   Galapagos NV. "Multiple Ascending Dose Study of GLPG0492 in Healthy Subjects," Available at:
         https://clinicaltrials.gov/ct2/show/NCT01397370?term=NCT01397370&rank=1, **2011**. Last
         accessed: 16/02/2020

[88]   Galapagos NV. "GLPG0492 Pharmacodynamics," Available at:
         https://clinicaltrials.gov/ct2/show/NCT01538420?term=NCT01538420&rank=1, **2012**. Last
         accessed: 16/02/2020

[89]   "PIPELINE DT-200: MUSCLE BUILDER," Available at: https://akashirx.com/pipeline/, Last
         accessed: 16/02/2020

[90]   GlaxoSmithKline. "Safety, Tolerability, Pharmacokinetics, and Pharmacodynamics Study of
         GSK2881078 in Single and Repeat Doses," Available at:
         https://clinicaltrials.gov/ct2/show/NCT02045940?term=NCT02045940&rank=1, **2014**. Last
         accessed: 16/02/2020

[91]   GlaxoSmithKline. "Safety, Tolerability, Pharmacokinetic (PK), and Pharmacodynamic Study of
         GSK2881078 and Study to Evaluate the Effect of CYP3A4 Inhibition on PK of GSK2881078,"
         Available at: https://clinicaltrials.gov/ct2/show/NCT02567773?term=NCT02567773&rank=1, **2015**.
         Last accessed: 16/02/2020

[92]   D. Neil, R. V Clark, M. Magee, J. Billiard, A. Chan, Z. Xue, A. Russell. GSK2881078, a SARM,
         produces dose-dependent increases in lean mass in healthy older men and women. *J. Clin.
         Endocrinol. Metab.*, **2018**, *103*, 3215–3224.

[93]   GlaxoSmithKline. "A Study to Evaluate the Safety, Tolerability, Pharmacokinetics, and

Pharmacodynamics of GSK2849466 in Healthy Male Subjects," Available at: https://clinicaltrials.gov/ct2/show/NCT01696604?term=NCT01696604&rank=1, **2012**. Last accessed: 16/02/2020

[94] GlaxoSmithKline. "Study to Test Safety, Tolerability and Blood Levels of GSK971086 After 1 Dose & 7 Days of Dosing in Healthy Adult Males," Available at: https://clinicaltrials.gov/ct2/show/NCT00540553?term=NCT00540553&rank=1, **2007**. Last accessed: 16/02/2020

[95] GlaxoSmithKline. "Study to Evaluate the Safety and Efficacy of 13 Weeks of the Selective Androgen Receptor Modulator (SARM) GSK2881078 in Chronic Obstructive Pulmonary Disease (COPD)," Available at: https://clinicaltrials.gov/ct2/show/NCT03359473?term=GSK2881078&rank=1, **2017**. Last accessed: 16/02/2020

[96] R. V Clark, M. C. Rhodes, A. C. Walker, A. Wolstenholme, J. a Wald, T. l Dimino, P. s Turnbull, A. Kapur, R. Goldwater. Use of Non-Clinical Toxicology Findings to Rapidly Terminate Early Clinical Progression of a Selective Androgen Receptor Modulator (SARM). *Eff. Regul. Sex Horm. Levels Men*, **2014**, *35*, 2055.

[97] Eli Lilly & Company. "Disposition of 14C-LY2452473 Following Oral Administration in Healthy Human Subjects," Available at: https://clinicaltrials.gov/ct2/show/NCT01275157?term=NCT01275157&rank=1, **2011**. Last accessed: 16/02/2020

[98] Eli Lilly & Company. "A Bioavailability Study of LY2452473 and Tadalafil," Available at: https://clinicaltrials.gov/ct2/show/NCT01401543?term=NCT01401543&rank=1, **2011**. Last accessed: 16/02/2020

[99] Dana-Faber Cancer Institute. "A Selective Androgen Receptor Modulator for Symptom Management in Prostate Cancer," Available at: https://clinicaltrials.gov/ct2/show/NCT02499497?term=LY2452473&rank=3, **2015**. Last accessed: 16/02/2020

[100] Eli Lilly & Company. "A Study of LY900010 in Erectile Dysfunction," Available at: https://clinicaltrials.gov/ct2/show/NCT01160289?term=NCT01160289&rank=1, **2010**. Last accessed: 16/02/2020

[101] C. Benson. "SARM I/Tadalafil Phase II Combination Study for Erectile Dysfunction," Available at: https://www.ema.europa.eu/en/documents/presentation/presentation-sarm-i/tadalafil-pgase-ii-combination-study-erectile-dysfunction-modeling-simulation-optimize-study-design_en.pdf, **2014**. Last accessed: 16/02/2020

[102] Transition Therapeutics. "Transition Therapeutics Announces Dosing of First Patient in Phase 2 Study of Drug Candidate TT701," Available at: https://www.prnewswire.com/news-releases/transition-therapeutics-announces-dosing-of-first-patient-in-phase-2-study-of-drug-candidate-tt701-577017881.html, **2016**. Last accessed: 16/02/2020

[103] Transition Therapeutics. "Effects and Safety of OPK-88004 Doses in Men With Signs and Symptoms of Benign Prostatic Hyperplasia (BPH)," Available at: https://clinicaltrials.gov/ct2/show/study/NCT03297398?term=OPK88004&rank=1, **2017**. Last accessed: 16/02/2020

[104] Radius Pharmaceuticals. "A Phase 1, First-in-Human, Multi-Part Study of RAD140 in Postmenopausal Women With Hormone Receptor Positive Breast Cancer," Available at: https://clinicaltrials.gov/ct2/show/NCT03088527?term=RAD140&rank=1, **2017**. Last accessed: 16/02/2020

[105] J. T. Dalton. The long and winding road for selective androgen receptor modulators. *Br. J. Clin. Pharmacol.*, **2017**, *83*, 2131–2133.

[106] K. C. H. Fearon, J. M. Argiles, V. E. Baracos, R. Bernabei, A. J. S. Coats, J. Crawford, N. E. Deutz, W. Doehner, W. J. Evans, L. Ferrucci. Request for regulatory guidance for cancer cachexia intervention trials. *J. Cachexia. Sarcopenia Muscle*, **2015**, *6*, 272–274.

[107] J. G. Le-Rademacher, J. Crawford, W. J. Evans, A. Jatoi. Overcoming obstacles in the design of cancer anorexia/weight loss trials. *Crit. Rev. Oncol. Hematol.*, **2017**, *117*, 30–37.

[108] Havah Therapeutics Pty Ltd. "Enobosarm and Anastrozole in Pre-menopausal Women With High Mammographic Breast Density," Available at: https://clinicaltrials.gov/ct2/show/NCT03264651?term=GTx-024&draw=3&rank=13, **2017**. Last accessed: 16/02/2020

[109] WADA. "List of Prohibited Substances and Methods," Available at: https://www.wada-ama.org/en/content/what-is-prohibited, **2020**. Last accessed: 16/02/2020

[110] WADA. "International Standard for Laboratories (ISL)," Available at: https://www.wada-

ama.org/en/resources/laboratories/international-standard-for-laboratories-isl-2019-newly-approved, **2019**. Last accessed: 16/02/2020

[111] F. Badoud, D. Guillarme, J. Boccard, E. Grata, M. Saugy, S. Rudaz, J.-L. Veuthey. Analytical aspects in doping control: Challenges and perspectives. *Forensic Sci. Int.*, **2011**, *213*, 49–61.

[112] IFHA. "International Agreement on Breeding, Racing and Wagering and Appendixes," Available at: https://www.ifhaonline.org/resources/ifAgreement.pdf, **2019**. Last accessed: 16/02/2020

[113] J. K. Y. Wong, T. S. M. Wan. Doping control analyses in horseracing: A clinician's guide. *Vet. J.*, **2014**, *200*, 8–16.

[114] A. G. Fragkaki, N. Kioukia-Fougia, P. Kiousi, M. Kioussi, M. Tsivou. Challenges in detecting substances for equine anti-doping. *Drug Test. Anal.*, **2017**, *9*, 1291-1303.

[115] FEI. "Anti-Doping Rules," Available at: https://inside.fei.org/content/anti-doping-rules, **2019**. Last accessed: 16/02/2020

[116] ILAC. "ILAC-G7. Accreditation Requirements and Operating Criteria for Horseracing Laboratories.," Available at: https://ilac.org/publications-and-resources/ilac-guidance-series/, **2016**. Last accessed: 16/02/2020

[117] European Council. Council Directive 96/22/EC of 29 April 1996 concerning the prohibition on the use in stockfarming of certain substances having a hormonal other thyrostatic action and of beta-agonist, and repealing Directives 81/602. *Off. J. Eur. Communities*, **1996**, *125*, 3–9.

[118] European Council. Council Directive 96/23/EC of 29 April 1996 on measures to monitor certain substances and residues thereof in live animals and animal products and repealing Directives 85/358/EEC and 86/469/EEC and Decisions 89/187/EEC and 91/664/EEC. *Off. J. Eur. Communities*, **1996**, *125*, 10–31.

[119] European Commission. 97/747/EC: Commission Decision of 27 October 1997 fixing the levels and frequencies of sampling provided for by Council Directive 96/23/EC for the monitoring of certain substances and residues thereof in certain animal products. *Off. J. Eur. Communities*, **1997**, 12–15.

[120] European Commission. 2002/657/EC: Commission decision of 12 August 2002 implementing Council Directive 96/23/EC concerning the performance of analytical methods and the interpretation of results. *Off. J. Eur. Communities*, **2002**, *221*, 8.

[121] Council of the European Union. Regulation (EC) No 882/2004 of the European Parliament and of the Council of 29 April 2004 on official controls performed to ensure the verification of compliance with feed and food law, animal health and animal welfare rules. *Off. J. Eur. Communities*, **2004**, *Chapter 3*, 200–251.

[122] M. Kohler, A. Thomas, H. Geyer, M. Petrou, W. Schänzer, M. Thevis. Confiscated black market products and nutritional supplements with non-approved ingredients analyzed in the cologne doping control laboratory 2009. *Drug Test. Anal.*, **2010**, *2*, 533–537.

[123] O. Krug, A. Thomas, K. Walpurgis, T. Piper, G. Sigmund, W. Schänzer, T. Laussmann, M. Thevis. Identification of black market products and potential doping agents in Germany 2010–2013. *Eur. J. Clin. Pharmacol.*, **2014**, *70*, 1303–1311.

[124] C. Weber, O. Krug, M. Kamber, M. Thevis. Qualitative and Semiquantitative Analysis of Doping Products Seized at the Swiss Border. *Subst. Use Misuse*, **2017**, *52*, 742–753.

[125] M. Thevis. Detection of the arylpropionamide-derived selective androgen receptor modulator (SARM) S-4 (Andarine) in a black-market product. *Drug Test. Anal.*, **2009**, *1*, 387–392.

[126] M. Thevis, H. Geyer, A. Thomas, W. Schänzer. Trafficking of drug candidates relevant for sports drug testing: Detection of non-approved therapeutics categorized as anabolic and gene doping agents in products distributed via the Internet. *Drug Test. Anal.*, **2011**, *3*, 331–336.

[127] L. Geldof, O. J. Pozo, L. Lootens, W. Morthier, P. Van Eenoo, K. Deventer. In vitro metabolism study of a black market product containing SARM LGD-4033. *Drug Test. Anal.*, **2017**, *9*, 168–178.

[128] A. Z. Temerdashev, A. A. Azaryan, A. V Labutin, M. A. Dikunets, I. O. Zvereva, I. I. Podol'skii, G. T. Berodze, I. A. Balabaev. Application of chromatography–mass spectrometry methods to the control of sport nutrition and medicines marketed via internet. *J. Anal. Chem.*, **2017**, *72*, 1184–1192.

[129] R. M. Van Wagoner, A. Eichner, S. Bhasin, P. A. Deuster, D. Eichner. Chemical Composition and Labeling of Substances Marketed as Selective Androgen Receptor Modulators and Sold via the Internet. *Jama*, **2017**, *318*, 2004–2010.

[130] B. Starcevic, B. D. Ahrens, A. W. Butch. Detection of the selective androgen receptor modulator S-4 (Andarine) in a doping control sample. *Drug Test. Anal.*, **2013**, *5*, 377–379.

[131] A. T. Cawley, C. Smart, C. Greer, M. L. Lau, J. Keledjian. Detection of the selective androgen receptor modulator andarine (S-4) in a routine equine blood doping control sample. *Drug Test. Anal.*, **2016**, *8*, 257–261.

[132] H. D. Cox, D. Eichner. Detection of LGD-4033 and its metabolites in athlete urine samples. *Drug Test. Anal.*, **2017**, *9*, 127–134.

[133] E. Grata, L. Perrenoud, M. Saugy, N. Baume. SARM-S4 and metabolites detection in sports drug testing: A case report. *Forensic Sci. Int.*, **2011**, *213*, 104–108.

[134] WADA. "2012 Anti-Doping Testing Figures Report," Available at: https://www.wada-ama.org/en/resources/laboratories/anti-doping-testing-figures-report, **2012**. Last accessed: 16/02/2020

[135] WADA. "2013 Anti-Doping Testing Figures Report," Available at: https://www.wada-ama.org/en/resources/laboratories/anti-doping-testing-figures-report, **2013**. Last accessed: 16/02/2020

[136] WADA. "2014 Anti-Doping Testing Figures Report," Available at: https://www.wada-ama.org/en/resources/laboratories/anti-doping-testing-figures-report, **2014**. Last accessed: 16/02/2020

[137] WADA. "2015 Anti-Doping Testing Figures Report," Available at: https://www.wada-ama.org/en/resources/laboratories/anti-doping-testing-figures-report, **2015**. Last accessed: 16/02/2020

[138] WADA. "2016 Anti-Doping Testing Figures Report," Available at: https://www.wada-ama.org/en/resources/laboratories/anti-doping-testing-figures-report, **2016**. Last accessed: 16/02/2020

[139] WADA. "2017 Anti-Doping Testing Figures Report," Available at: https://www.wada-ama.org/en/resources/laboratories/anti-doping-testing-figures-report, **2017**. Last accessed: 16/02/2020

[140] WADA. "2018 Anti-Doping Testing Figures Report," Available at: https://www.wada-ama.org/en/resources/laboratories/anti-doping-testing-figures-report, **2018**. Last accessed: 16/02/2020

[141] E. de Rijke, M. L. Essers, J. C. W. Rijk, M. Thevis, T. F. H. Bovee, L. A. van Ginkel, S. S. Sterk. Selective androgen receptor modulators: in vitro and in vivo metabolism and analysis. *Food Addit. Contam. Part A*, **2013**, *30*, 1517–1526.

[142] N. Cesbron, A. Sydor, M. Penot, S. Prevost, B. Le Bizec, G. Dervilly-Pinel. Analytical strategies to detect enobosarm administration in bovines. *Food Addit. Contam. Part A*, **2017**, *34*, 632–640.

[143] L. Beucher, G. Dervilly-Pinel, N. Cesbron, M. Penot, A. Gicquiau, F. Monteau, B. Le Bizec. Specific characterization of non-steroidal selective androgen peceptor modulators using supercritical fluid chromatography coupled to ion-mobility mass spectrometry: application to the detection of enobosarm in bovine urine. *Drug Test. Anal.*, **2017**, *9*, 179–187.

[144] M. Thevis, M. Kamber, W. Schänzer. Screening for metabolically stable aryl-propionamide-derived selective androgen receptor modulators for doping control purposes. *Rapid Commun. Mass Spectrom.*, **2006**, *20*, 870–876.

[145] M. Thevis. Screening for 2-quinolinone-derived selective androgen receptor agonists in doping control analysis. *Rapid Commun. Mass Spectrom.*, **2007**, *21*, 3477–3486.

[146] M. Thevis, M. Kohler, A. Thomas, N. Schlörer, W. Schänzer. Doping control analysis of tricyclic tetrahydroquinoline-derived selective androgen receptor modulators using liquid chromatography/electrospray ionization tandem mass spectrometry. *Rapid Commun. Mass Spectrom.*, **2008**, *22*, 2471–2478.

[147] M. Thevis, M. Kohler, A. Thomas, J. Maurer, N. Schlörer, M. Kamber, W. Schänzer. Determination of benzimidazole- and bicyclic hydantoin-derived selective androgen receptor antagonists and agonists in human urine using LC-MS/MS. *Anal. Bioanal. Chem.*, **2008**, *391*, 251–261.

[148] M. Thevis, A. Thomas, G. Fußhöller, S. Beuck, H. Geyer, W. Schänzer. Mass spectrometric characterization of urinary metabolites of the selective androgen receptor modulator andarine (S-4) for routine doping control purposes. *Rapid Commun. Mass Spectrom.*, **2010**, *24*, 2245–2254.

[149] M. Thevis, A. Thomas, M. Kohler, S. Beuck, W. Schänzer. Emerging drugs: mechanism of action, mass spectrometry and doping control analysis. *J. Mass Spectrom.*, **2009**, *44*, 442–460.

[150] M. Thevis, M. Kohler, N. Schlörer, G. Fußhöller, W. Schänzer. Screening for two selective androgen receptor modulators using gas chromatography-mass spectrometry in doping control analysis. *Eur. J. Mass Spectrom.*, **2008**, *14*, 153–161.

[151] E. Gerace, A. Salomone, F. Fasano, R. Costa, D. Boschi, A. Di Stilo, M. Vincenti. Validation of a GC/MS method for the detection of two quinolinone-derived selective androgen receptor modulators in doping control analysis. *Anal. Bioanal. Chem.*, **2011**, *400*, 137–144.

[152] A. Musenga, D. A. Cowan. Use of ultra-high pressure liquid chromatography coupled to high resolution mass spectrometry for fast screening in high throughput doping control. *J. Chromatogr. A*, **2013**, *1288*, 82–95.

[153] S. Guddat, E. Solymos, A. Orlovius, A. Thomas, G. Sigmund, H. Geyer, M. Thevis, W. Schänzer. High-throughput screening for various classes of doping agents using a new 'dilute-and-shoot' liquid

chromatography-tandem mass spectrometry multi-target approach. *Drug Test. Anal.*, **2011**, *3*, 836–850.

[154]   M. Thevis, O. Krug, H. Geyer, W. Schänzer. Expanding Analytical Options in Sports Drug Testing: Mass Spectrometric Detection of Prohibited Substances in Exhaled Breath. *Rapid Commun. Mass Spectrom.*, **2017**, *31*, 1290–1296.

[155]   W. H. Kwok, T. L. S. Choi, Y. Y. K. Tsoi, G. N. W. Leung, T. S. M. Wan. Screening of over 100 drugs in horse urine using automated on-line solid-phase extraction coupled to liquid chromatography-high resolution mass spectrometry for doping control. *J. Chromatogr. A*, **2017**, *1490*, 89–101.

[156]   J. K. Y. Wong, T. L. S. Choi, K. Y. Kwok, E. N. Y. Lei, T. S. M. Wan. Doping control analysis of 121 prohibited substances in equine hair by liquid chromatography–tandem mass spectrometry. *J. Pharm. Biomed. Anal.*, **2018**, *158*, 189–203.

[157]   B. Gray, M. Viljanto, E. Menzies, L. Vanhaecke. Detection of prohibited substances in equine hair by ultra-high performance liquid chromatography–triple quadrupole mass spectrometry–application to doping control samples. *Drug Test. Anal.*, **2018**, *10*, 1050–1060.

[158]   K. S. Schmidt, J. Mankertz. In-house validation of a liquid chromatography–tandem mass spectrometry method for the determination of selective androgen receptor modulators (SARMS) in bovine urine. *Food Addit. Contam. Part A*, **2018**, *35*, 1292–1304.

[159]   D. Rojas, G. Dervilly-Pinel, N. Cesbron, M. Penot, A. Sydor, S. Prévost, B. Le Bizec. Selective androgen receptor modulators: comparative excretion study of bicalutamide in bovine urine and faeces. *Drug Test. Anal.*, **2017**, *9*, 1017–1025.

[160]   E. Ventura, A. Gadaj, G. Monteith, A. Ripoche, J. Healy, F. Botrè, S. S. Sterk, T. Buckley, M. H. Mooney. Development and validation of a semi-quantitative ultra-high performance liquid chromatography-tandem mass spectrometry method for screening of selective androgen receptor modulators in urine. *J. Chromatogr. A*, **2019**, *1600*, 183–196.

[161]   A. Gadaj, E. Ventura, A. Ripoche, M. H. Mooney. Monitoring of selective androgen receptor modulators in bovine muscle tissue by ultra-high performance liquid chromatography-tandem mass spectrometry. *Food Chem. X*, **2019**, *4*, 100056.

[162]   M. Zhu, H. Zhang, W. G. Humphreys. Drug metabolite profiling and identification by high-resolution mass spectrometry. *J. Biol. Chem.*, **2011**, *286*, 25419–25425.

[163]   E. L. Schymanski, J. Jeon, R. Gulde, K. Fenner, M. Ruff, H. P. Singer, J. Hollender. Identifying small molecules via high resolution mass spectrometry: communicating confidence. **2014**, *48*, 2097-2098.

[164]   A. Hansson, H. Knych, S. Stanley, M. Thevis, U. Bondesson, M. Hedeland. Characterization of equine urinary metabolites of selective androgen receptor modulators (SARMs) S1, S4 and S22 for doping control purposes. *Drug Test. Anal.*, **2015**, *7*, 673–683.

[165]   A. Hansson, H. Knych, S. Stanley, M. Thevis, U. Bondesson, M. Hedeland. Investigation of the selective androgen receptor modulators S1, S4 and S22 and their metabolites in equine plasma using high-resolution mass spectrometry. *Rapid Commun. Mass Spectrom.*, **2016**, *30*, 833–842.

[166]   E. V Dmitrieva, A. Z. Temerdashev, A. A. Azaryan, E. M. Gashimova. Determination of andarine (S-4), a selective androgen receptor modulator, and ibutamoren (MK-677), a nonpeptide growth hormone secretagogue, in urine by ultra-high performance liquid chromatography with tandem mass-spectrometric detection. *J. Anal. Chem.*, **2018**, *73*, 674–678.

[167]   A. Temerdashev, E. Dmitrieva, A. Azaryan, E. Gashimova. A novel approach to the quantification of urinary aryl-propionamide-derived SARMs by UHPLC–MS/MS. *Biomed. Chromatogr.*, **2020**, *34*, e4700.

[168]   C. Görgens, S. Guddat, A. Thomas, P. Wachsmuth, A.-K. Orlovius, G. Sigmund, M. Thevis, W. Schänzer. Simplifying and expanding analytical capabilities for various classes of doping agents by means of direct urine injection high performance liquid chromatography high resolution/high accuracy mass spectrometry. *J. Pharm. Biomed. Anal.*, **2016**, *131*, 482–496.

[169]   A. Thomas, S. Guddat, M. Kohler, O. Krug, W. Schänzer, M. Petrou, M. Thevis. Comprehensive plasma-screening for known and unknown substances in doping controls. *Rapid Commun. Mass Spectrom.*, **2010**, *24*, 1124–1132.

[170]   A. Thomas, H. Geyer, W. Schänzer, C. Crone, M. Kellmann, T. Moehring, M. Thevis. Sensitive determination of prohibited drugs in dried blood spots (DBS) for doping controls by means of a benchtop quadrupole/Orbitrap mass spectrometer. *Anal. Bioanal. Chem.*, **2012**, *403*, 1279–1289.

[171]   L. Luosujärvi, M. Haapala, M. Thevis, V. Saarela, S. Franssila, R. a. Ketola, R. Kostiainen, T. Kotiaho. Analysis of Selective Androgen Receptor Modulators by Gas Chromatography-Microchip Atmospheric Pressure Photoionization-Mass Spectrometry. *J. Am. Soc. Mass Spectrom.*, **2010**, *21*, 310–316.

[172] A. Knoop, O. Krug, M. Vincenti, W. Schänzer, M. Thevis. In vitro metabolism studies on the selective androgen receptor modulator LG121071 and its implementation into human doping controls using liquid chromatography-mass spectrometry. *Eur. J. Mass Spectrom.*, **2015**, *21*, 27–36.

[173] M. Thevis, S. Beuck, A. Thomas, B. Kortner, M. Kohler, G. Rodchenkov, W. Schänzer. Doping control analysis of emerging drugs in human plasma – identification of GW501516, S-107, JTV-519, and S-40503. *Rapid Commun. Mass Spectrom.*, **2009**, *23*, 1139–1146.

[174] M. Polet, W. Van Gansbeke, P. Van Eenoo. Development and validation of an open screening method for doping substances in urine by gas chromatography quadrupole time-of-flight mass spectrometry. *Anal. Chim. Acta*, **2018**, *1042*, 52–59.

[175] M. Thevis, A. Thomas, I. Möller, H. Geyer, J. T. Dalton, W. Schänzer. Mass spectrometric characterization of urinary metabolites of the selective androgen receptor modulator S-22 to identify potential targets for routine doping controls. *Rapid Commun. Mass Spectrom.*, **2011**, *25*, 2187–2195.

[176] T. Sobolevsky, M. Dikunets, G. Sukhanova, Irina Rodchenkov. Applicability of routine analytical procedures to detect andarine and ostarine. A comparative study, in *Recent Adv. Doping Anal. Proc. Manfred Donike Work. 30th Col. Work. Dope Anal.*, (Eds: W. Schänzer, M. Thevis, H. Geyer, U. Mareck), **2012**, pp. 116–120.

[177] M. Thevis, E. Gerace, A. Thomas, S. Beuck, H. Geyer, N. Schlörer, J. D. Kearbey, J. T. Dalton, W. Schänzer. Characterization of in vitro generated metabolites of the selective androgen receptor modulators S-22 and S-23 and in vivo comparison to post-administration canine urine specimens. *Drug Test. Anal.*, **2010**, *2*, 589–598.

[178] T. Sobolevsky, M. Dikunets, G. Dudko, G. Rodchenkov. Metabolism study of the selective androgen receptor modulator LGD-4033, in *Recent Adv. Doping Anal. Proc. Manfred Donike Work. 33rd Col. Work. Dope Anal.*, (Eds: W. Schänzer, M. Thevis, H. Geyer, U. Mareck), **2015**, pp. 75–79.

[179] A. G. Fragkaki, P. Sakellariou, P. Kiousi, N. Kioukia-Fougia, M. Tsivou, M. Petrou, Y. Angelis. Human in vivo metabolism study of LGD-4033. *Drug Test. Anal.*, **2018**, *10*, 1635–1645.

[180] A. Hansson, H. Knych, S. Stanley, E. Berndtson, L. Jackson, U. Bondesson, M. Thevis, M. Hedeland. Equine in vivo-derived metabolites of the SARM LGD-4033 and comparison with human and fungal metabolites. *J. Chromatogr. B*, **2018**, *1074*, 91–98.

[181] T. Sobolevsky, M. Dikunets, G. Rodchenkov. In vitro and in vivo metabolism of RAD140, a novel non-steroidal SARM, in *Recent Adv. Doping Anal. Proc. Manfred Donike Work. 31th Col. Work. Dope Anal.*, (Eds: W. Schänzer, M. Thevis, H. Geyer, U. Mareck), **2013**, pp. 121–124.

[182] M. Thevis, A. Thomas, T. Piper, O. Krug, P. Delahaut, W. Schänzer. Liquid chromatography-high resolution/high accuracy (tandem) mass spectrometry-based identification of in vivo generated metabolites of the selective androgen receptor modulator ACP-105 for doping control purposes. *Eur. J. Mass Spectrom.*, **2014**, *20*, 73–83.

[183] P. Kintz, A. Ameline, L. Gheddar, J.-S. Raul. LGD-4033, S-4 and MK-2866–Testing for SARMs in hair: About 2 doping cases. *Toxicol. Anal. Clin.*, **2019**, *31*, 56–63.

[184] T. Kuuranne, A. Leinonen, W. Schänzer, M. Kamber, R. Kostiainen, M. Thevis. Aryl-priopionamide-derived selective androgen receptor modulators: liquid chromatography-tandem mass spectrometry characterization of the in vitro synthesized metabolites for doping. *Drug Metab. Dispos.*, **2008**, *36*, 571–581.

[185] O. Krug, A. Thomas, S. Beuck, I. Schenk, M. Machnik, W. Schänzer, U. Bondesson, M. Hedeland, M. Thevis. Characterization of In Vitro Synthesized Equine Metabolites of the Selective Androgen Receptor Modulators S24 and S4. *J. Equine Vet. Sci.*, **2012**, *32*, 562–568.

[186] A. Lagojda, D. Kuehne, O. Krug, A. Thomas, T. Wigger, U. Karst, W. Schänzer, M. Thevis. Identification of selected in vitro-generated phase-I metabolites of the steroidal selective androgen receptor modulator MK-0773 for doping control purposes. *Eur. J. Mass Spectrom.*, **2016**, *22*, 49–59.

[187] P. R. Ortiz de Montellano. Cytochrome P450-activated prodrugs. *Future Med. Chem.*, **2013**, *5*, 213–228.

[188] P. F. Guengerich, D. C. Liebler, D. L. Reed. Enzymatic activation of chemicals to toxic metabolites. *CRC Crit. Rev. Toxicol.*, **1985**, *14*, 259–307.

[189] C. Klaassen. *Casarett & Doull's Toxicology: The Basic Science of Poisons*, McGraw-Hill Professional, **2013**.

[190] G. G. Gibson, P. Skett. *Introduction to Drug Metabolism*, Nelson Thornes Publishers, **2001**.

[191] M. Hacker, W. S. Messer, K. A. Bachmann. *Pharmacology: Principles and Practice*, Academic Press, **2009**.

[192] F. P. Guengerich. Common and Uncommon Cytochrome P450 Reactions Related to Metabolism and Chemical Toxicity. *Chem. Res. Toxicol.*, **2001**, *14*, 611–650.

[193] D. F. V. Lewis. Chapter 3: The P450 catalytic cycle, in *Guid. to Cytochromes P450 Struct. Funct.*, CRC Press, **2001**.

[194] A. I. Cederbaum. Redox Biology Molecular mechanisms of the microsomal mixed function oxidases and biological and pathological implications. *Redox Biol.*, **2015**, *4*, 60–73.

[195] D. F. V Lewis, P. Hlavica. Interactions between redox partners in various cytochrome P450 systems : functional and structural aspects. *Biochim. Biophys. Acta (BBA)-Bioenergetics*, **2000**, *1460*, 353–374.

[196] D. F. V Lewis. *Cytochromes P450: Structure, Function and Mechanism.*, Taylor & Francis Ltd, **1996**.

[197] F. Elahian, Z. Sepehrizadeh, B. Moghimi, S. A. Mirzaei. Human cytochrome b5 reductase: structure, function, and potential applications. *Crit. Rev. Biotechnol.*, **2014**, *34*, 134–143.

[198] D. S. Riddick, X. Ding, C. R. Wolf, T. D. Porter, A. V Pandey, Q. Zhang, J. Gu, R. D. Finn, S. Ronseaux, L. A. McLaughlin, C. J. Henderson, L. Zou, C. E. Flück. NADPH − Cytochrome P450 Oxidoreductase : Roles in Physiology, Pharmacology, and Toxicology. *Drug Metab. Dispos.*, **2013**, *41*, 12–23.

[199] M. J. Coon, W. C. Rose. Enzyme Ingenuity in Biological Oxidations : a Trail Leading to Cytochrome P450. *J. Biol. Chem.*, **2005**, *277*, 28351–28363.

[200] T. D. Porter. The roles of cytochrome b5 in cytochrome P450 reactions. *J. Biochem. Mol. Toxicol.*, **2002**, *16*, 311–316.

[201] U. H. N. Dürr, L. Waskell, A. Ramamoorthy. The cytochromes P450 and b5 and their reductases-Promising targets for structural studies by advanced solid-state NMR spectroscopy. *Biochim. Biophys. Acta - Biomembr.*, **2007**, *1768*, 3235–3259.

[202] L. A. McLaughlin, S. Ronseaux, R. D. Finn, C. J. Henderson, C. Roland Wolf. Deletion of microsomal cytochrome b5 profoundly affects hepatic and extrahepatic drug metabolism. *Mol. Pharmacol.*, **2010**, *78*, 269–278.

[203] T. Omura, R. Sato. The Carbon Monoxide-binding Pigmentof Liver Microsomes: II. Solubilization, purification, and properties. *J. Biol. Chem.*, **1964**, *239*, 2379–2385.

[204] L. Waskell, J.-J. P. Kim. Chapter 2: Electron Transfer Partners of Cytochrome P450, in *Cytochrome P450 Struct. Mech. Biochem.*, (Ed: P.R.O. de Montellano), Springer, **2015**, pp. 33–68.

[205] P. A. Hubbard, A. L. Shen, R. Paschke, C. B. Kasper, J. J. P. Kim. NADPH-cytochrome P450 oxidoreductase. Structural basis for hydride and electron transfer. *J. Biol. Chem.*, **2001**, *276*, 29163–29170.

[206] M. Seliskar, D. Rozman. Mammalian cytochromes P450 -importance of tissue specificity. *Biochim Biophys Acta*, **2007**, *1770*, 458–466.

[207] F. P. Guengerich, M. V Martin, C. D. Sohl, Q. Cheng. Measurement of cytochrome P450 and NADPH-cytochrome P450 reductase. *Nat. Protoc.*, **2009**, *4*, 1245–1251.

[208] D. E. R. Hoeven, A. Arbor. Preparation and Properties of Partially Purified Cytochrome P-450 and Reduced Nicotinamide Adenine Dinucleotide P-450 Reductase from Rabbit Liver Microsomes. *J. Biol. Chem.*, **1974**, *249*, 6302–6311.

[209] M. J. Coon, D. A. Haugen, F. P. Guengerich, J. L. Vermilion, W. L. Dean. Liver microsomal membranes: reconstitution of the hydroxylation system containing cytochrome P-450, in *Struct. Basis Membr. Funct.*, (Eds: H. Youssef, L. Djavadi-Ohaniance), Academic Press, New York, **1976**, pp. 409–427.

[210] D. Garfinkel. Studies on pig liver microsomes I. Enzymic and pigment composition of different microsomal fractions 1. *Arch. Biochem. Biophys.*, **1958**, *77*, 493–509.

[211] M. Klingenberg. Pigments of rat liver microsomes 1. *Arch. Biochem. Biophys.*, **1958**, *75*, 376–386.

[212] R. W. Estabrook, J. Werringloer. The measurements of difference spectra: application to the cytochromes of microsomes, in *Methods Enzymol. Vol. 52; Biomembr. Part C.*, (Eds: S. Fleischer, L. Packer), Academic Press, New York, USA, **1978**, pp. 212–220.

[213] T. Matsubara, R. A. Prough, M. D. Burke, R. W. Estabrook. The Preparation of Microsomal Fractions of Rodent Respiratory Tract and Their Characterization. *Cancer Res.*, **1974**, *34*, 2196–2203.

[214] T. Matsubara, M. Koike, A. Touchi, Y. Tochino, K. Sugeno. Quantitative determination of cytochrome P-450 in rat liver homogenate. *Anal. Biochem.*, **1976**, *75*, 596–603.

[215] B. Schoene, R. A. Fleischmann, H. Remmer. Determination of Drug Metabolizing Enzymes in Needle Biopsies of Human Liver. *Eur. J. Clin. Pharmacol.*, **1972**, *4*, 65–73.

[216] D. R. Nelson. Cytochrome P450 nomenclature 2004. *Methods Mol. Biol.*, **2006**, *320*, 1–10.

[217] D. R. Nelson. The Cytochrome P450 Homepage. *Hum. Genomics*, **2009**, *4*, 59–65.

[218] M. F. Paine, H. L. Hart, S. S. Ludington, R. L. Haining, A. E. Rettie, D. C. Zeldin. The human intestinal cytochrome P450 "pie." *Drug Metab. Dispos.*, **2006**, *34*, 880–886.

[219] E. Tydén, H. Tjälve, P. Larsson. Gene and protein expression and cellular localisation of cytochrome P450 enzymes of the 1A, 2A, 2C, 2D and 2E subfamilies in equine intestine and liver. *Acta Vet. Scand.*, **2014**, *56*, 69.

[220] B. Achour, J. Barber, A. Rostami-hodjegan. Cytochrome P450 Pig Liver Pie : Determination of

Individual Cytochrome P450 Isoform Contents in Microsomes from Two Pig Livers Using Liquid Chromatography in Conjunction with Mass Spectrometry. *Drug Metab. Dispos.*, **2011**, *39*, 2130–2134.

[221] S. Michaels, M. Z. Wang. The Revised Human Liver Cytochrome P450 " Pie " : Absolute Protein Quantification of CYP4F and CYP3A Enzymes Using Targeted Quantitative Proteomics. *Drug Metab. Dispos.*, **2014**, *42*, 1241–1251.

[222] S. B. Yanni. Drug–Drug Interaction: From Bench to Drug Label, in *Transl. ADMET Drug Ther.*, John Wiley & Sons, Inc, **2015**, pp. 139–178.

[223] O. Pelkonen, M. Turpeinen, J. Hakkola, P. Honkakoski, J. Hukkanen, H. Raunio. Inhibition and induction of human cytochrome P450 enzymes: Current status. *Arch. Toxicol.*, **2008**, *82*, 667–715.

[224] C. Ioannides. Cytochrome P450 expression in the liver of food-producing animals. *Curr Drug Metab*, **2006**, *7*, 335–348.

[225] A. Parkinson, B. W. Ogilvie, B. L. Paris, T. ni N. Hensley, G. J. Loewen. Chapter 1.7: Drug metabolism from a chemical perspective, in *Biotransformation Metab. Elucidation Xenobiotics Charact. Identif.*, (Ed: Ala F. Nassar), John Wiley & Sons, **2010**.

[226] J. R. Cashman. Role of flavin-containing monooxgenase in drug development. *Expert Opin. Drug Metab. Toxicol.*, **2008**, *4*, 1507–1521.

[227] S. K. Krueger, D. E. Williams. Mammalian flavin-containing monooxygenases: Structure/function, genetic polymorphisms and role in drug metabolism. *Pharmacol. Ther.*, **2005**, *106*, 357–387.

[228] M. P. Lawton, J. R. Cashman, T. Cresteil, C. T. Dolphin, A. A. Elfarra, R. N. Hines, E. Hodgson, T. Kimura, J. Ozols, I. R. Phillips. A nomenclature for the mammalian flavin-containing monooxygenase gene family based on amino acid sequence identities. *Arch. Biochem. Biophys.*, **1994**, *308*, 254–257.

[229] J. Zhang, J. R. Cashman. Quantitative analysis of FMO gene mRNA levels in human tissues. *Drug Metab. Dispos.*, **2006**, *34*, 19–26.

[230] J. R. Cashman. Some distinctions between flavin-containing and cytochrome P450 monooxygenases. *Biochem. Biophys. Res. Commun.*, **2005**, *338*, 599–604.

[231] G. G. Gordon, P. Skett, Eds. . Pathways of drug metabolism, in *Introd. to Drug Metab.*, Blackie Academic & Professional, New York, **2001**, pp. 1–33.

[232] B. Wen, K. J. Coe, P. Rademacher, W. L. Fitch, M. Monshouwer, S. D. Nelson. Comparison of in vitro bioactivation of flutamide and its cyano analogue: Evidence for reductive activation by human NADPH:cytochrome P450 reductase. *Chem. Res. Toxicol.*, **2008**, *21*, 2393–2406.

[233] T. Fukami, T. Yokoi. The emerging role of human esterases. *Drug Metab. Pharmacokinet.*, **2012**, *27*, 466–477.

[234] G. G. Gordon, P. Skett, Eds. . Pathways of drug metabolism, in *Introd. to Drug Metab.*, Nelson Thornes Publishers, **2001**, pp. 1–33.

[235] T. Satoh, M. Hosokawa. The mammalian carboxylesterases: from molecules to functions. *Annu. Rev. Pharmacol. Toxicol.*, **1998**, *38*, 257–288.

[236] P. I. Mackenzie, K. W. Bock, B. Burchell, C. Guillemette, S. Ikushiro, T. Iyanagi, J. O. Miners, I. S. Owens, D. W. Nebert. Nomenclature update for the mammalian UDP glycosyltransferase (UGT) gene superfamily. *Pharmacogenet. Genomics*, **2005**, *15*, 677–685.

[237] M. B. Fisher, M. F. Paine, T. J. Strelevitz, S. A. Wrighton. The role of hepatic and extrahepatic UDP-glucuronosyltransferases in human drug metabolism. *Drug Metab. Rev.*, **2001**, *33*, 273–297.

[238] D. J. Clarke, B. Burchell. Chapter 1: The uridine diphosphate glucuronosyltransferase multigene family: function and regulation, in *Conjug. React. Drug Metab. Toxic.*, (Ed: F.C. Kauffman), Springer Berlin Heidelberg, **1994**, pp. 3–43.

[239] R. Meech, P. I. Mackenzie. Structure and function of uridine diphosphate glucuronnosyltransferases. *Clin. Exp. Pharmacol. Physiol.*, **1997**, *24*, 907–915.

[240] K. He, S. J. Ludtke, W. T. Heller, H. W. Huang. Mechanism of alamethicin insertion into lipid bilayers. *Biophys. J.*, **1996**, *71*, 2669–2679.

[241] J. M. Little, P. A. Lehman, S. Nowell, V. Samokyszyn, A. Radominska. Glucuronidation of all-trans-retinoic acid and 5, 6-epoxy-all-trans-retinoic acid: activation of rat liver microsomal UDP-glucuronosyltransferase activity by alamethicin. *Drug Metab. Dispos.*, **1997**, *25*, 5–11.

[242] L. Oleson, M. H. Court. Effect of the β-glucuronidase inhibitor saccharolactone on glucuronidation by human tissue microsomes and recombinant UDP-glucuronosyltransferases. *J. Pharm. Pharmacol.*, **2008**, *60*, 1175–1182.

[243] M. Y. Malik, S. Jaiswal, A. Sharma, M. Shukla, J. Lal. Role of enterohepatic recirculation in drug disposition: cooperation and complications. *Drug Metab. Rev.*, **2016**, *48*, 281–327.

[244] L. Oleson, M. H. Court. Effect of the β-glucuronidase inhibitor saccharolactone on glucuronidation by human tissue microsomes and recombinant UDP-glucuronosyltransferases. *J. Pharm. Pharmacol.*, **2008**, *60*, 1175–1182.

[245] G. A. A. Levvy. The Preparation and Properties of ß-Glucuronidase. 4. Inhibition by sugar acids and

their lactones. *J. Biol. Chem.*, **1952**, *52*, 464–472.

[246]   Z. Riches, E. L. Stanley, J. C. Bloomer, M. W. H. Coughtrie. Quantitative Evaluation of the Expression and Activity of Five Major Sulfotransferases (SULTs) in Human Tissues : The SULT "Pie." *Drug Metab. Dispos.*, **2009**, *37*, 2255–2261.

[247]   Y. Alnouti, C. D. Klaassen. Tissue Distribution and Ontogeny of Sulfotransferase Enzymes in Mice. *Toxicol. Sci.*, **2006**, *93*, 242–255.

[248]   R. L. Blanchard, R. R. Freimuth, J. Buck, R. M. Weinshilboum, M. W. Coughtrie. A proposed nomenclature system for the cytosolic sulfotransferase (SULT) superfamily. *Pharmacogenet. Genomics*, **2004**, *14*, 199–211.

[249]   M. W. H. Coughtrie. Sulfotransferases, in *Metab. Drugs Other Xenobiotics*, (Eds: P. Anzenbacher, U.M. Zanger), **2012**, pp. 117–145.

[250]   C. D. Klaassen, W. Boles. The importance phosphosulfate (PAPS) in the regulation of sulfation. *FASEB J.*, **1997**, *11*, 404–418.

[251]   M. Davis, C. J. Simmons, N. G. Harrison. Paracetamol Overdose in Man : Relationship between Pattern of Urinary Metabolites and Severity of liver Damage. *QJM An Int. J. Med.*, **1976**, *45*, 181–191.

[252]   M. O. James. Enzyme kinetics of conjugating enzymes: PAPS sulfotransferase., in *Methods Mol. Biol.*, (Eds: S. Nagar, U.A. Argikar, D.J. Tweedie), Humana Press, **2014**, pp. 187–201.

[253]   A. Parkinson, B. W. Ogilvie. Biotransformation of Xenobiotics, in *Casarett Doull's Toxicol. Basic Sci. Poisons*, (Ed: C. Klaassen), **2013**.

[254]   D. J. Hearse, W. W. Weber. Multiple N-Acetyltransferases and Drug Metabolism. *Biochem. J.*, **1973**, *132*, 519–526.

[255]   K. F. Windmill, A. Gaedigk, P. D. M. Hall, H. Samaratunga, D. M. Grant, M. E. Mcmanus. Localization of N -acetyltransferases NAT1 and NAT2 in human tissues. *Toxicol. Sci.*, **2000**, *54*, 19–29.

[256]   K. P. Vatsis, W. W. Weber, D. A. Bell, J.-M. Dupret, D. A. P. Evans, D. M. Grant, D. W. Hein, H. J. Lin, U. A. Meyer, M. V Relling. Nomenclature for N-acetyltransferases. *Pharmacogenet. Genomics*, **1995**, *5*, 1–17.

[257]   D. W. Hein, D. M. Grant, E. Sim. Update on consensus arylamine N-acetyltransferase gene nomenclature. *Pharmacogenet. Genomics*, **2000**, *10*, 291–292.

[258]   D. W. Hein, S. Boukouvala, D. M. Grant, R. F. Minchin, E. Sim. Changes in consensus arylamine N-acetyltransferase gene nomenclature. *Pharmacogenet. Genomics*, **2008**, *18*, 367–368.

[259]   S. Boukouvala. "The Database of Arylamine N-Acetyltransferases (NATs)," Available at: http://nat.mbg.duth.gr/background_2013.html, Last accessed: 16/02/2020

[260]   E. Sim, N. Lack, C. J. Wang, H. Long, I. Westwood, E. Fullam, A. Kawamura. Arylamine N-acetyltransferases: Structural and functional implications of polymorphisms. *Toxicology*, **2008**, *254*, 170–183.

[261]   S. Rendic, F. P. Guengerich. Update information on drug metabolism systems—2009, part II. Summary of information on the effects of diseases and environmental factors on human cytochrome P450 (CYP) enzymes and transporters. *Curr. Drug Metab.*, **2010**, *11*, 4–84.

[262]   M. Giantin, M. Carletti, F. Capolongo, S. Pegolo, R. M. Lopparelli, F. Gusson, C. Nebbia, M. Cantiello, P. Martin, T. Pineau, M. Dacasto. Effect of Breed upon Cytochromes P450 and Phase II Enzyme Expression in Cattle Liver. *Drug Metab. Dispos.*, **2008**, *36*, 885–893.

[263]   M. Dacasto, C. Eeckhoutte, F. Capolongoa, J. Dupuy, M. Carletti, C. Calleja, C. Nebbia, M. Alvinerie, P. Caltier. Effect of breed and gender on bovine liver cytochrome comparison with other domestic ruminants. *Vet. Res.*, **2005**, *36*, 179–190.

[264]   C. Nebbia, M. Dacasto, M. Carletti. Postnatal development of hepatic oxidative, hydrolytic and conjugative drug-metabolizing enzymes in female horses. *Life Sci.*, **2004**, *74*, 1605–1619.

[265]   P.-L. Toutain, A. Ferran, A. Bousquet-Mélou. Species differences in pharmacokinetics and pharmacodynamics. *Handb. Exp. Pharmacol.*, **2010**, 19–48.

[266]   P. C. Hirom, J. R. Idle, P. Millburn. Drug metabolism - from microbe to man: a symposium in honour of Richard Tecwyn Williams, (Eds: D. V. Parke, R.L. Smith), Taylor And Francis, **1977**, pp. 299–329.

[267]   Y. Kwon, Ed. . Chapter 8: Metabolism, in *Handb. Essent. Pharmacokinet. Pharmacodyn. Drug Metab. Ind. Sci.*, Springer US, **2002**, pp. 121–168.

[268]   J. Caldwell. Comparative Aspects of Detoxification in Mammals, in *Biochem. Pharmacol. Toxicol. A Ser. Monogr. Enzym. Basis Detoxif. Voluume I*, (Ed: W.B. Jakoby), Academic Press, **1980**, p. 85.

[269]   F. P. Guengerich. Comparisons of catalytic selectivity of cytochrome P450 subfamily enzymes from different species. **1997**, *106*, 161–182.

[270]   F. Gusson, M. Carletti, A. Giuliano Albo, M. Dacasto, C. Nebbia. Comparison of hydrolytic and conjugative biotransformation pathways in horse, cattle, pig, broiler chick, rabbit and rat liver subcellullar fractions. *Vet. Res. Commun.*, **2006**, *30*, 271–283.

[271] C. Nebbia, M. Dacasto, a. Rossetto Giaccherino, a. Giuliano Albo, M. Carletti. Comparative expression of liver cytochrome P450-dependent monooxygenases in the horse and in other agricultural and laboratory species. *Vet. J.*, **2003**, *165*, 53–64.

[272] J. Fink-Gremmels. Implications of hepatic cytochrome P450-related biotransformation processes in veterinary sciences. *Eur. J. Pharmacol.*, **2008**, *585*, 502–509.

[273] B. Szotáková, V. Baliharová, J. Lamka, E. Nožinová, V. Wsól, J. Velí, M. Machala, J. Neča, P. Souček, S. Šusová. Comparison of in vitro activities of biotransformation enzymes in pig, cattle, goat and sheep. *Res. Vet. Sci.*, **2004**, *76*, 43–51.

[274] M. R. Juchau. Species and Organ Differences in the Biotransformation of Chemical Carcinogens, in *Organ Species Specif. Chem. Carcinog.*, (Eds: R. Langenbach, S. Nesnow, J.M. Rice), Springer US, Boston, MA, **1983**, pp. 273–281.

[275] L. G. Yengi, L. Leung, J. Kao. The evolving role of drug metabolism in drug discovery and development. *Pharm. Res.*, **2007**, *24*, 842.

[276] G. N. Kumar, S. Surapaneni. Role of drug metabolism in drug discovery and development. *Med. Res. Rev.*, **2001**, *21*, 397–411.

[277] D. K. Wissenbach, M. R. Meyer, D. Remane, A. A. Philipp, A. A. Weber, H. H. Maurer. Drugs of abuse screening in urine as part of a metabolite-based LC-MSn screening concept. *Anal. Bioanal. Chem.*, **2011**, *400*, 3481–3489.

[278] D. K. Wissenbach, M. R. Meyer, D. Remane, A. A. Weber, H. H. Maurer. Development of the first metabolite-based LC-MSn urine drug screening procedure-exemplified for antidepressants. *Anal. Bioanal. Chem.*, **2011**, *400*, 79–88.

[279] I. Ojanperä, M. Kolmonen, A. Pelander. Current use of high-resolution mass spectrometry in drug screening relevant to clinical and forensic toxicology and doping control. *Anal. Bioanal. Chem.*, **2012**, *403*, 1203–1220.

[280] A. A. M. Stolker, U. A. T. Brinkman. Analytical strategies for residue analysis of veterinary drugs and growth-promoting agents in food-producing animals—a review. *J. Chromatogr. A*, **2005**, *1067*, 15–53.

[281] J. D. MacNeil, J. F. Kay. Basic Considerations for the Analyst for Veterinary Drug Residue Analysis in Animal Tissues. *Chem. Anal. Non‑antimicrobial Vet. Drug Residues Food*, **2016**, 1–26.

[282] R. J. B. Peters, A. A. M. Stolker, J. G. J. Mol, A. Lommen, E. Lyris, Y. Angelis, A. Vonaparti, M. Stamou, C. Georgakopoulos, M. W. F. Nielen. Screening in veterinary drug analysis and sports doping control based on full-scan, accurate-mass spectrometry. *TrAC Trends Anal. Chem.*, **2010**, *29*, 1250–1268.

[283] K. Diehl, R. Hull, D. Morton, R. Pfister, Y. Rabemampianina, D. Smith, J. Vidal, C. Van De Vorstenbosch. A good practice guide to the administration of substances and removal of blood, including routes and volumes. *J. Appl. Toxicol.*, **2001**, *21*, 15–23.

[284] E. M. Isin, C. S. Elmore, G. N. Nilsson, R. A. Thompson, L. Weidolf. Use of radiolabeled compounds in drug metabolism and pharmacokinetic studies. *Chem. Res. Toxicol.*, **2012**, *25*, 532–542.

[285] N. Penner, L. J. Klunk, C. Prakash. Human radiolabeled mass balance studies: objectives, utilities and limitations. *Biopharm. Drug Dispos.*, **2009**, *30*, 185–203.

[286] P. Anielski. Hair analysis of anabolic steroids in connection with doping control—results from horse samples. *J. Mass Spectrom.*, **2008**, *43*, 1001–1008.

[287] K. Zhang, X. Liang, C. Su, C. Tang, Q. Zhao, J. Zhang, Q. Meng. Salbutamol residues in plasma, urine and hair of heifers after a single dose and throughout. *J. Anal. Toxicol.*, **2016**, *40*, 454–459.

[288] H. A. Kuiper, M. Y. Noordam, M. M. van Dooren-Flipsen, R. Schilt, A. H. Roos. Illegal use of beta-adrenergic agonists: European Community. *J. Anim. Sci.*, **1998**, *76*, 195–207.

[289] H. H. Maurer, K. Pfleger, A. A. Weber. *Mass Spectral and GC Data of Drugs, Poisons, Pesticides, Pollutants, and Their Metabolites*, John Wiley & Sons, **2016**.

[290] R. L. Gomes, W. Meredith, C. E. Snape, M. a. Sephton. Analysis of conjugated steroid androgens: Deconjugation, derivatisation and associated issues. *J. Pharm. Biomed. Anal.*, **2009**, *49*, 1133–1140.

[291] P. B. Grace, E. C. Drake, P. Teale, E. Houghton. Quantification of 19‑nortestosterone sulphate and boldenone sulphate in urine from male horses using liquid chromatography/tandem mass spectrometry. *Rapid Commun. Mass Spectrom.*, **2008**, *22*, 2999–3007.

[292] E. Houghton, L. Grainger, M. C. Dumasia, P. Teale. Application of gas chromatography/mass spectrometry to steroid analysis in equine sports: problems with enzyme hydrolysis. *J. Mass Spectrom.*, **1992**, *27*, 1061–1070.

[293] A. E. Schwaninger, M. R. Meyer, H. H. Maurer. Gas Chromatography-Mass Spectrometry Detection of a Norfluoxetine Artifact in Hydrolyzed Urine Samples May Falsely Indicate Tranylcypromine Ingestion. *J. Anal. Toxicol.*, **2010**, *34*, 45–48.

[294] J. P. Scarth, H. a. Spencer, S. C. Hudson, P. Teale, B. P. Gray, L. L. Hillyer. The application of in vitro

technologies to study the metabolism of the androgenic/anabolic steroid stanozolol in the equine. *Steroids*, **2010**, *75*, 57–69.

[295]   A. Clarke, J. Scarth, P. Teale, C. Pearce, L. Hillyer. The use of in vitro technologies and high-resolution/accurate-mass LC-MS to screen for metabolites of "designer" steroids in the equine. *Drug Test. Anal.*, **2011**, *3*, 74–87.

[296]   C. Gómez, O. J. Pozo, L. Garrostas, J. Segura, R. Ventura. A new sulphate metabolite as a long-term marker of metandienone misuse. *Steroids*, **2013**, *78*, 1245–1253.

[297]   M. T. Donato, A. Lahoz, J. V Castell, M. J. Gomez-Lechon. Cell lines: a tool for in vitro drug metabolism studies. *Curr. Drug Metab.*, **2008**, *9*, 1–11.

[298]   J. Zhang, J. Lu, Y. Wu, X. Wang, Y. Xu, Y. Zhang, Y. Wang. New Potential Biomarker for Methasterone Misuse in Human Urine by Liquid Chromatography Quadrupole Time of Flight Mass Spectrometry. *Int. J. Mol. Sci.*, **2016**, *17*, 1628.

[299]   P. Meuleman, L. Libbrecht, R. De Vos, B. de Hemptinne, K. Gevaert, J. Vandekerckhove, T. Roskams, G. Leroux-Roels. Morphological and biochemical characterization of a human liver in a uPA-SCID mouse chimera. *Hepatology*, **2005**, *41*, 847–856.

[300]   O. J. Pozo, L. Lootens, P. Van Eenoo, K. Deventer, P. Meuleman, G. Leroux-Roels, M. K. Parr, W. Schänzer, F. T. Delbeke. Combination of liquid-chromatography tandem mass spectrometry in different scan modes with human and chimeric mouse urine for the study of steroid metabolism. *Drug Test. Anal.*, **2009**, *1*, 554–567.

[301]   L. Lootens, P. Meuleman, G. Leroux-Roels, P. Van Eenoo. Metabolic studies with promagnon, methylclostebol and methasterone in the uPA+/+-SCID chimeric mice. *J. Steroid Biochem. Mol. Biol.*, **2011**, *127*, 374–381.

[302]   L. Geldof, L. Lootens, M. Polet, D. Eichner, T. Campbell, V. Nair, F. Botrè, P. Meuleman, G. Leroux-Roels, K. Deventer. Metabolism of methylstenbolone studied with human liver microsomes and the uPA+/+-SCID chimeric mouse model. *Biomed. Chromatogr.*, **2014**, *28*, 974–985.

[303]   L. Lootens, P. Van Eenoo, P. Meuleman, O. J. Pozo, P. Van Renterghem, G. Leroux-Roels, F. T. Delbeke. Steroid metabolism in chimeric mice with humanized liver. *Drug Test. Anal.*, **2009**, *1*, 531–537.

[304]   L. Lootens, P. Meuleman, O. J. Pozo, P. Van Eenoo, G. Leroux-Roels, F. T. Delbeke. uPA+/+-SCID mouse with humanized liver as a model for in vivo metabolism of exogenous steroids: methandienone as a case study. *Clin. Chem.*, **2009**, *55*, 1783–1793.

[305]   L. Lootens, P. Van Eenoo, P. Meuleman, G. Leroux-roels, F. T. Delbeke. The uPA +/+-SCID Mouse with Humanized Liver as a Model for in Vivo Metabolism of 4-Androstene-3 , 17-dione. *Drug Metab. Dispos.*, **2009**, *37*, 2367–2374.

[306]   C. Hollands. The Animals (Scientific Procedures) Act 1986. *Lancet*, **1986**, *328*, 32–33.

[307]   U.S. FDA. Guidance for industry: Drug metabolism/drug interaction studies in the drug development process: Studies in vitro. **1997**.

[308]   L. Di, C. Keefer, D. O. Scott, T. J. Strelevitz, G. Chang, Y. Bi, Y. Lai, J. Duckworth, K. Fenner, M. D. Troutman, R. S. Obach. Mechanistic insights from comparing intrinsic clearance values between human liver microsomes and hepatocytes to guide drug design. *Eur. J. Med. Chem.*, **2012**, *57*, 441–448.

[309]   H. M. Mehendale. Application of isolated organ perfusion techniques in toxicology, in *Princ. Methods Toxicol.*, (Ed: A.W. Hayes), Raven Press, New York, **2007**, pp. 1157–1200.

[310]   A. Maier-Salamon, G. Trauner, R. Hiltscher, G. Reznicek, B. Kopp, T. Thalhammer, W. Jäger. Hepatic metabolism and biliary excretion of valerenic acid in isolated perfused rat livers: role of Mrp2 (Abcc2). *J. Pharm. Sci.*, **2009**, *98*, 3839–3849.

[311]   A. Maier-Salamon, B. Hagenauer, G. Reznicek, T. Szekeres, T. Thalhammer, W. Jäger. Metabolism and disposition of resveratrol in the isolated perfused rat liver: role of Mrp2 in the biliary excretion of glucuronides. *J. Pharm. Sci.*, **2008**, *97*, 1615–1628.

[312]   R. L. Fisher, A. E. M. Vickers. Preparation and culture of precision-cut organ slices from human and animal. *Xenobiotica*, **2013**, *43*, 8–14.

[313]   I. a M. de Graaf, P. Olinga, M. H. de Jager, M. T. Merema, R. de Kanter, E. G. van de Kerkhof, G. M. M. Groothuis. Preparation and incubation of precision-cut liver and intestinal slices for application in drug metabolism and toxicity studies. *Nat. Protoc.*, **2010**, *5*, 1540–1551.

[314]   R. De Kanter, M. H. De Jager, A. L. Draaisma, J. U. Jurva, P. Olinga, D. K. F. Meijer, G. M. M. Groothuis. Drug-metabolizing activity of human and rat liver, lung, kidney and intestine slices. *Xenobiotica*, **2002**, *32*, 349–362.

[315]   R. L. Fisher, A. J. Gandolfi, K. Brendel. Human liver quality is a dominant factor in the outcome of in vitro studies. *Cell Biol. Toxicol.*, **2001**, *17*, 179–189.

[316]   I. A. M. De Graaf, D. Van Der Voort, J. Brits, H. J. Koster. Increased post-thaw viability and phase I

and II biotransformation activity in cryopreserved rat liver slices after improvement of a fast-freezing method. *Drug Metab. Dispos.*, **2000**, *28*, 1100–1106.

[317] P. M. van Midwoud, G. M. M. Groothuis, M. T. Merema, E. Verpoorte. Microfluidic biochip for the perifusion of precision-cut rat liver slices for metabolism and toxicology studies. *Biotechnol. Bioeng.*, **2010**, *105*, 184–194.

[318] I. A. M. De Graaf, C. E. Van Meijeren, F. Pektaş, H. J. Koster. Comparison of in vitro preparations for semi-quantitative prediction of in vivo drug metabolism. *Drug Metab. Dispos.*, **2002**, *30*, 1129–1136.

[319] M. Martignoni, G. Groothuis, R. de Kanter. Comparison of mouse and rat cytochrome P450-mediated metabolism in liver and intestine. *Drug Metab. Dispos.*, **2006**, *34*, 1047–1054.

[320] G. MM Groothuis, I. AM de Graaf. Precision-cut intestinal slices as in vitro tool for studies on drug metabolism. *Curr. Drug Metab.*, **2013**, *14*, 112–119.

[321] I. A. M. de Graaf, R. de Kanter, M. H. de Jager, R. Camacho, E. Langenkamp, E. G. van de Kerkhof, G. M. M. Groothuis. Empirical validation of a rat in vitro organ slice model as a tool for in vivo clearance prediction. *Drug Metab. Dispos.*, **2006**, *34*, 591–599.

[322] S. Wang, J. C. W. Rijk, J. H. Riethoff-Poortman, S. Van Kuijk, A. Peijnenburg, T. F. H. Bovee. Bovine liver slices combined with an androgen transcriptional activation assay: an in-vitro model to study the metabolism and bioactivity of steroids. *Anal. Bioanal. Chem.*, **2010**, *397*, 631–641.

[323] J. C. W. Rijk, T. F. H. Bovee, A. A. C. M. Peijnenburg, M. J. Groot, I. M. C. M. Rietjens, M. W. F. Nielen. Bovine liver slices: A multifunctional in vitro model to study the prohormone dehydroepiandrosterone (DHEA). *Toxicol. Vitr.*, **2012**, *26*, 1014–1021.

[324] P. M. van Midwoud, M. T. Merema, E. Verpoorte, G. M. M. Groothuis. A microfluidic approach for in vitro assessment of interorgan interactions in drug metabolism using intestinal and liver slices. *Lab Chip*, **2010**, *10*, 2778–2786.

[325] A. Blouin, R. P. Bolender, E. R. Weibel. Distribution of organelles and membranes between hepatocytes and nonhepatocytes in the rat liver parenchyma. A stereological study. *J. Cell Biol.*, **1977**, *72*, 441–455.

[326] E. L. LeCluyse, E. Alexandre, G. A. Hamilton, C. Viollon-Abadie, D. J. Coon, S. Jolley, L. Richert. Isolation and culture of primary human hepatocytes. *Basic Cell Cult. Protoc.*, **2005**, 207–229.

[327] A. Bakala, W. Karlik, M. Wiechetek. Preparation of equine isolated hepatocytes. *Toxicol. Vitr.*, **2003**, *17*, 615–621.

[328] A. Stefanski, M. Mevissen, a. M. Möller, K. Kuehni-Boghenbor, A. Schmitz. Induction of cytochrome P450 enzymes in primary equine hepatocyte culture. *Toxicol. Vitr.*, **2013**, *27*, 2023–2030.

[329] Z.-G. Zhang, X.-B. Li, L. Gao, G.-W. Liu, T. Kong, Y.-F. Li, H.-B. Wang, C. Zhang, Z. Wang, R.-H. Zhang. An updated method for the isolation and culture of primary calf hepatocytes. *Vet. J.*, **2012**, *191*, 323–326.

[330] G. A. E. Van 't Klooster, F. M. A. Woutersen-van Nijnanten, W. R. Klein, B. J. Blaauboer, J. Noordhoek, A. Van Miert. Effects of various medium formulations and attachment substrata on the performance of cultured ruminant hepatocytes in biotransformation studies. *Xenobiotica*, **1992**, *22*, 523–534.

[331] M. E. M. Kuilman, R. F. M. Maas, D. J. Judah, J. Fink-Gremmels. Bovine hepatic metabolism of aflatoxin B1. *J. Agric. Food Chem.*, **1998**, *46*, 2707–2713.

[332] P. Papeleu, T. Vanhaecke, T. Henkens, G. Elaut, M. Vinken, S. Snykers, V. Rogiers. Isolation of rat hepatocytes. *Cytochrome P450 Protoc.*, **2006**, 229–237.

[333] D. Li, E. G. Schuetz, P. S. Guzelian. [32] Hepatocyte culture in study of P450 regulation. *Methods Enzymol.*, **1991**, *206*, 335–344.

[334] F.-Y. Meng, Z.-S. Chen, M. Han, X.-P. Hu, X.-X. He, Y. Liu, W.-T. He, W. Huang, H. Guo, P. Zhou. Porcine hepatocyte isolation and reversible immortalization mediated by retroviral transfer and site-specific recombination. *World J. Gastroenterol. WJG*, **2010**, *16*, 1660.

[335] G. Elaut, P. Papeleu, M. Vinken, T. Henkens, S. Snykers, T. Vanhaecke, V. Rogiers. Hepatocytes in suspension. *Cytochrome P450 Protoc.*, **2006**, 255–263.

[336] T. Vanhaecke, V. Rogiers. Hepatocyte cultures in drug metabolism and toxicological research and testing. *Cytochrome P450 Protoc.*, **2006**, 209–227.

[337] A. P. Li. Primary hepatocyte cultures as an in vitro experimental model for the evaluation of pharmacokinetic drug–drug interactions. *Adv. Pharmacol.*, **1997**, *43*, 103–130.

[338] A. K. Nussler, A. Wang, P. Neuhaus, J. Fischer, J. Yuan, L. Liu, K. Zeilinger, J. Gerlach, P. J. Arnold, W. Albrecht. The suitability of hepatocyte culture models to study various aspects of drug metabolism. *ALTEX*, **2001**, *18*, 91–101.

[339] K. H. Lin, H. Hino, S. Maeda, H. Inagaki, J. V. Airat, T. Saito. Albumin synthesis by rat hepatocytes cultured on collagen gels is sustained specifically by heparin. *Exp. Cell Res.*, **1995**, *219*, 717–721.

[340] S. R. Khetani, S. N. Bhatia. Microscale culture of human liver cells for drug development. *Nat.*

Biotechnol., **2008**, *26*, 120.

[341]   S. S. Bale, I. Golberg, R. Jindal, W. J. McCarty, M. Luitje, M. Hegde, A. Bhushan, O. B. Usta, M. L. Yarmush. Long-term coculture strategies for primary hepatocytes and liver sinusoidal endothelial cells. *Tissue Eng. Part C Methods*, **2014**, *21*, 413–422.

[342]   P. J. Lee, P. J. Hung, L. P. Lee. An artificial liver sinusoid with a microfluidic endothelial-like barrier for primary hepatocyte culture. *Biotechnol. Bioeng.*, **2007**, *97*, 1340–1346.

[343]   G. Ambrosino, S. M. M. Basso, S. Varotto, E. Zardi, A. Picardi, D. F. D'amico. Isolated hepatocytes versus hepatocyte spheroids: in vitro culture of rat hepatocytes. *Cell Transplant.*, **2005**, *14*, 397–401.

[344]   T. Ohkura, K. Ohta, T. Nagao, K. Kusumoto, A. Koeda, T. Ueda, T. Jomura, T. Ikeya, E. Ozeki, K. Wada. Evaluation of human hepatocytes cultured by three-dimensional spheroid systems for drug metabolism. *Drug Metab. Pharmacokinet.*, **2014**, *29*, 373–378.

[345]   C. Y. Li, K. R. Stevens, R. E. Schwartz, B. S. Alejandro, J. H. Huang, S. N. Bhatia. Micropatterned cell–cell interactions enable functional encapsulation of primary hepatocytes in hydrogel microtissues. *Tissue Eng. Part A*, **2014**, *20*, 2200–2212.

[346]   L. Guo, S. Dial, L. Shi, W. Branham, J. Liu, J.-L. Fang, B. Green, H. Deng, J. Kaput, B. Ning. Similarities and differences in the expression of drug metabolizing enzymes between human hepatic cell lines and primary human hepatocytes. *Drug Metab. Dispos.*, **2010**, *39*, 528–538.

[347]   C. Rodriguez-Antona, M. T. Donato, A. Boobis, R. J. Edwards, P. S. Watts, J. V. Castell, M.-J. Gómez-Lechón. Cytochrome P450 expression in human hepatocytes and hepatoma cell lines: molecular mechanisms that determine lower expression in cultured cells. *Xenobiotica*, **2002**, *32*, 505–520.

[348]   K. Köck, K. L. R. Brouwer. A perspective on efflux transport proteins in the liver. *Clin. Pharmacol. Ther.*, **2012**, *92*, 599–612.

[349]   K. Ito, J. B. Houston. Comparison of the use of liver models for predicting drug clearance using in vitro kinetic data from hepatic microsomes and isolated hepatocytes. *Pharm. Res.*, **2004**, *21*, 785–792.

[350]   X. Ponsoda, E. Pareja, M.-J. Gómez-Lechón, R. Fabra, E. Carrasco, R. Trullenque, J. V. Castell. Drug biotransformation by human hepatocytes. In vitro/in vivo metabolism by cells from the same donor. *J. Hepatol.*, **2001**, *34*, 19–25.

[351]   D. Dalvie, R. S. Obach, P. Kang, C. Prakash, C. Loi, A. Nedderman, L. Goulet, E. Smith, H. Bu, D. A. Smith, S. Hurst. Assessment of Three Human in Vitro Systems in the Generation of Major Human Excretory and Circulating Metabolites Assessment of Three Human in Vitro Systems in the Generation of Major Human Excretory and Circulating Metabolites. *Chem. Res. Toxicol.*, **2009**, *22*, 357–368.

[352]   A.-S. Clouet, B. Le Bizec, F. Boerlen, F. Monteau, F. André. Calf primary hepatocyte culture as a tool for anabolic steroid metabolism studies. *Analyst*, **1998**, *123*, 2489–2492.

[353]   D. Hooijerink, R. Schilt, R. Hoogenboom, M. Huveneers-Oorsprong. Identification of metabolites of the anabolic steroid methandienone formed by bovine hepatocytes in vitro. *Analyst*, **1998**, *123*, 2637–2641.

[354]   J.-F. Lévesque, E. Templeton, L. Trimble, C. Berthelette, N. Chauret. Discovery, biosynthesis, and structure elucidation of metabolites of a doping agent and a direct analogue, tetrahydrogestrinone and gestrinone, using human hepatocytes. *Anal. Chem.*, **2005**, *77*, 3164–3172.

[355]   J. Gauthier, D. Goudreault, D. Poirier, C. Ayotte. Identification of drostanolone and 17-methyldrostanolone metabolites produced by cryopreserved human hepatocytes. *Steroids*, **2009**, *74*, 306–314.

[356]   M. Giantin, G. Gallina, S. Pegolo, R. M. Lopparelli, C. Sandron, V. Zancanella, C. Nebbia, D. Favretto, F. Capolongo, C. Montesissa. Primary hepatocytes as an useful bioassay to characterize metabolism and bioactivity of illicit steroids in cattle. *Toxicol. Vitr.*, **2012**, *26*, 1224–1232.

[357]   J. Graham. Fractionation of subcellular organelles, in *Biol. Centrifugation*, Bios Scientific Publishers Limited, **2001**, pp. 103–139.

[358]   J. M. Graham. Homogenization of tissues and cells, in *Subcell. Fractionation A Pract. Approach*, (Ed: J.M. Graham), IRL Press, **1997**, pp. 1–29.

[359]   R. H. Hinton, B. M. Mullock. Isolation of subcellular fractions, in *Subcell. Fractionation A Pract. Approach*, (Ed: J.M. Graham), IRL Press, **1997**, pp. 31–69.

[360]   J. W. Depierre, G. Dallner. Structural aspects of the membrane of the endoplasmatic reticulum. *Biochim. Biophys. Acta*, **1975**, *415*, 411–472.

[361]   J. R. Tata. Preparation and properties of microsomal and submicrosomal fractions from animal cells, in *Subcell. Components Prep. Fractionation*, (Eds: G.D. Birnie, S.M. Fox), Plenum, New York, **1969**, pp. 83–107.

[362]   F. P. Guengerich. Analysis and characterization of enzymes and nucleic acids relevant to toxicology. *Hayes' Princ. Methods Toxicol.*, **2014**, *6*, 1905–1964.

[363]   D. Li, Y. Han, X. Meng, X. Sun, Q. Yu, Y. Li, L. Wan, Y. Huo, C. Guo. Effect of Regular Organic Solvents on Cytochrome P450 Mediated Metabolic Activities in Rat Liver Microsomes. *Drug Metab.*

Dispos., **2010**, *38*, 1922–1925.

[364] J. C. Kalvass, D. A. Tess, C. Giragossian, M. C. Linhares, T. S. Maurer. Influence of microsomal concentration on apparent intrinsic clearance: implications for scaling in vitro data. *Drug Metab. Dispos.*, **2001**, *29*, 1332–1336.

[365] H. M. Jones, J. B. Houston. Substrate depletion approach for determining in vitro metabolic clearance: time dependencies in hepatocyte and microsomal incubations. *Drug Metab. Dispos.*, **2004**, *32*, 973–982.

[366] J. P. Scarth, H. a. Spencer, S. E. Timbers, S. C. Hudson, L. L. Hillyer. The use of in vitro technologies coupled with high resolution accurate mass LC-MS for studying drug metabolism in equine drug surveillance. *Drug Test. Anal.*, **2010**, *2*, 1–10.

[367] P. Taylor, J. P. Scarth, L. L. Hillyer. Use of in vitro technologies to study phase II conjugation in equine sports drug surveillance. *Bioanalysis*, **2010**, *2*, 1971–1988.

[368] J. K. Y. Wong, G. H. M. Chan, D. K. K. Leung, F. P. W. Tang, T. S. M. Wan. Generation of phase II in vitro metabolites using homogenized horse liver. *Drug Test. Anal.*, **2015**, *8*, 241–247.

[369] J. K. Y. Wong, F. P. W. Tang, T. S. M. Wan. In vitro metabolic studies using homogenized horse liver in place of horse liver microsomes. *Drug Test. Anal.*, **2011**, *3*, 393–399.

[370] K. Y. Kwok, G. H. M. Chan, W. H. Kwok, J. K. Y. Wong, T. S. M. Wan. In vitro phase I metabolism of selective estrogen receptor modulators in horse using ultra-high performance liquid chromatography-high resolution mass spectrometry. *Drug Test. Anal.*, **2017**, *9*, 1349–1362.

[371] E. de Rijke, P. W. Zoontjes, D. Samson, S. Oostra, S. S. Sterk, L. A. van Ginkel. Investigation of the presence of prednisolone in bovine urine. *Food Addit. Contam. Part A*, **2014**, *31*, 605–613.

[372] J. C. W. Rijk, T. F. H. Bovee, M. J. Groot, a. a C. M. Peijnenburg, M. W. F. Nielen. Evidence of the indirect hormonal activity of prohormones using liver S9 metabolic bioactivation and an androgen bioassay. *Anal. Bioanal. Chem.*, **2008**, *392*, 417–425.

[373] R. Merlanti, G. Gallina, F. Capolongo, L. Contiero, G. Biancotto, M. Dacasto, C. Montesissa. An in vitro study on metabolism of 17β-boldenone and boldione using cattle liver and kidney subcellular fractions. *Anal. Chim. Acta*, **2007**, *586*, 177–183.

[374] M. Martignoni, G. M. M. Groothuis, R. de Kanter. Species differences between mouse, rat, dog, monkey and human CYP-mediated drug metabolism, inhibition and induction. *Expert Opin. Drug Metab. Toxicol.*, **2006**, *2*, 875–894.

[375] R. E. Pearce, C. J. McIntyre, A. Madan, U. Sanzgiri, A. J. Draper, P. L. Bullock, D. C. Cook, L. A. Burton, J. Latham, C. Nevins, A. Parkinson. Effects of freezing, thawing, and storing human liver microsomes on cytochrome P450 activity. *Arch. Biochem. Biophys.*, **1996**, *331*, 145–169.

[376] C. L. Crespi, V. P. Miller. The use of heterologously expressed drug metabolizing enzymes — state of the art and prospects for the future. *Pharmacol. Ther.*, **1999**, *84*, 121–131.

[377] C.-H. Yun, S.-K. Yim, D.-H. Kim, T. Ahn. Functional expression of human cytochrome P450 enzymes in Escherichia coli. *Curr. Drug Metab.*, **2006**, *7*, 411–429.

[378] H. K. DiMaio Knych, C. DeStefano Shields, A. R. Buckpitt, S. D. Stanley. Equine cytochrome P450 2C92: cDNA cloning, expression and initial characterization. *Arch. Biochem. Biophys.*, **2009**, *485*, 49–55.

[379] H. K. D. Knych, D. S. McKemie, S. D. Stanley. Molecular cloning, expression, and initial characterization of members of the CYP3A family in horses. *Drug Metab. Dispos.*, **2010**, *38*, 1820–1827.

[380] H. K. D. Knych, S. D. Stanley. Complementary DNA cloning, functional expression and characterization of a novel cytochrome P450, CYP2D50, from equine liver. *Biochem. Pharmacol.*, **2008**, *76*, 904–911.

[381] L. M. Peters, S. Demmel, G. Pusch, J. T. M. Buters, W. Thormann, J. Zielinski, T. Leeb, M. Mevissen, A. Schmitz. Equine cytochrome P450 2B6 -genomic identification, expression and functional characterization with ketamine. *Toxicol. Appl. Pharmacol.*, **2013**, *266*, 101–108.

[382] A. Schmitz, S. Demmel, L. M. Peters, T. Leeb, M. Mevissen, B. Haase. Comparative human–horse sequence analysis of the CYP3A subfamily gene cluster. *Anim. Genet.*, **2010**, *41*, 72–79.

[383] M. Natsuhori, M. van Raak, M. Ligtenberg, L. Kleij, D. ten Berge, W. M. Zweers-Zeilmaker, E. M. de Groene, A. S. van Miert, R. F. Witkamp, G. J. Horbach. Isolation of a bovine full length cytochrome P450 (CYP3A) cDNA sequence and its functional expression in V79 cells. *Environ. Toxicol. Pharmacol.*, **1997**, *3*, 17–24.

[384] M. Kojima, T. Morozumi. Cloning of six full-length cDNAs encoding pig cytochrome P450 enzymes and gene expression of these enzymes in the liver and kidney. *J. Heal. Sci.*, **2004**, *50*, 518–529.

[385] M. Thevis, W. Lohmann, Y. Schrader, M. Kohler, W. Bornatsch, U. Karst, W. Schänzer. Use of an electrochemically synthesised metabolite of a selective androgen receptor modulator for mass spectrometry-based sports drug testing. *Eur. J. Mass Spectrom.*, **2008**, *14*, 163–170.

[386] S. Jahn, S. Beuck, I. Möller, M. Thevis, U. Karst. Using electrochemistry for metabolite simulation and synthesis in preventive doping research: application to the Rycal S107 and the PPARδ-agonist GW1516. *Anal. Methods*, **2013**, *5*, 1214–1224.

[387] A. P. Bruins. An overview of electrochemistry combined with mass spectrometry. *TrAC Trends Anal. Chem.*, **2015**, *70*, 14–19.

[388] T. Gul, R. Bischoff, H. P. Permentier. Electrosynthesis methods and approaches for the preparative production of metabolites from parent drugs. *TrAC Trends Anal. Chem.*, **2015**, *70*, 58–66.

[389] E. A. Abourashed, A. M. Clark, C. D. Hufford. Microbial models of mammalian metabolism of xenobiotics: an updated review. *Curr. Med. Chem.*, **1999**, *6*, 359–374.

[390] D. Zhang, Y. Yang, J. E. A. Leakey, C. E. Cerniglia. Phase I and phase II enzymes produced by Cunninghamella elegans for the metabolism of xenobiotics. *FEMS Microbiol. Lett.*, **1996**, *138*, 221–226.

[391] S. Asha, M. Vidyavathi. Cunninghamella–a microbial model for drug metabolism studies–a review. *Biotechnol. Adv.*, **2009**, *27*, 16–29.

[392] A. Rydevik, M. Thevis, O. Krug, U. Bondesson, M. Hedeland. The fungus Cunninghamella elegans can produce human and equine metabolites of selective androgen receptor modulators (SARMs). *Xenobiotica*, **2013**, *43*, 409–420.

[393] A. Rydevik, U. Bondesson, M. Thevis, M. Hedeland. Mass spectrometric characterization of glucuronides formed by a new concept, combining Cunninghamella elegans with TEMPO. *J. Pharm. Biomed. Anal.*, **2013**, *84*, 278–284.

[394] A. Rydevik, U. Bondesson, M. Hedeland. Structural elucidation of phase I and II metabolites of bupivacaine in horse urine and fungi of the Cunninghamella species using liquid chromatography/multi-stage mass spectrometry. *Rapid Commun. Mass Spectrom.*, **2012**, *26*, 1338–1346.

[395] A. Tevell Åberg, C. Olsson, U. Bondesson, M. Hedeland. A mass spectrometric study on meloxicam metabolism in horses and the fungus Cunninghamella elegans, and the relevance of this microbial system as a model of drug metabolism in the horse. *J. Mass Spectrom.*, **2009**, *44*, 1026–1037.

[396] S. Guddat, G. Fußhöller, S. Beuck, A. Thomas, H. Geyer, A. Rydevik, U. Bondesson, M. Hedeland, A. Lagojda, W. Schänzer, M. Thevis. Synthesis, characterization, and detection of new oxandrolone metabolites as long-term markers in sports drug testing. *Anal. Bioanal. Chem.*, **2013**, *405*, 8285–8294.

[397] A. Rydevik, A. Lagojda, M. Thevis, U. Bondesson, M. Hedeland. Isolation and characterization of a β-glucuronide of hydroxylated SARM S1 produced using a combination of biotransformation and chemical oxidation. *J. Pharm. Biomed. Anal.*, **2014**, *98*, 36–39.

[398] J. Kirchmair, A. H. Göller, D. Lang, J. Kunze, B. Testa, I. D. Wilson, R. C. Glen, G. Schneider. Predicting drug metabolism: experiment and/or computation? *Nat. Rev. Drug Discov.*, **2015**, *14*, 387.

[399] E. Tyrkkö, A. Pelander, R. a. Ketola, I. Ojanperä. In silico and in vitro metabolism studies support identification of designer drugs in human urine by liquid chromatography/quadrupole-time-of-flight mass spectrometry. *Anal. Bioanal. Chem.*, **2013**, *405*, 6697–6709.

[400] H. T'jollyn, K. Boussery, R. J. Mortishire-Smith, K. Coe, B. De Boeck, J. F. Van Bocxlaer, G. Mannens. Evaluation of three state-of-the-art metabolite prediction software packages (Meteor, MetaSite, and StarDrop) through independent and synergistic use. *Drug Metab. Dispos.*, **2011**, *39*, 2066–2075.

[401] V. A. Narkar, M. Downes, T. Y. Ruth, E. Embler, Y.-X. Wang, E. Banayo, M. M. Mihaylova, M. C. Nelson, Y. Zou, H. Juguilon. AMPK and PPARδ agonists are exercise mimetics. *Cell*, **2008**, *134*, 405–415.

[402] Y.-X. Wang, C.-L. Zhang, T. Y. Ruth, H. K. Cho, M. C. Nelson, C. R. Bayuga-Ocampo, J. Ham, H. Kang, R. M. Evans. Regulation of muscle fiber type and running endurance by PPARδ. *PLoS Biol.*, **2004**, *2*, e294.

[403] M. Thevis, S. Beuck, A. Thomas, M. Kohler, N. Schlörer, I. Vajiala, W. Schänzer. Screening for the calstabin-ryanodine receptor complex stabilizers JTV-519 and S-107 in doping control analysis. *Drug Test. Anal.*, **2009**, *1*, 32–42.

[404] M. Thevis, T. Kuuranne, H. Geyer. Annual banned-substance review: Analytical approaches in human sports drug testing. *Drug Test. Anal.*, **2019**, *11*, 8–26.

[405] M. Thevis, W. Schänzer. Detection of SARMs in doping control analysis. *Mol. Cell. Endocrinol.*, **2018**, *464*, 34–45.

[406] M. Thevis, W. Schänzer. Current role of LC–MS (/MS) in doping control. *Anal. Bioanal. Chem.*, **2007**, *388*, 1351–1358.

[407] B. D. Ahrens, B. Starcevic, A. W. Butch. Detection of prohibited substances by liquid chromatography tandem mass spectrometry for sports doping control, in *LC-MS Drug Anal.*, (Eds: L.J. Langman, C.L.H. Snozek), Humana Press, **2012**, pp. 115–128.

[408] J. P. Scarth, A. D. Clarke, P. Teale, C. M. Pearce. Comparative in vitro metabolism of the "designer" steroid estra-4,9-diene-3,17-dione between the equine, canine and human: identification of target metabolites for use in sports doping control. *Steroids*, **2010**, *75*, 643–52.

[409] V. R. Potter, C. A. Elvehjem. A modified method for the study of tissue oxidations. *J. Biol. Chem.*, **1936**, *114*, 495–504.

[410] C. De Duve, J. Berthet. The use of differential centrifugation in the study of tissue enzymes. *Int. Rev. Cytol.*, **1954**, *3*, 225–275.

[411] M. Otsuka, T. Mine, E. Ohuchi, S. Ohmori. A detoxication route for acetaldehyde: metabolism of diacetyl, acetoin, and 2, 3-butanediol in liver homogenate and perfused liver of rats. *J. Biochem.*, **1996**, *119*, 246–251.

[412] G. K. Poon, B. Walter, P. E. Lønning, M. N. Horton, R. McCague. Identification of tamoxifen metabolites in human Hep G2 cell line, human liver homogenate, and patients on long-term therapy for breast cancer. *Drug Metab. Dispos.*, **1995**, *23*, 377–382.

[413] O. Pelkonen, A. Tolonen, T. Rousu, L. Tursas, M. Turpeinen, J. Hokkanen, J. Uusitalo, M. B. d'Yvoire, S. Coecke. Comparison of metabolic stability and metabolite identification of 55 ECVAM/ICCVAM validation compounds between human and rat liver homogenates and microsomes-a preliminary analysis. *ALTEX-Alternatives to Anim. Exp.*, **2009**, *26*, 214–222.

[414] A. A. J. J. L. Rutten, H. E. Falke, J. F. Catsburg, R. Topp, B. J. Blaauboer, I. Holsteijn van, F. X. R. Doorn, Lambertm Leeuwen van. Interlaboratory comparison of total cytochrome P-450 and protein determinations in rat liver microsomes. *Arch. Toxicol.*, **1987**, *61*, 27–33.

[415] B. G. Lake. Preparation and characteristation of microsomal fractions for studies of xenobiotic metabolism., in *Biochem. Toxicol. A Pract. Approach*, (Eds: K. Snell, B. Mullock), IRL Press, Oxford, **1987**, pp. 183–215.

[416] C. H. Williams, H. Kamin. Microsomal triphosphopyridine nucleotide-cytochrome c reductase of liver. *J. Biol. Chem.*, **1962**, *237*, 587–595.

[417] J. Lampinen, M. Raitio, A. Peraia, H. Oranen, R.-R. Harinen. Microplate based pathlength correction method for photometric DNA quantification assay. *Vantaa Thermo Fish. Appl. Note*, **2012**.

[418] D. J. Waxman, T. K. H. Chang. Use of 7-ethoxycoumarin to monitor multiple enzymes in the human CYP1, CYP2, and CYP3 families. *Methods Mol. Biol.*, **2006**, *320*, 153–156.

[419] F. P. Guengerich. Mechanisms of cytochrome P450-catalyzed oxidations. *ACS Catal.*, **2018**, *8*, 10964–10976.

[420] A. Altuve, S. Silchenko, K.-H. Lee, K. Kuczera, S. Terzyan, X. Zhang, D. R. Benson, M. Rivera. Probing the differences between rat liver outer mitochondrial membrane cytochrome b5 and microsomal cytochromes b5. *Biochemistry*, **2001**, *40*, 9469–9483.

[421] M. R. Waterman. [48] Spectral characterization of human hemoglobin and its derivatives, in *Methods Enzymol.*, Elsevier, **1978**, pp. 456–463.

[422] P. Strittmatter, S. F. Velick. The isolation and properties of microsomal cytochrome. *J. Biol. Chem.*, **1956**, *221*, 253–264.

[423] B. Wahl, D. Reichmann, D. Niks, N. Krompholz, A. Havemeyer, B. Clement, T. Messerschmidt, M. Rothkegel, H. Biester, R. Hille. Biochemical and spectroscopic characterization of the human mitochondrial amidoxime reducing components hmARC-1 and hmARC-2 suggests the existence of a new molybdenum enzyme family in eukaryotes. *J. Biol. Chem.*, **2010**, *285*, 37847–37859.

[424] W. Gao, J. S. Johnston, D. D. Miller, J. T. Dalton. Interspecies differences in pharmacokinetics and metabolism of S-3-(4-acetylamino-phenoxy)-2-hydroxy-2-methyl-N-(4-nitro-3-trifluoromethylphenyl)-propionamide: the role of N-acetyltransferase. *Drug Metab. Dispos.*, **2006**, *34*, 254–260.

[425] L. Perrenoud, C. Schweizer Grundisch, N. Baume, M. Saugy, R. Nicoli. Risk of false positive results to SARM S-4 in case of therapeutic use of antineoplastic/antiandrogen drug containing flutamide: a case study. *Drug Test. Anal.*, **2016**, *8*, 1109–1113.

[426] W. Gao, Z. Wu, C. E. Bohl, J. Yang, D. D. Miller, J. T. Dalton. Characterization of the in vitro metabolism of selective androgen receptor modulator using human, rat, and dog liver enzyme preparations. *Drug Metab. Dispos.*, **2006**, *34*, 243–253.

[427] J. Rosen, A. Negro-Vilar. Novel, non-steroidal, selective androgen receptor modulators (SARMs) with anabolic activity in bone and muscle and improved safety profile. *J. Musculoskelet. Neuronal Interact.*, **2002**, *2*, 222–224.

[428] W. Gao, P. J. Reiser, C. C. Coss, M. A. Phelps, J. D. Kearbey, D. D. Miller, J. T. Dalton. Selective androgen receptor modulator treatment improves muscle strength and body composition and prevents bone loss in orchidectomized rats. *Endocrinology*, **2005**, *146*, 4887–4897.

[429] W. Gao, J. T. Dalton. Ockham's razor and selective androgen receptor modulators (SARMs): are we overlooking the role of 5α-reductase? *Mol. Interv.*, **2007**, *7*, 10.

[430] B. Wen, M. Zhu. Applications of mass spectrometry in drug metabolism: 50 years of progress. *Drug Metab. Rev.*, **2015**, *47*, 71–87.

[431] M. J. Cohen, F. W. Karasek. Plasma chromatography™—a new dimension for gas chromatography and mass spectrometry. *J. Chromatogr. Sci.*, **1970**, *8*, 330–337.

[432] S. M. Stow, T. J. Causon, X. Zheng, R. T. Kurulugama, T. Mairinger, J. C. May, E. E. Rennie, E. S. Baker, R. D. Smith, J. A. McLean. An interlaboratory evaluation of drift tube ion mobility–mass spectrometry collision cross section measurements. *Anal. Chem.*, **2017**, *89*, 9048–9055.

[433] E. A. Mason, H. W. Schamp Jr. Mobility of gaseous Ions in weak electric fields. *Ann. Phys. (N. Y.)*, **1958**, *4*, 233–270.

[434] J. C. May, C. B. Morris, J. A. McLean. Ion mobility collision cross section compendium. *Anal. Chem.*, **2016**, *89*, 1032–1044.

[435] V. d'Atri, T. Causon, O. Hernandez-Alba, A. Mutabazi, J. Veuthey, S. Cianferani, D. Guillarme. Adding a new separation dimension to MS and LC–MS: What is the utility of ion mobility spectrometry? *J. Sep. Sci.*, **2018**, *41*, 20–67.

[436] C. Tejada-Casado, M. Hernández-Mesa, F. Monteau, F. J. Lara, M. del Olmo-Iruela, A. M. García-Campaña, B. Le Bizec, G. Dervilly-Pinel. Collision cross section (CCS) as a complementary parameter to characterize human and veterinary drugs. *Anal. Chim. Acta*, **2018**, *1043*, 52–63.

[437] M. Hernández-Mesa, B. Le Bizec, F. Monteau, A. M. García-Campaña, G. Dervilly-Pinel. Collision Cross Section (CCS) database: An additional measure to characterize steroids. *Anal. Chem.*, **2018**, *90*, 4616–4625.

[438] L. Righetti, M. Fenclova, L. Dellafiora, J. Hajslova, M. Stranska-Zachariasova, C. Dall'Asta. High resolution-ion mobility mass spectrometry as an additional powerful tool for structural characterization of mycotoxin metabolites. *Food Chem.*, **2018**, *245*, 768–774.

[439] E. Reading, J. Munoz-Muriedas, A. D. Roberts, G. J. Dear, C. V Robinson, C. Beaumont. Elucidation of drug metabolite structural isomers using molecular modeling coupled with ion mobility mass spectrometry. *Anal. Chem.*, **2016**, *88*, 2273–2280.

[440] M. Thevis, J. Dib, A. Thomas, S. Höppner, A. Lagojda, D. Kuehne, M. Sander, G. Opfermann, W. Schänzer. Complementing the characterization of in vivo generated N-glucuronic acid conjugates of stanozolol by collision cross section computation and analysis. *Drug Test. Anal.*, **2015**, *7*, 1050–1056.

[441] M. Hernández-Mesa, F. Monteau, B. Le Bizec, G. Dervilly-Pinel. Potential of ion mobility-mass spectrometry for both targeted and non-targeted analysis of phase II steroid metabolites in urine. *Anal. Chim. Acta X*, **2019**, *1*, 100006.

[442] S. V. F. Hansen, T. Ulven. Oxalyl chloride as a practical carbon monoxide source for carbonylation reactions. *Org. Lett.*, **2015**, *17*, 2832–2835.

[443] K. M. A. Johannesen, J. DePierre. Measurement of cytochrome P-450 in the presence of large amounts of contaminating hemoglobin and methemoglobin. *Anal. Biochem.*, **1978**, *86*, 725–732.

[444] B. X. MacLean, B. S. Pratt, J. D. Egertson, M. J. MacCoss, R. D. Smith, E. S. Baker. Using Skyline to Analyze Data-Containing Liquid Chromatography, Ion Mobility Spectrometry, and Mass Spectrometry Dimensions. *J. Am. Soc. Mass Spectrom.*, **2018**, 2182–2188.

[445] S. E. Kandel, J. N. Lampe. Role of protein–protein interactions in cytochrome P450-mediated drug metabolism and toxicity. *Chem. Res. Toxicol.*, **2014**, *27*, 1474–1486.

[446] L. Reed, R. Indra, I. Mrizova, M. Moserova, H. H. Schmeiser, C. R. Wolf, C. J. Henderson, M. Stiborova, D. H. Phillips, V. M. Arlt. Application of hepatic cytochrome b5/P450 reductase null (HBRN) mice to study the role of cytochrome b5 in the cytochrome P450-mediated bioactivation of the anticancer drug ellipticine. *Toxicol. Appl. Pharmacol.*, **2019**, *366*, 64–74.

[447] N. Negreira, C. Erratico, T. Kosjek, A. L. N. van Nuijs, E. Heath, H. Neels, A. Covaci. In vitro phase I and phase II metabolism of α-pyrrolidinovalerophenone (α-PVP), methylenedioxypyrovalerone (MDPV) and methedrone by human liver microsomes and human liver cytosol. *Anal. Bioanal. Chem.*, **2015**, *407*, 5803–5816.

[448] M. Grapp, C. Kaufmann, M. Ebbecke. Toxicological investigation of forensic cases related to the designer drug 3, 4-methylenedioxypyrovalerone (MDPV): Detection, quantification and studies on human metabolism by GC–MS. *Forensic Sci. Int.*, **2017**, *273*, 1–9.

[449] J. Bolleddula, K. DeMent, J. P. Driscoll, P. Worboys, P. J. Brassil, D. L. Bourdet. Biotransformation and bioactivation reactions of alicyclic amines in drug molecules. *Drug Metab. Rev.*, **2014**, *46*, 379–419.

[450] M. F. Mesleh, J. M. Hunter, A. A. Shvartsburg, G. C. Schatz, M. F. Jarrold. Structural information from ion mobility measurements: effects of the long-range potential. *J. Phys. Chem.*, **1996**, *100*, 16082–16086.

[451] I. Campuzano, M. F. Bush, C. V Robinson, C. Beaumont, K. Richardson, H. Kim, H. I. Kim. Structural characterization of drug-like compounds by ion mobility mass spectrometry: comparison of theoretical

and experimentally derived nitrogen collision cross sections. *Anal. Chem.*, **2011**, *84*, 1026–1033.

[452] Z. Zhou, X. Xiong, Z.-J. Zhu. MetCCS predictor: a web server for predicting collision cross-section values of metabolites in ion mobility-mass spectrometry based metabolomics. *Bioinformatics*, **2017**, *33*, 2235–2237.

[453] Z. Zhou, X. Shen, J. Tu, Z.-J. Zhu. Large-scale prediction of collision cross-section values for metabolites in ion mobility-mass spectrometry. *Anal. Chem.*, **2016**, *88*, 11084–11091.

[454] S. M. Colby, D. G. Thomas, J. R. Nunez, D. J. Baxter, K. R. Glaesemann, J. M. Brown, M. A. Pirrung, N. Govind, J. G. Teeguarden, T. O. Metz. ISiCLE: A molecular collision cross section calculation pipeline for establishing large in silico reference libraries for compound identification. *arXiv Prepr. arXiv1809.08378*, **2018**.

[455] P.-L. Plante, E. Francovic-Fontaine, J. C. May, J. A. McLean, E. S. Baker, F. Laviolette, M. Marchand, J. Corbeil. Predicting Ion Mobility Collision Cross-Sections Using a Deep Neural Network: DeepCCS. *Anal. Chem.*, **2019**, *91*, 5191–5199.

[456] K. L. Helke, K. N. Nelson, A. M. Sargeant, B. Jacob, S. McKeag, J. Haruna, V. Vemireddi, M. Greeley, D. Brocksmith, N. Navratil. Pigs in toxicology: breed differences in metabolism and background findings. *Toxicol. Pathol.*, **2016**, *44*, 575–590.

[457] R. W. Estabrook. A passion for P450s (remembrances of the early history of research on cytochrome P450). *Drug Metab. Dispos.*, **2003**, *31*, 1461–1473.

[458] D. W. Nebert, K. Wikvall, W. L. Miller. Human cytochromes P450 in health and disease. *Philos. Trans. R. Soc. B Biol. Sci.*, **2013**, *368*, 20120431.

[459] K. Walton, J.-L. C. M. Dorne, A. G. Renwick. Default factors for interspecies differences in the major routes of xenobiotic elimination. *Hum. Ecol. Risk Assess. An Int. J.*, **2001**, *7*, 181–201.

[460] J. B. Watkins III, C. D. Klaassen. Xenobiotic biotransformation in livestock: comparison to other species commonly used in toxicity testing. *J. Anim. Sci.*, **1986**, *63*, 933–942.

[461] V. Zancanella, M. Giantin, M. Dacasto. Absolute quantification and modulation of cytochrome P450 3A isoforms in cattle liver. *Vet. J.*, **2014**, *202*, 106–111.

[462] M. Mazzarino, X. de la Torre, I. Fiacco, A. Palermo, F. Botrè. Drug-drug interaction and doping, part 1: An in vitro study on the effect of non-prohibited drugs on the phase I metabolic profile of toremifene. *Drug Test. Anal.*, **2014**, *6*, 482–491.

[463] M. Mazzarino, X. de la Torre, I. Fiacco, F. Botrè. Drug-drug interaction and doping, part 2: An in vitro study on the effect of non-prohibited drugs on the phase I metabolic profile of stanozolol. *Drug Test. Anal.*, **2014**, *6*, 969–977.

[464] A. Palermo, F. Botrè, X. De La Torre, I. Fiacco, M. Iannone, M. Mazzarino. Drug-drug interactions and masking effects in sport doping: influence of miconazole administration on the urinary concentrations of endogenous anabolic steroids. *Forensic Toxicol.*, **2016**, *34*, 386–397.

[465] M. Mazzarino, F. L. Khevenhüller-Metsch, I. Fiacco, M. K. Parr, X. de la Torre, F. Botrè. Drug–drug interaction and doping: Effect of non-prohibited drugs on the urinary excretion profile of methandienone. *Drug Test. Anal.*, **2018**, *10*, 1554–1565.

[466] B. W. Ogilvie, E. Usuki, P. Yerino, A. Parkinson. In vitro approaches for studying the inhibition of drug-metabolizing enzymes and identifying the drug-metabolizing enzymes responsible for the metabolism of drugs (reaction phenotyping) with emphasis on cytochrome P450, in *Drug-Drug Interact.*, (Ed: A.D. Rodrigues), CRC Press, **2008**, pp. 231–358.

[467] T. W. Harper, P. J. Brassil. Reaction phenotyping: current industry efforts to identify enzymes responsible for metabolizing drug candidates. *AAPS J.*, **2008**, *10*, 200–207.

[468] T. De Vijlder, D. Valkenborg, F. Lemière, E. P. Romijn, K. Laukens, F. Cuyckens. A tutorial in small molecule identification via electrospray ionization-mass spectrometry: The practical art of structural elucidation. *Mass Spectrom. Rev.*, **2018**, *37*, 607–629.

[469] A. Tolonen, M. Turpeinen, O. Pelkonen. Liquid chromatography–mass spectrometry in in vitro drug metabolite screening. *Drug Discov. Today*, **2009**, *14*, 120–133.

[470] D. Q. Liu, C. E. C. A. Hop. Strategies for characterization of drug metabolites using liquid chromatography–tandem mass spectrometry in conjunction with chemical derivatization and on-line H/D exchange approaches. *J. Pharm. Biomed. Anal.*, **2005**, *37*, 1–18.

[471] D. Q. Liu, Y. Xia, R. Bakhtiar. Use of a liquid chromatography/ion trap mass spectrometry/triple quadrupole mass spectrometry system for metabolite identification. *Rapid Commun. Mass Spectrom.*, **2002**, *16*, 1330–1336.

[472] D. R. Nelson. Cytochrome P450 and the individuality of species. *Arch. Biochem. Biophys.*, **1999**, *369*, 1–10.

[473] C. Orr. Characterisation of equine cytochrome P450s, University Of Nottingham, **2016**.

[474] V. Zancanella, M. Giantin, R. M. Lopparelli, T. Patarnello, M. Dacasto, E. Negrisolo. Proposed new nomenclature for Bos taurus cytochromes P450 involved in xenobiotic drug metabolism. *J. Vet.*

Pharmacol. Ther., **2010**, *33*, 528–536.

[475] A. J. Draper, A. Madan, A. Parkinson. Inhibition of coumarin 7-hydroxylase activity in human liver microsomes. *Arch. Biochem. Biophys.*, **1997**, *341*, 47–61.

[476] R. L. Walsky, A. V. Astuccio, R. S. Obach. Evaluation of 227 Drugs for In Vitro Inhibition of Cytochrome P450 2B6. *J. Clin. Pharmacol.*, **2006**, *46*, 1426–1438.

[477] M. Turpeinen, H. Raunio, O. Pelkonen. The functional role of CYP2B6 in human drug metabolism: substrates and inhibitors in vitro, in vivo and in silico. *Curr. Drug Metab.*, **2006**, *7*, 705–714.

[478] J. Zielinski, M. Mevissen. Inhibition of in vitro metabolism of testosterone in human, dog and horse liver microsomes to investigate species differences. *Toxicol. Vitr.*, **2015**, *29*, 468–478.

[479] D. J. Newton, R. W. Wang, A. Y. Lu. Cytochrome P450 inhibitors. Evaluation of specificities in the in vitro metabolism of therapeutic agents by human liver microsomes. *Drug Metab. Dispos.*, **1995**, *23*, 154–158.

[480] M. Bourrié, V. Meunier, Y. Berger, G. Fabre. Cytochrome P450 isoform inhibitors as a tool for the investigation of metabolic reactions catalyzed by human liver microsomes. *J. Pharmacol. Exp. Ther.*, **1996**, *277*, 321–332.

[481] D. M. Stresser, E. S. Perloff, A. K. Mason, A. P. Blanchard, S. S. Dehal, T. P. Creegan, R. Singh, E. T. Gangl. Selective time- and NADPH-dependent inhibition of human CYP2E1 by clomethiazole. *Drug Metab. Dispos.*, **2016**, *44*, 1424–1430.

[482] J. Yang, B. Yan. Photochemotherapeutic agent 8-methoxypsoralen induces cytochrome P450 3A4 and carboxylesterase HCE2: evidence on an involvement of the pregnane X receptor. *Toxicol. Sci.*, **2006**, *95*, 13–22.

[483] S. D. Krämer, B. Testa. The Biochemistry of Drug Metabolism–An Introduction: Part 6. Inter-Individual Factors Affecting Drug Metabolism. *Chem. Biodivers.*, **2008**, *5*, 2465–2578.

[484] V. A. Eagling, J. F. Tjia, D. J. Back. Differential selectivity of cytochrome P450 inhibitors against probe substrates in human and rat liver microsomes. *Br. J. Clin. Pharmacol.*, **1998**, *45*, 107–114.

[485] X.-Q. Li, A. Björkman, T. B. Andersson, M. Ridderström, C. M. Masimirembwa. Amodiaquine clearance and its metabolism to N-desethylamodiaquine is mediated by CYP2C8: a new high affinity and turnover enzyme-specific probe substrate. *J. Pharmacol. Exp. Ther.*, **2002**, *300*, 399–407.

[486] P. McManus, G. Albrecht, R. Graham. *The Global Horseracing Industry: Social, Economic, Environmental and Ethical Perspectives*, Routledge, **2012**.

[487] J. Chen, J. Kim, J. T. Dalton. Discovery AND Therapeutic Promise OF Selective Androgen Receptor Modulators. *Mol Interv.*, **2005**, *5*, 173–188.

[488] M. L. Mohler, V. a Nair, D. J. Hwang, I. M. Rakov, R. Patil, D. D. Miller. Nonsteroidal tissue selective androgen receptor modulators: a promising class of clinical candidates. *Expert Opin. Ther. Pat.*, **2005**, *15*, 1565–1585.

[489] N. Dodman, N. Blondeau, A. M. Marini. Association of phenylbutazone usage with horses bought for slaughter: A public health risk. *Food Chem. Toxicol.*, **2010**, *48*, 1270–1274.

[490] European Commission. Commission Implementing Regulation (EU) 2015/262 of 17 February 2015 laying down rules pursuant to Council Directives 90/427/EEC and 2009/156/EC as regards the methods for the identification of equidae (Equine Passport Regulation). *Off. J. Eur. Union*, **2015**, *L 59*.

[491] W. Schänzer, H. Geyer, G. Fußhöller, N. Halatcheva, M. Kohler, M. Parr, S. Guddat, A. Thomas, M. Thevis. Mass spectrometric identification and characterization of a new long-term metabolite of metandienone in human urine. *Rapid Commun. Mass Spectrom.*, **2006**, *20*, 2252–2258.

[492] P. Pavek, Z. Dvorak. Xenobiotic-induced transcriptional regulation of xenobiotic metabolizing enzymes of the cytochrome P450 superfamily in human extrahepatic tissues. *Curr. Drug Metab.*, **2008**, *9*, 129–143.

[493] E. Tydén, M. Löfgren, S. Pegolo, F. Capolongo, H. Tjälve, P. Larsson. Differential gene expression of CYP3A isoforms in equine liver and intestines. *J. Vet. Pharmacol. Ther.*, **2012**, *35*, 588–595.

[494] E. Tydén, M. Löfgren, M. Hakhverdyan, H. Tjälve, P. Larsson. The genes of all seven CYP 3A isoenzymes identified in the equine genome are expressed in the airways of horses. *J. Vet. Pharmacol. Ther.*, **2013**, *36*, 370–375.

[495] P. Fasinu, P. J. Bouic, B. Rosenkranz. Liver-Based In Vitro Technologies for Drug Biotransformation Studies - A Review. *Curr. Drug Metab.*, **2012**, *13*, 215–224.

[496] A. Damre, S. R. Mallurwar, D. Behera. Preparation and Characterization of Rodent Intestinal Microsomes : Comparative Assessment of Two Methods. *Indian J. Pharm. Sci.*, **2016**, *71*, 75–77.

[497] M. Thevis, D. A. Volmer. Recent instrumental progress in mass spectrometry: advancing resolution, accuracy, and speed of drug detection. *Drug Test. Anal.*, **2012**, *4*, 242–245.

[498] C. L. Litterst, E. G. Mimnaugh, R. L. Reagan, T. E. Gram. Comparison of in vitro drug metabolism by lung, liver, and kidney of several common laboratory species. *Drug Metab. Dispos.*, **1975**, *3*, 259–265.

[499] D. J. Waxman, D. P. Lapenson, T. Aoyama, H. V Gelboin, F. J. Gonzalez, K. Korzekwa. Steroid

hormone hydroxylase specificities of eleven cDNA-expressed human cytochrome P450s. *Arch. Biochem. Biophys.*, **1991**, *290*, 160–166.

[500] A. Schmitz, C. J. Portier, W. Thormann, R. Theurillat, M. Mevissen. Stereoselective biotransformation of ketamine in equine liver and lung microsomes. *J. Vet. Pharmacol. Ther.*, **2008**, *31*, 446–455.

[501] M. H. Court. Acetaminophen UDP-glucuronosyltransferase in ferrets: species and gender differences, and sequence analysis of ferret UGT1A6. *J. Vet. Pharmacol. Ther.*, **2001**, *24*, 415–422.

[502] N. D. Pickwell. Equine UDP-glucuronosyltransferases and their role in phase II metabolism, University Of Nottingham, **2018**.

[503] C. M. Wade, E. Giulotto, S. Sigurdsson, M. Zoli, S. Gnerre, F. Imsland, T. L. Lear, D. L. Adelson, E. Bailey, R. R. Bellone. Genome sequence, comparative analysis, and population genetics of the domestic horse. *Science (80-.).*, **2009**, *326*, 865–867.

[504] P. Teale, E. Houghton. Metabolism of anabolic steroids and their relevance to drug detection in horseracing. *Bioanalysis*, **2010**, *2*, 1085–1107.

[505] A. R. McKinney. Modern techniques for the determination of anabolic-androgenic steroid doping in the horse. *Bioanalysis*, **2009**, *1*, 785–803.

[506] C. Chang, A. Saltzman, S. Yeh, W. Young, E. T. Keller, H.-J. Lee, C. Wang, A. Mizokami. Androgen receptor: an overview. *Crit. Rev. Eukaryot. Gene Expr.*, **1995**, *5*, 97–125.

[507] D. Li, W. Zhou, J. Pang, Q. Tang, B. Zhong, C. Shen, L. Xiao, T. Hou. A magic drug target: Androgen receptor. *Med. Res. Rev.*, **2018**.

[508] R. A. Davey, M. Grossmann. Androgen receptor structure, function and biology: from bench to bedside. *Clin. Biochem. Rev.*, **2016**, *37*, 3–15.

[509] A. G. Fragkaki, Y. S. Angelis, M. Koupparis, A. Tsantili-Kakoulidou, G. Kokotos, C. Georgakopoulos. Structural characteristics of anabolic androgenic steroids contributing to binding to the androgen receptor and to their anabolic and androgenic activities: applied modifications in the steroidal structure. *Steroids*, **2009**, *74*, 172–197.

[510] R. Narayanan, M. L. Mohler, C. E. Bohl, D. D. Miller, J. T. Dalton. Selective androgen receptor modulators in preclinical and clinical development. *Nucl. Recept. Signal.*, **2008**, *6*, e010.

[511] M. L. Mohler, C. E. Bohl, A. Jones, C. C. Coss, R. Narayanan, Y. He, J. H. Dong, J. T. Dalton, D. D. Miller. Nonsteroidal Selective Androgen Receptor Modulators (SARMs): Dissociating the anabolic and androgenic activities of the androgen receptor for therapeutic benefit. *J. Med. Chem.*, **2009**, *52*, 3597–3617.

[512] C. C. Coss, A. Jones, J. T. Dalton. Selective androgen receptor modulators as improved androgen therapy for advanced breast cancer. *Steroids*, **2014**, *90*, 94–100.

[513] Z. Yu, S. He, D. Wang, H. K. Patel, C. P. Miller, J. L. Brown, G. Hattersley, J. C. Saeh. Selective Androgen Receptor Modulator RAD140 Inhibits the Growth of Androgen/Estrogen Receptor–Positive Breast Cancer Models with a Distinct Mechanism of Action. *Clin. Cancer Res.*, **2017**, *23*, 7608–7620.

[514] K. Tsarouhas, N. Kioukia–Fougia, P. Papalexis, A. Tsatsakis, D. Kouretas, F. Bacopoulou, C. Tsitsimpikou. Use of nutritional supplements contaminated with banned doping substances by recreational adolescent athletes in Athens, Greece. *Food Chem. Toxicol.*, **2018**, *115*, 447–450.

[515] A. L. Goldman, H. G. Pope Jr, S. Bhasin. The Health Threat Posed by the Hidden Epidemic of Anabolic Steroid Use and Body Image Disorders Among Young Men. *J. Clin. Endocrinol. Metab.*, **2018**, *104*, 1069–1074.

[516] M. Uhlén, L. Fagerberg, B. M. Hallström, C. Lindskog, P. Oksvold, A. Mardinoglu, Å. Sivertsson, C. Kampf, E. Sjöstedt, A. Asplund. Tissue-based map of the human proteome. *Science (80-.).*, **2015**, *347*, 1260419.

[517] R. P. Horgan, L. C. Kenny. 'Omic'technologies: genomics, transcriptomics, proteomics and metabolomics. *Obstet. Gynaecol.*, **2011**, *13*, 189–195.

[518] J. S. Cassoli, P. C. Guest, A. G. Santana, D. Martins-de-Souza. Employing proteomics to unravel the molecular effects of antipsychotics and their role in schizophrenia. *Proteomics Clin. Appl.*, **2016**, *10*, 442–455.

[519] K. S. Lilley, D. B. Friedman. All about DIGE: quantification technology for differential-display 2D-gel proteomics. *Expert Rev. Proteomics*, **2004**, *1*, 401–409.

[520] UniProt Consortium. UniProt: a worldwide hub of protein knowledge. *Nucleic Acids Res.*, **2018**, *47*, D506–D515.

[521] H. Mi, A. Muruganujan, X. Huang, D. Ebert, C. Mills, X. Guo, P. D. Thomas. Protocol Update for large-scale genome and gene function analysis with the PANTHER classification system (v. 14.0). *Nat. Protoc.*, **2019**, *14*, 703–721.

[522] A. Fabregat, S. Jupe, L. Matthews, K. Sidiropoulos, M. Gillespie, P. Garapati, R. Haw, B. Jassal, F. Korninger, B. May. The reactome pathway knowledgebase. *Nucleic Acids Res.*, **2017**, *46*, D649–D655.

[523] S. T. Reddy, D. J. Wadleigh, V. Grijalva, C. Ng, S. Hama, A. Gangopadhyay, D. M. Shih, A. J. Lusis,

M. Navab, A. M. Fogelman. Human paraoxonase-3 is an HDL-associated enzyme with biological activity similar to paraoxonase-1 protein but is not regulated by oxidized lipids. *Arterioscler. Thromb. Vasc. Biol.*, **2001**, *21*, 542–547.

[524] K. B. Rubinow, T. Vaisar, C. Tang, A. M. Matsumoto, J. W. Heinecke, S. T. Page. Testosterone replacement in hypogonadal men alters the HDL proteome but not HDL cholesterol efflux capacity. *J. Lipid Res.*, **2012**, *53*, 1376–1383.

[525] C. Nicholls, H. Li, J. Liu. GAPDH: a common enzyme with uncommon functions. *Clin. Exp. Pharmacol. Physiol.*, **2012**, *39*, 674–679.

[526] N. Harada, R. Yasunaga, Y. Higashimura, R. Yamaji, K. Fujimoto, J. Moss, H. Inui, Y. Nakano. Glyceraldehyde-3-phosphate dehydrogenase enhances transcriptional activity of androgen receptor in prostate cancer cells. *J. Biol. Chem.*, **2007**, *282*, 22651–22661.

[527] M. Ralser, M. M. Wamelink, A. Kowald, B. Gerisch, G. Heeren, E. A. Struys, E. Klipp, C. Jakobs, M. Breitenbach, H. Lehrach. Dynamic rerouting of the carbohydrate flux is key to counteracting oxidative stress. *J. Biol.*, **2007**, *6*, 10.

[528] E. R. Perri, C. J. Thomas, S. Parakh, D. M. Spencer, J. D. Atkin. The unfolded protein response and the role of protein disulfide isomerase in neurodegeneration. *Front. cell Dev. Biol.*, **2016**, *3*, 80.

[529] C. Grek, D. M. Townsend. Protein disulfide isomerase superfamily in disease and the regulation of apoptosis. *Endoplasmic reticulum Stress Dis.*, **2014**, *1*, 4–17.

[530] H. Zeeshan, G. Lee, H.-R. Kim, H.-J. Chae. Endoplasmic reticulum stress and associated ROS. *Int. J. Mol. Sci.*, **2016**, *17*, 327.

[531] M. Shankaran, T. W. Shearer, S. A. Stimpson, S. M. Turner, C. King, P. A. Wong, Y. Shen, P. S. Turnbull, F. Kramer, L. Clifton. Proteome-wide muscle protein fractional synthesis rates predict muscle mass gain in response to a selective androgen receptor modulator in rats. *Am. J. Physiol. Metab.*, **2015**, *310*, E405–E417.

[532] A. Pey, A. Saborido, I. Blázquez, J. Delgado, A. Megías. Effects of prolonged stanozolol treatment on antioxidant enzyme activities, oxidative stress markers, and heat shock protein HSP72 levels in rat liver. *J. Steroid Biochem. Mol. Biol.*, **2003**, *87*, 269–277.

[533] S. P. Frankenfeld, L. P. Oliveira, V. H. Ortenzi, I. C. C. Rego-Monteiro, E. A. Chaves, A. C. Ferreira, A. C. Leitão, D. P. Carvalho, R. S. Fortunato. The anabolic androgenic steroid nandrolone decanoate disrupts redox homeostasis in liver, heart and kidney of male Wistar rats. *PLoS One*, **2014**, *9*, e102699.

[534] E. Sadowska-Krępa, B. Kłapcińska, S. Jagsz, A. Nowara, I. Szołtysek-Bołdys, M. Chalimoniuk, J. Langfort, S. J. Chrapusta. High-dose testosterone enanthate supplementation boosts oxidative stress, but exerts little effect on the antioxidant barrier in sedentary adolescent male rat liver. *Pharmacol. Reports*, **2017**, *69*, 673–678.

[535] C. Ding, Y. Li, F. Guo, Y. Jiang, W. Ying, D. Li, D. Yang, X. Xia, W. Liu, Y. Zhao. A cell-type-resolved liver proteome. *Mol. Cell. Proteomics*, **2016**, *15*, 3190–3202.

[536] S. B. Azimifar, N. Nagaraj, J. Cox, M. Mann. Cell-type-resolved quantitative proteomics of murine liver. *Cell Metab.*, **2014**, *20*, 1076–1087.

[537] M. Dreger. Subcellular proteomics. *Mass Spectrom. Rev.*, **2003**, *22*, 27–56.

[538] J. R. Yates Iii, A. Gilchrist, K. E. Howell, J. J. M. Bergeron. Proteomics of organelles and large cellular structures. *Nat. Rev. Mol. Cell Biol.*, **2005**, *6*, 702–714.

[539] R. Drissi, M. Dubois, F. Boisvert. Proteomics methods for subcellular proteome analysis. *FEBS J.*, **2013**, *280*, 5626–5634.

[540] L. J. Foster, C. L. de Hoog, Y. Zhang, Y. Zhang, X. Xie, V. K. Mootha, M. Mann. A mammalian organelle map by protein correlation profiling. *Cell*, **2006**, *125*, 187–199.

[541] B. Cox, A. Emili. Tissue subcellular fractionation and protein extraction for use in mass-spectrometry-based proteomics. *Nat. Protoc.*, **2006**, *1*, 1872–1878.

[542] M. Kanehisa, Y. Sato, M. Furumichi, K. Morishima, M. Tanabe. New approach for understanding genome variations in KEGG. *Nucleic Acids Res.*, **2018**, *47*, D590–D595.

[543] S. X. Ge, D. Jung. ShinyGO : a graphical enrichment tool for animals and plants. *bioRxiv*, **2018**, 315150.

[544] D. Szklarczyk, A. L. Gable, D. Lyon, A. Junge, S. Wyder, J. Huerta-Cepas, M. Simonovic, N. T. Doncheva, J. H. Morris, P. Bork. STRING v11: protein–protein association networks with increased coverage, supporting functional discovery in genome-wide experimental datasets. *Nucleic Acids Res.*, **2018**, *47*, D607–D613.

[545] P. Bardou, J. Mariette, F. Escudié, C. Djemiel, C. Klopp. jvenn: an interactive Venn diagram viewer. *BMC Bioinformatics*, **2014**, *15*, 293.

[546] T. Rabilloud, C. Lelong. Two-dimensional gel electrophoresis in proteomics: a tutorial. *J. Proteomics*, **2011**, *74*, 1829–1841.

[547] L. A. Fahien, J. M. Schooler, G. A. Gehred, P. P. Cohen. Studies on the mechanism of action of

acetylglutamate as an activator of carbamyl phosphate synthetase. *J. Biol. Chem.*, **1964**, *239*, 1935–1941.

[548] T. Lam, A. Poljak, M. McLean, N. Bahl, K. K. Y. Ho, V. Birzniece. Testosterone prevents protein loss via the hepatic urea cycle in human. *Eur. J. Endocrinol.*, **2017**, *176*, 489–496.

[549] T. Sugino, T. Shirai, Y. Kajimoto, O. Kajimoto. L-ornithine supplementation attenuates physical fatigue in healthy volunteers by modulating lipid and amino acid metabolism. *Nutr. Res.*, **2008**, *28*, 738–743.

[550] B. J. Mutch, E. W. Banister. Ammonia metabolism in exercise and fatigue: a review. *Med. Sci. Sports Exerc.*, **1983**, *15*, 41–50.

[551] L. Nybo, M. K. Dalsgaard, A. Steensberg, K. Møller, N. H. Secher. Cerebral ammonia uptake and accumulation during prolonged exercise in humans. *J. Physiol.*, **2005**, *563*, 285–290.

[552] R. Blanqué, L. Lepescheux, M. Auberval, D. Minet, D. Merciris, C. Cottereaux, P. Clément-Lacroix, P. Delerive, F. Namour. Characterization of GLPG0492, a selective androgen receptor modulator, in a mouse model of hindlimb immobilization. *BMC Musculoskelet. Disord.*, **2014**, *15*, 291.

[553] W. Hu, C. Zhang, R. Wu, Y. Sun, A. Levine, Z. Feng. Glutaminase 2, a novel p53 target gene regulating energy metabolism and antioxidant function. *Proc. Natl. Acad. Sci.*, **2010**, *107*, 7455–7460.

[554] R. K. Berge, B. Bjørndal, E. Strand, P. Bohov, C. Lindquist, J. E. Nordrehaug, A. Svardal, J. Skorve, O. Nygård. Tetradecylthiopropionic acid induces hepatic mitochondrial dysfunction and steatosis, accompanied by increased plasma homocysteine in mice. *Lipids Health Dis.*, **2016**, *15*, 24.

[555] K. de Oliveira, D. F. Fachiolli, M. J. Watanabe, D. Tsuzukibashi, C. M. M. Bittar, C. Costa, M. L. Poiatti, P. R. de L. Meirelles. Dimethylglycine supplementation in horses performing incremental treadmill exercise. *Comp. Exerc. Physiol.*, **2015**, *11*, 167–172.

[556] M. Kurosaki, S. Demontis, M. M. Barzago, E. Garattini, M. Terao. Molecular cloning of the cDNA coding for mouse aldehyde oxidase: tissue distribution and regulation in vivo by testosterone. *Biochem. J.*, **1999**, *341*, 71–80.

[557] M. T. Valenti, F. Bertoldo, L. Dalle Carbonare, G. Azzarello, S. Zenari, M. Zanatta, E. Balducci, O. Vinante, V. Lo Cascio. The effect of bisphosphonates on gene expression: GAPDH as a housekeeping or a new target gene? *BMC Cancer*, **2006**, *6*, 49.

[558] E. G. Vajda, A. Hogue, K. N. Griffiths, W. Y. Chang, K. Burnett, Y. Chen, K. Marschke, D. E. Mais, B. Pedram, Y. Shen. Combination treatment with a selective androgen receptor modulator (SARM) and a bisphosphonate has additive effects in osteopenic female rats. *J. Bone Miner. Res.*, **2009**, *24*, 231–240.

[559] D. B. Hoffmann, M. Komrakova, S. Pflug, M. von Oertzen, D. Saul, L. Weiser, T. A. Walde, M. Wassmann, A. F. Schilling, W. Lehmann. Evaluation of ostarine as a selective androgen receptor modulator in a rat model of postmenopausal osteoporosis. *J. Bone Miner. Metab.*, **2018**, 1–13.

[560] C. J. Martyniuk, S. Alvarez, S. McClung, D. L. Villeneuve, G. T. Ankley, N. D. Denslow. Quantitative proteomic profiles of androgen receptor signaling in the liver of fathead minnows (Pimephales promelas). *J. Proteome Res.*, **2009**, *8*, 2186–2200.

[561] C. Tristan, N. Shahani, T. W. Sedlak, A. Sawa. The diverse functions of GAPDH: views from different subcellular compartments. *Cell. Signal.*, **2011**, *23*, 317–323.

[562] A. Tarze, A. Deniaud, M. Le Bras, E. Maillier, D. Mollé, N. Larochette, N. Zamzami, G. Jan, G. Kroemer, C. Brenner. GAPDH, a novel regulator of the pro-apoptotic mitochondrial membrane permeabilization. *Oncogene*, **2007**, *26*, 2606.

[563] D. Y. Gui, L. B. Sullivan, A. Luengo, A. M. Hosios, L. N. Bush, N. Gitego, S. M. Davidson, E. Freinkman, C. J. Thomas, M. G. Vander Heiden. Environment dictates dependence on mitochondrial complex I for NAD+ and aspartate production and determines cancer cell sensitivity to metformin. *Cell Metab.*, **2016**, *24*, 716–727.

[564] C. Turano, E. Gaucci, C. Grillo, S. Chichiarelli. ERp57/GRP58: a protein with multiple functions. *Cell. Mol. Biol. Lett.*, **2011**, *16*, 539.

[565] H. Meyer, C. C. Weihl. The VCP/p97 system at a glance: connecting cellular function to disease pathogenesis. *J. Cell Sci.*, **2014**, *127*, 3877–3883.

[566] D. B. Solit, H. I. Scher, N. Rosen. Hsp90 as a therapeutic target in prostate cancer. *Semin. Oncol.*, **2003**, *30*, 709–716.

[567] A. S. Lee. The accumulation of three specific proteins related to glucose-regulated proteins in a temperature-sensitive hamster mutant cell line K12. *J. Cell. Physiol.*, **1981**, *106*, 119–125.

[568] P. Agostinis, S. Afshin. *Endoplasmic Reticulum Stress in Health and Disease*, Springer, **2012**.

[569] A. S. Lee. Mammalian stress response: induction of the glucose-regulated protein family. *Curr. Opin. Cell Biol.*, **1992**, *4*, 267–273.

[570] R. Sano, J. C. Reed. ER stress-induced cell death mechanisms. *Biochim. Biophys. Acta (BBA)-Molecular Cell Res.*, **2013**, *1833*, 3460–3470.

[571] C. E. Moore, O. Omikorede, E. Gomez, G. B. Willars, T. P. Herbert. PERK activation at low glucose concentration is mediated by SERCA pump inhibition and confers preemptive cytoprotection to pancreatic β-cells. *Mol. Endocrinol.*, **2011**, *25*, 315–326.

[572] M. Manczak, B. S. Park, Y. Jung, P. H. Reddy. Differential expression of oxidative phosphorylation genes in patients with Alzheimer's disease. *Neuromolecular Med.*, **2004**, *5*, 147–162.

[573] B. A. Altenberg, K. O. Greulich. Genes of glycolysis are ubiquitously overexpressed in 24 cancer classes. *Genomics*, **2004**, *84*, 1014–1020.

[574] Y.-C. Tseng, S. G. Liva, A. M. Dauki, M. Sovic, S. E. Henderson, Y.-C. Kuo, J. A. Benedict, S. K. Kulp, M. Campbell, T. Bekaii-Saab. Overcoming Resistance to Anabolic Selective Androgen Receptor Modulator (SARM) Therapy in Experimental Cancer Cachexia with Histone Deacetylase Inhibitor AR-42. *bioRxiv*, **2018**, 214155.

[575] Y. H. Lee, H. T. Tan, M. C. M. Chung. Subcellular fractionation methods and strategies for proteomics. *Proteomics*, **2010**, *10*, 3935–3956.

[576] M. Shen, H. Shi. Sex hormones and their receptors regulate liver energy homeostasis. *Int. J. Endocrinol.*, **2015**, *2015*.

[577] E. Lundberg, G. H. H. Borner. Spatial proteomics: a powerful discovery tool for cell biology. *Nat. Rev. Mol. Cell Biol.*, **2019**, 20, 285-302.

[578] A. P. Diz, M. Truebano, D. O. F. Skibinski. The consequences of sample pooling in proteomics: an empirical study. *Electrophoresis*, **2009**, *30*, 2967–2975.

[579] N. A. Karp, K. S. Lilley. Investigating sample pooling strategies for DIGE experiments to address biological variability. *Proteomics*, **2009**, *9*, 388–397.

[580] G. Arentz, F. Weiland, M. K. Oehler, P. Hoffmann. State of the art of 2D DIGE. *PROTEOMICS–Clinical Appl.*, **2015**, *9*, 277–288.